DNA origami tools for biophysical and biochemical applications

Inaugural-Dissertation zur Erlangung des Doktorgrades

-Dr. rer. nat.-

der Fakultät für Biologie an der Universität Duisburg-Essen

vorgelegt von

Richard Johannes Kosinski (M. Sc.)

aus Essen

März 2022

DOI: 10.17185/duepublico/76126
URN: urn:nbn:de:hbz:465-20220705-115418-5

„Iucundi acti labores.“
(Arbeiten sind angenehm, wenn sie getan sind.)

- Marcus Tullius Cicero (De finibus II, 105)

„Nunc est bibendum!“
(Nun muss getrunken werden!)

- Horaz (Carmina, 1, 37, 1)

Die vorliegende Arbeit wurde im Zeitraum von Juni 2017 bis Dezember 2021 im Arbeitskreis von Prof. Dr. Barbara Saccà am Zentrum für medizinische Biotechnologie an der Universität Duisburg-Essen durchgeführt.

Tag der Disputation:	17.06.2022
1. Gutachter:	Prof. Dr. Barbara Saccà
2. Gutachter:	Prof. Dr. Andrea Musacchio
3. Gutachter:	Prof. Dr. Kurt Gothelf
Vorsitzende(r) der Prüfungskommission:	Prof. Dr. Elsa Sánchez-García

Zusammenfassung

Nanotechnologie ist die nötige und unausweichliche nächste Stufe für den technologischen Fortschritt. Das liegt darin begründet, dass sowohl die Miniaturisierung als auch die Nutzung von Quanteneffekten nicht nur wertvolle Ressourcen spart, sondern auch bestehende Prozesse deutlich effizienter macht und die Entwicklung neuer Prozesse ermöglicht. Ein großes Problem der Nanotechnologie ist die Schwierigkeit einzelne Moleküle präzise zu platzieren. DNA Nanotechnologie, speziell die Methode des DNA Origamis, ist besonders gut geeignet um genau dieses Problem zu behandeln, da es eine Plattform bietet, auf der sich Multi-Kompenenten-Systeme assemblieren lassen.

In dieser These werden drei Projekte präsentiert, wovon jedes einen anderen Aspekt der DNA Nanotechnologie untersucht. Die Hauptarbeit analysiert die Effekte der Bindung und räumlichen Einschränkung der Serin-Protease Thrombin an DNA Nanostrukturen (R. Kosinski *et al.* Sci. Adv. 2022). Das Enzym wird erfolgreich an verschiedene DNA Origamis gebunden und das kinetische Verhalten wird gründlich untersucht, speziell mit Rücksicht auf den Grad der räumlichen Einschränkung, dem Substrattypen und der Nanostrukturen. Generell wurde eine erhöhte Reaktionsrate für DNA-gebundene Enzyme festgestellt. Das Ausmaß ebendieses ist jedoch von vielen verschiedenen Faktoren abhängig, welche im Detail beschrieben werden. In dieser Arbeit werden viele der vorgeschlagenen Hypothesen bezüglich DNA-Enzym Konjugaten diskutiert und sie zeigt, dass voreilige Schlussfolgerungen in Bezug auf erhöhte Enzymaktivitäten zu vermeiden sind, da DNA-Enzym Konjugate ein komplexes kinetisches Verhalten aufweisen, trotz einer Reduzierung des Systems auf wenige Komponenten.

Des Weiteren wird der Faltungsprozess eines DNA Origamis untersucht und die Möglichkeit zwei verschiedene Strukturen zu erhalten (R. Kosinski *et al.* Nat. Comm. 2020). Es wird gezeigt, dass mechanischer Stress, ausgelöst durch ungünstige Hybridisierungen an den Rändern der Struktur und abhängig von der Sequenz, zu einer Isomerisierung führt, in dem Versuch die globale Struktur zu entspannen.

Letztlich wird die hierarchische Assemblierung von DNA Origami Strukturen für die selektive Bindung von Gast-Molekülen sowie deren räumlicher Zuwendung realisiert (M. Erkelenz*, R. Kosinski* *et al.* Chem. Comm. 2021; *gleicher Beitrag; eine weitere Co-Erstautorenschaft ist derzeit in Vorbereitung). Als erster Nachweis wird eine Nanopartikel-DNA Hybridstruktur konstruiert mit möglichen Anwendungen für SERS und M-FRET.

Abstract

Nanotechnology is the inevitable and necessary next step in technological advance. This is because the miniaturization of devices and the benefits derived by quantum effects do not only safe valuable resources, but they are also highly promising for making existing processes more efficient and for developing a completely new set of tools for basically every domain of life. One problem faced in this area of research is the extreme difficulty encountered when trying to precisely arrange molecules in an orchestrated fashion. DNA nanotechnology offers an exciting toolbox to specifically address this problem, as it allows the rational assembly of multi-component systems with nanometer accuracy.

In this thesis, three projects are presented that take on different aspects of DNA nanotechnology. The main work investigates the effects of the spatial confinement of the serine protease thrombin within DNA nanostructures (R. Kosinski *et al.* Sci. Adv. 2022). The enzyme is successfully bound to different DNA origami structures and its kinetics are carefully analyzed in dependence of various parameters, such as the degree of confinement, type of substrate and type of nanostructure. In general, increased reaction rates were observed for confined enzyme species, although the extent of improvement varied in a complex way upon many factors that will be described in detail. This work discusses many of the proposed hypotheses on the enhancement of reaction rates observed for DNA-enzyme conjugates and advocates for a careful investigation of these structures, which may show a complex kinetic behavior despite their apparent simplicity.

Furthermore, the folding pathway of a three-domain DNA origami structure was investigated in detail (R. Kosinski *et al.* Nat. Comm. 2020). In particular, the ability of each structurally identical domain to fold in one of two different isomers as a function of the mechanical stress applied at the edges and their sequence composition. The mechanical stress generated by the unfavorable hybridization of edge staples resulted in isomerization as a means to circumvent local structural frustrations, however in a sequence-dependent fashion.

Finally, a hierarchical assembly of DNA origami structures was realized for the selective encapsulation of cargos and regulation of their intermolecular distance through a reconfigurable platform that can reversibly switch among five distinct states (M. Erkelenz*, R. Kosinski* *et al.* Chem. Comm. 2021; *equal contributors; an additional first co-authorship is currently in preparation). As a proof-of-principle, a AuNP-DNA hybrid superstructure was constructed as a potential tool for optical analytics such as SERS and M-FRET.

Table of Contents

1 Introduction

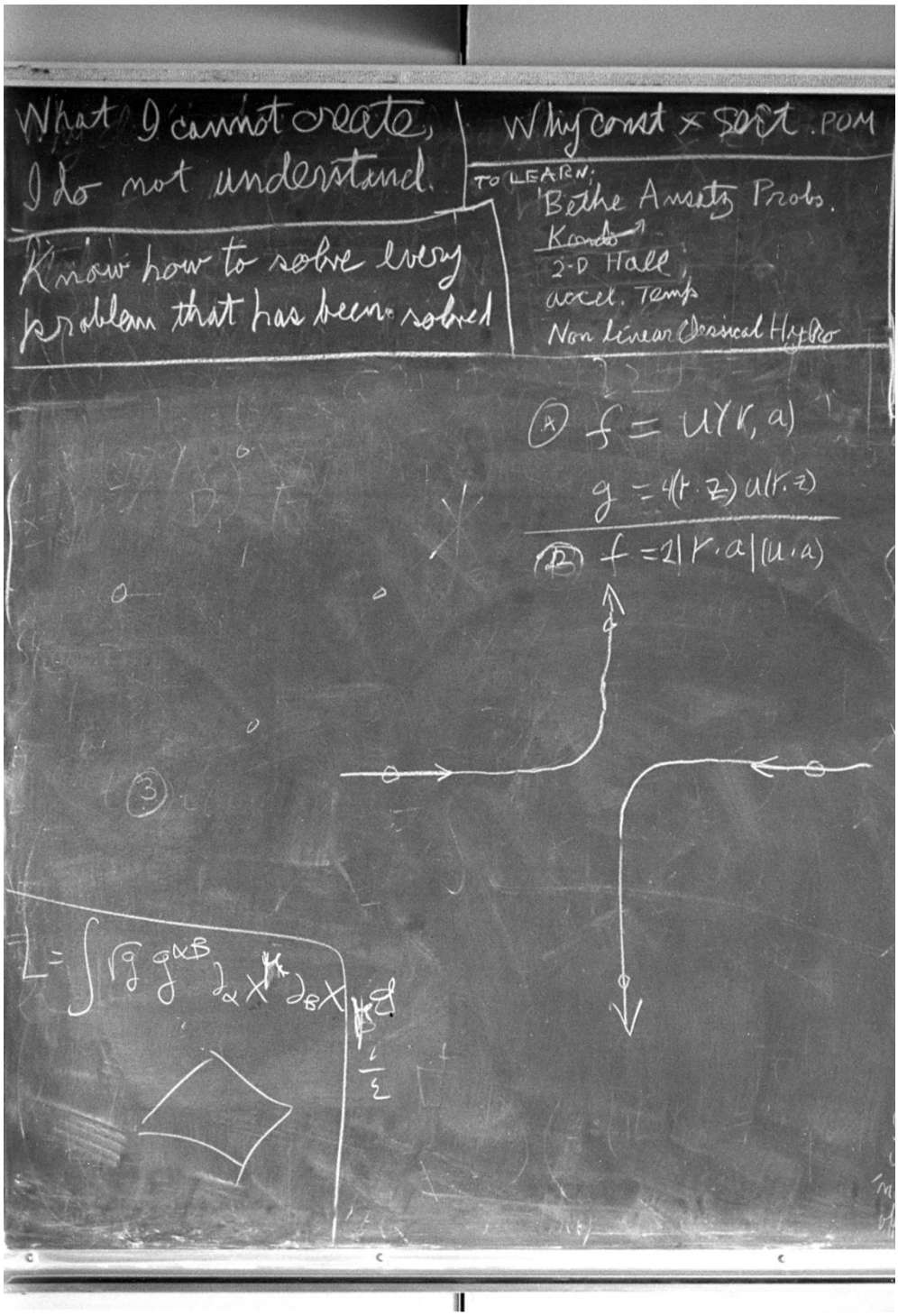

Figure 1: Feynman's blackboard at the time of his death. Kindly provided by Caltech Archives.

Probably no name is so much coupled to the term "*Nanotechnology*" as that of Richard P. Feynman. Since his groundbreaking talk "*There's Plenty of Room at the Bottom*"[1] in 1959 at the California Institute of Technology, where he anticipated the prodigious opportunities given by the miniaturization of machines down to the atomic level, he is regarded by many as the intellectual father of nanotechnology. Figure 1 shows his blackboard at the time of his death in 1988. On the upper left corner of the blackboard Feynman wrote "*What I cannot create, I do not understand*", a sentence that has been quoted countless times by now and leaves some room for interpretation.

One way of interpretation would be to include the sentence below: "*Know how to solve every problem that has been solved*". Arguably, Feynman may not have meant to precisely "create" something, but to be able to re-derive every formula and every natural phenomenon by starting with a blank piece of paper. The ability to do that requires a profound understanding in every "creation" step involved and the reasoning behind it. Eventually, one may recognize that even simple problems that seem to be easy to understand, reveal themselves to be growingly difficult the more detailed you look at them.[2]

On the other hand, it is also possible to stick more strictly to the quote and argue that we only truly understand something if we are able to literally create it. This may become increasingly apparent if we move down the scale in terms of size. While it is comparably easy for us to build macroscopic objects, difficulty mounts once we go downwards, eventually reaching the subcellular level. Here, most of the work so far has focused on observation and description. Systems are studied and dissected, taken apart to analyze their constituents and behavior to eventually derive a theoretical model that aims to predict the action of similar systems or to predict their response to a specific stimulus. While this method has undoubtedly proven to be successful in driving technological advance, many models are only applicable under a narrow set of conditions and can often describe only a fraction or an aspect of a complex system. It is therefore not surprising, and appears to be a general concept, that the opposite (bottom-up) process is far more challenging, i.e. to take a set of constituents and assemble them together into a working structure, as experienced by everybody who likes puzzle games.

1.1 Nanotechnology

Nanotechnology is the scientific discipline that deals with objects in the nanometer range, i.e. usually in the range of 1 to 100 nanometers (nm).[1,3] While this may appear simply as the "nano"-version of the definition of "microtechnology", we realize that at the nanosized scale important phenomena take place. First of all, while the size of a single cell, e.g. the *E. coli* bacterium, is about 1 µm[4], nanosized objects are at least 10 times smaller. We therefore leave the world of living matter once we enter the realms of nanosized objects. Also, since the resolution of light microscopes is limited to few hundreds of nanometers,[5] observation and visualization of nanosystems which are smaller than ca. 100 nm are oftentimes more laborious and require more sophisticated instrumentation. Much more important however is the fact that at these scales, other physical forces play a fundamental role, the occurrence of which is usually not even realized in the macroscopic world, while others are marginalized.[6,7] Newtonian physics loses its significance in the nanosized world, as the effect of gravity declines with smaller and lighter objects, while thermally-driven Brownian motion and surface effects start to dominate the events.[8,9] Additionally, many intrinsic properties, as e.g. conductivity,[10] optics,[11] stability,[12] or reactivity[13] of materials change when taking place in a nanoscaled environment. These changes are usually not observed when going from macro to micro. Possible benefits of nanotechnological applications therefore go beyond the interests of miniaturization and aim to take advantage of this "new" set of physics.

While several historical sources witness the usage of nanotechnology already millennia ago,[14] the manufacturing of nanoparticles has been carried out without any understanding of the underlying principles or even the existence of any such materials. First scientific descriptions of those nanoobjects were given by Graham and Faraday in the 19th century;[15,16] however, much before any possibility for precise manipulation of matter at these scales. It was not until 1959 that the actual advent of nanotechnology can be dated, when Richard Feynman first seeded the idea to set out into the nanoworld and yet still more than two decades were needed to convert his vision into reality.

With the invention of the first scanning tunneling microscope (STM),[17] the atomic force microscope (AFM)[18] and the discovery of fullerenes,[19] first experimental results were at hand that went beyond thought experiments or pure observations of nanoobjects done by transmission electron microscopy (TEM)[20] or light scattering techniques.[21] A scientific

breakthrough was then presented to the world a few years later by Donald Eigler and Erhard Schweizer. In a world's first demonstration, they arranged 35 Xenon molecules to spell out the IBM logo.[22] While this experiment required conditions that are highly unfeasible for any practical application, it represented an important step in the field, as it demonstrated the active and precise arrangement of individual atoms. This kind of superb manipulation precision is what many people share as the "grand vision" for nanotechnology, i.e. the creation of "molecular assemblers" that are able to create any type of molecule.[3] If this kind of machines are really possible, it is still a matter of debate,[23] but the applications of nanotechnology are so surprisingly increasing, that this endeavor may become feasible in the near future.

A lot of these nanotechnological applications include nano-"coatings", as e.g. in more efficient solar panels[24] or nanoparticles that are more limited to bulk applications, as e.g. in cosmetics, sunscreen[25] or in material sciences.[26–28] However, there are also more sophisticated applications, especially in the field of medicine. Nanodevices are already investigated and/or in practice as tumor therapeutics,[29,30] as drug delivery vehicles,[31–33] or as sensitive detection methods.[34,35] Finally, the ever-decreasing size of transistors for our electronic devices are probably the most noticeable and appreciated product of nanotechnology by now.[36,37]

Generally, the construction of nanomaterials falls under one of the following two categories:

- Top-Down: The construction of nano objects from larger precursors
- Bottom-Up: The construction of nano objects from the assembly of smaller precursors

Top-Down approaches

Most of today's applications of nanomaterials rely on the top-down methodology. Here, nanoobjects are generated by the breakdown of (or manipulation from) larger bulk material. Typical methods include photolithography or inkjet-printing.[38] Usually these procedures are linked to inorganic materials. In fact, one downside of this approach relies on the fact that the materials used oftentimes have very little chemical diversity.[39] Also, the diffraction limit of light is making lithography increasingly difficult for features of decreasing size. Although novel techniques can circumvent this problem, they normally require high production costs.[38]

Bottom-Up approaches

This approach relies on the self-assembly of small constituents into larger, more complex structures. This is the main construction route found in nature (e.g. self-organization of lipid

membranes, synthesis of amino acid chains that fold into functional proteins, protein-oligomerization, filament growth, etc.). This construction principle usually relies on non-covalent forces as molecular recognition, shape complementarity, Van-der-Waals forces, electrostatic interactions and/or hydrogen bonds.[39,40] The main advantage of bottom-up structures is that their formation and disruption is reversible. Thus, such structures may undergo deformation (lipid bilayers), denaturation (protein degradation) or disassembly (cytoskeleton) without spending too much energy on breaking the bonds that keep them together. Probably the most intriguing bottom-up fabricated materials in nature are proteins. The sheer existence of 20 different amino acids allows for such a huge variety of different proteins that a more or less endless reservoir of possible sequences, structures and electrostatic surface potentials can be achieved from a given set of amino acid residues (e.g. a protein with 100 amino acids could potentially give rise to 20^{100} distinct protein sequences). This blessing of diversity however comes along with a downside, i.e. it has been notoriously hard to foresee how an amino acid chain will fold, how it will behave and interact once folded. Only now, 64 years after the first crystal structure of a protein was reported,[41] we start to be able to predict these features with the help of advanced machine learning algorithms, and yet a lot of work remains to be done.[42] Therefore, scientists have come up with another building material for the construction of nanoobjects, i.e. DNA.

1.2 DNA Nanotechnology

In nature, DNA has evolved as the molecule for storage of genetic information. It contains the blueprints for all the proteins that are manufactured inside the cells,[43] and is therefore probably one of the most essential molecules of life, as we know it today. A DNA molecule is made up of a sequence of four different monomers. Each monomer is composed of a phosphate, a sugar (deoxyribose) and one of four nucleobases, namely Adenine (A), Guanine (G), Thymine (T) or Cytosine (C). The most common form of DNA is the B-DNA.[44] Here, two DNA single strands are arranged in a right-handed helix and are oriented in an antiparallel fashion to one another, with the nucleobases pointing inwards and the phosphates outwards, building the DNA "backbone" [45] (Figure 2 A). The nucleobases are capable of hydrogen bonding to one another, however only in a specific fashion. In the canonical Watson-Crick base pairing, A will bind T and C will bind G.[45] Interestingly, while being important for the stability and the self-

recognition properties of the DNA, the hydrogen bonds of the nucleobases are not the driving force in DNA duplex formation. In fact, the stacking interactions between the vertically aligned nucleobases of the same strand yield the major energetic contribution to the DNA duplex stability and are furthermore responsible for its helical structure.[46–48]

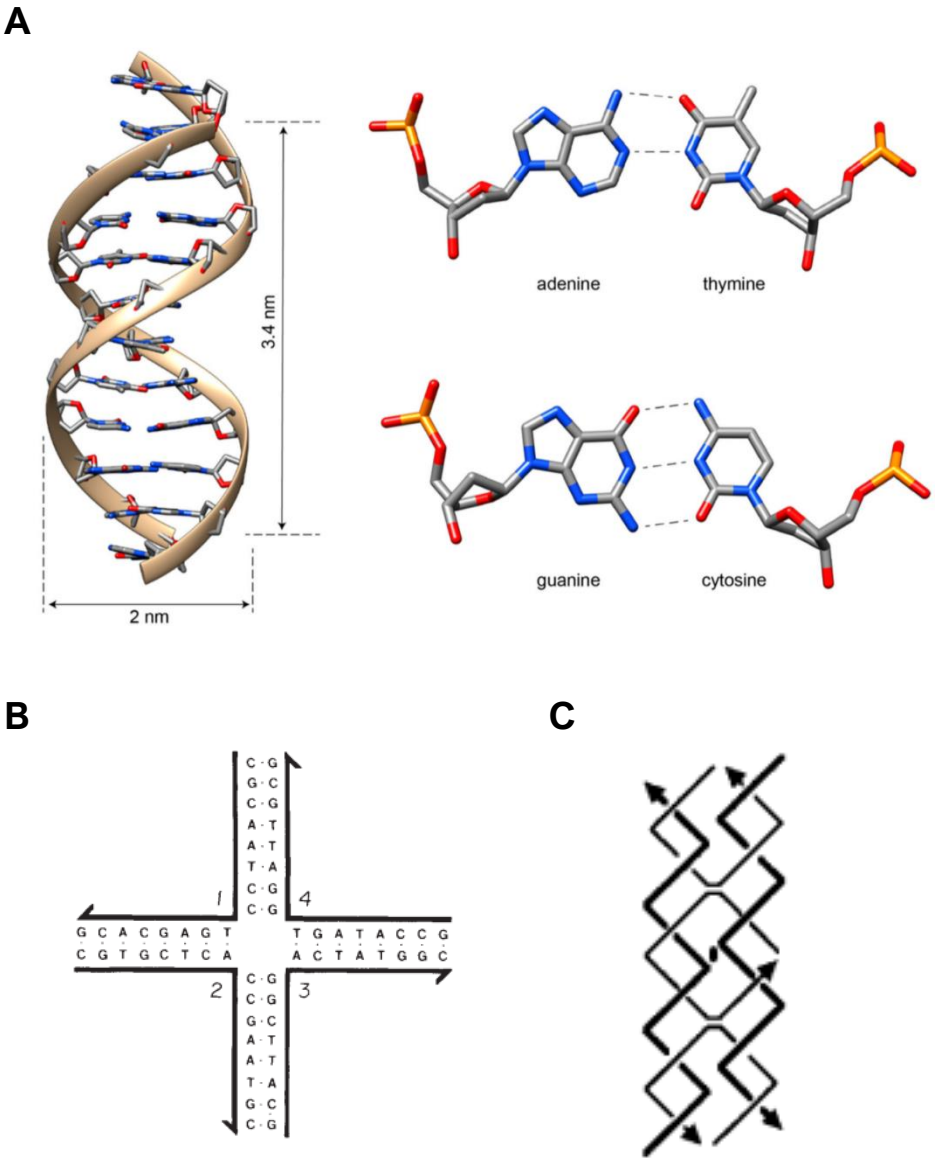

Figure 2: Structure and use of DNA in nanotechnology. (**A**) DNA double helix in its B-form (left). Bases in the inner part of the helix form hydrogen bonds. While AT pairs only form two bonds, GC pairs are stabilized by three bonds. (right) (**B**) Immobile Holliday junction made up by four oligonucleotides. Each oligonucleotide binds two other DNA single strands. Lack of symmetry prohibits migration of the junction. (**C**) Double-crossover tile with antiparallel double-helical domains and an even integer number of half helical turns between crossovers. (**A-C**) were reprinted and adapted with permission from references [49–51]. (**A**) Figure modified from open sources (Protein Data Bank (PDB): 1DUF) (**B**) Copyright 2022 by Springer Nature. (**C**) Copyright 2022 by American Chemical Society

DNA has several characteristics that make it a suitable candidate for nanotechnological applications. It is quite thermostable (especially in dry conditions)[52,53] as well as stable across a wide range of pH values and buffer systems.[54,55] Also, binding strengths of individual DNA motifs can be fine-tuned.[56] Furthermore, progress in chemical synthesis of DNA sequences make it readily available and affordable at relatively low costs. Additionally, while DNA itself is rather chemically inert,[57] a variety of functional moieties can be attached to it and are commercially available.[58] The true power of DNA as material for nanotechnology however lies in the nature of the specific binding of its nucleobases (A:T and C:G). This property makes the hybridization of two DNA single strands *predictable*. This is fundamentally different from proteins, where the folding cannot (at least for now) be easily predicted based on its primary structure (i.e. its amino acid sequence), despite powerful protein design strategies are rapidly evolving that may overcome this problem in a near future.[42,59,60]

Ned Seeman was among the first scientists who realized and applied the programmability of DNA to create molecular objects. In his groundbreaking theoretical and practical works in 1982 and 1983, Seeman firstly reported the construction of an immobile DNA junction (Figure 2B, C).[50,61] Since these immobile junctions are the fundamental "unit" of every DNA nanostructure, this work is usually regarded as the cornerstone of DNA nanotechnology. Further research led to the development of double crossover (DX) tiles,[51] where immobile junctions are connected to one another through crossovers of DNA strands. These tiles quickly became the building block of many different DNA nanostructures.[62–64] During the next decades, tile assemblies into DNA lattices and polyhedral architectures were further investigated, and many different approaches are pursued today.[65–67] While DNA tiles have been shown to allow the construction of a wide array of different assemblies and were used for the controlled placement of molecular moieties at specific locations, this method also suffers from major drawbacks. Generally, these systems are structurally more flexible and are rather sensitive to impurities and/or stoichiometric differences among the constituent oligonucleotides. The final result is a poor control of the assembly process.[68] To overcome these issues, an inherently different assembly strategy was presented by Paul Rothemund in 2006.[69] This strategy relies on the use of a long, single-stranded DNA *scaffold* strand as the main constituent of the assembly mixture and was termed "scaffolded DNA Origami".

1.3 DNA Origami

Origami (ori = “folding”, kami = “paper”) describes the art of folding a two-dimensional (2D) piece of paper into, usually, a three-dimensional (3D) object. Besides being beautiful pieces of crafting, origami found applications in various disciplines, most notably material sciences and engineering.[70,71] Very similar to this idea is the concept of DNA origami. Here, a 1D single-stranded DNA chain (scaffold) is folded into a desired structure by using hundreds of suitably designed short oligonucleotides (staple strands). These short DNA strands bind to discontinuous regions of the scaffold, bending it into a predictable shape. Within a DNA origami, helices are aligned in an antiparallel fashion and connected via immobile Holliday junctions, also called “cross-overs”.[69]

1.3.1 General information

While there are examples of scaffolded DNA assemblies earlier than 2006,[72,73] Rothemund’s paper (Figure 3A, B) is generally considered to be the pioneering work of DNA origami nanotechnology. That is because of several reasons: The use of a much longer, single-stranded phage-derived genome increases the yield of scaffold generation, which is demanded for working with DNA origami, as no restriction, ligation or denaturation is necessary. This choice therefore eases the use of DNA origami to a point where this method can be readily implemented in standard laboratories. Additionally, in his work, Rothemund already pioneered further concepts like multimerization, twist correction, cross-over rules and individual addressability.[69] All of these notions were later on picked up by other groups and studied in detail.[74–79]

DNA origami is an attractive branch of DNA nanotechnology as it holds many benefits over classical tile-based assembly. For example, the use of a scaffold strand has several advantages. First of all, it gives the structure a limit of growth and thus makes the assembly highly controllable in size. Also, using a molar excess of staple strands over the scaffold strand highly increases the yield of fully intact structures. This is because, during the assembly process, deleted or truncated staples (that may be present in commercially purchased oligonucleotides) will be displaced and finally replaced by the correct full sequences, which display a competitively higher number of base pairs. Indeed, by heating the assembly mixture

and slowly cooling it down, not only kinetic traps can be overcome, but also the structure will reach its thermodynamic minimum, which usually occurs when all bases are paired. This feature of DNA, to be able to displace other DNA strands that typically have a sub-optimal number of base pairs, is highly important for the DNA assembly process and has found applications in numerous works under the name of "toehold mediated strand displacement reactions".[80,81] Finally, binding of staple strands to the scaffold is a cooperative event. Once the first oligonucleotides bind discontinuous regions of the scaffold, thereby "pulling" it together, the adjacent scaffold sequences are in close proximity to one another and greatly facilitate the binding of neighboring staple strands, making the whole assembly much more efficient.

Today's repertoire of DNA origami structures is immense and, structurally, almost no restrictions apply.[74,76,82–85] Applications in research are manifold as DNA origamis find use as sensing devices,[86–88] cargo containers,[89–91] light harvesting structures,[92,93] molecular switches,[94,95] force spectroscopy tools,[96,97] rotor units [98,99] or as hosts for DNA walkers,[100] to name but a few. Additionally, differently sized DNA origamis were investigated. While it is usually no problem to simply use a smaller scaffold in order to achieve smaller structures,[101,102] increasing the length of the scaffold strand may complicate the folding process. Also, a heavily increased number of staple strands increases the production costs and sequences need to be carefully designed in order to ensure their uniqueness.[103] A more convenient approach is to bind individual DNA origami structures together, either *via* strand hybridization or base stacking. In this way, DNA origami mega-structures were achieved, yielding giga-Dalton molecular weight objects, with a size up to the micrometer scale.[74,104–106] This kind of hierarchical assembly, that goes from nanosized constituents to micrometer sized super-structures, is common to biological systems and DNA nanotechnology offers an ideal toolbox to mimic these processes.[107] This trend, i.e. to construct objects of ever-increasing size, may apparently contradict the notion of nanotechnology. However, it should be noted that these structures keep their nanosized features and these can be individually addressed.[104]

While structures are versatile and applications are numerous, the true power of DNA origami can be condensed to one simple fact: It allows the precise placement (on a DNA surface) of virtually any ligand molecule with nanometer resolution (Figure 3C). This characteristic is the fundamental motivation for the construction of any complex nanoobject. Ironically, by stripping the DNA of its protein-coding property and using it simply as a construction material, we incidentally add another code to it. Now, DNA sequences code for 3D coordinates rather than amino acids.

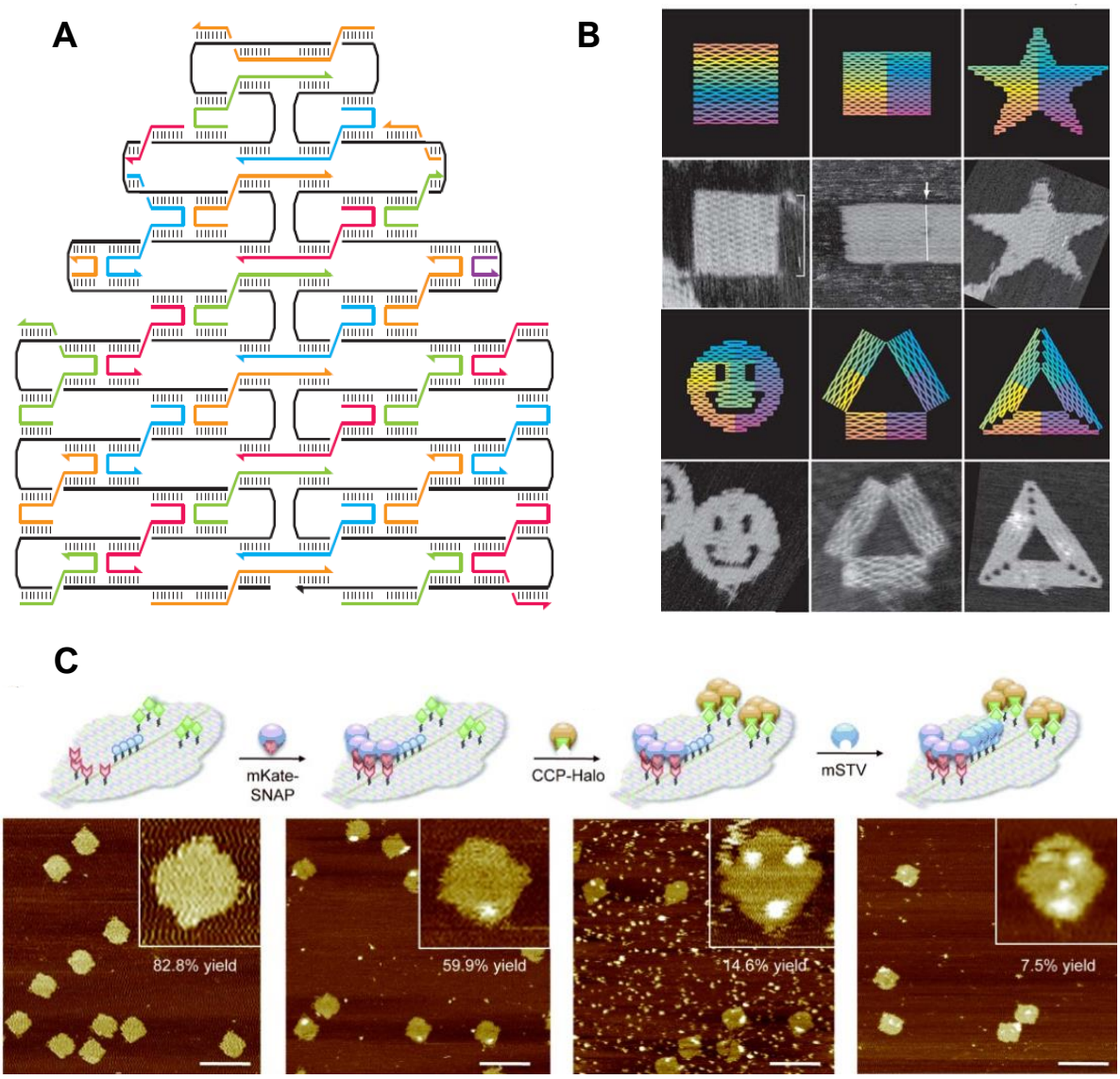

Figure 3: DNA Origami. (**A**) DNA origami design. Staples strands connect a long scaffold strand and bend it into a desired shape. Most staples connect three helices. Central staples connect the scaffold seam. (**B**) Various DNA origami designs and their corresponding structures as recorded by AFM imaging. First and third rows show the design. Second and fourth rows show the AFM images. (**C**) Orthogonally modified DNA origami. O6-benzylguanin (BG), 5-chlorohexane (CH) and biotin-derivatized staples were incorporated into the DNA origami, allowing the specific and serial binding of different proteins at designed positions. Scale bars are 100 nm. (**A-C**) were reprinted and adapted with permission from references [69,79]. (**A+B**) Copyright 2022 by Springer Nature. (**C**) Copyright 2022 by John Wiley and Sons.

In this work, three projects will be presented. All were pursued during the course of this doctoral thesis and resulted in three publications. Each project takes on a different topic of DNA nanotechnology. While the main work covered the topic of enzyme kinetics in DNA confined

spaces, the remaining two projects faced the problem of DNA origami folding and reconfigurable hierarchical DNA systems (these last two works will be presented in the appendix, see section 7.1 and 7.2). This thesis therefore treated both theoretical aspects of DNA origami self-assembly and its applications in protein and, as a proof-of-principle, nanoparticle-based materials. A short introduction will be given below to each aspect of DNA origami nanotechnology elaborated in this thesis, namely: 1) the kinetics of DNA-enzyme complexes, 2) the folding process of DNA origami structures, and 3) the structural reconfiguration of DNA origami constructs.

1.3.2 Kinetics of DNA-enzymes conjugates

Parts of this chapter are currently in press as a book chapter (*The Effect of DNA Boundaries on Enzymatic Reactions*, Richard Kosinski & Barbara Saccà) in *DNA Origami: Structures, Technology, and Applications* (2022, John Wiley and Sons Inc.)

Probably no other class of biomolecules is so much associated with the role of an "active" substance as enzymes. Since they catalyze a plethora of different chemical reactions, they are not only vital for any form of life, but they also appear "to do" things. It is therefore not surprising that, when observing fermentation processes, Louis Pasteur stated that this was caused by a "vital force" functioning only in living things.[108]

Today enzymes are understood as non-living biomolecules that can recognize and bind to target substrate molecules and encourage a chemical reaction by lowering the activation energy needed for it to occur.[109] Obviously this characteristic makes enzymes an interesting subject not only in research, but for numerous applications in every domain of our daily life, as e.g. in health care, brewing industry, biofuel industry, food processing, detergents etc.[110–112]

Since the large-scale production of enzymes is expensive, they are usually immobilized for industrial applications in order to use them for an extended period of time. Also, it is much easier in this way to separate the catalysts from the products. Additionally, it is often observed that immobilization improves the stability of enzymes, e.g. makes them more tolerant to high pH and high temperatures.[113,114] All of these properties aid in reducing the costs immensely and therefore help to keep the whole process economically viable.

In nature, immobilization or compartmentalization of enzymes is a common theme. Enzymes may be bound to membranes or kept in certain areas of the cell.[115] Oftentimes, enzymes taking part to the same reaction cascade are located next to each other.[116] This organized spatial distribution bears several advantages: It helps to protect enzymes from degradation, it increases the local concentration of catalysts and reactants, it prevents unwanted side reactions to occur and toxic intermediates are less likely to escape into the bulk solution.[115,117]

Given the above-mentioned benefits, enzymes have been quickly merged with DNA nanostructures. Their ability to precisely place guest molecules in space and time is ideal to explore compartmentalization strategies and/or create in vitro reaction cascades that cannot be found in nature. Interestingly, it was soon noted that enzymatic activities often change dramatically when attached to DNA structures.

1.3.2.1 Single enzymes on DNA scaffolds

Among the first to inspect the nature of DNA-enzyme hybrids was the Niemeyer group. Fruk *et al.*[118] covalently linked a heme group to a DNA oligonucleotide. This hybrid DNA strand could then bind to either apo-myoglobin (Mb) or horseradish peroxidase (HRP). Interestingly, while the activity of HRP-DNA was reduced (increased K_M and decreased k_{cat}), the activity of Mb-DNA was heavily increased, with a k_{cat} up to 18-fold larger than that of the native enzyme. The authors suggested that increased K_M values may be due to steric hindrance or electrostatic repulsion between substrate and DNA, while increased or decreased k_{cat} values can be attributed to unspecific interactions of the DNA with the protein surface. In a follow-up study, the same group investigated possible effects given by the length and sequence of the DNA oligo on the attached enzyme. In essence, the trends of the previous work were replicated, however to various degrees, depending on the type of oligo attached. No correlation between sequence and/or length and enzyme activity could be concluded though.[119] Along the same line is a finding of Rudiuk *et al.*,[120] where a 48.5 kbp-long lambda phage DNA was attached to β-lactamase. A moderate increase of the catalytic activity (3.3-fold) was observed, with no significant change in the K_M values. Taken together, these findings testify the difficulty to give a straightforward interpretation to the intriguing observations. Detected differences in catalytic efficiencies were mainly attributed to *unspecific interactions of the DNA and the enzyme*, struggling to pinpoint an exact mechanism.

Another possible explanation for increased reaction rates was suggested by the Wheeldon group. In two following works, they observed increased reaction rates when enzymes were attached to DNA oligos/motifs. Surprisingly, this could be attributed to favorable interactions of the DNA with the substrate. If the strength of this interaction was "just right", i.e. not too weak and not too strong, similar to the well-known "Sabatier Principle",[121] the local concentration of substrate near the enzyme was increased, effectively reducing its K_M values.[122,123] In this way, the matrix to which the enzyme is attached (in this case DNA) takes active part in the reaction and its role is usually referred to as *substrate steering*. Strikingly, Wheeldon and co-workers did not observe a reduced catalytic efficiency for HRP in case of 2,2'-azino-bis(3-ethylbenzothiazoline-6-solfonic acid) (ABTS) as substrate. This is in contrast to findings of the Niemeyer group and may well be attributed to differences in the experimental set-ups and DNA motifs used, highlighting again the complex nature of the subject.

A detailed analysis of entrapped enzymes was done by Zhao *et al.*[124] By studying the catalytic performance of six different enzymes, each separately encaged in a DNA container, increased reaction rates were recorded for all except one enzyme (Figure 4A) (3.5 up to 9.6-fold increase in the turnover numbers), similar to previous findings.[125] The authors ascribed this increase to a *structured layer of water molecules* inside the DNA box that spans the region from its walls to the protein surface. Multiple studies have shown that this can have a favorable and stabilizing effect on proteins[126,127] and a similar rationale was argued for the enhanced enzymatic performances observed.

Yet another explanation for the altered enzymatic behaviour was given by Ijäs *et al.*[90] Two-fold enhanced reaction rates of HRP inside a DNA container were attributed to a potential *decreased pH value*. Here, the authors argue that the microenvironment near the DNA walls is different from the bulk, as positively charged H^+ ions accumulate at the highly negatively charged DNA surface, therefore lowering the pH in the direct vicinity of the DNA scaffold. Since HRP is known to perform better at low pH regimes,[128] this rationale fits well with the experimental observations.

1.3.2.2 Enzyme cascades on DNA scaffolds

While there are several examples of studies of single enzymes on DNA structures (*vide supra*), the main body of scientific works on enzyme-DNA hybrid systems focuses on enzyme

cascades that are precisely placed on a DNA platform.[95,129–137] Within these cascades, a metabolite that has been processed by one enzyme is subsequently used as substrate for the next enzyme (Figure 4). This strategy is inspired by nature, where enzymes that take part in the same metabolic pathway are oftentimes located together.[138–140] Ideally, the substrates are *channeled* from the first enzyme to the second, preventing its escape into the bulk solution where it could be sequestered by unwanted side reactions. This process is termed *substrate channeling*.

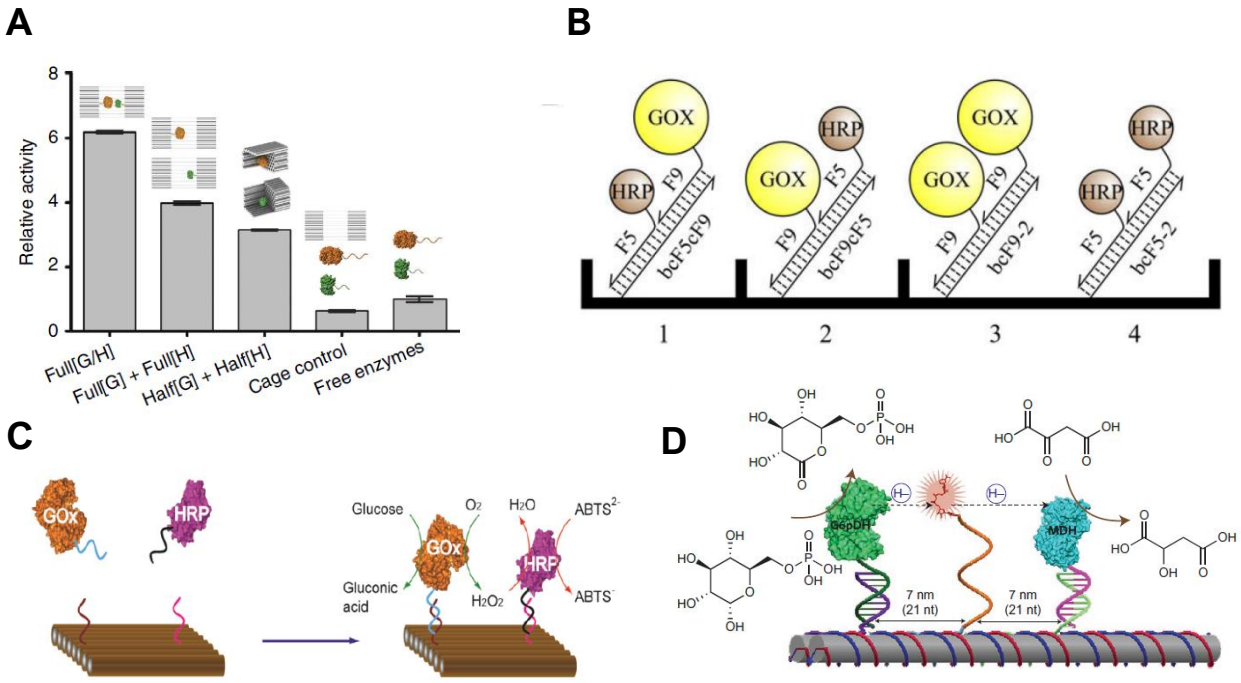

Figure 4: DNA-enzyme hybrid structures. (A) Single or enzyme pairs (GOx/HRP) are encapsulated within a 3D DNA cage. The relative activity increases for encapsulated enzymes. (**B**) Immobilization and co-localization of enzyme pairs via DNA strand hybridization. (**C**) GOx/HRP enzymes are co-assembled onto a 2D DNA sheet. The intermediate H_2O_2 is channeled between the enzymes. (**D**) Enzymes G6pDH and MDH are co-localized onto a DNA scaffold. A swinging arm in between carries the co-factor NAD^+. (**A-D**) were reprinted and adapted with permission from references [124,129–131]. (**B**) Copyright 2022 by Elsevier. (**C**) Copyright 2022 by American Chemical Society. (**D**) Copyright 2022 by Springer Nature.

Among the first to mimic this strategy was again the Niemeyer group.[129] By coupling a Glucose oxidase/Horseradish peroxidase (GOx/HRP) enzyme pair to a DNA scaffold they observed an up to 3-fold increase in catalytic activity as compared to an enzyme mix that is located on different scaffolds (Figure 4B). However, the introduction of a competing enzymatic reaction diminished this effect. One hallmark of substrate channeling is the fact that it cannot be affected by the presence of a third enzyme in solution, as this cannot in principle confiscate the intermediate channeled between the first and the second enzyme. Hence, these results

suggested that substrate channeling either did not take place or was not very efficient. Further investigations on this subject were carried out by multiple groups, which reported efficient activation of enzymatic cascades upon co-localization of both enzymes.[141–144] The concept was extended to *in vivo* applications, where not only DNA but also RNA and protein scaffolds were used to alter metabolic pathways.[145–148] In an often-cited work, Fu *et al.*[131] presented a GOx/HRP system on a 2D DNA origami (Figure 4C). Substrate turnover clearly increased with decreasing inter-enzyme distances. A form of *limited diffusion* was stated by the authors, where the intermediates were hindered from escaping into the bulk solution due to preferred movement along the hydration shells of the enzymes. These results were replicated more recently with another read-out system, strengthening the observations.[133] Along these lines was an elegant study from the Hao Yan group, in which a DNA origami was used that could undergo conformational changes from a planar 2D sheet into a 3D DNA nanotube, thereby changing the distances of attached enzymes to one another and essentially restricting the volume within which the molecular diffusion of the reacting species occured. Again, higher enzymatic activities were observed for closer inter-enzyme distances,[132] in line with similar works.[149] Notably, Ngo *et al.*[136] reported an enzyme pair system in which two intermediates were necessary for the second enzyme to generate the final product. Proximity of both enzymes increased greatly the reaction velocity (9.0-fold). Upon addition of one of the intermediates (xylitol) in excess, however, this enhancement dropped significantly (2.6-fold), indicating that in conditions where intermediates are rapidly available, the effect of spatial proximity is of little benefit.

A similar approach was investigated *inter alia* by Fu *et al*. (Figure 4D) which relied on fixing the co-factor nicotinamide adenine dinucleotide (NAD^+) via swinging arms in between the enzymes glucose-6-phosphate dehydrogenase (G6pDH) and malic dehydrogenase (MDH).[130,150] In this way, the *local concentration* of the co-factor was tremendously increased, thereby boosting enzymatic activity up to 90-fold and further.[151] Similar results were presented by other groups in which control over the distance of co-factor and enzyme could be applied to tune enzymatic activity.[95,152,153]

While all these works clearly indicate a relationship between inter-enzyme distances and reactivity, reported efficiencies vary quite dramatically, presumably due to different experimental set-ups, purities/efficiencies of DNA-enzyme hybridization, equipment and read-out systems. It is therefore difficult to decipher the actual origin of the altered kinetics of DNA-scaffolded enzymes and to which extent each factor contributes to the compelling observations.

1.3.2.3 Current discussion on proximity and other hypotheses

While a staggering amount of evidence has been found in support of the proximity model, several studies convincedly counteract this hypothesis. Interestingly, in some of these works, co-localization of enzymes did indeed increase reaction velocities, however only to a small degree. Notably, reaction speeds were increased for each individual enzyme upon conjugation to the DNA surface, making it hard to judge whether the observations only reflect the sum of the enhanced reaction rates of both enzymes.[124,135] In a more recent report, Klein *et al*.[134] further nourished the questions about the validity of the proximity model. By attaching a three-enzyme cascade on a DNA origami platform, significant increases in the reaction rates were observed. Remarkably, an even higher increase was observed when the enzymes were positioned at the farthest distances (about 100 nm) to one another. It was reasoned that other scaffold-dependent effects, as variations in the pH, hydrations layers or interactions of the scaffold with enzymes or substrates, must be the reason for the enhanced reaction velocities, rather than proximity induced effects.

The Hess group is one of the first groups that showed the inadequacy of the proximity model to explain the velocities observed in DNA-enzyme conjugates.[154] In a very basic experiment, utilizing the popular GOx/HRP enzyme pair, the concentration of HRP was varied between 1, 2 and 20 nM.[128] While an increase in reaction speed was observed within the first seconds to minutes, final velocities converged to a common value (about 15 nM/s). Hence, the measured speeds refer to the velocity of the rate-limiting enzyme GOx. In another insightful experiment, both enzymes were connected via a sulfosuccinimidyl 4-(N-maleimidomethyl)cyclohexane-1-carboxalte (sulfo-SMCC) linker. Again, no increase in the reaction velocity could be observed as compared to each enzyme individually and the reaction was successfully sequestered by catalase, thereby excluding any substrate channeling phenomenon. The point is that the reaction velocity of an enzyme cascade will always correspond to the velocity of the rate-limiting enzyme.[154] This is obvious if the first enzyme (E1) within the cascade is the rate-limiting one. If the second enzyme (E2) is the rate-limiting factor, the bulk will be soon filled up with intermediates (since E2 cannot process it as quickly as E1 produces it) until its concentration will be sufficiently high to saturate E2. In this scenario, substrate channeling can contribute to the reaction velocities only in the initial phase during which the bulk solution fills up with intermediates.[155] Under the experimental conditions typically used, this time period was calculated to be within milliseconds, i.e. beyond the time-

resolution limits of standard techniques.[154] Hess and co-authors admit however, that substrate channeling may indeed increase reaction speeds if a sequestering reaction runs in parallel or if molecular bridges or swinging arms are used to significantly increase the concentration of co-factors (as seen e.g. for NAD+).[151] Markedly, substrate channeling in nature usually relies on guidance or fixation of intermediate species, rather than on proximity alone.[150,156,157]

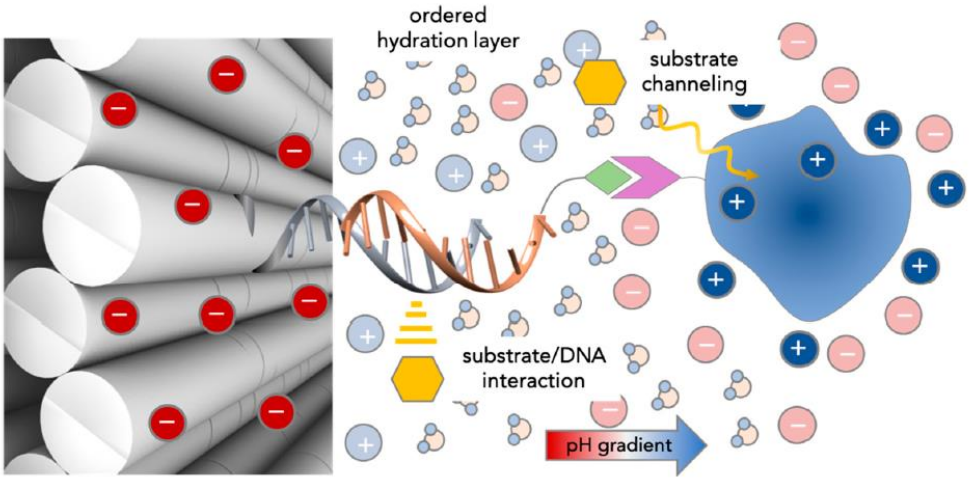

Figure 5: Hypotheses on altered behaviour of DNA-scaffolded enzymes. Substrate/DNA interactions can lead to a high local concentration of substrate (substrate/DNA interactions). Substrates can be channeled between enzymes, preventing escape to bulk solution (substrate channeling). A pH gradient can be established due to the high amount of negative charges of the DNA scaffold, effectively lowering the pH of the microenvironment around the enzyme (pH gradient). The negatively charged DNA structure can induce an ordered hydration layer that is thought to stabilize the enzyme and accelerate the reactions at its surface (ordered hydration layer). Reprinted and adapted with permission from reference [158].

Overlooking the wealth of publications on DNA-enzyme hybrid systems, it emerges that no hypothesis on increased reaction rates (Figure 5) could satisfactorily unite all experimental observations. A quite complex picture results, in which many different factors may (certainly) play a role, making it difficult to pinpoint each individual contribution. The situation is surely further impeded by the differing experimental set-ups. Therefore, the work presented in this thesis aimed at excluding *a priori* as many hypotheses as possible, through the investigation of a single and well-defined enzyme system and the systematic analysis of the role played by each individual component (i.e. substrate, enzyme, DNA) in detail.

1.3.3 Folding of DNA origami structures

While the hybridization of DNA duplexes has been extensively studied,[56,159–161] the formation of a DNA origami structure is a much more complex event that cannot be simply described by consecutive hybridizations of many staple strands to the scaffold. Arguably the most fundamental difference between the two assembly processes is that – in a DNA origami structure - each staple strand can be divided into several hybridization *domains*. Each of these domains binds to a distinct region of the scaffold strand and hence the process is different from the hybridization of a linear dsDNA. It has been independently shown by the Dietz group[77] and the Shih group[78] that the hybridization process is favorable if one of these domains exhibits a sufficiently long and consecutive binding region to act as a *seed*, thus favoring further contacts between adjacent staple domains and distinct parts of the scaffold. Binding of these domains, which eventually drives the folding of the scaffold, is of crucial importance. Building on theoretical and experimental findings of Arbona and others,[162–164] the Turberfield group demonstrated this in an equally simple as elegant experiment (Figure 6A).[165] By ligating two scaffold strands of the same sequence together, each staple strand had the "choice" to either bind regions within one scaffold or to connect regions of both scaffolds. AFM analysis revealed that folding trajectories are favored in which staples have binding domains within proximity or continuous regions. Different folding pathways could be tuned by purposefully omitting or incorporating such staples. This is because the folding of far-distant regions into a well-ordered, closely packed structure comes with an entropic penalty.[162] This contribution gets larger the more distant regions have to be connected. In other words: It becomes less likely for staple domains to make contacts with distant scaffold regions, the further apart they are. A consequence from this is that, once a staple fully binds to the scaffold, i.e. all domains are bound and the scaffold is crudely folded, binding of the neighboring staple strands is highly facilitated, since their yet unbound domains are now in close proximity to their target binding sequences.[162,163,165] This makes the assembly of DNA origamis a highly cooperative process,[166,167] as convincingly demonstrated by the Dietz group by isothermally assembling complex DNA structures. In their work, constant temperatures, slightly below the T_m values of the structures, were applied in order to obtain rapid assembly, i.e. within minutes.[168] The picture gets further complicated by the fact that (depending on the T_m of the staples) complete binding of an already partially bound staple is hindered by the presence of another partially bound staple of the same sequence.[162,169] More than one staple strand can thus compete for the same position

on the DNA origami and complete binding therefore requires a competitive displacement reaction, where one staple manages to detach the other.

Taken together these results testify that the folding process of a DNA origami is a complex sequence of events that is hard to describe with conventional DNA hybridization models. While a lot of progress has been made to describe the folding and some rules could be worked out, a complete understanding is still missing.

Another level of complexity was then presented by the Sugiyama group in 2014[170] when they observed that one origami design could assemble into two distinct structures, i.e. isomers. The same group later demonstrated that this isomerization could be triggered in a *post-assembly* process, by applying forces along different axes of the structure.[171] As an explanation, the authors suggested an isomerization of the Holliday junctions within the structure (Figure 6B, C). Already in 2007, the Ha group presented a sophisticated single molecule experiment which enabled to map the energy landscape of a single Holliday junction transition.[172] Previously, the same group showed that such a transition is faster at low magnesium concentrations, although the ratio between the two conformers at the equilibrium does not change.[173] This implies two things: first, that the effect of magnesium ions is on the activation energy between the two conformers and not on their relative stability; and second, that the transition between one conformer and the other must pass through an intermediate form, called the open structure.

If such isomerization events progress successively along the origami structure, a complete structural reconfiguration can take place, similar to the allosterically-induced conformational transitions of proteins.[174–177] While delicate control of the isomerization process has been demonstrated, these works usually apply a set of external stimuli that target exposed regions of the scaffold, thereby allosterically triggering the isomerization of Holliday junctions. The system is thereby purely mechanically actuated, without taking into account the crucial sequence-to-structure relationship typical of protein structures.

This work (see section 7.1) aims to highlight this relationship by evaluating and manipulating the folding trajectories of a three-parted structure. Each part is geometrically identical and differs from the other two parts solely in its sequence. Immense differences in their thermal stability and isomerization rates were observed, eventually leading to the conclusion that the assembly of a DNA origami is not only an entropically (i.e. mechanically) driven process but also a sequence-dependent process that, by evading unfavorable strain, takes on a more stable isomer conformation.

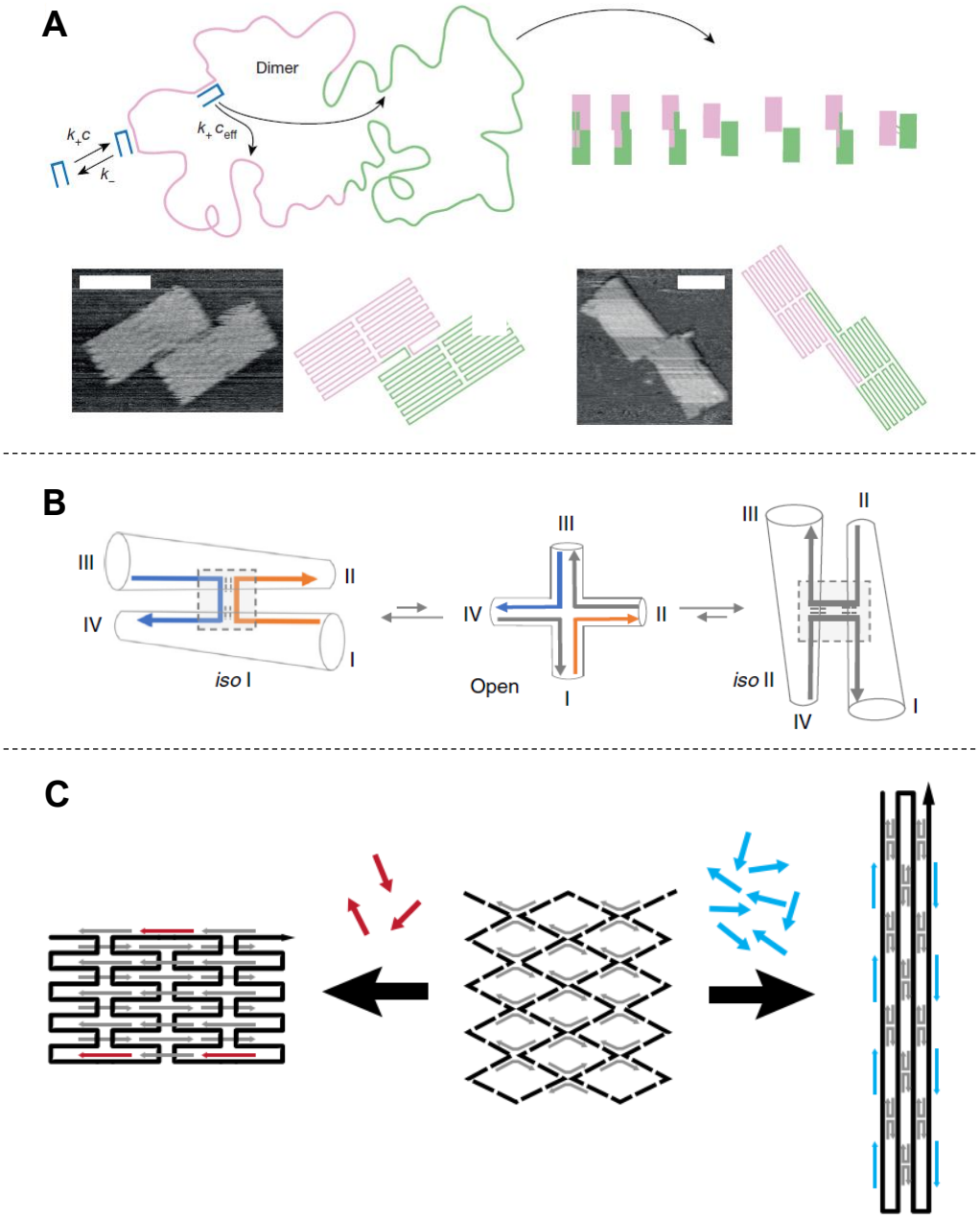

Figure 6: Dynamics of DNA origami assemblies. (A) Two scaffolds are fused together and allowed to assemble. Staples have the option to bind regions of the same scaffold (pink) or regions of the second scaffold that are more distant (green). Depending on these events, different structures are observed via AFM. (**B**) A Holliday junction can switch between two isomer states, in which the helices are in a stacked configuration. To switch from one form to the other, an intermediate „open“ form must be visited. (**C**) Depending on which type of „trigger strands“ are added to a DNA origami, two different isomers can be obtained. (**A-C**) were reprinted and adapted with permission from references [165,175,178]. (**A**) Copyright 2022 by Springer Nature. (**C**) Copyright 2022 by American Chemical Society

1.3.4 Reconfigurable DNA nanostructures for nanophotonic applications

Surface-enhanced Raman scattering (SERS) relies on the property of noble metal surfaces or noble metal particle to generate a *plasmon* (hybrid term: plasmonics = plasma oscillation + electronics) due to the interaction of the metal with a light wave.[179] A plasmon is a quasi-particle that is generated when an incoming light wave interacts with the conduction band electrons of the metal. In case of a noble metal particle, the irradiation with resonant laser light results in a damped harmonic oscillation of the particle plasmon (Figure 7). The non-propagating wave character of the plasmon within the nanoparticle is called localized surface plasmon resonance (LSPR). The resulting dipole generates a strong localized electromagnetic field. Rather unexpectedly, it was discovered that this effect could be used in order to increase the Raman signal of molecules absorbed on metal surfaces.[21,180] This finding is crucial, since Raman signals are usually so weak that they are impractical for many applications.[181] Highly sensitive analytical methods have been therefore developed which are based on the Raman scattering enhancement phenomenon at metal surfaces. Fundamentally, they rely on the fact that Raman spectra are a kind of chemical *fingerprint*, unique for every molecule and thus highly useful, especially for analytical purposes.[179,182]

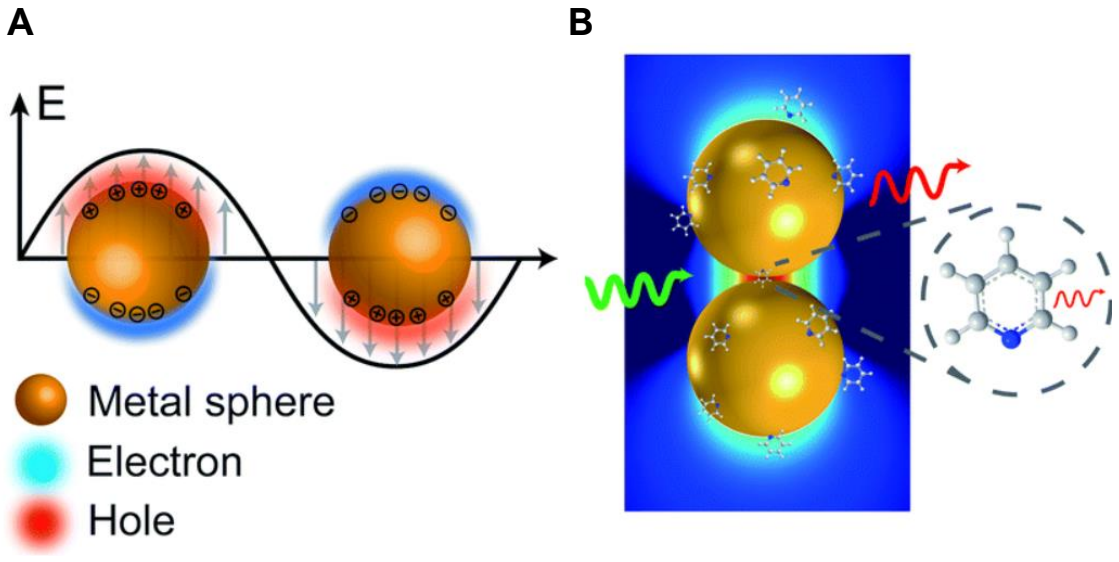

Figure 7: Nanoparticles for SERS. (A) Localized surface plasmon resonance (LSPR) effect. Light induces a collective oscillation of electrons within the gold spheres, yielding a quasi-particle, the plasmon. (**B**) Two metal nanospheres produce a hot spot in between both interfaces. The local electric field is enhanced. Molecules within the gap give a strongly enhanced Raman signal. Reproduced with permission from reference [183] and reprinted and adapted from reference [181]. Copyright 2022 by Springer Nature.

In addition to that, SERS is a non-destructive method and does not rely on labeling, further increasing its attractiveness. Another interesting aspect of SERS is that it is highly influenced by the size and the geometry of the metal nanoparticles.[184] Particularly, when two nanoparticles are brought together into very close proximity (few nanometers), a *hot spot* is generated,[185] in which the Raman signal can be enhanced up to 12 orders of magnitude, thus enabling to use this method for *single-molecule* detection. SERS is therefore a promising and popular analytical technique. The main challenge is to arrange two nanoparticles in such a precise manner to position them only few nanometers apart and possibly change their distance in a programmable fashion. With the advent of DNA nanotechnology and its ability to accurately organize guest molecules, a possible solution to this issue was found.

DNA was explored for the ordering of nanoparticles as early as 1996[186] and it has rapidly grown its repertoire of functionalized structures.[187–189] A downside of a lot of these structures however was the fact that the number and orientation of the attached nanoparticles was hard to adjust. A possible solution came with the introduction of DNA origami.[69]

In one of the first examples of DNA origami structures for the generation of a hot spot, the Tinnefeld group presented a nanoantenna, to which one or two 100 nm gold (Au) nanoparticles (NP) were attached[87] via strand hybridization. By placing a fluorophore in the middle of these nanoparticles (23 nm gap), a 117-fold fluorescence enhancement was obtained. Although this increase can be considered still rather low, the study undoubtedly demonstrated that a hot spot can be generated by the rationally designed placement of nanoparticles on DNA structures.

A classical example for plasmonic nanoantennas used for SERS was presented by Thacker *et al.*[190] By creating a DNA structure that has two docking sites for AuNPs and a "slit" in between, the authors were able to place both AuNPs at a distance of about 3.3 nm. Again, placement of the nanoparticles was achieved via DNA strand hybridization. By incubating the solution with the Raman reporter Rhoadmine 6G, local field enhancements of several orders of magnitude could be detected within the slit. Other NP shapes were investigated as well. The Sen group presented a DNA-AuNP system in which rectangular DNA origami platforms, capable of dimerization were used in order to bind Au nanostars. Upon binding, a hot spot was formed between the Au nanostars. Strong field enhancements of up to 2×10^{10} were detected for interparticle distances of about 7 nm, which was sufficient to detect characteristic Raman bands of single dye molecules, precisely located within the hot spot.[191]

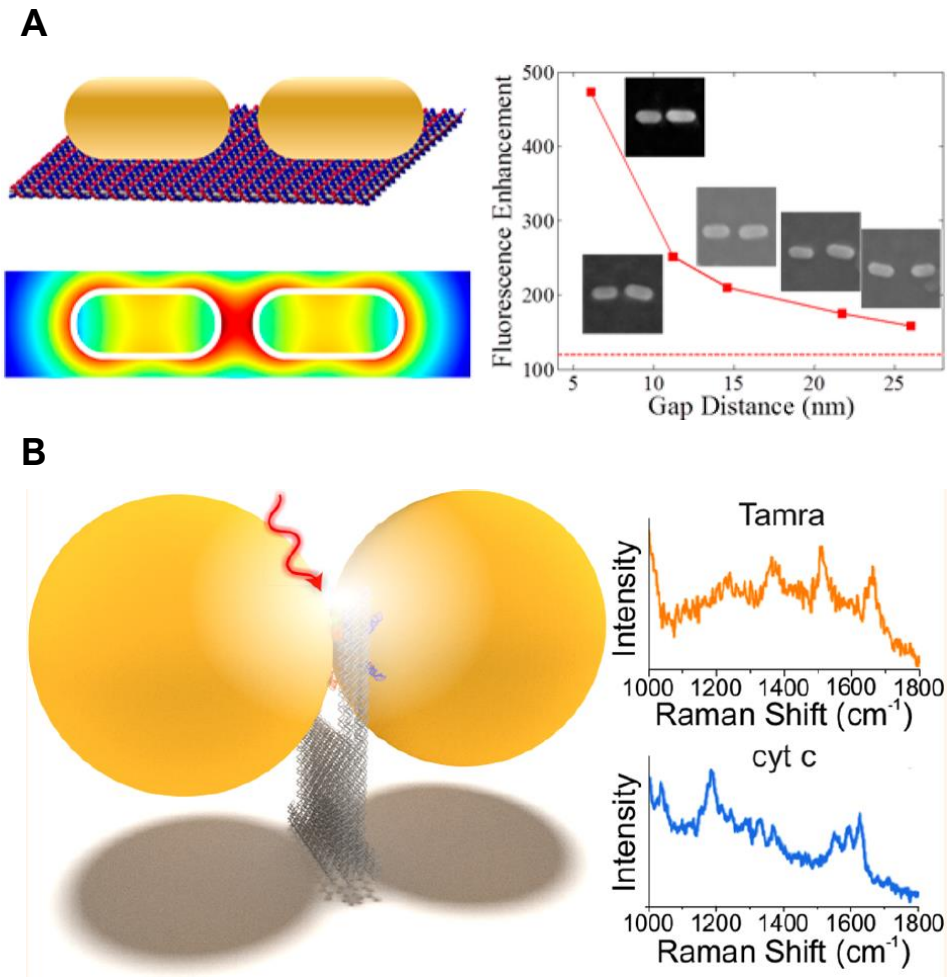

Figure 8: Enhanced fluorescence and SERS signals from AuNP dimers. (A) AuNR are precisely positioned on a 2D DNA origami sheet, with varying gap distances. Fluorescence of ATTO-655 is increased for decreasing gap distances. (**B**) AuNS are positioned onto a DNA origami „nanofork“. Reporter molecules (e.g. TAMRA or cytochrome c) are placed inside the gap, enabling single molecule measurements. Reprinted and adapted with permission from reference [192,193]. (**A**) Copyright 2022 by American Chemical Society. (**B**) Creative common license BY-NC-ND 4.0.

It is noteworthy to mention, that DNA-AuNP hybrid structures are not only used for SERS measurements, but also for other spectroscopic applications as CD-measurements,[194–196] metal-enhanced FRET (M-FRET)[192] or even the construction of gold nanowires.[197] In an interesting work, Xu and co-workers[192] investigated the effect of variable gap distances (6.1 – 26 nm) between two gold nanorods (AuNR) placed onto a flat DNA surface on the fluorescence enhancement of ATTO-655 molecules diffusing into that gap (Figure 8A). Detection of single burst-like signals were interpreted as single molecule detection of fluorophores inside the gap.

Another important step was achieved with the introduction of more dynamic structures.[195,198] In a compelling experimental work, the Liedl group utilized a dynamic DNA origami for the detection of virus RNA.[199] By equipping the origami with a chiral arrangement of gold nanorods, strong CD signals could be generated. Presence of viral DNA within the solution would then arrest the origami conformation in one of two possible chiral states. Liedl and co-workers were thus able to detect picomolar concentrations of viral RNA, proving the utility of such structures in medical applications.

While previous reports of single-molecule detection usually lack the control of the number of reporters inside the hot spot, a rather recent study by the Bald group demonstrated a fully controlled detection of different reporter molecules as well as proteins at a single-molecule level (Figure 8B).[193] By using a DNA "nanofork", two 60 nm AuNPs could be attached on each side of the construct with varying gap sizes down to 1.17 nm. In total, three different Raman reporters could be detected at the single-molecule level, even in non-resonant conditions, providing longer photostability. Additionally, single proteins could be detected. While the gap distances were too small to accommodate whole proteins, characteristic vibrational bands could be detected in each case.

To conclude, the application of spectroscopic methods as e.g. M-FRET and SERS, coupled to DNA nanostructures, has undergone immense progress since its dawn, producing highly sophisticated systems that allow single-molecule detection, making it a particularly interesting research area especially for sensing applications. Current drawbacks in these systems are the presence of ssDNA in the hot spot. These strands are usually used for the hybridization of nanoparticles onto DNA surfaces, leading to hot spots that are "contaminated" with DNA signals and may not be fully accessible. Omission of these ssDNAs however would lead to an increasing difficulty in binding, placement and stability of AuNPs, a central theme that is tackled within this work (see section 7.2). Furthermore, developing a system that can control the inter-particle distance in a modular fashion would be highly desirable. For this purpose, a hierarchical assembly of DNA origami structures is introduced that can dynamically tune the distance between two AuNPs positioned on top of a switchable DNA platform, enabling the generation of DNA-free hot spots with potentially various enhancement factors.

2 Results & Discussion

Parts of chapters 2, 3, and 4 are published in the following article: Kosinski, R. *et al.* The role of DNA nanostructures in the catalytic properties of an allosterically regulated protease. *Science advances* **8**, (2022)[200]

The human species portrays the climax of at least 3.5 billion years of evolution.[201] On average, each one of us consists of about 3.7 x 10^{13} cells.[202] Additionally, we harbor about the same amount of bacterial cells within or on our bodies.[203] In consideration of these huge numbers and the apparent complexity of the human organism, we tend to think about a single cell as being "simple". This is however far from reality. In fact, cells are highly sophisticated entities that can sense and interact with their surroundings, adapt to various external stimuli and conditions, produce and degrade numerous chemical compounds, move and migrate, replicate and self-sustain (the last points may not be true for all human cells). To accomplish all these tasks, a magnitude of chemical reactions is running simultaneously within a cell, making it a highly crowded place with a dynamic mixture of salts and biomolecules that interact with one another. From a human perspective, the inside of a cell would appear wild and chaotic.[204] This poses the need to segregate certain parts from the rest of the cell in order to avoid cross talk between chemical reactions. Therefore, in nature, enzymatic reactions are often confined within or restricted to certain areas of the cell.[115,117]

As the restriction of enzymatic reactions to confined spaces is highly interesting for applications in many other fields, as e.g. human medicine, chemical industry or basic scientific research, one branch of DNA nanotechnology focuses on the study of enzymes that are attached to or enclosed within DNA nanostructures.

Since the early investigations on enzyme-DNA hybrid structures by the Niemeyer group and others,[118,119,141] a lot of research has been undertaken to create far more sophisticated systems. Nowadays, enzymes can be fully encapsulated within 3D DNA origami structures[124,135,205,206] or whole enzymatic cascades can be tuned by dynamically regulating enzyme pair distances.[132,152] A highly interesting observation is that the enzymatic activity of these systems can change dramatically -oftentimes increasing- when the enzyme is in close proximity to DNA structures and this issue is probably the most intensively investigated subject

within this field. Different hypotheses have been brought forward to interpret these observations.[90,118,122,124,131,207] Those efforts though have been complicated by partially contradicting results and vastly differing enzymatic enhancement rates.[118,123]

We therefore developed two DNA origami host systems, one being a 2D quasi-planar DNA sheet, the other one being a 3D DNA box, which are capable of binding single thrombin molecules. This feature is achieved by equipping DNA structures with thrombin binding aptamers (TBAs) that are able to bind the enzyme in a non-covalent fashion with high affinity.[208] The focus here relies on the characterization of a single enzyme and its changed behavior as opposed to an enzymatic cascade. This bears the advantage of a much simpler system that can exclude proximity-caused effects as e.g. substrate channeling, *a priori*. Upon verification of thrombin binding to the DNA hosts, enzymatic activity is recorded by fluorescent readout. Three different, rationally designed, synthetic substrates were applied, which, upon cleavage, liberate a fluorophore from its quencher. Extensive control experiments were added for interpretation of the gathered data in order to get a deep understanding of the origin of the altered enzymatic behavior and exclude/support/adjust common hypotheses that have been brought forward to explain the compelling observations.

2.1 Design of the DNA-enzyme constructs

Our DNA-enzyme systems consist of three parts: 1) the enzyme, 2) the substrates and 3) the DNA microenvironment. The only constant in this system is the enzyme, i.e. α-human thrombin, whereas the other two elements are systematically changed in order to understand the role played by each individual part. In all our samples, thrombin catalyzes the hydrolysis of a synthetic, fluorogenic substrate of sequence FAM-GGfPR│SGGGK(BHQ-1)K-Aaa-OH (where f indicates a D-phenylalanine residue, Aaa is the variable amino acid, FAM is 6-Carboxyfluorescein and BHQ-1 is Black Hole Quencher 1; Figure 9B). Each substrate carries a FRET pair (FAM/BHQ-1), with the donor and quencher being in close proximity to one another (P5 and P5’ position of the peptide). Upon cleavage of the substrate, the donor is liberated from its quencher, giving a fluorescence signal, which is then used to monitor the reaction during time. All three substrates differ only in their C-terminal amino acid (Aaa). In particular, Gly, Asp or Lys residues were incorporated, giving to each peptide either a neutral (0), negative (-1) or positive (+1) net charge at pH 7.00 (Figure S 1). Substrates are henceforth

denoted as S(0), S(-1) and S(+1). The second variable in our system is the DNA microenvironment. Two aptamers were used in order to bind thrombin to its DNA hosts. Specifically, we employed the 15-mer thrombin binding aptamer TBA1 of sequence 5'-GGTTGGTGTGGTTGG-3' and the 29-mer TBA2 of sequence 5'AGTCCGTGGTAGGGCAGGTTGGGGTGACT-3' to specifically recognize the exosite I and exosite II of thrombin, respectively (Figure 9A). The aptamers contain a single stranded DNA elongation which in turn is able to hybridize to a protruding staple on the DNA hosts. This enables the attachment of thrombin to the DNA nanostructures (Figure 9).

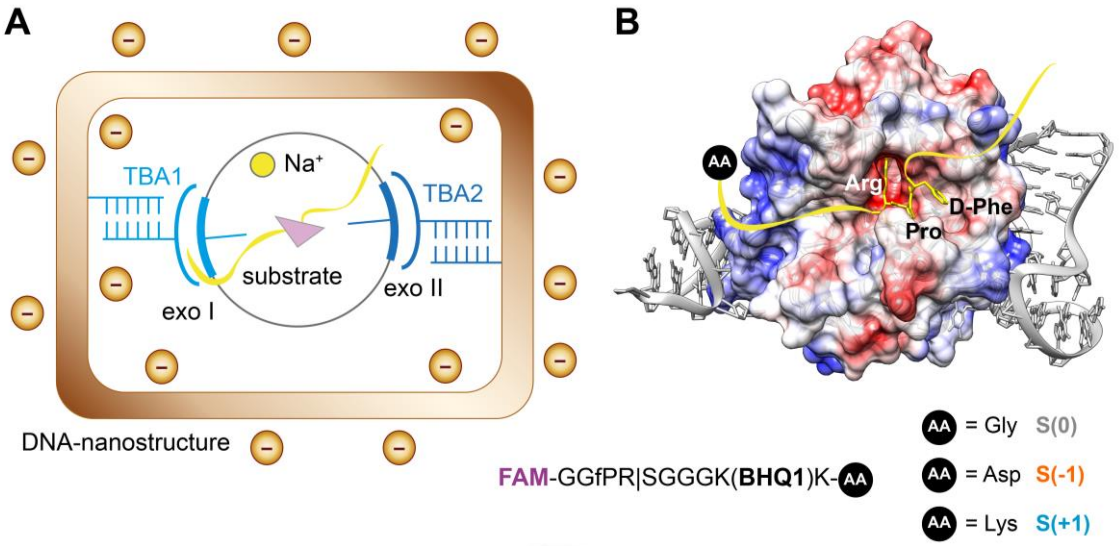

Figure 9: Binding and encapsulation of thrombin to the DNA hosts. (**A**) Schematic representation of the DNA origami/thrombin system. Thrombin is non-covalently fixed to the negatively charged origami by DNA aptamers (TBA1/TBA2 (Protein Data Bank: 4DIH and 4I7Y)). Substrate (yellow line) can bind to its catalytic cleft (purple triangle) to be hydrolyzed. A sodium (yellow circle) binding site is present that is allosterically affecting thrombin activity upon binding.[209,210] (**B**) Molecular model of thrombin. The enzyme is bound by two DNA aptamers. Substrate is bound to its catalytic cleft.[209] The protein surface is color coded: red = negatively charged, blue = positively charged. Substrate sequence is given below. The terminal amino acid is variable for all three substrates. Reprinted and adapted from reference [200].

Efficient binding of aptamers to the exosites requires correct folding of the DNA sequences into a G-quadruplex structure (Figure 9B). To ensure G-quadruplex formation, FRET-labeled TBA sequences were used, where FRET can be observed once the correct secondary structure is achieved. Correct formation of the aptamer motifs under the experimental conditions used were verified as well as their efficient integration into the DNA origami structure (Figure S 2, Figure S 3).

Two different DNA origami hosts were utilized in this work, which are denoted "rect" and "box". While "rect" is a 2D quasi-planar DNA monolayer, "box" is a 3D dual-layered DNA

container. Both structures carry an internal cavity of about 20 x 20 nm size, into which the TBAs protrude, leaving about 5 nm space in between the two aptamers. This largely ensures binding of only a single thrombin molecule to each host (Figure S 4). Binding of thrombin to each host was verified by atomic force microscopy (AFM) and transmission electron microscopy (TEM) (Figure 10, Figure S 5, Figure S 6). Furthermore, a fluorescently labeled thrombin was used in order to confirm the specificity of protein-binding to its TBA-modified DNA cages (Figure S 7, Figure S 8)

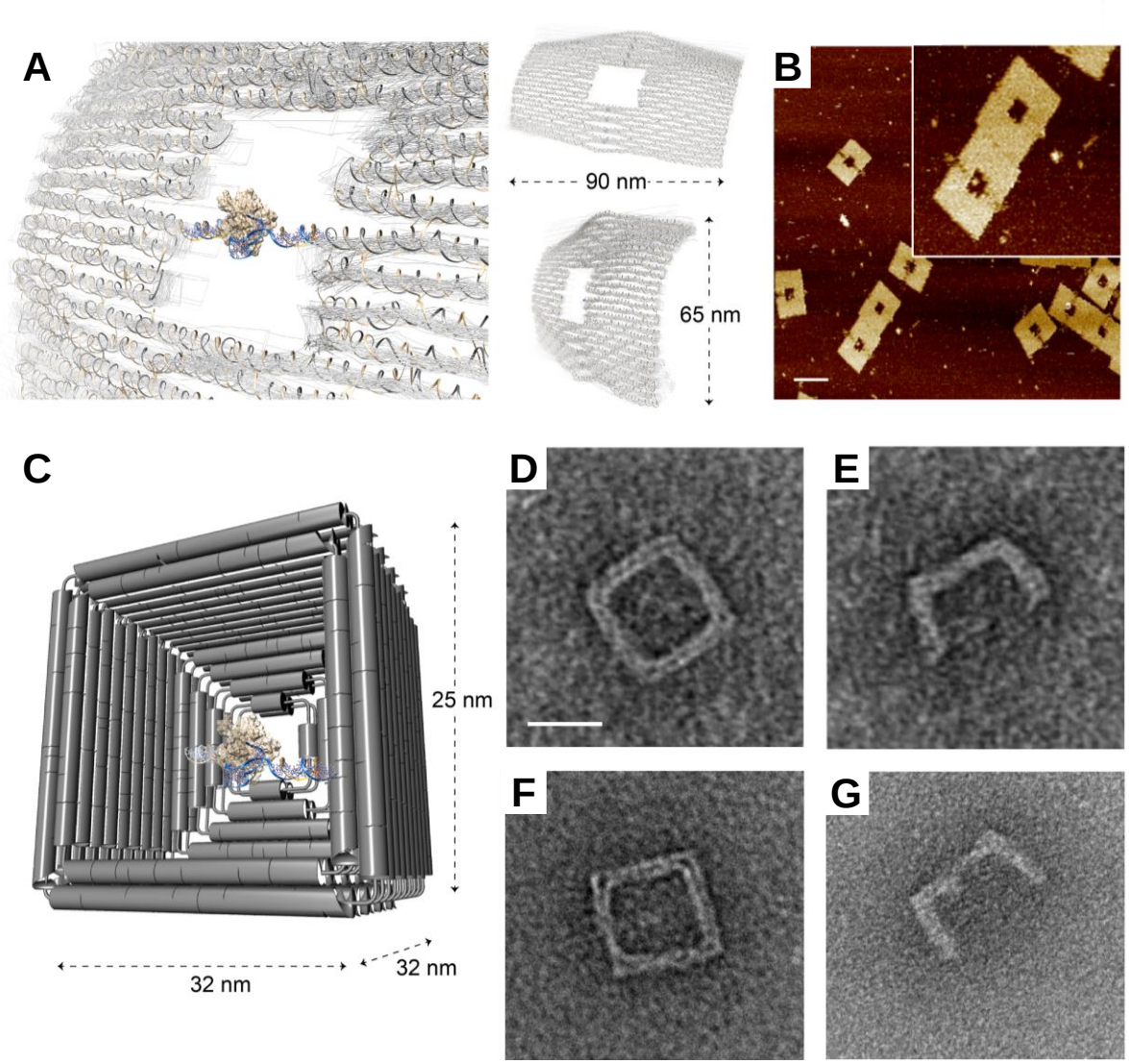

Figure 10: Binding of thrombin to the DNA hosts. (**A**) Left: Molecular model of thrombin bound to the rectangular DNA origami. Right: Front and side view (**B**) Representative AFM image of the thrombin/origami system. Scale bar is 100 nm. (**C**) Molecular model of thrombin bound to the box DNA origami. (**D**-**G**) Raw TEM images of the unloaded (**D, E**) and loaded (**F, G**) DNA boxes (front and side view respectively). Scale bar is 25 nm. AFM image was recorded by Dr. Elisa Schöneweiß, former member of the group of Prof. Saccà. TEM images were recorded by Dr. Michael Erkelenz of the group of Prof. Schlücker. Reprinted and adapted from reference [200].

In order to evaluate the effect of the DNA origami host and the confinement of the enzyme to it, a number of different DNA host systems were used in this work, as well as a number of controls, where no DNA origami was employed. For a matter of clarity, the following nomenclature was applied: All TBA modified DNA origamis used in this work are indicated as "rect" or "box", followed by an apex number that represents the type of aptamer interlinked to the DNA cage (i.e. 1, 2 or 1/2 for TBA1, TBA2 or both). Furthermore, two different variations of the "rect1/2" structure were investigated, different in the structural flexibility that the aptamers can experience. In both, the flex ("flex") and the rigid ("rig") versions, the aptamers are bound to the inner cavity of the host through a DNA duplex (Figure S 9). However, in the "flex" version, the presence of a nick and/or a single unpaired base at the origami/aptamer interface allows for considerably more freedom of aptamers orientation. This freedom is somewhat limited for the "rig" version as both DNA strands (TBA as well as the protruding strand) are integrated within the origami and adopt a fixed orientation with respect to the inner cavity of the structure. Additional controls were applied to estimate the geometric as well as the electrostatic contributions of the DNA cages on thrombin activity. A pre-melted DNA structure carrying both aptamers ($flex_{1/2}^{melt}$) was used in order to investigate the importance of the structural integrity of the DNA host. Moreover, DNA cages lacking both aptamers (rect and box) were studied to evaluate the effect of unspecific electrostatic interactions between the protein and the DNA origami surface on the enzymatic activity. Finally, an equimolar mixture of short single stranded DNA (ssDNA) as well as a phosphate solution of identical ionic strength (phosph) permitted to determine whether the spatial density of negative charges around the enzyme is of importance. All constructs used in this work are schematically illustrated in Figure 11.

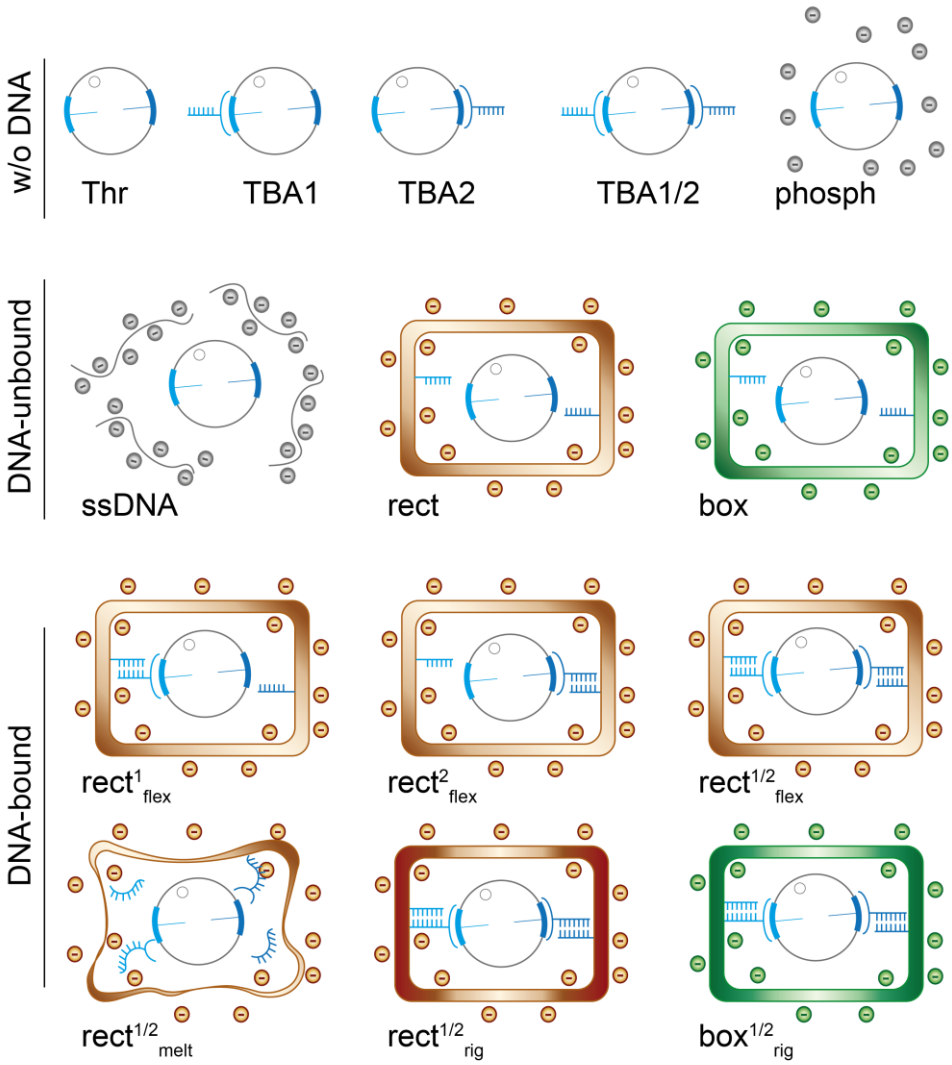

Figure 11: Constructs used in this work. All constructs used in this work can be categorized into three domains. In the first one (top), thrombin is free in solution (Thr), either in presence of aptamers (TBA1, TBA2 or both) or in a buffer of high ionic strength (phosph). In the second category (middle), DNA origami structures (rect or box), or the same amount of DNA as short oligonucleotides (ssDNA) are present, however without TBAs, in order to evaluate unspecific thrombin-DNA interactions. Finally, the effect of scaffolding thrombin to a DNA host is investigated in the third group, where DNA origami structures equipped with TBAs ($rect_1^{flex}$, $rect_2^{flex}$, and $rect_{1/2}^{flex}$, $rect_{1/2}^{rig}$ $box_{1/2}^{rig}$ and $rect_{1/2}^{melt}$) are able to bind thrombin (bottom). Reprinted and adapted from reference [200].

2.2 Effect of DNA on thrombin catalysis

If not stated otherwise, in all the kinetic assays presented here 1.2 nM thrombin were incubated with 1 nM aptamers in a suitable reaction buffer (TEMg 1x) at 37°C for 1 h in order to equilibrate the system prior to kinetic analysis. Aptamers were present either as free-floating species or attached to DNA origami structures (*vide supra*). Upon addition of the substrate (0 – 25 µM final conc.), the proteolytic activity of thrombin was measured as a function of time by monitoring the increase in fluorescence signal that results from the cleavage of the substrate and therefore the liberation of the fluorophore from its quencher (Figure 12).

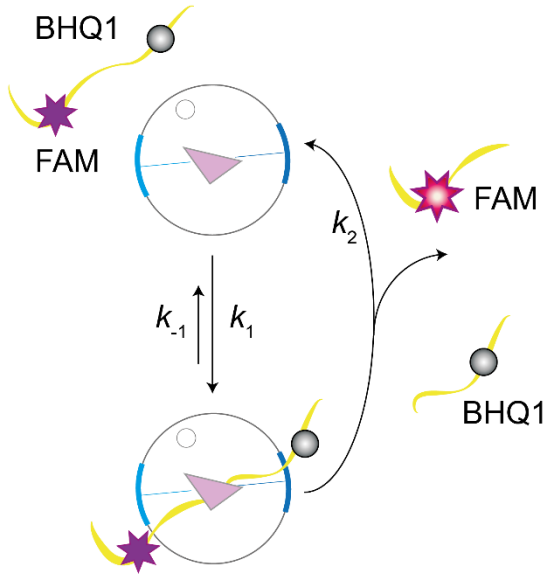

Figure 12: Substrate cleavage by thrombin. Substrate (yellow thread) binds to the proteolytic cleft of thrombin (purple triangle) where it is hydrolyzed. Subsequently the fluorophore (FAM) is allowed to diffuse away from its quencher (BHQ1), yielding a fluorescence signal. Reprinted and adapted from reference [200].

Product concentrations were assigned to each fluorescence value by recording a reference signal for each substrate concentration used in the kinetic assays. The substrate used as reference however is lacking the quencher unit, thereby imitating the cleavage product. Standard curves were obtained by non-linear fitting of the obtained values (Figure S 10, Figure S 11, Figure S 12). Fluorescence background signal was recorded by measuring each substrate concentration in absence of enzyme and DNA and was found to be negligible. Furthermore, the signal was stable over time, therefore not interfering with the *relative change* of fluorescence that is recorded during the enzymatic reactions (Figure S 13). Thrombin stability under the experimental conditions used for the reaction was verified by SDS-PAGE in order to exclude any bias due to protein degradation (Figure S 14). Furthermore, a linearity test was performed, recording thrombin activity over a wide range of enzyme concentrations. Thrombin showed a linear response over the whole scale,

strengthening the assumption that no protein degradation or aggregation occurs under the experimental conditions used (Figure S 15).

Each reaction was performed under identical conditions and the data obtained were mediated over three replicates. For each substrate, 14 distinct reactions were recorded, differing in the microenvironment experienced by the protein, yielding a total of 42 reactions. Progress curves of each reaction are presented in the supplementary materials (Figure S 16, Figure S 17, Figure S 18). All kinetic profiles (velocity *vs*. substrate concentration) for S(0) are given in Figure 13 (analog curves for S(-1) and S(+1) are reported in Figure 17 and will be discussed later).

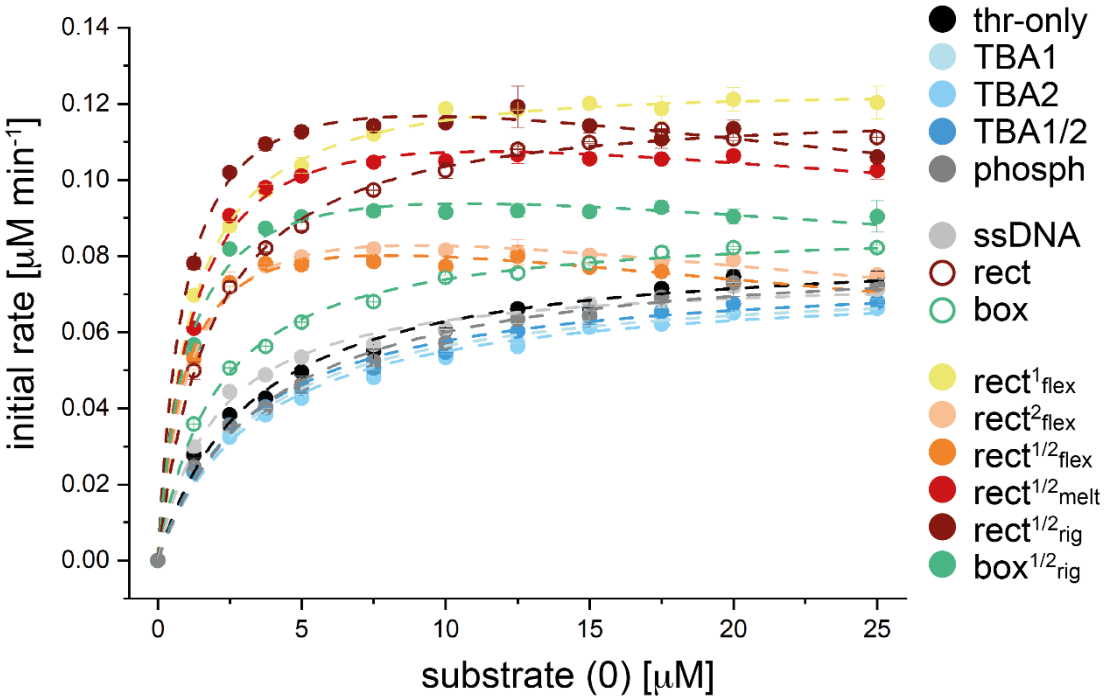

Figure 13: Kinetic profiles of thrombin catalyzed hydrolysis of substrate (0). Initial rates of the thrombin catalyzed hydrolysis of substrate (0) in different conditions (i.e. microenvironments). Each data point represents the slope of the first five minutes of the reaction. Reprinted and adapted from reference [200].

The catalytic activity of thrombin is described by the following three-step mechanism[210] (Figure 14), where an enzyme (E) catalyzes the hydrolysis of a substrate (S) to a product (P). In a first step, E and S bind to form an enzyme-substrate complex (ES). This binding is a reversible reaction and is described by the rate constants k_1 (association) and k_{-1} (dissociation). Subsequently, an irreversible acetylation reaction occurs (EP'), followed by a final deacetylation reaction (E+P), where eventually both E and P are released. Each of the two reactions, acetylation and deacetylation, is expressed by a rate constant, i.e. k_2 and k_3, respectively (k_3 also includes the rate of diffusion of the product away from the enzyme).

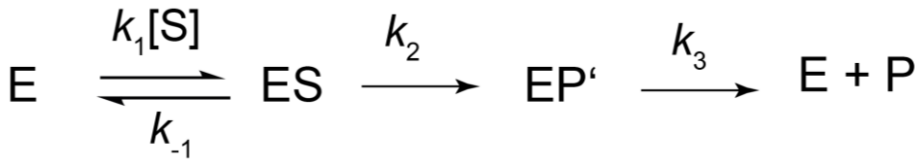

Figure 14: Reaction mechanism of an enzyme catalyzed hydrolysis of a substrate S. Reprinted and adapted from reference [200].

Since the deacetylation step is usually much faster than the acetylation step (i.e. $k_3 >> k_2$), EP' does not accumulate in the solution and the whole reaction can be treated as a two-step reaction whose velocity of product formation over time, $v = \frac{d[P]}{dt}$, obeys the Michaelis-Menten (MM) equation (for steady-state conditions) as depicted in Eq. 1.

$$\boldsymbol{v = \frac{k_{cat}[E]_0[S]}{K_M+[S]}} \qquad \textbf{Eq. 1}$$

In a similar fashion, the kinetic parameters K_M (Michaelis-Menten constant) and k_{cat} (turnover number) can be simplified as shown below and converge to the common representation of a classic two-step MM reaction. For K_M it follows:

$$\boldsymbol{K_M = \frac{k_3(k_{-1}+k_2)}{k_1(k_2+k_3)}} \qquad \textbf{Eq. 2}$$

$$\boldsymbol{\lim_{k_3 \gg k_2} \frac{k_3k_{-1}+k_3k_2}{k_1k_3} = \frac{k_3}{k_3} \times \frac{k_{-1}+k_2}{k_1} = \frac{k_{-1}+k_2}{k_1}} \qquad \textbf{Eq. 3}$$

For k_{cat} it follows:

$$\boldsymbol{k_{cat} = \frac{k_2k_3}{k_2+k_3}} \qquad \textbf{Eq. 4}$$

$$\boldsymbol{\lim_{k_3 \gg k_2} \frac{k_2k_3}{k_3} = k_2} \qquad \textbf{Eq. 5}$$

All kinetic curves obtained follow the MM behavior, with DNA-origami tethered enzymes suffering from substrate inhibition at high substrate concentrations (i.e. [S] > 5 µM). Therefore, K_M and k_{cat} values can be extracted by applying Eq. 1, modified for substrate inhibition when necessary (Supplementary Text 1). Values of K_M, k_{cat}, k_{cat}/K_M (specificity constant) and K_i (dissociation constant of the inhibited enzyme/substrate complex) are shown in Figure 15, Figure S 19, Figure S 20 and listed in Table 1.

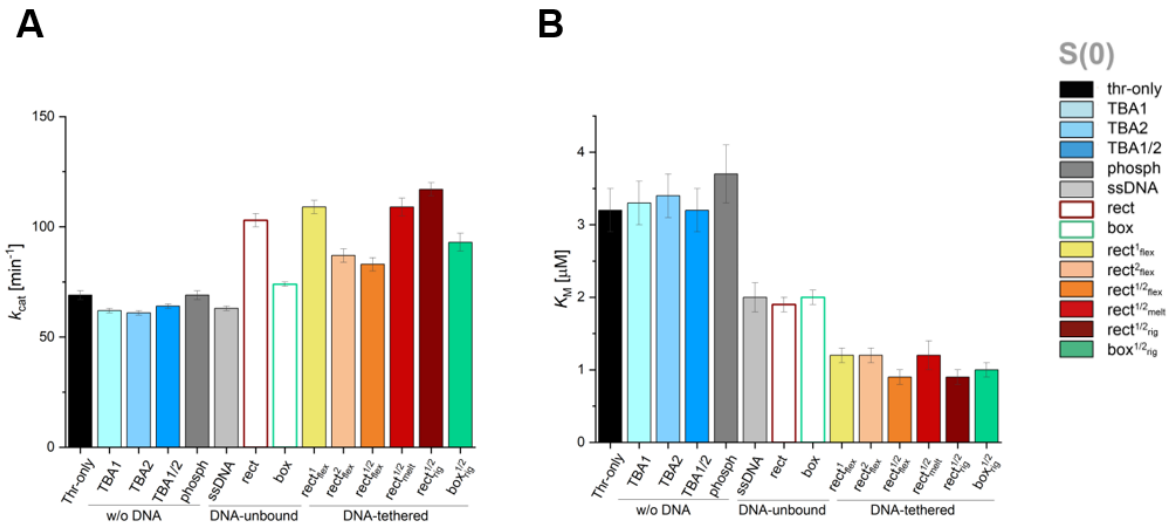

Figure 15: Extracted kinetic parameters for the thrombin catalyzed hydrolysis of substrate (0). Michaelis-Menten parameters (**A**) K_M, (**B**) k_{cat} and when necessary the inhibition constant *K*i (see Table 1) were extracted from the velocity profiles of the hydrolysis of S(0). The kinetics of thrombin were investigated either in a thrombin-only solution (black), in presence of aptamers (light to dark blue), in presence of phosphate ions (dark grey) or in presence of equivalent amounts (in respect to DNA origami samples) of single-stranded DNA (light grey). Control samples with origamis lacking the aptamers were included (red and green unfilled). To analyze the effect of scaffolding, thrombin bound to flexible (yellow to orange), rigid (brown) or pre-melted (red) rectangular, or box-like (green) DNA-origamis were investigated. Reprinted and adapted from reference [200].

Taking a close look at the data, especially Figure 15B, three classes of enzyme species can be identified, which are hereby denoted as “w/o DNA”, “DNA-unbound” and “DNA-bound”. Within the “w/o DNA” class, thrombin is freely floating in the solution, either in presence of aptamers (TBA1, TBA2, TBA1/2; light to dark blue) or in their absence, or within a buffer of high ionic strength (phosph; dark grey). This class behaves very similar to the control sample which features thrombin in absence of any additional agent (thrombin-only; black). In contrast to this, the “DNA-unbound” class comprises enzymes in presence of large amounts of DNA, either in form of freely floating single stranded oligonucleotides (ssDNA; light grey), or as compact DNA origami structures (rect, box; brown unfilled, green unfilled). These structures

however lack any TBAs and are therefore not able to bind thrombin specifically. This class displays a significant reduction of the average K_M value to about 60% (2.0 ± 0.1 µM) of its initial value, accompanied by an increase in the k_{cat} value of about 16% (80 ± 21 min^{-1}). Finally, the third class - "DNA-bound" - includes enzymes that are tethered to DNA origami. It includes either rect or box with one, two or both TBAs anchored to its surface. The type ($rect^{1/2}_{flex}$ *vs*. $rect^{1/2}_{rig}$; orange, brown) and amount of TBAs ($rect^{1}_{flex}$ *vs*. $rect^{2}_{flex}$ *vs*. $rect^{1/2}_{flex}$; yellow, pink, orange), as well as the type of origami ($rect^{1/2}_{rig}$ *vs*. $box^{1/2}_{rig}$; brown, green) does not seem to affect the kinetic parameters significantly, as most values are comparable. Furthermore, the structural integrity of the origami does not seem to play a huge role, as also the control sample ($rect^{1/2}_{melt}$; red) shows a behaviour that is similar to its counterparts that have not been exposed to high temperatures before the assay (See also Table 1).

However, in contrast to the thrombin-only control sample, this group of DNA-bound enzyme species exhibits a reduced K_M to about 34% of its original value (1.1 ± 0.2 µM) and on average a 45% increase in k_{cat} of (100 ± 14 min^{-1}), which again is significantly different from the "DNA-unbound" group. Recalling Eq. 1, an increased reaction speed can be achieved by either reducing K_M or increasing k_{cat}, or by applying both changes simultaneously, as is the case here (to be accurate, an increase in enzyme concentration would also result in an increased reaction speed. Since this variable is set to a fixed value in all experiments, it is of no concern here). Noteworthy, this is valid for all substrate concentrations, which is apparent from Figure 15. Therefore, it has to be reasoned that the driving factor for the increased reaction rates observed is the immobilization of the enzyme to the DNA nanostructures and its prolonged residence in a microenvironment that is characterized by a large amount of densely packed charges in close proximity to the enzyme. Interestingly to note is that the same effect applies for the second class of enzymes (DNA-unbound), however to a much lower extent. One can speculate that such an observation is the result of unspecific binding and/or weak interactions of the enzyme to DNA nanostructures, thereby triggering the same effect however to a lower degree. Although such unspecific interactions could be excluded by agarose gel electrophoresis (Figure S 8), the electrostatic forces applied during gel migration might falsify the outcome. Unspecific binding of a comparably small molecule to a huge DNA nanostructure is experimentally challenging to prove and could neither be rejected nor demonstrated in the scope of this work but will be part of ongoing research. It should be stressed here, that while the *concentration* of DNA is always the same (i.e. 1 nM) for all samples analyzed, the *amount* of DNA does differ tremendously, since the molecular weights of the DNA species are of different magnitude (TBA aptamers *vs*. DNA origami). Therefore, the environment experienced by the

enzyme varies significantly amongst the groups. Taken together, we observe a gradual decrease of the initial K_M value from the w/o DNA group to the DNA-unbound group (60%) until the DNA-bound group (34%), correlating with the amount of DNA in solution and its organization around the enzyme. This reduction of the K_M value is accompanied by a moderate increase in the k_{cat} value of 16% (DNA-unbound) up to 45% (DNA-bound).

Table 1: Kinetic parameters of the hydrolysis of S(0) by thrombin. Application of the MM equation corrected for substrate inhibition (when necessary) on the recorded kinetic profiles allowed for the extraction of the kinetic parameters of the reaction, namely, the catalytic efficiency or turnover number (k_{cat}), the MM constant (K_M), the specificity constant (k_{cat}/K_M), and, when relevant, the inhibition constant (K_I). Reported values are the result of at least three replicates. Reprinted and adapted from reference [200].

	Thr/S(0)	**k_{cat} [min^{-1}]**	**K_M [mM]**	**k_{cat}/K_M [min^{-1}mM^{-1}]**	**K_I [mM]**
thrombin only	-	69 ± 2	3.2 ± 0.3	21 ± 2	-
w/o DNA	TBA1	62 ± 1	3.3 ± 0.3	19 ± 2	-
	TBA2	61 ± 1	3.4 ± 0.3	18 ± 2	-
	TBA1/2	64 ± 1	3.2 ± 0.3	20 ± 2	-
	phosph	69 ± 2	3.7 ± 0.4	18 ± 2	-
DNA-unbound	ssDNA	63 ± 1	2.0 ± 0.2	31 ± 3	-
	rect	103 ± 3	1.9 ± 0.1	55 ± 4	-
	box	74 ± 1	2.0 ± 0.1	37 ± 2	-
DNA-bound	$rect^1_{flex}$	109 ± 3	1.2 ± 0.1	93 ± 8	-
	$rect^2_{flex}$	87 ± 3	1.2 ± 0.1	75 ± 9	70 ± 13
	$rect^{1/2}_{flex}$	83 ± 3	0.9 ± 0.1	87 ± 12	68 ± 13
	$rect^{1/2}_{melt}$	109 ± 4	1.2 ± 0.2	88 ± 12	106 ± 28
	$rect^{1/2}_{rig}$	117 ± 3	0.9 ± 0.1	124 ± 13	90 ± 14
	$box^{1/2}_{rig}$	93 ± 4	1.0 ± 0.1	89 ± 13	110 ± 31

Assuming a simple MM model, we then applied the transition state theory[211] (TS-theory) to interpret the data in respect to relative changes in energy levels experienced by the interacting species along the reaction coordinate. In its simplest portrayal, the TS-theory postulates that within an enzymatic reaction, the substrate must pass through a so called “transition state”, in which chemical bonds are broken and established and which is energetically most unfavorable.

The interesting aspect of the TS-theory is that it relates the kinetic parameters of the reaction to the difference in the energy levels between the ground state (E + S), the enzyme-substrate complex (ES) and the transition state ($ES^{\ddagger}$). To say it more exactly, the *relative* changes in the energy levels of the enzyme species in two distinct scenarios are mathematically related to the *ratio* of the corresponding kinetic parameters of the two distinct reactions. This enables the comparison of the same enzymatic reaction under different conditions, e.g. in the existence or absence of DNA nanostructures. Here, the difference in the energy levels between the unreacted species E + S and ES is given by the Gibbs free energy of binding between the two molecules (ΔG_{ES}) which, in case of a MM mechanism, is proportional to the K_M. Consequently, the energy difference between ES and the transition state $ES^{\ddagger}$ is related to k_{cat} ($\Delta G^{\ddagger}$). Finally, the activation energy for the reaction to occur, i.e. the difference between the ground state and the transition state ($\Delta G^{\ddagger}_{TS}$) can be related to the pseudo second-order rate coefficient of the reaction between E and S and is referred to as k_{cat}/K_M. As this theory relies on the relative changes in energies rather than their absolute values, it is assumed that the energy level of the initial species (E + S) is the same for every reaction. Since the changes in the energy levels are linked to K_M and k_{cat} values, the variation of those changes can be extracted by the ratio of the associated kinetic parameters, as described below:

$$\Delta\Delta \boldsymbol{G_{ES}} = -\boldsymbol{RT} \ln\left(\frac{\boldsymbol{K_M}}{\boldsymbol{K'_M}}\right) \qquad \textbf{Eq. 6}$$

$$\Delta\Delta \boldsymbol{G^{\ddagger}} = -\boldsymbol{RT} \ln\left(\frac{\boldsymbol{k_{cat}}}{\boldsymbol{k'_{cat}}}\right) \qquad \textbf{Eq. 7}$$

$$\Delta\Delta \boldsymbol{G^{\ddagger}_{TS}} = -\boldsymbol{RT} \ln\left(\frac{\frac{\boldsymbol{k_{cat}}}{\boldsymbol{K_M}}}{\frac{\boldsymbol{k'_{cat}}}{\boldsymbol{K'_M}}}\right) \qquad \textbf{Eq. 8}$$

where k'_{cat}, K'_M and k'_{cat}/K'_M refer to the kinetic parameters observed under a condition that is different from that at which k_{cat}, K_M and k_{cat}/K_M were measured (e.g. when comparing the hydrolysis of the same substrate by two distinct enzyme species, e.g. S(0)/thrombin in presence or absence of DNA; or when comparing the hydrolysis of two distinct substrates by the same enzyme species, e.g. thrombin-only with S(0) or S(-1)). Now it is possible to depict an arbitrary energy diagram, using a control reaction as reference (thrombin-only sample) and observe how the energy barriers move in respect to the reference under certain conditions (see Figure 16). Two different substrate regimes are considered for this analysis. In the first one the substrate

concentration is below the K_M value ([S] < K_M) and hence ES will be poorly populated. Therefore, ES will lay above E + S. In the second regime, the substrate concentration will approach saturation and will thus be far higher than K_M ([S] > K_M). As a consequence, ES will lay below E + S.

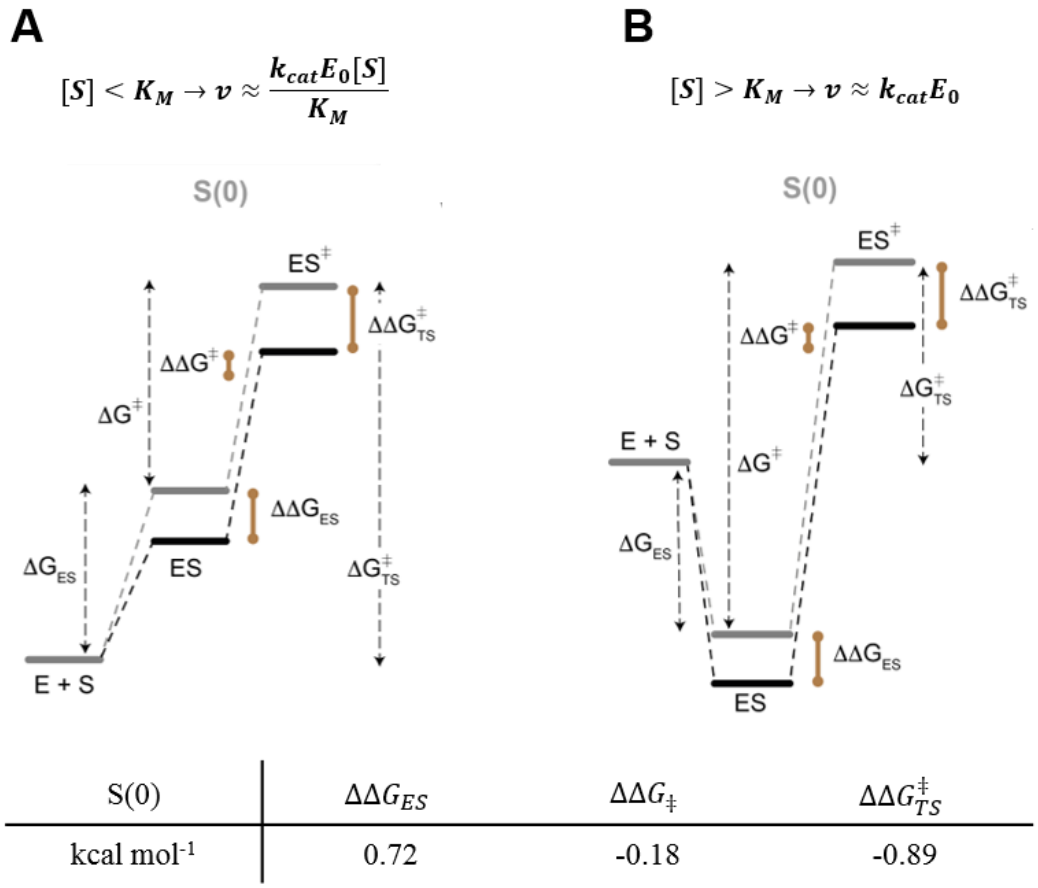

S(0)	$\Delta\Delta G_{ES}$	$\Delta\Delta G_{\ddagger}$	$\Delta\Delta G^{\ddagger}_{TS}$
kcal mol^{-1}	0.72	-0.18	-0.89

Figure 16: Application of the transition state theory on the hydrolysis of S(0) by thrombin only and box$^{1/2}_{rig}$. Assuming a simple MM mechanism, the transition state theory allows to depict changes in the energy barriers of an enzymatic reaction that progresses from the unreacted E + S through the ES complex to the transition state ES‡ and finally to the products. It enables comparisons between the same enzymatic reaction within different conditions (e.g. thrombin-only (light lanes) vs box$^{1/2}_{rig}$ (dark lanes)). Two substrate regimes are considered, S < K_M (**A**) and S > K_M (**B**). The reaction of S(0) with thrombin only is taken as a reference, and its energy diagram is arbitrarily drawn. Diagrams of the other substrates and reactions are drawn to scale and are therefore fully comparable. For all reactions it was assumed that the unbound state E + S is energetically identical. Numerical values of the differences in the energy barriers are given in the table below. Reprinted and adapted from reference [200].

As we shall see, this has important repercussions. According to Eq. 9 and Eq. 10, for [S] < K_M, the value of k_{cat}/K_M will be of major importance and the change in $\Delta G^{\ddagger}_{TS}$ will dictate the change in the reaction velocity. For [S] > K_M, the situation is different. Here, only k_{cat} affects the velocity of the reaction and therefore $\Delta G^{\ddagger}$ will mostly influence the reaction rate.

$$[\boldsymbol{S}] < \boldsymbol{K_M} \rightarrow \boldsymbol{v} \approx \frac{\boldsymbol{k_{cat}[E]_0[S]}}{\boldsymbol{K_M}} \qquad \textbf{Eq. 9}$$

$$[\boldsymbol{S}] > \boldsymbol{K_M} \rightarrow \boldsymbol{v} \approx \boldsymbol{k_{cat}[E]_0} \qquad \textbf{Eq. 10}$$

Figure 16 illustrates the investigation of two experimental conditions for S(0) (i.e. thrombin-only, light lines, and $box^{1/2}_{rig}$, dark lines). The analysis shows that the surrounding DNA scaffold stabilizes the ES complex and, to a slightly larger extent, stabilizes the $ES^{‡}$, too. This is sometimes termed a *uniform* binding energy effect.[212,213] Specifically, in presence of the DNA nanostructure, ES is stabilized by 0.72 kcal mol^{-1} ($\Delta\Delta G_{ES}$) while the energy level of $ES^{‡}$ is lowered by -0.89 kcal mol^{-1} ($\Delta\Delta G^{‡}_{TS}$**)**. Note that the conversion from ES to $ES^{‡}$ is hence only marginally affected (with $\Delta\Delta G^{‡}$ = -0.18 kcal mol^{-1}). This is interesting because it can explain the different reaction speeds observed in the two substrate regimes. For [S] < K_M, a reduction of $\Delta G^{‡}_{TS}$ causes the velocity of the reaction to increase significantly, as confirmed by the drastically increased values of k_{cat}/K_M (Figure S 19). On the contrary, for [S] > K_M, i.e. at saturating substrate concentrations, basically all E is already in form of ES. This implies that only the transition from ES to $ES^{‡}$ (k_{cat}, or $\Delta G^{‡}$) is important for the velocity. Since $\Delta\Delta G^{‡}$ is rather small, the effect of DNA at this substrate concentration regimes should not be that pronounced, i.e. an increase in reaction velocity should be observed mainly for low substrate concentrations and somewhat fade out for higher substrate regimes. This prediction perfectly matches with the measured reaction speeds (Figure 13) and thus gives confidence in the suitability of the TS-theory for the analysis of the kinetic data and its help in rationalizing the outcomes under a unifying picture.

Taken together, the results and subsequent analysis by application of the TS-theory imply that DNA nanostructures cause a stabilization of the ES and $ES^{‡}$ complexes and therefore increase reaction velocities, especially pronounced for low substrate concentrations.

2.3 Effect of substrate charge on thrombin kinetics

After successful extraction of the kinetic parameters and their analysis by application of the TS-theory for a net-neutral substrate, we next performed the same enzymatic reactions with substrates (+1) and (-1). To recall, both substrates are identical to substrate (0), however, instead of a Gly, they bear an Asp (-1) or a Lys (+1) residue at the C-terminal region of the peptide. This leads to a net-charge of +1 or -1 under the pH conditions used within the experiments. The C-terminus of natural thrombin substrates is known to establish critical electrostatic interactions with the exosite I on the surface of the enzyme. These interactions have an impact on nearby hydrophobic interactions and are thought to be responsible for the high specificity of substrate recognition and thrombin allosteric regulation.[214–216] It is important to note here, that the substrates do not interfere with binding of TBAs to the exosite I (Figure S 21).

By comparing the kinetics observed for samples without DNA nanostructures, it is possible to isolate the effect of the C-terminal residue, since this is the only variable of such class of compounds. Indeed, as it can be seen from Figure 17, tremendous differences appear when comparing the hydrolysis of (almost identical) substrates by enzyme species of the w/o DNA class. In comparison to S(0), K_M and k_{cat} values of S(-1) are increased more than 3-fold (ca. 9 µM and 200 min^{-1} respectively). Contrarily, substrate S(+1) shows a highly reduced K_M and notably reduced k_{cat} value (ca. 0.5 µM and 45 min^{-1} respectively). Clearly, the kinetic profile of the enzyme is affected by electrostatic interactions between the C-terminal region of the substrate and the exosite I of thrombin (See also Table S 6 and Table S 7).

Again, application of the TS-theory allows us to analyze the extracted kinetic data (Figure 18, Figure S 22). Figure 18 shows an energy diagram similar to the one presented in Figure 16 for S(0). Energetic diagrams for S(-1) (orange/red) and S(+1) (light blue/dark blue) are also reported. Again, for all substrates, the relative changes in the energy barriers are presented for samples of thrombin only (light lines) and $box^{1/2}_{rig}$ (dark lines), enabling the comparison of substrate hydrolysis for all substrate classes and between different enzyme species (“no DNA” vs “DNA-bound”).

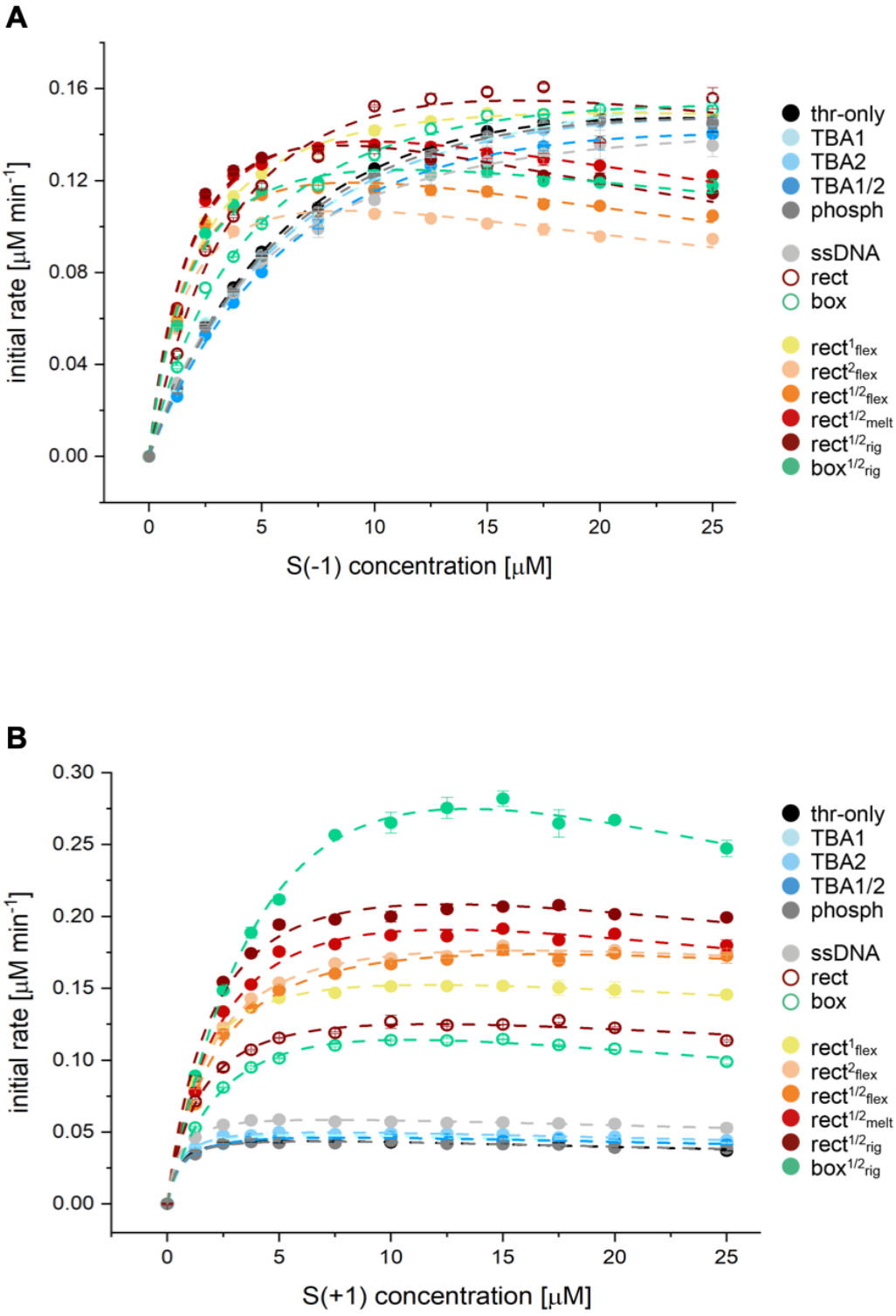

Figure 17: Kinetic profiles of thrombin catalyzed hydrolysis of substrate S(-1) (A) and S(+1) (B). The constructs used for the kinetic assays are the same employed for substrate S(0), as described in Figure 15. Reprinted and adapted from reference [200].

In particular, when comparing S(-1) with S(0), the negative charge of the substrate weakly destabilizes the ES complex (ES, grey *vs.* orange lines), while leaving $ES^{‡}$ mostly unaffected ($ES^{‡}$, grey *vs.* orange lines). This increases ΔG_{ES} while simultaneously reducing $\Delta G^{‡}$ and therefore increases both K_M and k_{cat}. On the other hand, the addition of a positive charge on the substrate, i.e. S(+1), stabilizes the ES complex significantly (ES, grey *vs.* light blue lines), while supporting $ES^{‡}$ moderately ($ES^{‡}$, grey *vs.* light blue lines). This results in a decreased K_M (ΔG_{ES}) and decreased k_{cat} (increased $\Delta G^{‡}$). To resume, in absence of DNA, S(-1) is a superior substrate over S(0), especially at high substrate concentrations (Figure 18B), while S(+1) performs very poorly here. The situation gets different when thrombin is tethered to a DNA nanostructure (Figure 18, Figure S 23). For S(-1), both the ES complex as well as the $ES^{‡}$ complex (ES and $ES^{‡}$, red *vs.* orange lines), are stabilized by the presence of DNA surrounding the enzyme, similar to what observed for substrate S(0) (ES and $ES^{‡}$, black *vs.* grey lines). Therefore, reaction rates are elevated, especially for $S < K_M$ (Figure 18A), while only slightly increased for $S > K_M$ (Figure 18B). After all, S(-1) and S(0) substrates behave rather comparably, although differing in the details. The opposite is true for substrate S(+1). Here, when DNA nanostructures are introduced into the reaction, a complete reversal of the enzyme behavior can be observed. Instead of stabilizing the ES complex, as seen for the S(0) and S(-1) substrates, the hydrolysis of a S(+1) substrate by a DNA-thrombin complex results in the heavily destabilization of ES complex (ES, dark *vs.* light blue lines), while the transition state is barely untouched ($ES^{‡}$, dark *vs.* light blue lines). This condition is especially favorable for high substrate concentrations where maximum reaction speeds are recorded (up to 0.30 µM min^{-1}, Figure 17B).

To resume, two conclusions can be drawn from these data:

1. The introduction of a negative charge at the C-terminal region of the substrate causes a destabilization of the ES complex, which is critical to the improved performance of the enzyme. In absence of DNA, S(-1) is therefore the superior substrate.
2. The unfavorable contributions given by the positive charge of S(+1) are compensated by the DNA nanostructures. Again, the destabilization of the ES complex is important for enhanced catalytic efficiency. In presence of DNA, S(+1) is the best substrate.

There can be several reasons for the DNA-induced effect on the ES and $ES^{‡}$ complexes and are hard to pinpoint experimentally. Only structural studies can shed light into this complex system and help to unravel the exact mechanisms responsible for the intriguing observations. Clearly, the charge of the substrate is of utmost importance in the establishment of interactions, both with protein and DNA, thereby fundamentally influencing the kinetic profiles.

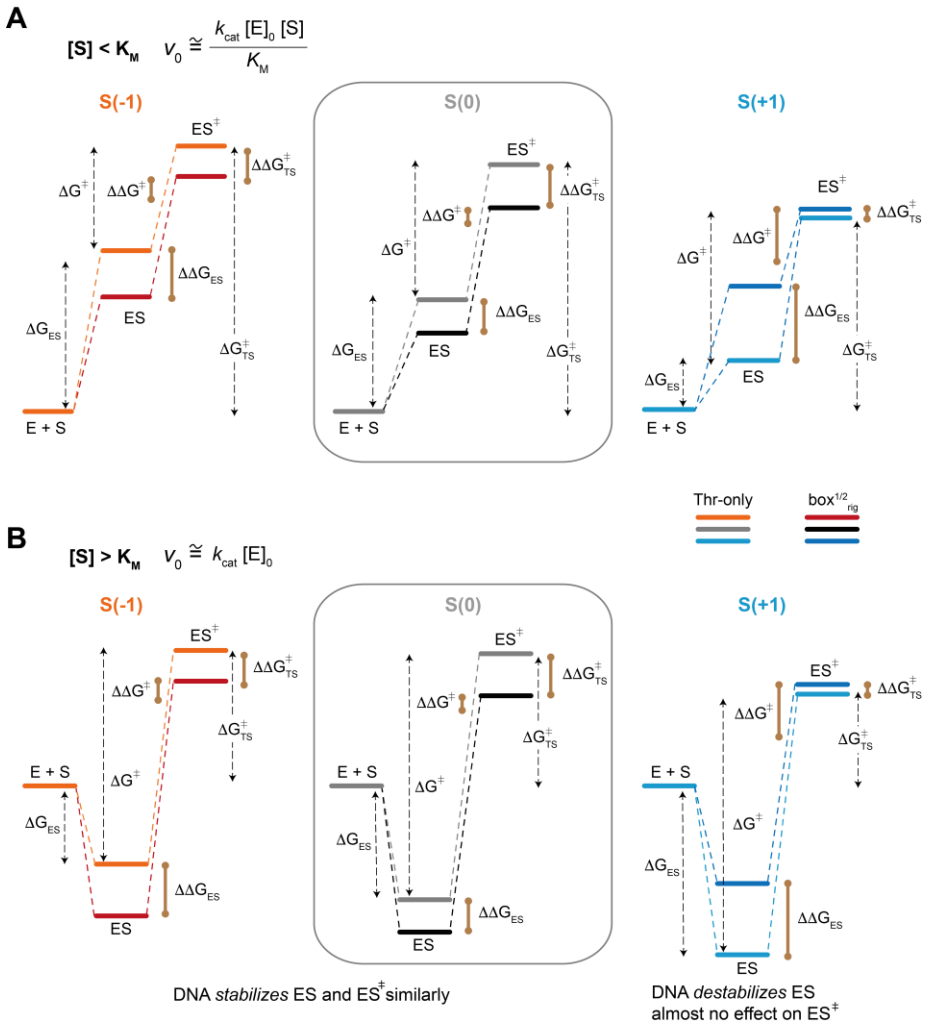

kcal mol^{-1}	S(-1)	S(0)	S(+1)
$\Delta\Delta G_{ES}$	0.96	0.72	-1.63
$\Delta\Delta G^{\ddagger}$	0.27	-0.18	-1.46
$\Delta\Delta G^{\ddagger}_{TS}$	-0.69	-0.89	0.17

Figure 18: Application of the transition state theory on the thrombin catalyzed hydrolysis of S(-1), S(0) and S(+1) for thrombin only box$^{1/2}_{rig}$. Assuming a simple MM mechanism, the transition state theory allows to depict changes in the energy barriers of an enzymatic reaction that progresses from the unreacted E + S through the ES complex to the transition state ES+ and finally to the products. It enables comparisons between the same enzymatic reaction within different conditions (e.g. thrombin-only (light lanes) vs box$^{1/2}_{rig}$ (dark lanes)). Two substrate regimes are considered, S < K_M (**A**) and S > K_M (**B**). The reaction of S(0) with thrombin only is taken as a reference, and its energy diagram is arbitrarily drawn. Diagrams of the other substrates and reactions are drawn to scale and are therefore fully comparable. For all reactions it was assumed that the unbound state E + S is energetically identical. Numerical values of the differences in the energy barriers are given in the table below. Reprinted and adapted from reference [200].

To get a better understanding of the different behaviors of the substrates, Gaussian accelerated Molecular Dynamics (GaMD) simulations of the protein/substrate complex were performed (Figure 19, upper panel). Three model systems were built, that use the crystal structure of the dPhe-Pro-Arg chloromethylketone inhibitor bound to the protein.[217,218] This structure contains the P1-P3 portion of the peptides properly oriented within the deep cleft of the protein that features the catalytic site of thrombin. The goal of the simulations was to investigate the influence of the C-terminal amino acid on the interactions with exosite I. This allosteric site features a large number of positively charged amino acid residues (six Lys and three Arg) and is therefore expected to have varying affinities towards the three different substrates due to dominant electrostatic interactions in this region of the protein.[215] Since substrate (+1) features three Lys residues at the C-terminus, it is anticipated to have the lowest affinity to exosite I due to electrostatic repulsion, which is supported by MD simulations (Figure S 24), showing no close contact between exosite I and S(+1). On the contrary, the positive surface charges of exosite I should attract the C-terminus of S(-1). Again, GaMD simulations support that view, showing that the C-terminal Asp of S(-1) interacts favorably with exosite I (i.e. Lys 60F and Arg 35 and to a less extent Arg 73, Figure S 25). Additionally, density maps of the C-terminal Asp and Lys residues of S(-1) and S(+1) were calculated (Figure 19, lower panel). Those maps represent the region of the protein with the highest probability of residence of these residues. Calculations clearly suggest that the C-terminal residue of S(-1) overlaps with the regions of exosite I (Figure 19A) while the C-terminus of S(+1) rather covers areas of the enzyme, distant from exosite I (Figure 19C). Finally, GaMD simulations indicate that S(0) behaves similar to S(-1) (Figure 19B). A possible explanation for this relies on the C-terminal Gly of S(0), that does not hinder electrostatic interactions of the negatively charged carboxylate group of the peptide with the positively charged exosite I of thrombin (mainly with Arg 35 and Arg 75, Figure S 26).

Taken together, molecular dynamics simulations indicate that C-terminal amino acid residues of the peptides are of crucial importance to establish interactions with the allosteric regulatory exosite I of thrombin. Negative or neutral charges at the C-terminus allow or even support interactions, thus probably triggering enzyme activation. Meanwhile, positive charges impede those interactions through electrostatic repulsion, therefore downregulating enzyme activity. These simulations implicate that even very small changes in the pattern of interactions around the protein surface may have tremendous effects on the enzymatic activity. It is therefore reasonable to assume that huge, electrostatically charged structures like DNA origami can interact with the protein surface and alter its behavior in a similar fashion.

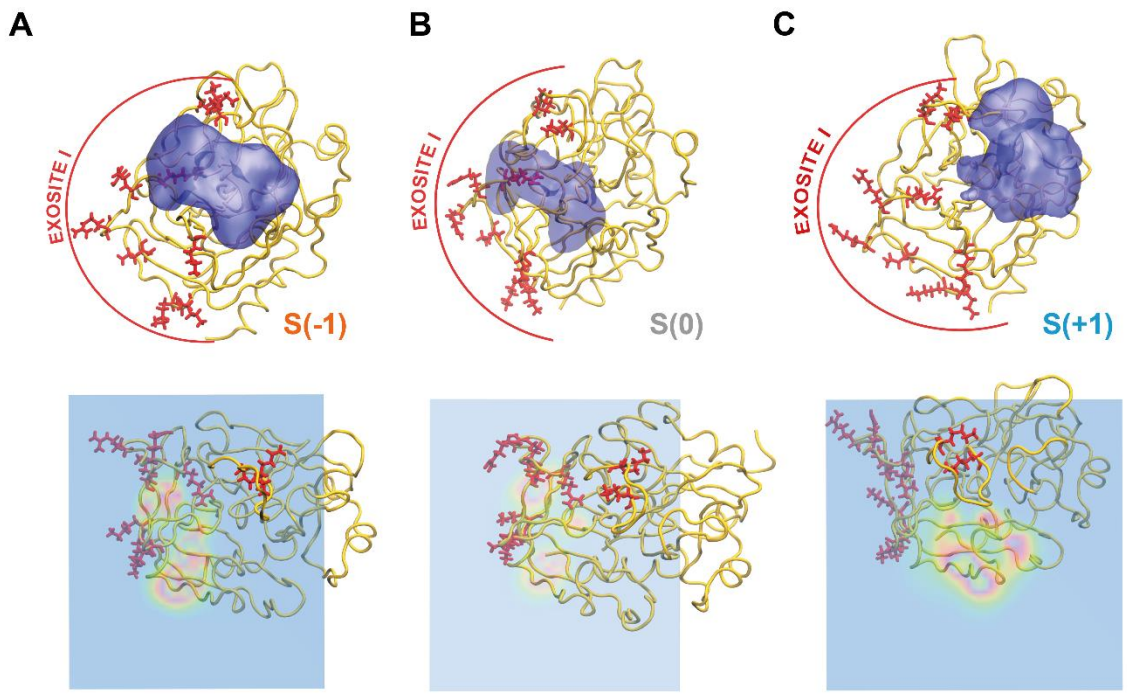

Figure 19: Molecular dynamics simulations of thrombin and C-terminal substrate region interactions. A to **C** top panel shows the regions with the highest residence probability of the C-terminal region of each substrate during the GaMD simulations and are shown as mass densities at isovalues of 0.01. Lower panels show horizontal slices along the xz plane with an offset value of 0.6 (representing the position of the slice with respect to the y axis in a scale from 0 to 1). The brighter areas represent larger values of the density while blue areas correspond to zero or very low densities. Reprinted and adapted from reference [200]. Simulations were performed by the group of Prof. Sánchez-García, University of Duisburg-Essen.

2.4 The combined effect of substrate net charge and DNA scaffolding on thrombin kinetics

The experimental observations presented so far highlight the role of electrostatic interactions between the substrates and the enzyme, but also between the DNA nanostructures and the enzyme and/or substrate. To facilitate the contributions given by each of the three components, 3D plots were generated (Figure 20A, B), in which the kinetic parameters K_M and k_{cat} are illustrated in respect to a reference sample (z-axis). Values are presented in dependence of two variables, which are 1) the extent of DNA/enzyme confinement (x-axis), and 2) the substrate net charge (y-axis). Two sets of samples are analyzed for each substrate. The first set comprises TBA1/2, rect and $rect^{1/2}_{rig}$ (light-colored bars), while the second set consists of TBA1/2, box and $box^{1/2}_{rig}$ (dark-colored bars). In the z-axis are the values of the kinetic

parameters divided by the corresponding values obtained for the thrombin-only sample ($K_M/K_{M(Thr)}$ and $k_{cat}/k_{cat(Thr)}$). The samples are compared with respect to a reference, which is constituted by thrombin in presence of TBA1/2. By moving along the x-axis, the influence of DNA-enzyme confinement can be read-out (w/o DNA, DNA-unbound, DNA-bound). On the other hand, moving along the y-axis, the impact of the substrates can be revealed (S(-1) – orange; S(0) – grey; S(+1) – blue). Finally, the influence that the geometry of the DNA nanostructures imposes on the system can be seen by comparing rect to box samples (light-colored vs. dark-colored).

Focusing on the x-axis first, it is apparent that increased DNA/enzyme interactions lead to a decrease in K_M, when substrates are S(-1) and S(0), meaning that the ES complex is stabilized (Figure 20A, inset). Specifically, ΔG_{ES} is reduced by about 0.90 kcal mol^{-1} for both, rect$^{1/2}_{rig}$ and box$^{1/2}_{rig}$. For S(+1), the opposite is true (Figure 20, blue bars). Enzyme confinement to DNA nanostructures has a destabilizing effect on ES and therefore hugely increases the K_M (up to 14-fold). This effect is particularly obvious for box$^{1/2}_{rig}$, where the enzyme is confined within a 3D DNA structure (ΔG_{ES} increased by 1.42 kcal mol^{-1}). A somewhat similar trend emerges for the k_{cat} values (Figure 20B). Here, S(-1) shows a slight decrease in k_{cat} for DNA-bound enzyme species, while S(0) exhibits a moderate increase (ca. 1.7-fold for rect$^{1/2}_{rig}$). Again, the most dominant change appears for S(+1), with an up to 10-fold increase of the turnover number for box$^{1/2}_{rig}$. Following the plot along the y-axis, it seems that the addition of aptamers to the free enzyme in solution (w/o DNA species) does not change its performance considerably, for any substrate. This is somewhat surprising but may be due to the low concentrations used in these experiments. Binding appears to be facilitated when the aptamers are scaffolded to a DNA nanostructure, especially when equipped with both TBAs. Introduction of DNA origamis to the solution, however, reveals vast differences between the substrates (DNA-unbound and DNA-bound; along the y-axis), with the largest kinetic effects given when the enzyme is tethered inside a 3D DNA box (blue bars in Figure 20A, B). This is particularly interesting, as it shows that favorable DNA/substrate interactions can compensate for, or even surpass, unfavorable enzyme/substrate binding. Thus, depending on the degree of confinement within a DNA nanostructure, a poorly performing substrate can be turned into a very efficient one. (Figure 20C).

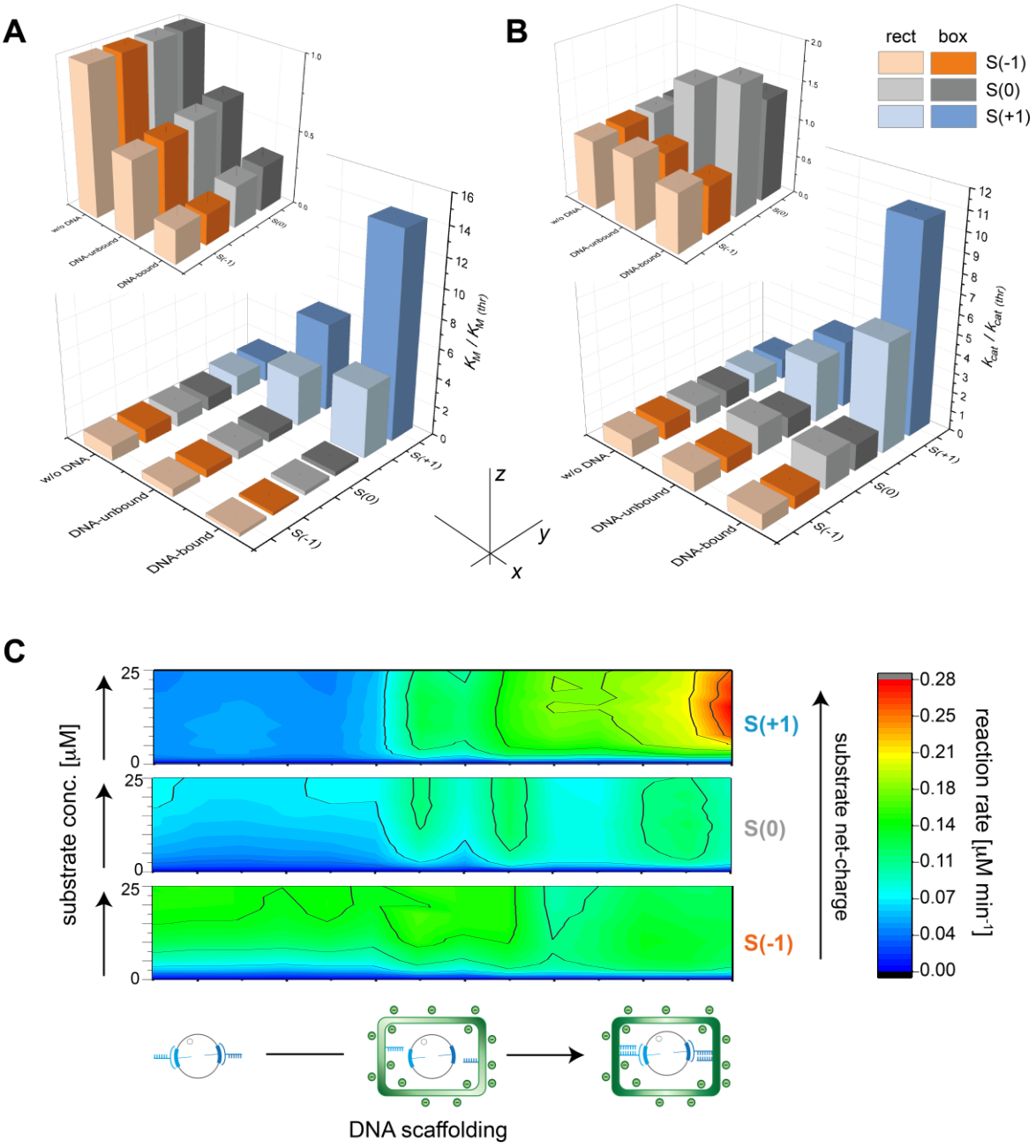

Figure 20: Altered enzyme kinetics through DNA. (A, B) K_M and k_{cat} values of thrombin-catalyzed substrate hydrolysis are presented in a 3D diagram. Data are shown as relative values in respect to the thrombin-only sample ($K_{M(thr)}$, $k_{cat(Thr)}$). The Y-axis breaks down the effect of the substrate net charge on the catalysis, while the X-axis shows the effect of DNA scaffolding. Insets show S(-1) and S(0) data enlarged. Data are shown for two representative samples, namely TBA1/2 rect and rect$^{1/2}{}_{rig}$ (light-colored bars) and the TBA1/2, box and box$^{1/2}{}_{rig}$ (dark-colored bars. (**C**) 2D contour plot illustrating the reaction speed as a function of substrate concentration (Y-axis) and DNA scaffolding (X-axis) for each substrate. Reaction rates are shown as a heat-map, with blue showing the lowest rates and red showing the highest rates (0 to 0.28 µM min^{-1}). In general, reaction speeds increase for increased degree of DNA scaffolding, with S(+1) becoming the best performing substrate. Reprinted and adapted from reference [200].

In order to get a deeper understanding of the DNA/enzyme system, a coarse-grained (CG) model of the rectangular origami was built ($rect^{1/2}_{flex}$). Here, a thrombin molecule was attached to the aptamers and the complex was solvated in a CG model of water. In total, more than 3 million CG particles were incorporated in this model. This complex was used as a starting point for three independent molecular dynamics simulations (Figure 21) with time scales of 120, 140 and 400 ns. Several important conclusions can be drawn from these simulations. It is apparent, that the monolayered DNA origami is a highly flexible complex, that does not keep its planar configuration in solution. This finding was also shown elsewhere[219] and confirms the validity of the simulations. A second important finding is that the protein stays within the 20 nm x 20 nm cavity and remains bound to the aptamers for the entire time of the simulations (Figure 21B). This fortifies the suitability of the DNA host system for the specific confinement of thrombin. Lastly, the spatial distribution of positively charged ions in close proximity to the DNA nanostructure was analyzed. It can be assumed that a huge, negatively charged polymeric structure like a DNA origami does attract cations. Therefore, sodium ions were used as probes and sodium density maps were generated (Figure 21C, D). Indeed, these maps indicate that the cations are mostly concentrated nearby the origami.

Accordingly, it is reasonable to assume that also S(+1) is likely to accumulate around the DNA origamis. In full agreement with this idea, it was observed that DNA origamis tend to aggregate at substrate concentrations above ca. 10 µM (Figure S 29, Figure S 30). This phenomenon was observed only in presence of S(+1), with no aggregation taking place for S(0) and S(-1) even at [S] = 25 µM (Figure S 27, Figure S 28, Figure S 30). Analysis of these curves and extraction of the kinetic parameters is still possible however, since the early phase of the reaction is free from aggregation events (onset of aggregation is time dependent and occurs at later stages of the reaction, see Figure S 31). Another interesting aspect of the enzymatic hydrolysis of S(+1) is the appearance of a hysteresis around 5 – 7.5 µM of substrate concentration. This leads to a sigmoidal, rather than hyperbolic, shape (see Figure S 32, Figure S 33), indicating that the reaction velocity actually increases at a certain time point during the reaction.

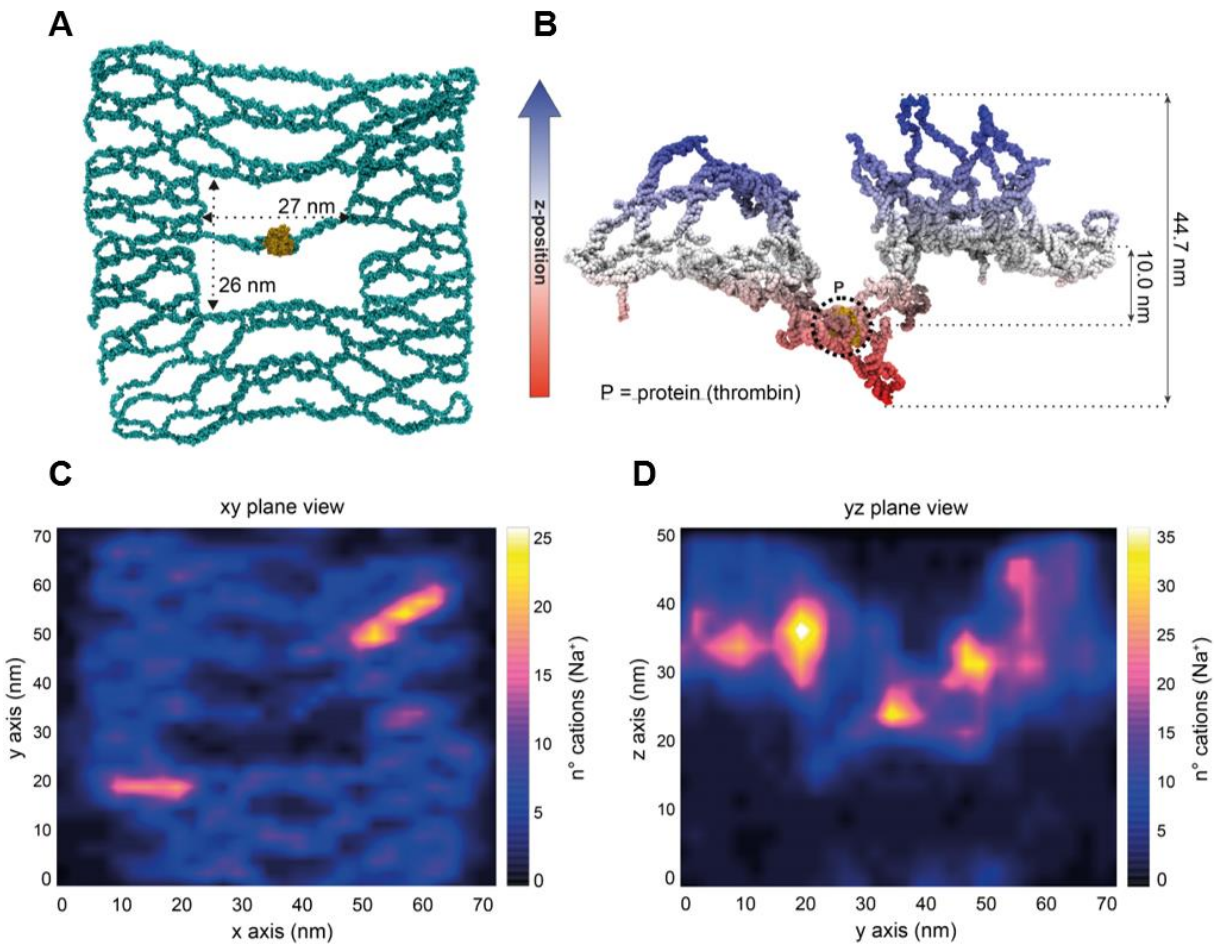

Figure 21: CG model of thrombin bound to rect$^{1/2}_{flex}$. (**A**) The model shows thrombin (yellow) located in the middle of the DNA origami structure, bound by both aptamers. (**B**) Side view of the protein (P) bound to the DNA origami. The protein is located at the bottom of a topological depression. Heights along the Z-axis are color coded. Red parts are located deeper, while blue regions are located higher. (**C, D**) Distribution of sodium ions within the DNA origami are shown within a 2D projection of the XY-plane (**C**) and the YZ-plane (**D**). Brighter regions correspond to increased sodium concentrations. Reprinted and adapted from reference [200]. Simulations were performed by the group of Prof. Sánchez-García, University of Duisburg-Essen

This is different from a usual MM reaction, where the maximal speed of the enzyme takes place at the very start of the reaction and is the one that is typically acquired for constructing the velocity *vs*. substrate concentration curves.[220,221] Interestingly, this sigmoidal behavior is also observed at low substrate concentrations, when the variable parameter is the DNA origami concentration (Figure 22). Here, the same enzymatic reaction was recorded, however this time, the substrate concentration was fixed (10 µM S(+1)) and the DNA origami concentration (rect$^{1/2}_{rig}$) was varied. Clearly, even very low concentrations of DNA origami drastically affect the reaction rate (0.3 nM). Also, above this concentration, product curves take on a sigmoidal shape, with increased reaction rates appearing about 10 minutes after addition of the substrate.

This increase is also rather considerable. Indeed, while initial reaction speeds plateau at about 0.15 µM min^{-1}, maximum rates peak at above 0.3 µM min^{-1} (Figure 22B). Interestingly, this enhancement is not proportional to the DNA origami concentration but levels off above a concentration of about 2 nM, which roughly corresponds to a 1:2 ratio of enzyme to DNA host and finally takes on a hyperbolic shape again for high origami concentrations (10 nM). These findings further support the idea that substrate S(+1) electrostatically interacts with the DNA origamis in a complex way. In presence of small amounts of DNA (ca 0.3-0.5 nM), DNA-protein interactions accelerate the reaction while preserving the typical MM kinetics. Above that concentration (0.5-2 nM), a further and time-delayed increase in reaction speed takes place, which protein- and/or substrate-DNA aggregates may be responsible for. Finally, further increase in DNA concentration (5-10 nM) deteriorates the effectiveness of catalysis.

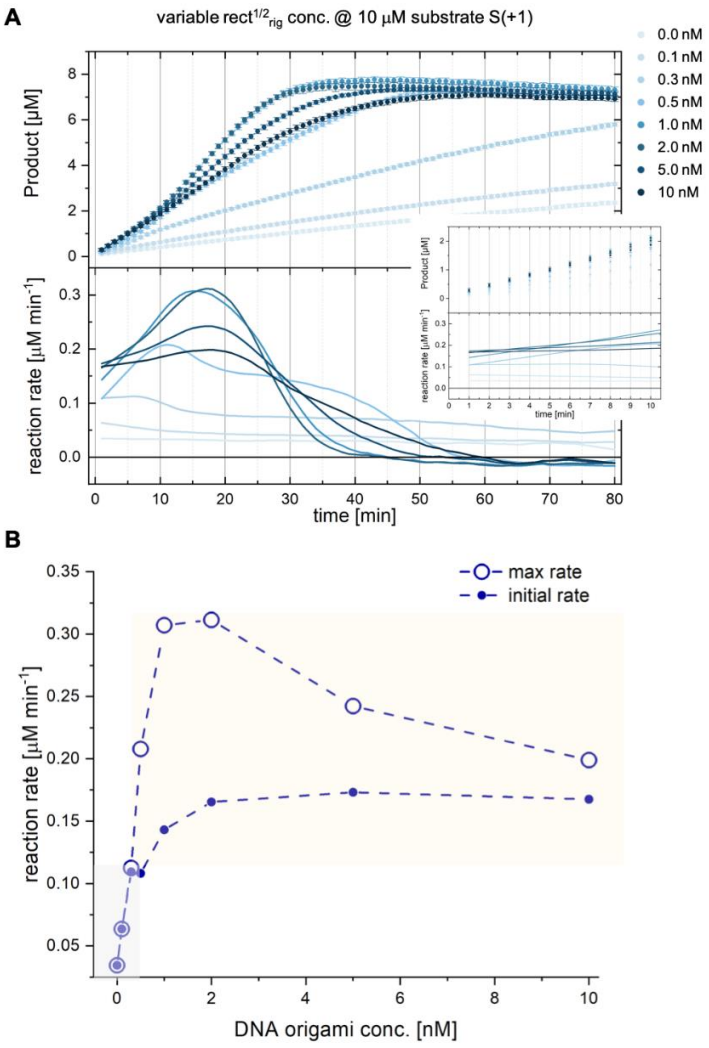

Figure 22: Effect of DNA origami concentration on the catalytic activity of thrombin for S(+1). (**A**, top panel) Thrombin catalyzes the hydrolysis of S(+1). Rising concentrations of $rect^{1/2}_{rig}$ (0 - 10 nM) increase product formation as well as reaction rates (**A**, bottom panel). Progress curves assume a sigmoidal shape above a certain DNA concentration but become again hyperbolic for concentrations above 5 nM. Samples contain 1.2 nM thrombin and 10 µM S(+1) in 1X TEMg at 37°C. (**B**) DNA origami does not increase reactions rates linearly. Both, maximum rates as well as initial rates peak at about 2 nM origami concentration. Maximum reaction rates differ from the initial rates above a DNA origami concentration of about 0.3 nM. Here, max rates are reached later in the time course of the reaction (ca. min 10). Reprinted and adapted from reference [200].

It has been suggested elsewhere[90,128] that the altered enzymatic behavior observed when enzymes are tethered to DNA structures originates from the establishment of a pH gradient from the surface of the DNA structure to the bulk solution. The hypothesis founds on the enormous amount of negative charges near the DNA surface, which attracts H^+ ions, thereby lowering the pH value in its vicinity.

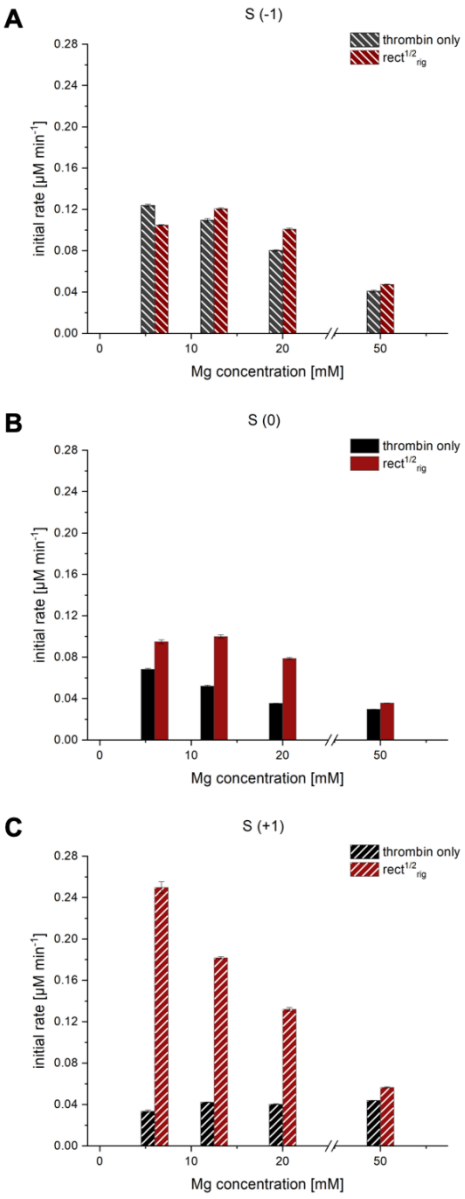

Figure 23: Effect of Mg ions concentration on the catalytic activity of thrombin. The enzymatic activity assays were performed as described in the Materials and Methods (see 4.2.11). Two types of reactions (thrombin only – black bars, $rect^{1/2}_{rig}$ – red bars) were recorded for all three substrates (**A** to **C**), while the magnesium concentration was varied (6 mM, 12.5 mM, 20 mM and 50 mM). Initial reaction rates were documented and plotted. Reprinted and adapted from reference [200].

To test whether this effect might be liable for the observed increase in enzymatic reaction speeds, a control experiment was performed with thrombin catalyzing the hydrolysis of S(+1) at different pH values (Figure S 34). The data show that the pH value indeed affects the reaction, however in a negative fashion. Lower pH values result in a diminished reaction speed until almost no activity is present at all. This excludes the hypothesis of a pH gradient as the driving force of increased reaction velocities in our experiments and is in line with literature reports of a decreased thrombin activity at low pH values.[222] Possibly, additional ions other than hydrogen ions (e.g. sodium) might be involved in interactions with critical amino acid residues on the protein surface.[210] Furthermore, the effect of decreased or elevated Mg^{2+} ion concentrations on the hydrolysis of all three substrates was investigated and the initial reaction

rates were plotted (Figure 23). Again, the electrostatic contributions of both the substrate and the DNA are obvious from the plots. S(-1) and S(0) show once more a comparable behavior, with S(+1) deviating far from them. Thrombin-only samples (black bars) confirm anew the differences in reaction rates due to substrate charges only, with S(-1) > S(0) > S(+1). In presence of DNA origamis, the trend is inverted, with S(+1) being the fastest substrate. The difference is even increased the lower the Mg^{2+} concentration becomes (6 mM), with peak reaction rates for S(+1) of about 0.25 µM min^{-1}. On the other hand, the higher the magnesium concentration, the lower are the variations in enzymatic activity between the substrates. At 50 mM Mg^{2+} ions, such differences are almost negligible. At these high Mg^{2+} concentrations aggregation events may probably occur, canceling out any positive effect given by the DNA nanostructures.

Taken together, the results show that in general thrombin activity is affected by the concentration of ions in the solution, which may be especially pronounced in presence of DNA nanostructures. Here, an up to 6-fold difference in reaction speeds can be accomplished (cfr. S(+1) at 6 mM magnesium ions) by varying the Mg^{2+} concentration, thereby either screening the negative charges (in case of high Mg^{2+} concentrations) or emphasizing them (in case of low Mg^{2+} concentrations) and thus altering the electrostatic interactions between substrate, DNA and enzyme.

2.5 The effect of multiple enzyme species on thrombin catalysis

A key element of this work is the binding of thrombin to the DNA hosts which relies on non-covalent binding mechanisms. This has two advantages: 1) the enzyme is not altered in its chemical makeup since no chemical bonds are formed or broken, 2) since covalent binding is often achieved through non-regiospecific coupling to lysine or cysteine residues, a multitude of different enzyme species is usually generated. This is not the case here. On the other hand, non-covalent binding has one disadvantage, which is important to keep in mind: it is an equilibrium binding, i.e. depending on the strength of the interactions and the surrounding environment, only a fraction of reacting molecules is actually bound into the non-covalent complex. This is also true for the DNA-enzyme systems described in this work. Binding of thrombin to the DNA-hosts is not quantitative. Several attempts have been undertaken to isolate pure DNA-enzyme species by using excess amounts of thrombin (50-fold to 500-fold), variations of incubation

times (from 2h to overnight) and/or variations of incubation and re-solvation temperatures (24/37°C and 24/4°C respectively). However, no change in binding yield was observed, suggesting that – in the experimental conditions used – the DNA-enzyme complex equilibrates with its products of dissociation, the unbound DNA and enzyme species. To bypass this issue, very high DNA-enzyme concentrations should be used (>> K_D). Unfortunately, spectroscopic analysis to quantify the binding constant of the complex also failed due to unwanted aggregation taking place at high DNA origami concentrations (> 200 nM). Taken together, the upscaling of DNA-enzyme complexes was unsuccessful and remains a challenge to be accomplished in future works. Alternatively, other methods should be employed to determine the K_D of the complex.

Since it is reasonable to assume that the effects on thrombin kinetics observed in presence of DNA nanostructures result from the contribution of the enzymes that are actually bound to these structures, it is very likely that the calculated enhancement rates for the DNA-bound compounds are underestimated. Quantification of thrombin binding to DNA origami was performed by AFM imaging and varied from 5% ($rect^1_{flex}$) to a maximum of 44% ($rect^{1/2}_{flex}$) (Figure S 5, Figure S 6). Although AFM might slightly falsify these yields due to surface adhesion effects and sample preparation/purification issues, the data match very well with the expected theoretical values for a binding constant in the low nM range. Assuming the DNA-enzyme complex has a K_D = 1 nM (given by the strong affinity of the TBA2 to thrombin),[223] the following equation will relate the concentration of the three possible species at the equilibrium:

$$\boldsymbol{K_D = \frac{[E][DNA]}{[E_{DNA}]} = \frac{(1.2-x)(1-x)}{x}} \qquad \textbf{Eq. 11}$$

Where [E], [DNA] and [E_{DNA}] represent the concentration of free enzyme, unbound DNA structures and DNA-enzyme complexes, respectively. Solving Eq. 11 for a solution containing 1.2 nM free enzyme and 1 nM DNA structures, as used in the enzymatic assays, will yield 0.77 nM free enzyme, 0.57 nM unbound DNA structures and 0.43 nM DNA-enzyme complexes. The theoretical values therefore match the experimentally observed ones very closely (i.e., about 60% unbound and 40% bound). This hypothesis lets us conclude that the observed enzymatic enhancement rates are likely caused by a minority of enzyme species and thus, the

enhancement rates caused by isolated DNA-enzyme complexes may be much higher than those presented here.

Since isolation of pure, non-covalently bound DNA-enzyme species is most challenging and has not been accomplished in this work, a theoretical framework is needed to analyze *mixtures* of enzyme species. A possible solution was introduced by Di Cera and coauthors,[224] who implemented the so-called kinetic linkage scheme. The idea here is that, at any time, there is not a single thrombin species in solution, rather more than one, since binding of sodium or phosphates or indeed any other allosteric effector will create a new thrombin species. These enzyme species perform the same catalytic reaction, but their kinetics may vary from one another. Therefore, a number of different kinetic fluxes coexist, as many as the distinct enzyme species are, and those fluxes are interlinked with one another by specific rate coefficients (Figure 24). By assigning constant values to some of these rate coefficients while setting others as variables, one can simulate the kinetics of the system and extract useful information about the participating enzyme species. In particular, one can observe how the steady-state rate of the reaction is affected by the kinetic fluxes among the various enzyme species.

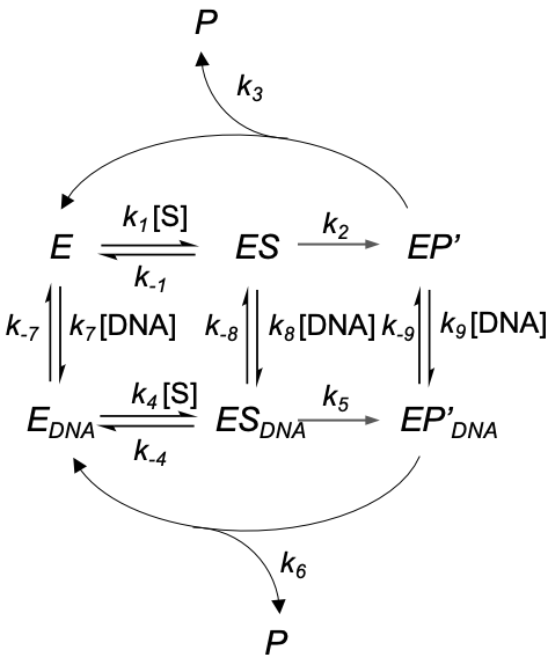

Figure 24: Kinetic linkage scheme of thrombin in presence of DNA nanostructures. In presence of DNA, the classical MM-reaction scheme is expanded with a parallel enzymatic flux. Different enzyme (E, E_{DNA}) species co-exist and are in pseudo-equilibrium with one another, each one contributing to the final reaction rate. Reprinted and adapted from reference [200].

For the purpose of this work, the kinetic linkage scheme was simplified to a system consisting of only two enzyme species, namely E (freely diffusing thrombin) and E_{DNA} (DNA-thrombin complexes). On the upper panel of Fig. 24, the kinetic flux of freely diffusing thrombin is presented, with k_1, k_{-1}, k_2 and k_3 being the rate constants of each step. Values for k_1 to k_3 were taken from the literature for thrombin in similar buffer conditions.[210,224] The lower panel shows the flux of the DNA-enzyme complexes and is described by the rate constants k_4 to k_6. These rate constants are set as variable for the

simulations. Finally, the connection between these two kinetic cycles is given by the rate constants k_7 to k_9. Figure 25 depicts the first set of simulations.

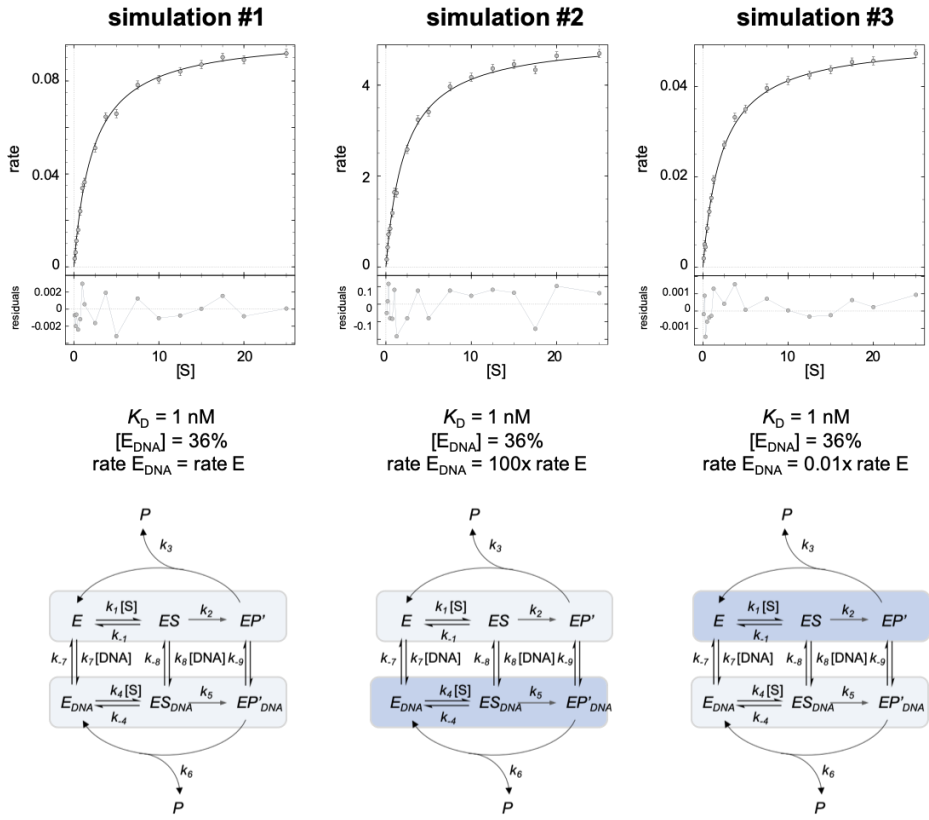

Figure 25: Simulations of thrombin catalyzed hydrolysis for varying parameters (K_D = 1 nM). Simulations (top) show the reaction rates that result from reaction mixtures featuring several enzyme species, namely thrombin free in solution (E) or bound to a DNA cage (E_{DNA}). Both enzyme species perform the classical MM kinetic cycle and are connected by the association and dissociation (k_7 to k_9) of thrombin to the TBA-modified DNA cage. The rate coefficients of the two pathways were chosen such to result into an apparent MM behavior. Rate coefficients (k_4 to k_6) can vary between the enzyme species and are modelled for three scenarios (from E_{DNA} = 0.01x E, E_{DNA} = E and E_{DNA} = 100x E). Kinetic fluxes that dominate the reaction are labeled in blue (lower panel). Reprinted and adapted from reference [200].

Here, three different rates for E_{DNA} in respect to E were chosen, i.e. k_1-k_3 = k_4-k_6 (Simulation #1), k_1-k_3 = 0.01 x k_4-k_6 (Simulation #2) and k_1-k_3 = 100 x k_4-k_6 (Simulation #3) (For a detailed description of the simulation see Supplementary Text 2). When both kinetic fluxes are equally fast (sim. #1), the reaction rate plateaus at about 0.08 µM min^{-1}. However, when E_{DNA} is considerably faster than E (sim. #2), the maximal reaction speed significantly increases (about 50-fold). On the other hand, if E_{DNA} is considerably slower than E (sim. #3), the effect is almost negligible, with the maximal reaction speed being cut by half the initial value. While somewhat intuitive, these simulations clearly demonstrate that the faster kinetic

flux dominates the reaction, even if its enzyme species might be the minor component in solution.

In another set of simulations (Simulation #4-12, Figure S 35), the rate constants between E and E_{DNA} were varied between 0.1 nM and 1 µM in order to investigate the effect of different K_D values of the DNA-enzyme complex on the reaction rate. Clearly, the higher the K_D (the less E_{DNA} present), the lower is the impact given by this kinetic cycle. The maximal reaction velocity therefore increases only moderately (Simulation #4-6) or almost not at all (Simulation #10-12). If the situation is reversed and the K_D is very small, a lot of DNA-enzyme complexes will be formed, and the contribution given by this species will be huge. In this case, if E_{DNA} = 100x rate E (Simulation #8), the max reaction velocity is almost 100-fold increased. In contrast, if E_{DNA} = 0.01x rate E (Simulation #9), the max reaction rate will drop to about 1/10 of that of E.

Taken together, the different kinetics of the substrates are likely caused by allosteric effects, originating from interactions of the C-terminus of the peptide with the exosite I of thrombin and can be simulated by choosing slightly favorable rate coefficients for S(0) and S(-1) when compared to S(+1) (Figure S 36A, B). When DNA origamis are introduced, a new kinetic pathway emerges. This pathway competes with that of the free enzyme. Assuming that the E_{DNA} pathway is faster than E (for an, up to now, unknown reason), as observed in the enzymatic assays, a higher flux into this pathway (i.e. a lower K_D and/or a faster kinetics), will be beneficial for the reactions in all cases. This increase is however different for the substrates. While S(0) and S(-1) only moderately benefit from the DNA nanostructures, S(+1) is immensely affected by DNA, rising from the worst substrate to the best performing substrate. A final set of simulation was run in which the E_{DNA} rate was chosen so that the maximal reaction velocities approximate those observed in the experiments (Figure S 36C, D). Clearly, the E_{DNA} pathway is dominating the reaction for S(+1) (10x faster than E), while it is only moderately superior in case of S(0) (3x faster than E).

It is important to note, that these simulations do not attempt to give estimations about the rate coefficients. They are much more intended to demonstrate the concept of kinetic linkage schemes and their usefulness for the understanding of complex kinetic reactions.

3 Conclusion

In this work, the kinetic behavior of the allosterically regulated thrombin, a member of the serine protease family, was studied when confined within DNA nanostructures. Three different, rationally designed, fluorogenic substrates were used, which differ in their C-terminal amino acid residue, putatively implicated in the allosteric regulation of thrombin activity. Furthermore, two DNA origami designs were evaluated, one being a 2D DNA rectangle, the other being a newly designed 3D DNA box. For each substrate, a total of 14 distinct enzymatic assays were performed, differing in the chemical nature of the environment surrounding the protein (e.g. presence or absence of DNA nanostructures), yielding a sum of 42 reactions in total. For all reactions recorded, a typical Michaelis-Menten behavior was observed and kinetic parameters such as k_{cat} and K_M values could be extracted. Analysis of the data allowed for the classification of the samples into three main categories, i.e. "w/o DNA", "DNA-unbound" and "DNA bound". The data show that within the first group (no DNA nanostructures), tremendous differences exist between the substrates. While S(0) and S(-1) behave similarly and are hydrolyzed quite rapidly, S(+1) in contrast is a very poor substrate. Molecular dynamics simulations helped to understand this observation by showing that S(0) as well as S(-1) interact with the allosteric site of thrombin (exosite I) with their C-terminal amino acid residue. These interactions are mainly driven by electrostatic interactions. On the other hand, S(+1) does not interact with exosite I for the same reason. Its positive charge at the C-terminus rejects the positively charged exosite I. The situation is reversed when thrombin is tethered to DNA nanostructures. S(+1) is now the best performing substrate, with thrombin exhibiting peak reaction speeds of up to 0.3 µM min^{-1}. Interestingly, also catalysis of S(0) and S(-1) accelerates, however only in a moderate fashion and in a concentration-dependent manner. Application of the transition state theory helps to reveal the energetic contributions which are responsible for the change in the enzymatic behaviors observed, although only structural analyses can give a clear explanation of the mechanistic reasons behind this phenomenon. Notoriously, electrostatic interactions play a fundamental role in thrombin activity and for many other allosterically-regulated serine proteases. Therefore, it is reasonable to assume that large, massively charged objects around the enzyme may influence the local environment of the enzyme, e.g. in terms of ionic strength, thereby changing the pK of critical ionizable residues or triggering ion-dependent mechanisms of allosteric regulation. These alterations of the enzyme create different enzyme species, each of which capable of performing its own catalytic cycle. The enzyme

species may have vastly differing kinetics, which can result in one flux dominating over the others, even if the corresponding enzyme species represents only a minor part of the total. This would explain the inversion of the catalytic profile of the substrates used in this work, with the slowest substrate becoming the fastest one and the fastest becoming the slowest instead. Additionally, DNA structures may not only interact with the enzyme, but also with the substrates. As demonstrated by TEM imaging and further supported by CG models, positively charged ions interact with the DNA origamis and even induce aggregation upon high S(+1) concentrations. It is known that scaffolding enzymes can increase the local concentration of substrates when interactions of moderate strength occur between scaffold and substrate.[122] This so-called *substrate steering* effect may be present for S(0) and S(-1) since K_M values decrease upon thrombin-binding to DNA nanostructures. On the other hand, interactions with S(+1) may be too strong, therefore rather trapping the substrates on the DNA. In this way, the local substrate concentration around the enzyme would decrease, which would be coherent with the highly increased K_M values observed. Quantification of these interactions are needed in order to test this hypothesis and may be an interesting subject for further research. Finally, a possible contribution given by a reduced pH value near the DNA origami surface could be excluded. It can therefore be concluded with high confidence, that the main driving forces for the altered behavior of thrombin in this work are the electrostatic interactions of all three players involved, i.e. DNA/enzyme, enzyme/substrate and DNA/substrate. This may inspire future works, in which DNA structures can be employed not only to increase and/or modulate enzymatic reactions, but also to improve the catalysis of one substrate over others. Clearly, to accomplish these goals, more research for the identification and quantification of these electrostatic interactions is needed as well as a clear separation of the electrostatic contributions from the contributions given by the confinement of enzymes alone.

4 Materials & Methods

4.1 Materials

Table S 1: General Equipment

Equipment	Manufacturer
Analytical balance	Sartorius AG
Atomic force microscope, MultiMode8	Bruker corporation
Centrifuge 5424R, 5430R, 5810R	Eppendorf AG
CFX96 RealTime PCR-System	Bio-Rad Laboratories Inc.
DS11 Spectrophotometer	DeNovix
Electrophoresis systems	VWR International GmbH/Bio-Rad Laboratories Inc.
Glow discharger	Pelco easiGlow
Shaking Incubator	New Brunswick scientific
JEM 1400Plus	JEOL
Microwave	Sharp business systems, Deutschland GmbH
Pipettes: Eppendorf Research Plus	Eppendorf AG
Poly acrylamide gel system	VWR International GmbH/Bio-Rad Laboratories Inc.
Precision balance	Sartorius AG
SPROUT mini centrifuge 12 V	Heathrow scientific
Tecan Spark 10 M	Tecan
Thermocycler	Eppendorf AG
Typhoon FLA 9000	GE Healthcare Life sciences
Vortex mixer, VV3	VWR International GmbH
WTW Inolab pH 920	Xylem Analytics Germany sales GmbH & Co. KG

Table S 2: Consumables

Consumables	Manufacturer
96 well plate	Bio-Rad Laboratories Inc.
96 well black flat bottom polystyrene NBS	Corning
AFM tips ScanAsyst air/liquid	Bruker Nano Inc.
AFM metal specimen discs	Ted Pella Inc.
Amicon Ultra Centrifugal Filter Units 3, 50 & 100 kDa	Sartorius/Millipore
AssayMix qRT-PCR	Thermo Fisher Scientific
Cryotubes (2 mL)	Sarstedt
Dye Removal Column	Thermo Fisher Scientific
Formvar/coal coated copper grids S-162	Plano GmbH
Human α-Thrombin	Cayman Chemical Company
Mica	Plano GmbH
p7249	Affymetrix
p8064	Tilibit Nanosystems GmbH
PCR tubes (0.2 mL)	VWR
Pipetting tips (20 µL, 200 µL, 1000 µL, 5 mL, 10 mL)	Eppendorf AG
Protein low binding reaction tubes (0.5 mL, 1.5 mL, 2.0 mL)	Eppendorf AG
Qunatum Prep Freeze ‘N Squeeze DNA Gel extraction columns	Bio-Rad Laboratories Inc.
Reaction tubes (0.5 mL, 1.5 mL, 2.0 mL, 5 mL)	Sarstedt AG & Co.
Reaction tubes (15 mL, 50 mL)	VWR
Taq Man Gene Expression Assay Master Mix	Thermo Fisher Scientific
XL1-Blue *E. coli* bacteria	Agilent technologies

Table S 3: Chemicals & miscellaneous reagents

Chemicals & miscellaneous reagents	Manufacturer
1 kb DNA ladder + gel loading buffer	Carl Roth GmbH + Co. KG
Acrylamide/bis solution (37.5:1, 30 % w/v)	Merck
Agarose	Lonza
APS	Carl Roth GmbH + Co. KG
Aqua dest.	Milli-Q® Integral Water purification System
Bacto tryptone	Becton, Dickinson and company
Bacto yeast extract	Merck
Boric acid	Carl Roth GmbH + Co. KG
Bromophenol blue sodium salt	Merck
Coomassie R250	Thermo Fisher scientific
Dithiothreitol (DTT)	Merck
Dimethylsulfoxid (DMSO)	Merck
Ethylenediamine tetraacetic acid disodium salt dihydrate (EDTA)	Merck
Ethanol	VWR
Ethidium bromide	Merck
Glycerol	Merck
HCl	Merck
Isopropanol	VWR
Lysis-buffer (0.2 M NaOH, 1 % SDS)	Macherey-Nagel
Magnesium acetate	Merck
Magnesiumchlorid hexahydrate	Merck
Na_2EDTA	Merck
Neutralization buffer (3 M KOAc, pH 5.5)	Macherey-Nagel

NHS-A488	Thermo Fisher
N-Z-Amine (NZA)	Merck
Polyethylene glycol 8000	Merck
Precision Plus Protein™ Unstained Protein Standards	Bio-Rad
Sodium Chloride	Carl Roth GmbH + Co. KG
Sodium dodecyl sulfate (SDS)	Merck
Sodium phosphate	VWR Chemicals
Substrates S(+1), S(0), S(-1)	INTAVIS Peptide Services GmBH & Co. KG
TCEP	Merck
TEMED	Carl Roth GmbH + Co. KG
Tetracycline	Merck
Tris base	Merck
Tris-HCl	Merck
Tween20	Merck
Urea	Merck
X-gal [100 µg/mL]	Merck

Note: All Gold nanoparticles used in this work were synthesized in the group of Prof. S. Schlücker (Faculty of Chemistry, University of Duisburg-Essen).

Table S 4: Buffers, media and solutions

Buffers/Media/Solutions	**Composition**
2x YT Medium	16 g/l bacto tryptone, 10 g/l bacto yeast extract, 5 g/l NaCl
Buffer CA	25 % (v/v) isopropanol, 10 % (v/v) acetate, 0.05 % (w/v) Coomassie R250
Buffer CB	10 % (v/v) isopropanol, 10 % (v/v) acetate, 0.005 % (w/v) Coomassie R250
Buffer CC	10 % (v/v) acetate, 0.002 % (w/v) Coomassie R250
Buffer CD	10 % (v/v) acetate

Loading dye for den. PAGE	80 % formamide (v/v), 20 % TBE 5x (v/v)
Loading dye for agarose gel electrophoresis	60 % ddH_2O (v/v), 30 % glycerol (v/v), 10 % 10x TEMg (v/v)
NZA-Medium	10 g/l NZA, 5 g/l bacto yeast extract, 10 g/l NaCl
PEG buffer	5 mM tris base, 1 mM EDTA, 505 mM NaCl, 15 % (w/v) PEG 8000
SDS PAGE gel-loading buffer (w/ or w/o DTT)	200 mM tris HCl (pH 6.8), 8 % SDS, 40 % glycerol, 0.004 % bromophenolblue, (DTT 30 mM)
SDS resolving gel buffer (4x)	500 mM tris/HCl (pH = 6.8), 4 g/l SDS
SDS running buffer (1x)	250 mM tris, 950 mM glycine, 5 g/l SDS
Standard I agar	37 g/l agar
TBEMg (1x)	40 mM tris base, 20 mM boric acid, 2 mM EDTA, 12.5 mM Mg acetate, pH 8.0
TEMg (1x)	40 mM tris base, 2 mM EDTA, 12.5 mM $MgCl_2$, pH 7.6
TEMg(X) (1x)	40 mM tris base, 2 mM EDTA, X mM $MgCl_2$, pH 7.6
Thrombin storage buffer	5 mM sodium citrate, 20 mM NaCl, 0.01 % PEG, pH 6.5
Tris-buffer (1x)	10 mM tris-base, pH 8.5

Table S 5: Software

Software	Comment
caDNAno2	All DNA origami designs were created using the cadnano2 software.[225] Staple sequences were exported as .csv file.
CanDo	For schematic representations and in silico modeling of the designed structures the CanDo online tool was used.[219,226]
CPX Manager	FAM signals for assembly/disassembly or quantification of origami concentration were programmed and characterized with the CFX Manager TM 3.0 (Bio-Rad) software.
Design_analyzer.app	Sequence optimization and estimation of melting temperatures of staple domains were done with this software.[77]
Dynafit	Kinetic simulations were performed using the Dynafit software that is free-of-charge at http://www.biokin.com/dynafit/suite.
ImageJ	This software, developed at the National Institutes of Health, USA, was used for graphical presentation of gel images and to calculate band intensities. Version 1.53 was used.
Mfold software tool	For the calculation of melting temperatures of individual staples, the Mfold software tool was used.[227]
Nanoscope 1.9	AFM images were flattened analyzed and prepared for presentation using this software.

4.2 Methods

4.2.1 Design and assembly of DNA nanostructures

All DNA origami structures presented in this work were designed using caDNAno (v2.2.0) either as stand-alone program or as plug-in for Autodesk Maya 2015.

4.2.1.1 Rect

Assembly of rect was achieved by folding the single stranded p7249 plasmid, produced from phage DNA in *E. coli* (see 4.2.2), into a rectangular, quasi-planar DNA monolayer, as previously reported.[228,229] The construct has a calculated length of about 97 nm and a width of 78 nm (calculated with interhelical distances of 1 nm as previously reported[69]) and consists of two halves that are connected by a central seam. Staples that span the central seam possess a 15 b hairpin motif ($C_5T_5G_5$), that can be stretched out if needed (not applied in this work). Unpaired scaffold regions extrude from both ends of the central seam (140 b and 141 b respectively). In its middle, the structure features an internal cavity of about 20 nm x 20 nm, into which oligonucleotides can protrude. These protruding arms can hybridize TBA-modified oligonucleotides, which in turn bind thrombin (see Figure S 4). A three-dimensional modeling of the structure was done using the CanDo online software tool.[219,226] This software predicts the shape and the flexibility of a DNA structure by applying a mechanical model that represents the DNA double-helix as a homogeneous elastic rod with axial, twisting and bending moduli, based on experimentally investigated data[230] (Figure 26). A detailed design of the structure as well as a list of all staples and scaffold sequences is given in the supplementary materials (Figure S 37 and section 6.3).

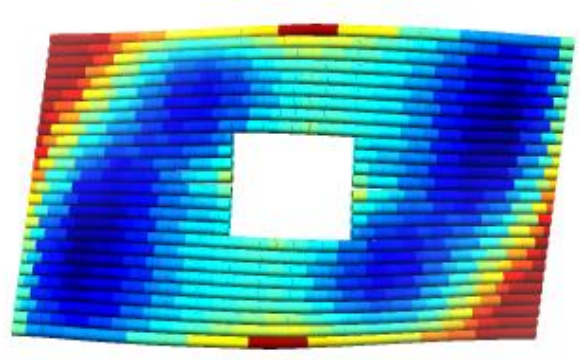

Figure 26: CanDo simulation of rect. The flexibility of the structure is represented as root mean square flexibility (rmsf) and color coded from blue (minimal) to red (maximal). For this simulation, unpaired scaffold and staple regions were omitted.

Rect was assembled using a 1:6 molar ratio between p7249 (40 nM) and staple strands (240 nM). Assembly buffer was 1X TEMg (20 mM Tris, 2 mM EDTA, 12.5 mM MgCl2, pH 7.6). Thermal annealing was performed by gradually decreasing the temperature from 80°C – 20°C at -1°C/min (see Figure 27) in a Thermocycler Mastercycler nexus gradient (Eppendorf).

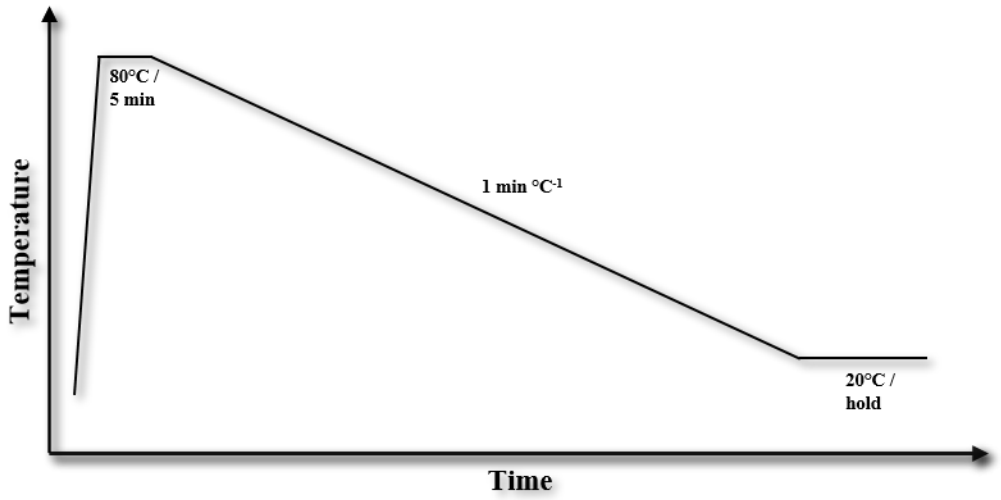

Figure 27: Thermal annealing ramp of rect. Upon an initial denaturation step of 5 min at 80°C the solution was allowed to gradually cool down to 20°C.

4.2.1.2 Box

Box was assembled by folding the p8064 single stranded plasmid, produced from phage DNA in *E. coli* (see 4.2.2), into a box-like, three-dimensional, dual-layered structure, as previously reported.[231] Briefly, the structures square bottom plate has a calculated width of about 31 nm and a height of ca. 25 nm. The inner diameter is about 21 nm. An unpaired scaffold loop of 74 bases extrudes from one side of the structure. The box is made up of four parts, that each consists of a triangular bottom segment and a square-like wall. All four parts are connected

by either 3 bases of unpaired scaffold (bottom plate) or 3 bases of unpaired staple strands (walls). To give the structure more rigidity, it was designed as a dual-layered object in square lattice organization. Four staple strands (Two protruding staples and two TBA-carrying staples), protrude into the inner cavity of the structure in order to bind thrombin (see Figure S 4). A three-dimensional modeling of the structure was done using the CanDo online software tool.[219,226] A detailed design of the structure, as well as a list of all staple and scaffold sequences used is given in the supplementary materials (Figure S 38 and section 6.3).

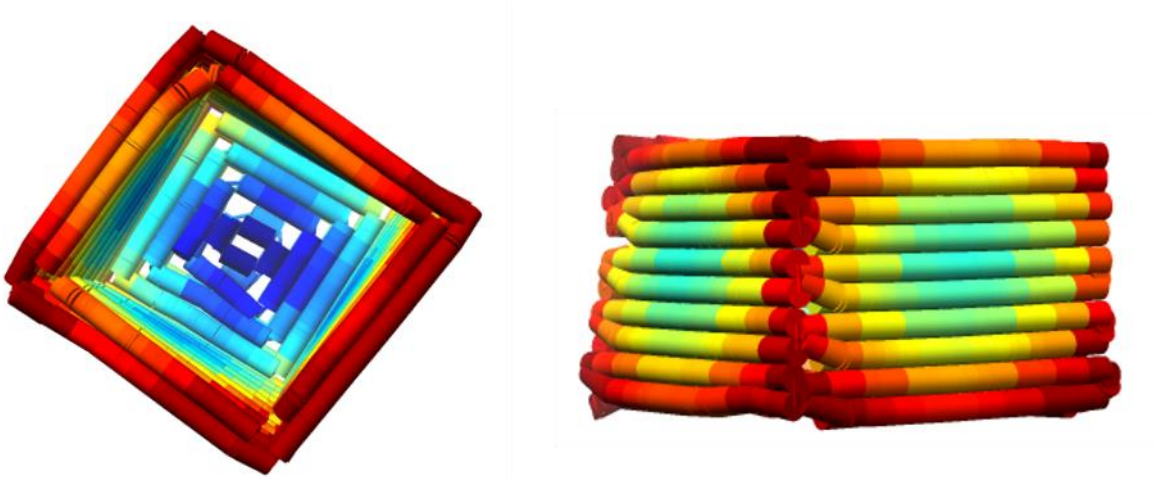

Figure 28: CanDo simulation of box. The flexibility of the structure is represented as root mean square flexibility (rmsf) and color coded from blue (minimal) to red (maximal). For this simulation unpaired, connecting region in between the four parts were adjusted in length in order to get a relaxation of the structure.

Box was assembled using a 1:6 molar ratio of p8064 scaffold (20 nM) and staple strands (120 nM). Assembly buffer was 1X TEMg (20 mM Tris, 2 mM EDTA, 12.5 mM $MgCl_2$, pH 7.6). Thermal annealing was performed by an initial denaturing step at 80°C and subsequent careful cooling the structure over several hours. For a detailed view of the annealing protocol see Figure 29. The instrument used was a Thermocycler Mastercycler nexus gradient (Eppendorf).

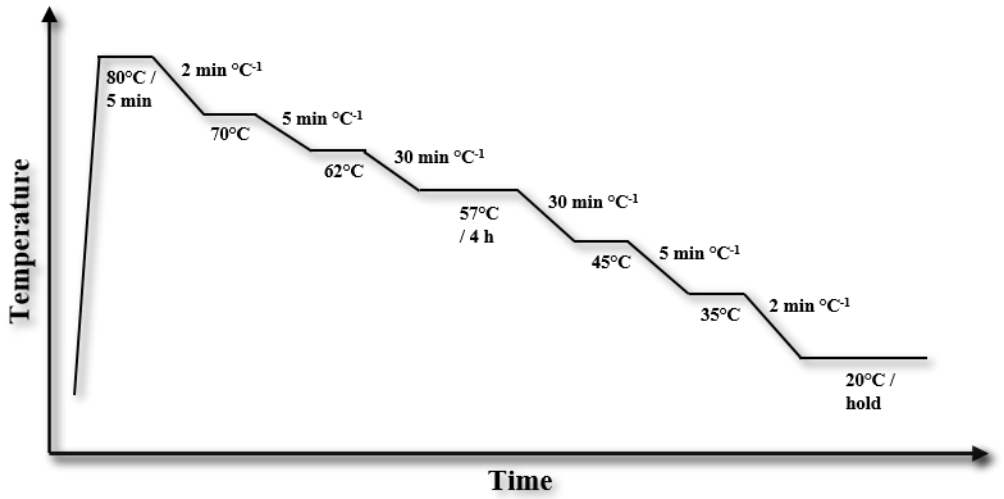

Figure 29: Thermal annealing ramp of box. Upon initial denaturation of all sequences, a careful cooling ramp over a sufficiently long timespan was used in order to ensure correct folding of the structure.

4.2.2 Preparation of the scaffold

For the assembly of the presented DNA nanostructures, a long circular, single-stranded DNA scaffold is needed. For rect, the scaffold p7249 was chosen, which is identical to the m13mp18 phage vector. For box, p8064, a derivative of the aforementioned, was used. Both scaffolds were prepared in the same way, as previously reported.[226,232]

Briefly, 25 µL of competent *E. coli* XL1-Blue cells were obtained from the freezer and allowed to thaw. 5 µL of the respective plasmid (p7249 or p8064) were added to a final concentration of about 20 nM. The solution was incubated on ice for 10 min. Afterwards, cells were heat shocked at 42 °C for 30 seconds and put back on ice for another 5 minutes. 1 mL of recovery medium was added, and cells were incubated at 37 °C while shaking at 600 rpm for 60 min. 200 µL of this solution was plated onto X-Gal selection plates (Standard agar plates supplemented with X-Gal, IPTG and tetracycline). Plates were placed in an incubator at 37 °C overnight. In parallel, a liquid overnight culture was prepared by scraping -80°C XL1-Blue cells from a glycerol stock and inoculating 200 mL of NZA medium (including tetracycline). Cells were incubated at 37°C while shaking at 120 rpm.

Next day, 3 l of 2x YT medium (with tetracycline) were inoculated with the overnight culture in a 1:40 ratio. Cells were allowed to grow to an OD of about 0.3. At this point, plaques from the X-Gal selection plate were scraped off, employing the open end of a pipette tip and

used for the inoculation of the 3 l cell culture. The culture was grown for another 4 hours at 37 °C while shaking. Subsequently, cells were pelleted by centrifugation (4,000 rcf, 4 °C, 15 min). The supernatant (containing the phage) was taken and further supplemented with PEG8000 (40 g/l) and NaCl (30 g/l) in order to precipitate phage particles. The solution was cooled in an ice bath and incubated, while stirring, for 45 minutes, until the solution appeared cloudy. Afterwards, the solution was centrifuged again (4,000 rcf, 4 °C, 15 min). The supernatant was discarded, and the phage pellet resuspended in 20 mL 10 mM Tris (pH 8.5). Residual *E. coli* cells were cleared out by centrifugation at 21,000 rcf for 15 min at 4 °C. Supernatant was transferred to a new tube and stored at -20 °C until the next day.

To lyse the phages, 2 volumes of lysis buffer (Macherey Nagel) were added. The solution was gently mixed by inversion. Subsequently, 1.5 volumes of neutralization buffer were added and again, the solution was mixed by inversion. Afterwards, the solution was incubated on ice for 15 minutes and then centrifuged at 16,000 rcf for 10 min at 4 °C. The supernatant was transferred to a new flask and 1 volume of absolute ethanol was added in order to precipitate phage DNA. The solution was centrifuged at 16,000 rcf for 15 min at 4 °C. The supernatant was discarded, and pelleted DNA was washed twice with 75 % ethanol. Finally, the pellet was resuspended in a suitable amount of 10 mM Tris buffer (pH 8.5) and the concentration was determined by spectrometry (Nanodrop, DeNovix).

To verify the purity and correct sequence of isolated phage DNA, samples were sent to a sequencing lab (GATC) with suitable primers for sequencing (Primers 1-20, see 6.3). Evaluation of sequencing results was done by using the CodonCode aligner software (CodonCode Corp.).

4.2.3 Agarose gel electrophoresis

Agarose gel electrophoresis was performed using 1 % agarose (Lonza) gels in 1X TBEMg buffer (40 mM tris base, 20 mM Boric acid, 2 mM EDTA, 12.5 mM Mg acetate, pH 8.0). Electrophoresis was run at 80 V for 2 h in an ice-water bath. Gels were scanned with a Typhoon FLA9000 (GE healthcare Life Sciences) at different wavelengths, depending on the fluorophores. Finally, gels were stained and imaged with EtBr.

4.2.4 Purification of DNA nanostructures

If not stated otherwise, DNA origami structures were purified using PEG (Poly(ethylene glycol)) purification. This method can be used for purification or buffer exchange purposes.[233] The PEG-induced precipitation approach relies on the depletion of high-molecular-weight species by excluded volume effects. Importantly, this method cannot be used to separate DNA origami monomers from dimers, since both have high molecular weight. Staple strands and other smaller molecules as e.g. proteins are however efficiently removed. Briefly, one volume of PEG buffer (5 mM Tris base, 1 mM EDTA, 505 mM NaCl, 15 % PEG8000 (w/v)) was supplemented with $MgCl_2$ so that the final Mg concentration was the same as in the DNA origami sample. Then, PEG buffer and sample were mixed in a 1:1 ratio and mixed by inversion. Following, the mixture was centrifuged for 25 min at 16,000 rcf at room temperature. The supernatant was removed, and the pellet dissolved in a suitable amount of TEMg buffer overnight.

4.2.5 Quantification of DNA nanostructures

DNA nanostructures were quantified using either the DS-11 Spectrophotometer FX+ (DeNovix) by measuring the concentration of ds DNA, or by means of qRT-PCR. In the latter case, a specific TaqMan probe, i.e. an oligonucleotide containing a fluorophore and a quencher, targeting the m13mp18 backbone, was designed (Thermo Fisher scientific). Upon replication of the target sequence, the polymerase disintegrates the probe and the fluorophore is freed, thereby generating a fluorescent readout signal. A calibration curve was obtained by using a serial dilution of the m13mp18 plasmid and fitted to a linear function with which the concentration of the sample could be calculated. The instrument used was a CFX96 real time system. The software was the CFX Manager™ 3.0 (BioRad). Running parameters are listed in Table 2 and Table 3.

Table 2: Reaction mixture for qRT-PCR.

Reagents	Volume [µL]
Mastermix (#4369016)	10
Assay-Mix (#4331348)	1
DNAse free water	7
DNA origami sample	2

Table 3: qRT-PCR cycle parameters.

Time	Temperature [°C]	Cycles
2 min	50	1
10 min	95	1
15 sec	95	40
1 min	60	40

4.2.6 Atomic Force Microscopy

Imaging of DNA nanostructures via AFM was performed by depositing the sample on a freshly cleaved mica surface. The sample was allowed to absorb to the surface for 3 min. Samples were scanned in ScanAsyst PeakForce Tapping Mode using a MultiMode™ microscope (Bruker) equipped with a Nanoscope V controller. ScanAsyst Fluid+, with sharpened pyramidal tips, in 1X TEMg buffer, were used for imaging. Images were acquired from different locations of the mica to ensure reproducibility. All images were analyzed with the NanoScope Analysis 1.5 software.

4.2.7 Transmission electron microscopy

For TEM analysis, 5 µL of sample was deposited onto glow charged (30 s, 15 µA, 25 mbar) 400 mesh carbon-coated copper grids (Quantifoil) and allowed to absorb to the surface for 2 min. Excess liquid was blotted off. The sample was washed with 5 µL of 1 % uranyl

formate staining solution and then incubated for 2 min with staining solution. Finally, the stain was blotted off and the sample was allowed to air dry. TEM imaging was carried out with a JOEL JEM 1400+ instrument, at 120 kV.

4.2.8 Protein labeling

To minimize the effect of attached fluorophores on the binding of thrombin to the DNA nanostructures, the labeling reaction was carried out in a 1:5 ratio of thrombin to fluorophore. Therefore, 150 µL of thrombin stock solution (≈ 8.7 µM) were mixed with 1 µL of 6.4 mM NHS-A488 dye (ThermoFisher). Samples were incubated at room temperature for 1 h, protected from light. The buffer used was the thrombin storage buffer (5 mM sodium citrate, 20 mM NaCl, 0.01 % (w/v) PEG8000, pH 6.5). Excess fluorophores were removed by using dye-removal columns (ThermoFisher) according to the manufacturer's instructions.

4.2.9 SDS-PAGE

Autodigestion of thrombin was analyzed via SDS-PAGE. For the gel, acrylamide/bis solution (37.5:1, 30 % w/v, Sigma Aldrich) was used. For the stacking gel, a 4.5 % solution was used. For the resolving gel, a 12 % solution was used. Samples were supplemented with 5X SDS loading buffer, either containing DTT or not. Samples were heated for 5 min at 95 °C prior to loading. Gels were run in Mini-PROTEAN electrophoresis cells (BioRad) with 1X SDS-buffer, for 60 min at 200 V, ice cooled.

4.2.10 Thrombin binding to DNA origami structures

For the AFM analysis of thrombin binding to the DNA nanostructures, a 5 equimolar excess of thrombin over DNA origamis were used. The mixture was incubated for 1 h at room temperature and then PEG purified. The pellet was resuspended in 1X TEMg buffer over night and imaged the next day.

4.2.11 Enzymatic activity assay

For the kinetic analysis of thrombin, the enzyme (α-human thrombin, Cayman Chemicals, #13188, MW 38 kDa) was diluted in 1X TEMg buffer from its stock solution to 1.2 nM in the final reaction mixture (100 µL reaction volume). Depending on the experiment, free TBAs or PEG-purified DNA origamis (exceptions: 2 nM for ssDNA; 14.5 µM sodium phosphate (VWR Chemicals)) were added to reach a final 1 nM concentration. 50 µL of the mixture were added to each well of a 96-well plate (Corning, #3991). The mixture was incubated for 1 h at 37 °C. Finally, 50 µL of pre-warmed substrate was added to each well (Intavis, 0-25 µM final concentration, diluted in 1X TEMg buffer). Plates were immediately transferred to a plate reader (TECAN Spark10M) and the fluorescence signal was recorded over a time period of 80 min. The fluorescence signal was correlated to the amount of product by using a standard curve of substrate that contains no quencher. Each sample was measured as a triplicate. Time intervals of each measurement was 1 min. Data were analyzed with the OriginPro Software and the kinetic parameters were extracted using a nonlinear Michaelis-Menten fit. Running parameters are detailed in Table 4.

Table 4: TECAN running parameters for enzyme studies.

Parameter	Setting
Mode	Shaking
Shaking (Double Orbital) Duration	30 s
Shaking (Double Orbital) Position	Current
Shaking (Double Orbital) Amplitude	1.5 mm
Shaking (Double Orbital) Frequency	180 rpm
Mode	Kinetic
Kinetic cycles	80
Interval time	00:01:00 (hh:mm:ss)
Mode	Fluorescence top reading
Excitation	Monochromator
Excitation wavelength	482 nm

Excitation bandwidth	20 nm
Emission	Monochromator
Emission wavelength	20 nm
Gain	42
Mirror	Automatic
Number of flashes	30
Integration time	40 µs
Lag time	0 µs
Settle time	0 ms
Z-Position	18455 µm
Z-Position mode	Manual

4.2.12 Kinetic simulations

All kinetic simulations were performed using the DynaFit program, freely available at http://www.biokin.com/dynafit/suite. As depicted in Figure 25 a kinetically linked system was simulated with two kinetic fluxes. Starting parameters were the following: $[E]_0$ = 1.2 nM, $[DNA]_0$ = 1 nM. For the unbound thrombin pathway (E) the following rate coefficients were chosen: k_1 = 6,000 min^{-1} μM^{-1}, k_{-1} = 16,000 min^{-1}, k_2 = 100 min^{-1}, k_3 = 500 min^{-1}. These values were taken from literature for thrombin-catalyzed degradation of peptides in buffer conditions similar to those used in the experiments presented in this work.[210,224] Similar to the E pathway, the reaction of bound thrombin (E_{DNA}) was simulated with rate coefficients k_4, k_{-4}, k_5 and k_6. Values for these coefficients were chosen to be either equal, 100-fold or 0.01-fold the values of, respectively, k_1, k_{-1}, k_2 and k_3. Furthermore, the K_D value was varied for different simulations, with values being either 0.1 nM, 1 nM, 10 nM or 1 µM ($k_7 = k_8 = k_9$ = 10.000 min^{-1} μM^{-1} and, respectively, $k_{-7} = k_{-8} = k_{-9}$ = 1 min^{-1}, 10 min^{-1}, 100 min^{-1} and 10,000 min^{-1}). For simulations in Figure S 36, the rate coefficients of E_{DNA} were modified in order to simulate experimentally gained reaction rates of thrombin-catalyzed hydrolysis of either S(0) or S(+1). The K_D for these simulations was set to 1 nM.

4.2.13 Molecular dynamics simulations

Note: All molecular dynamics simulations were performed by coworkers of the group of Prof. Sánchez-García (acknowledged as co-authors of this article) (Faculty of Biology, University of Duisburg-Essen). Software used in these simulations are referenced in the respective descriptions of the method.

For the molecular dynamics simulations, the DNA origamis were simulated as a reduced, coarse-grained model, solvated in water, with the total number of particles being about 3 million. The SIRAH 2.0 force field[234] and the Gromacs 2019.2 software[235] were used for the simulations. Since no coarse-grained sodium ions fit into the ion binding pockets of the aptamers, harmonic restraints were used for the G-quadruplex structures. Three independent replicas of simulations were performed, each with a respective length of 120, 140 and 400 ns. Note that the simulations are set up with monovalent counter ions (i.e. Na^+ or Cl^-) instead of Mg^{2+}, since the SIRAH force field is parameterized for those. The initial coordinates of the protein/substrate model were extracted from the crystal structure of the dPhe-Pro-Arg fragment in complex with thrombin (PDB ID: 1PPB).[217] The peptide/thrombin systems were solvated in explicit TIP3P water molecules[236] and after equilibration they were subjected to three independent production runs of Gaussian accelerated Molecular Dynamics simulations (GaMD)[237] of 100 ns each. The simulations were done using a time step of 2 fs, at a constant pressure of 1 bar and a temperature of 300 K. The first 10 ns of production MD were discarded for the analysis of the trajectories. PME[238] was employed for the treatment of long-range electrostatic interactions. The simulations were performed using NAMD 2.13[239,240] and the CHARMM36m force field.[241,242] For the fluorophores, the parameters were obtained from the Swissparam server[243] and the Match server[244] except for the diazo region for which parameters from the literature were used.[245] For the visualization and analysis of the simulations the program VMD 1.9.3[246] was employed. A cut-off of 5.0 Å for the RMSD was used for the clustering analysis.

5 References

1. Feynman, R. P. There's plenty of room at the bottom. *Engineering and Science magazine* **18** (1960).
2. Eichenlaub, M. Answer to: What did Richard Feynman mean when he said, "What I cannot create, I do not understand"? Available at https://www.quora.com/What-did-Richard-Feynman-mean-when-he-said-What-I-cannot-create-I-do-not-understand. Last visited 02.2022.
3. Drexler, K. E. *Engines of Creation: The Coming Era of Nanotechnology* (New York, 1987).
4. Ron, M., Milo, R. & Phillips, R. *Cell biology by the numbers* (Garland Science Taylor & Francis Group, New York, NY, Abingdon, 2016).
5. Born, M., Wolf, E. & Knight, P. *Principles of optics.* 60th ed. (Cambridge University Press, Cambridge, 2019).
6. Gray, H. B. & Winkler, J. R. Electron tunneling through proteins. *Quarterly reviews of biophysics* **36,** 341–372; 10.1017/S0033583503003913 (2003).
7. Nagel, Z. D. & Klinman, J. P. Tunneling and Dynamics in Enzymatic Hydride Transfer. *ChemInform* **37**; 10.1002/chin.200643274 (2006).
8. Hänggi, P. & Marchesoni, F. Artificial Brownian motors: Controlling transport on the nanoscale. *Rev. Mod. Phys.* **81,** 387–442; 10.1103/RevModPhys.81.387 (2009).
9. Nishiyama, M., Muto, E., Inoue, Y., Yanagida, T. & Higuchi, H. Substeps within the 8-nm step of the ATPase cycle of single kinesin molecules. *Nature cell biology* **3,** 425–428; 10.1038/35070116 (2001).
10. Kaiser, A. B. & Skákalová, V. Electronic conduction in polymers, carbon nanotubes and graphene. *Chemical Society reviews* **40,** 3786–3801; 10.1039/c0cs00103a (2011).
11. Burda, C., Chen, X., Narayanan, R. & El-Sayed, M. A. Chemistry and properties of nanocrystals of different shapes. *Chemical reviews* **105,** 1025–1102; 10.1021/cr030063a (2005).
12. Sundaram, D. S., Yang, V. & Zarko, V. E. Combustion of nano aluminum particles (Review). *Combust Explos Shock Waves* **51,** 173–196; 10.1134/S0010508215020045 (2015).
13. Xu, L., Liang, H.-W., Yang, Y. & Yu, S.-H. Stability and Reactivity: Positive and Negative Aspects for Nanoparticle Processing. *Chemical reviews* **118,** 3209–3250; 10.1021/acs.chemrev.7b00208 (2018).
14. Kokarneswaran, M. *et al.* Discovery of carbon nanotubes in sixth century BC potteries from Keeladi, India. *Scientific reports* **10,** 19786; 10.1038/s41598-020-76720-z (2020).
15. Graham, T. Liquid diffusion applied to analysis. *Phil. Trans. R. Soc.* **151,** 183–224; 10.1098/rstl.1861.0011 (1861).
16. Faraday, M. The Bakerian Lecture. —Experimental relations of gold (and other metals) to light. *Phil. Trans. R. Soc.* **147,** 145–181; 10.1098/rstl.1857.0011 (1857).

17. Binnig, G. & Rohrer, H. Scanning tunneling microscopy. *Surface Science* **126,** 236–244; 10.1016/0039-6028(83)90716-1 (1983).

18. Binnig, Quate & Gerber. Atomic force microscope. *Physical review letters* **56,** 930–933; 10.1103/PhysRevLett.56.930 (1986).

19. Kroto, H. W., Heath, J. R., O'Brien, S. C., Curl, R. F. & Smalley, R. E. C60: Buckminsterfullerene. *Nature* **318,** 162–163; 10.1038/318162a0 (1985).

20. Knoll, M. & Ruska, E. Das Elektronenmikroskop. *Z. Physik* **78,** 318–339; 10.1007/BF01342199 (1932).

21. Jeanmaire, D. L. & van Duyne, R. P. Surface raman spectroelectrochemistry. *Journal of Electroanalytical Chemistry and Interfacial Electrochemistry* **84,** 1–20; 10.1016/S0022-0728(77)80224-6 (1977).

22. Eigler, D. M. & Schweizer, E. K. Positioning single atoms with a scanning tunnelling microscope. *Nature* **344,** 524–526; 10.1038/344524a0 (1990).

23. Drexler, E. K. & Smalley, R. E. Nanotechnology: Drexler and Smalley make the case for and against 'molecular assemblers'. *American Chemical Society* **81,** 37–42; 10.1021/cen-v081n036.p037 (2003).

24. Serrano, E., Rus, G. & García-Martínez, J. Nanotechnology for sustainable energy. *Renewable and Sustainable Energy Reviews* **13,** 2373–2384; 10.1016/j.rser.2009.06.003 (2009).

25. Santos, A. C. *et al.* Nanotechnology for the development of new cosmetic formulations. *Expert opinion on drug delivery* **16,** 313–330; 10.1080/17425247.2019.1585426 (2019).

26. Jaggessar, A., Shahali, H., Mathew, A. & Yarlagadda, P. K. D. V. Bio-mimicking nano and micro-structured surface fabrication for antibacterial properties in medical implants. *Journal of nanobiotechnology* **15,** 64; 10.1186/s12951-017-0306-1 (2017).

27. Li, X. *et al.* Surface treatments on titanium implants via nanostructured ceria for antibacterial and anti-inflammatory capabilities. *Acta biomaterialia* **94,** 627–643; 10.1016/j.actbio.2019.06.023 (2019).

28. Gao, H., Jian, Y. & Yan, Y. The effects of bio-inspired micro/nano scale structures on anti-icing properties. *Soft matter* **17,** 447–466; 10.1039/d0sm01683g (2021).

29. Burke, A. *et al.* Long-term survival following a single treatment of kidney tumors with multiwalled carbon nanotubes and near-infrared radiation. *Proceedings of the National Academy of Sciences of the United States of America* **106,** 12897–12902; 10.1073/pnas.0905195106 (2009).

30. Abadeer, N. S. & Murphy, C. J. Recent Progress in Cancer Thermal Therapy Using Gold Nanoparticles. *J. Phys. Chem. C* **120,** 4691–4716; 10.1021/acs.jpcc.5b11232 (2016).

31. Huh, A. J. & Kwon, Y. J. "Nanoantibiotics": a new paradigm for treating infectious diseases using nanomaterials in the antibiotics resistant era. *Journal of controlled release : official journal of the Controlled Release Society* **156,** 128–145; 10.1016/j.jconrel.2011.07.002 (2011).

32. Osman, N. *et al.* Surface modification of nano-drug delivery systems for enhancing antibiotic delivery and activity. *Wiley interdisciplinary reviews. Nanomedicine and nanobiotechnology* **14,** e1758; 10.1002/wnan.1758 (2022).

33. Li, S. *et al.* A DNA nanorobot functions as a cancer therapeutic in response to a molecular trigger in vivo. *Nature biotechnology* **36,** 258–264; 10.1038/nbt.4071 (2018).

34. Tran, V., Walkenfort, B., König, M., Salehi, M. & Schlücker, S. Rapid, Quantitative, and Ultrasensitive Point-of-Care Testing: A Portable SERS Reader for Lateral Flow Assays in Clinical Chemistry. *Angewandte Chemie (International ed. in English)* **58,** 442–446; 10.1002/anie.201810917 (2019).

35. Lew, T. T. S. *et al.* Epitope-Functionalized Gold Nanoparticles for Rapid and Selective Detection of SARS-CoV-2 IgG Antibodies. *ACS nano*; 10.1021/acsnano.1c04091 (2021).

36. Lee, H. *et al.* Sub-5nm All-Around Gate FinFET for Ultimate Scaling. In *2006 Symposium on VLSI Technology, 2006. Digest of Technical Papers* (IEEETuesday, June 13, 2006), pp. 58–59.

37. IBM. IBM Unveils World's First 2 Nanometer Chip Technology, Opening a New Frontier for Semiconductors. Available at https://newsroom.ibm.com/2021-05-06-IBM-Unveils-Worlds-First-2-Nanometer-Chip-Technology,-Opening-a-New-Frontier-for-Semiconductors (Last visited 2022).

38. Biswas, A. *et al.* Advances in top-down and bottom-up surface nanofabrication: techniques, applications & future prospects. *Advances in colloid and interface science* **170,** 2–27; 10.1016/j.cis.2011.11.001 (2012).

39. Seeman, N. C. & Belcher, A. M. Emulating biology: building nanostructures from the bottom up. *Proceedings of the National Academy of Sciences of the United States of America* **99 Suppl 2,** 6451–6455; 10.1073/pnas.221458298 (2002).

40. Wong, T.-S., Brough, B. & Ho, C.-M. Creation of Functional Micro/Nano Systems through Top-down and Bottom-up Approaches. *Molecular & cellular biomechanics : MCB* **6,** 1–55 (2009).

41. KENDREW, J. C. *et al.* A three-dimensional model of the myoglobin molecule obtained by x-ray analysis. *Nature* **181,** 662–666; 10.1038/181662a0 (1958).

42. Jumper, J. *et al.* Highly accurate protein structure prediction with AlphaFold. *Nature* **596,** 583–589; 10.1038/s41586-021-03819-2 (2021).

43. CRICK, F. H., BARNETT, L., BRENNER, S. & WATTS-TOBIN, R. J. General nature of the genetic code for proteins. *Nature* **192,** 1227–1232; 10.1038/1921227a0 (1961).

44. Richmond, T. J. & Davey, C. A. The structure of DNA in the nucleosome core. *Nature* **423,** 145–150; 10.1038/nature01595 (2003).

45. WATSON, J. D. & CRICK, F. H. Molecular structure of nucleic acids; a structure for deoxyribose nucleic acid. *Nature* **171,** 737–738; 10.1038/171737a0 (1953).

46. Yakovchuk, P., Protozanova, E. & Frank-Kamenetskii, M. D. Base-stacking and base-pairing contributions into thermal stability of the DNA double helix. *Nucleic acids research* **34,** 564–574; 10.1093/nar/gkj454 (2006).

47. Sponer, J. *et al.* Nature and magnitude of aromatic base stacking in DNA and RNA: Quantum chemistry, molecular mechanics, and experiment. *Biopolymers* **99,** 978–988; 10.1002/bip.22322 (2013).

48. *DNA. Das Molekül und seine Funktionsweise.* 3rd ed. (Elsevier Spektrum Akad. Verl., Heidelberg, München, 2006).

49. Jaekel, A., Lill, P., Whitelam, S. & Saccà, B. Insights into the Structure and Energy of DNA Nanoassemblies. *Molecules (Basel, Switzerland)* **25**; 10.3390/molecules25235466 (2020).

50. Kallenbach, N. R., Ma, R.-I. & Seeman, N. C. An immobile nucleic acid junction constructed from oligonucleotides. *Nature* **305,** 829–831; 10.1038/305829a0 (1983).

51. Fu, T. J. & Seeman, N. C. DNA double-crossover molecules. *Biochemistry* **32,** 3211–3220; 10.1021/bi00064a003 (1993).

52. Pillers, M. A. & Lieberman, M. Thermal stability of DNA origami on mica. *Journal of Vacuum Science & Technology B, Nanotechnology and Microelectronics: Materials, Processing, Measurement, and Phenomena* **32,** 40602; 10.1116/1.4879417 (2014).

53. Nizioł, J. *et al.* Thermal stability of the solid DNA as a novel optical material. *Optical Materials* **66,** 344–350; 10.1016/j.optmat.2017.02.035 (2017).

54. Kielar, C. *et al.* On the Stability of DNA Origami Nanostructures in Low-Magnesium Buffers. *Angewandte Chemie (International ed. in English)* **57,** 9470–9474; 10.1002/anie.201802890 (2018).

55. Ramakrishnan, S., Ijäs, H., Linko, V. & Keller, A. Structural stability of DNA origami nanostructures under application-specific conditions. *Computational and structural biotechnology journal* **16,** 342–349; 10.1016/j.csbj.2018.09.002 (2018).

56. JOHN SANTALUCIA, JR. A unified view of DNA nearest-neighbor thermodynamics. SantaLucia. 1997.

57. Seeman, N. C. & Sleiman, H. F. DNA nanotechnology. *Nat Rev Mater* **3**; 10.1038/natrevmats.2017.68 (2018).

58. Sigma Aldrich. *Custom DNA Oligo Synthesis (last accessed: 04.02.2022)*. Available at https://www.sigmaaldrich.com/DE/de/configurators/tube?product=standard ,

59. Kuhlman, B. & Bradley, P. Advances in protein structure prediction and design. *Nature reviews. Molecular cell biology* **20,** 681–697; 10.1038/s41580-019-0163-x (2019).

60. Ljubetič, A. *et al.* Design of coiled-coil protein-origami cages that self-assemble in vitro and in vivo. *Nature biotechnology* **35,** 1094–1101; 10.1038/nbt.3994 (2017).

61. Seeman, N. C. Nucleic acid junctions and lattices. *Journal of Theoretical Biology* **99,** 237–247; 10.1016/0022-5193(82)90002-9 (1982).

62. Liu, D., Park, S. H., Reif, J. H. & LaBean, T. H. DNA nanotubes self-assembled from triple-crossover tiles as templates for conductive nanowires. *Proceedings of the National Academy of Sciences of the United States of America* **101,** 717–722; 10.1073/pnas.0305860101 (2004).

63. LaBean, T. H. *et al.* Construction, Analysis, Ligation, and Self-Assembly of DNA Triple Crossover Complexes. *J. Am. Chem. Soc.* **122,** 1848–1860; 10.1021/ja993393e (2000).

64. He, Y., Tian, Y., Ribbe, A. E. & Mao, C. Highly connected two-dimensional crystals of DNA six-point-stars. *J. Am. Chem. Soc.* **128,** 15978–15979; 10.1021/ja0665141 (2006).

65. Yan, H., Park, S. H., Finkelstein, G., Reif, J. H. & LaBean, T. H. DNA-templated self-assembly of protein arrays and highly conductive nanowires. *Science (New York, N.Y.)* **301,** 1882–1884; 10.1126/science.1089389 (2003).

66. He, Y. *et al.* Sequence symmetry as a tool for designing DNA nanostructures. *Angewandte Chemie (International ed. in English)* **44,** 6694–6696; 10.1002/anie.200502193 (2005).

67. Ke, Y., Ong, L. L., Shih, W. M. & Yin, P. Three-dimensional structures self-assembled from DNA bricks. *Science (New York, N.Y.)* **338,** 1177–1183; 10.1126/science.1227268 (2012).

68. Agrawal, D. K. *et al.* Terminating DNA Tile Assembly with Nanostructured Caps. *ACS nano* **11,** 9770–9779; 10.1021/acsnano.7b02256 (2017).

69. Rothemund, P. W. K. Folding DNA to create nanoscale shapes and patterns. *Nature* **440,** 297–302; 10.1038/nature04586 (2006).

70. Faber, J. A., Arrieta, A. F. & Studart, A. R. Bioinspired spring origami. *Science (New York, N.Y.)* **359,** 1386–1391 (2018).

71. Merali, Z. Profile: Zhong You. 'Origami engineer' flexes to create stronger, more agile materials. *Science (New York, N.Y.)* **332,** 1376–1377; 10.1126/science.332.6036.1376 (2011).

72. Yan, H., LaBean, T. H., Feng, L. & Reif, J. H. Directed nucleation assembly of DNA tile complexes for barcode-patterned lattices. *Proceedings of the National Academy of Sciences of the United States of America* **100,** 8103–8108; 10.1073/pnas.1032954100 (2003).

73. Shih, W. M., Quispe, J. D. & Joyce, G. F. A 1.7-kilobase single-stranded DNA that folds into a nanoscale octahedron. *Nature* **427,** 618–621; 10.1038/nature02307 (2004).

74. Gerling, T., Wagenbauer, K. F., Neuner, A. M. & Dietz, H. Dynamic DNA devices and assemblies formed by shape-complementary, non-base pairing 3D components. *Science (New York, N.Y.)* **347,** 1446–1452; 10.1126/science.aaa5372 (2015).

75. Pfeifer, W., Lill, P., Gatsogiannis, C. & Saccà, B. Hierarchical Assembly of DNA Filaments with Designer Elastic Properties. *ACS nano* **12,** 44–55; 10.1021/acsnano.7b06012 (2018).

76. Dietz, H., Douglas, S. M. & Shih, W. M. Folding DNA into twisted and curved nanoscale shapes. *Science (New York, N.Y.)* **325,** 725–730; 10.1126/science.1174251 (2009).

77. Martin, T. G. & Dietz, H. Magnesium-free self-assembly of multi-layer DNA objects. *Nature communications* **3,** 1103; 10.1038/ncomms2095 (2012).

78. Ke, Y., Bellot, G., Voigt, N. V., Fradkov, E. & Shih, W. M. Two design strategies for enhancement of multilayer-DNA-origami folding: underwinding for specific intercalator rescue and staple-break positioning. *Chemical science* **3,** 2587–2597; 10.1039/C2SC20446K (2012).

79. Saccà, B. *et al.* Orthogonal protein decoration of DNA origami. *Angewandte Chemie (International ed. in English)* **49,** 9378–9383; 10.1002/anie.201005931 (2010).

80. Yurke, B., Turberfield, A. J., Mills, A. P., Simmel, F. C. & Neumann, J. L. A DNA-fuelled molecular machine made of DNA. *Nature* **406,** 605–608; 10.1038/35020524 (2000).

81. Simmel, F. C., Yurke, B. & Singh, H. R. Principles and Applications of Nucleic Acid Strand Displacement Reactions. *Chemical reviews* **119,** 6326–6369; 10.1021/acs.chemrev.8b00580 (2019).

82. Han, D. *et al.* DNA origami with complex curvatures in three-dimensional space. *Science (New York, N.Y.)* **332,** 342–346; 10.1126/science.1202998 (2011).

83. Douglas, S. M. *et al.* Self-assembly of DNA into nanoscale three-dimensional shapes. *Nature* **459,** 414–418; 10.1038/nature08016 (2009).

84. Liedl, T., Högberg, B., Tytell, J., Ingber, D. E. & Shih, W. M. Self-assembly of three-dimensional prestressed tensegrity structures from DNA. *Nature nanotechnology* **5,** 520–524; 10.1038/nnano.2010.107 (2010).

85. Grome, M. W., Zhang, Z., Pincet, F. & Lin, C. Vesicle Tubulation with Self-Assembling DNA Nanosprings. *Angewandte Chemie (International ed. in English)* **57,** 5330–5334; 10.1002/anie.201800141 (2018).

86. Selnihhin, D., Sparvath, S. M., Preus, S., Birkedal, V. & Andersen, E. S. Multifluorophore DNA Origami Beacon as a Biosensing Platform. *ACS nano* **12,** 5699–5708; 10.1021/acsnano.8b01510 (2018).

87. Acuna, G. P. *et al.* Fluorescence enhancement at docking sites of DNA-directed self-assembled nanoantennas. *Science (New York, N.Y.)* **338,** 506–510; 10.1126/science.1228638 (2012).

88. Shen, X. *et al.* Three-dimensional plasmonic chiral tetramers assembled by DNA origami. *Nano letters* **13,** 2128–2133; 10.1021/nl400538y (2013).

89. Sprengel, A. *et al.* Tailored protein encapsulation into a DNA host using geometrically organized supramolecular interactions. *Nature communications* **8,** 14472; 10.1038/ncomms14472 (2017).

90. Ijäs, H., Hakaste, I., Shen, B., Kostiainen, M. A. & Linko, V. Reconfigurable DNA Origami Nanocapsule for pH-Controlled Encapsulation and Display of Cargo. *ACS nano* **13,** 5959–5967; 10.1021/acsnano.9b01857 (2019).

91. Shawn M. Douglas, Ido Bachelet, George M. Church. A Logic-Gated Nanorobot for Targeted Transport of Molecular Payloads. *Science (New York, N.Y.)* **335,** 828–831; 10.1126/science.1216697 (2012).

92. Hemmig, E. A. *et al.* Programming Light-Harvesting Efficiency Using DNA Origami. *Nano letters* **16,** 2369–2374; 10.1021/acs.nanolett.5b05139 (2016).

93. Stein, I. H., Steinhauer, C. & Tinnefeld, P. Single-molecule four-color FRET visualizes energy-transfer paths on DNA origami. *J. Am. Chem. Soc.* **133,** 4193–4195; 10.1021/ja1105464 (2011).

94. Erkelenz, M., Kuo, C.-H. & Niemeyer, C. M. DNA-mediated assembly of cytochrome P450 BM3 subdomains. *J. Am. Chem. Soc.* **133,** 16111–16118; 10.1021/ja204993s (2011).

95. Ke, G. *et al.* Directional Regulation of Enzyme Pathways through the Control of Substrate Channeling on a DNA Origami Scaffold. *Angewandte Chemie (International ed. in English)* **55,** 7483–7486; 10.1002/anie.201603183 (2016).

96. Derr, N. D. *et al.* Tug-of-war in motor protein ensembles revealed with a programmable DNA origami scaffold. *Science (New York, N.Y.)* **338,** 662–665; 10.1126/science.1226734 (2012).

97. Nickels, P. C. *et al.* Molecular force spectroscopy with a DNA origami-based nanoscopic force clamp. *Science (New York, N.Y.)* **354,** 305–307; 10.1126/science.aah5974 (2016).

98. Kosuri, P., Altheimer, B. D., Dai, M., Yin, P. & Zhuang, X. Rotation tracking of genome-processing enzymes using DNA origami rotors. *Nature* **572,** 136–140; 10.1038/s41586-019-1397-7 (2019).

99. Ketterer, P., Willner, E. M. & Dietz, H. Nanoscale rotary apparatus formed from tight-fitting 3D DNA components. *Science advances* **2,** e1501209; 10.1126/sciadv.1501209 (2016).

100. Lund, K. *et al.* Molecular robots guided by prescriptive landscapes. *Nature* **465,** 206–210; 10.1038/nature09012 (2010).

101. Erkelenz, M. *et al.* A facile method for preparation of tailored scaffolds for DNA-origami. *Small* **10,** 73–77; 10.1002/smll.201300701 (2014).

102. Engelhardt, F. A. S. *et al.* Custom-Size, Functional, and Durable DNA Origami with Design-Specific Scaffolds. *ACS nano* **13,** 5015–5027; 10.1021/acsnano.9b01025 (2019).

103. Marchi, A. N., Saaem, I., Vogen, B. N., Brown, S. & LaBean, T. H. Toward larger DNA origami. *Nano letters* **14,** 5740–5747; 10.1021/nl502626s (2014).

104. Tikhomirov, G., Petersen, P. & Qian, L. Fractal assembly of micrometre-scale DNA origami arrays with arbitrary patterns. *Nature* **552,** 67–71; 10.1038/nature24655 (2017).

105. Wagenbauer, K. F., Sigl, C. & Dietz, H. Gigadalton-scale shape-programmable DNA assemblies. *Nature* **552,** 78–83; 10.1038/nature24651 (2017).

106. Zhang, T. *et al.* 3D DNA Origami Crystals. *Advanced materials (Deerfield Beach, Fla.)* **30,** e1800273; 10.1002/adma.201800273 (2018).

107. Pfeifer, W. & Saccà, B. From Nano to Macro through Hierarchical Self-Assembly: The DNA Paradigm. *Chembiochem : a European journal of chemical biology* **17,** 1063–1080; 10.1002/cbic.201600034 (2016).

108. Manchester, K. L. Louis Pasteur (1822–1895) — chance and the prepared mind. *Trends in biotechnology* **13,** 511–515; 10.1016/S0167-7799(00)89014-9 (1995).

109. Fersht, A. *Enzyme structure and mechanism.* 2nd ed. (Freeman, New York, 1995).

110. Meghwanshi, G. K. *et al.* Enzymes for pharmaceutical and therapeutic applications. *Biotechnology and applied biochemistry* **67,** 586–601; 10.1002/bab.1919 (2020).

111. Liu, X. & Kokare, C. Microbial Enzymes of Use in Industry. In *Biotechnology of Microbial Enzymes* (Elsevier2017), pp. 267–298.

112. Li, S., Yang, X., Yang, S., Zhu, M. & Wang, X. Technology prospecting on enzymes: application, marketing and engineering. *Computational and structural biotechnology journal* **2,** e201209017; 10.5936/csbj.201209017 (2012).

113. Mateo, C., Palomo, J. M., Fernandez-Lorente, G., Guisan, J. M. & Fernandez-Lafuente, R. Improvement of enzyme activity, stability and selectivity via immobilization techniques. *Enzyme and Microbial Technology* **40,** 1451–1463; 10.1016/j.enzmictec.2007.01.018 (2007).

114. Guzik, U., Hupert-Kocurek, K. & Wojcieszyńska, D. Immobilization as a strategy for improving enzyme properties-application to oxidoreductases. *Molecules (Basel, Switzerland)* **19,** 8995–9018; 10.3390/molecules19078995 (2014).

115. Martin, W. Evolutionary origins of metabolic compartmentalization in eukaryotes. *Philosophical transactions of the Royal Society of London. Series B, Biological sciences* **365,** 847–855; 10.1098/rstb.2009.0252 (2010).

116. Katchalski, E., Silman, I. & Goldman, R. Effect of the microenvironment on the mode of action of immobilized enzymes. *Advances in enzymology and related areas of molecular biology* **34,** 445–536; 10.1002/9780470122792.ch7 (1971).

117. Chen, A. H. & Silver, P. A. Designing biological compartmentalization. *Trends in cell biology* **22,** 662–670; 10.1016/j.tcb.2012.07.002 (2012).

118. Fruk, L., Müller, J. & Niemeyer, C. M. Kinetic analysis of semisynthetic peroxidase enzymes containing a covalent DNA-heme adduct as the cofactor. *Chemistry (Weinheim an der Bergstrasse, Germany)* **12,** 7448–7457; 10.1002/chem.200501613 (2006).

119. Glettenberg, M. & Niemeyer, C. M. Tuning of peroxidase activity by covalently tethered DNA oligonucleotides. *Bioconjugate chemistry* **20,** 969–975; 10.1021/bc800558g (2009).

120. Rudiuk, S., Venancio-Marques, A. & Baigl, D. Enhancement and modulation of enzymatic activity through higher-order structural changes of giant DNA-protein multibranch conjugates. *Angewandte Chemie (International ed. in English)* **51,** 12694–12698; 10.1002/anie.201206962. (2012).

121. Knözinger, H. & Kochloefl, K. Heterogeneous Catalysis and Solid Catalysts. In *Ullmann's Encyclopedia of Industrial Chemistry* (Wiley-VCH Verlag GmbH & Co. KGaA, Weinheim, Germany, 2000).

122. Lin, J.-L. & Wheeldon, I. Kinetic Enhancements in DNA–Enzyme Nanostructures Mimic the Sabatier Principle. *ACS Catal.* **3,** 560–564; 10.1021/cs300766d (2013).

123. Gao, Y., Roberts, C. C., Toop, A., Chang, C.-E. A. & Wheeldon, I. Mechanisms of Enhanced Catalysis in Enzyme-DNA Nanostructures Revealed through Molecular Simulations and Experimental Analysis. *Chembiochem : a European journal of chemical biology* **17,** 1430–1436; 10.1002/cbic.201600224 (2016).

124. Zhao, Z. *et al.* Nanocaged enzymes with enhanced catalytic activity and increased stability against protease digestion. *Nature communications* **7,** 10619; 10.1038/ncomms10619 (2016).

125. Timm, C. & Niemeyer, C. M. Assembly and purification of enzyme-functionalized DNA origami structures. *Angewandte Chemie (International ed. in English)* **54,** 6745–6750; 10.1002/anie.201500175 (2015).

126. Zhao, H. *et al.* Effect of kosmotropicity of ionic liquids on the enzyme stability in aqueous solutions. *Bioorganic chemistry* **34,** 15–25; 10.1016/j.bioorg.2005.10.004. (2006).

127. Levy, Y. & Onuchic, J. N. Water and proteins: a love-hate relationship. *Proceedings of the National Academy of Sciences of the United States of America* **101,** 3325–3326; 10.1073/pnas.0400157101 (2004).

128. Zhang, Y., Tsitkov, S. & Hess, H. Proximity does not contribute to activity enhancement in the glucose oxidase-horseradish peroxidase cascade. *Nature communications* **7,** 13982; 10.1038/ncomms13982 (2016).

129. Müller, J. & Niemeyer, C. M. DNA-directed assembly of artificial multienzyme complexes. *Biochemical and biophysical research communications* **377,** 62–67; 10.1016/j.bbrc.2008.09.078 (2008).

130. Fu, J. *et al.* Multi-enzyme complexes on DNA scaffolds capable of substrate channelling with an artificial swinging arm. *Nature nanotechnology* **9,** 531–536; 10.1038/nnano.2014.100 (2014).

131. Fu, J., Liu, M., Liu, Y., Woodbury, N. W. & Yan, H. Interenzyme substrate diffusion for an enzyme cascade organized on spatially addressable DNA nanostructures. *J. Am. Chem. Soc.* **134,** 5516–5519; 10.1021/ja300897h (2012).

132. Fu, Y. *et al.* Single-step rapid assembly of DNA origami nanostructures for addressable nanoscale bioreactors. *Journal of the American Chemical Society* **135,** 696–702; 10.1021/ja3076692 (2013).

133. Ge, Z. *et al.* Constructing Submonolayer DNA Origami Scaffold on Gold Electrode for Wiring of Redox Enzymatic Cascade Pathways. *ACS applied materials & interfaces* **11,** 13881–13887; 10.1021/acsami.8b12374 (2019).

134. Klein, W. P. *et al.* Enhanced Catalysis from Multienzyme Cascades Assembled on a DNA Origami Triangle. *ACS nano* **13,** 13677–13689; 10.1021/acsnano.9b05746 (2019).

135. Linko, V., Eerikäinen, M. & Kostiainen, M. A. A modular DNA origami-based enzyme cascade nanoreactor. *Chemical communications (Cambridge, England)* **51,** 5351–5354; 10.1039/c4cc08472a (2015).

136. Ngo, T. A., Nakata, E., Saimura, M. & Morii, T. Spatially Organized Enzymes Drive Cofactor-Coupled Cascade Reactions. *J. Am. Chem. Soc.* **138,** 3012–3021; 10.1021/jacs.5b10198 (2016).

137. Liu, M. *et al.* A Three-Enzyme Pathway with an Optimised Geometric Arrangement to Facilitate Substrate Transfer. *Chembiochem : a European journal of chemical biology* **17,** 1097–1101; 10.1002/cbic.201600103 (2016).

138. Srere, P. A. Complexes of sequential metabolic enzymes. *Annual review of biochemistry* **56,** 89–124; 10.1146/annurev.bi.56.070187.000513 (1987).

139. Küchler, A., Yoshimoto, M., Luginbühl, S., Mavelli, F. & Walde, P. Enzymatic reactions in confined environments. *Nature nanotechnology* **11,** 409–420; 10.1038/nnano.2016.54 (2016).

140. Sweetlove, L. J. & Fernie, A. R. The spatial organization of metabolism within the plant cell. *Annual review of plant biology* **64,** 723–746; 10.1146/annurev-arplant-050312-120233 (2013).

141. Wilner, O. I. *et al.* Enzyme cascades activated on topologically programmed DNA scaffolds. *Nature nanotechnology* **4,** 249–254; 10.1038/nnano.2009.50 (2009).

142. Wang, Z.-G., Wilner, O. I. & Willner, I. Self-assembly of aptamer-circular DNA nanostructures for controlled biocatalysis. *Nano letters* **9,** 4098–4102; 10.1021/nl902317p (2009).

143. Wilner, O. I., Shimron, S., Weizmann, Y., Wang, Z.-G. & Willner, I. Self-assembly of enzymes on DNA scaffolds: en route to biocatalytic cascades and the synthesis of metallic nanowires. *Nano letters* **9,** 2040–2043; 10.1021/nl900302z (2009).

144. Freeman, R., Sharon, E., Teller, C. & Willner, I. Control of biocatalytic transformations by programmed DNA assemblies. *Chemistry (Weinheim an der Bergstrasse, Germany)* **16,** 3690–3698; 10.1002/chem.200902559 (2010).

145. Lee, J. H. *et al.* Improved production of L-threonine in Escherichia coli by use of a DNA scaffold system. *Applied and environmental microbiology* **79,** 774–782; 10.1128/AEM.02578-12 (2013).

146. Sachdeva, G., Garg, A., Godding, D., Way, J. C. & Silver, P. A. In vivo co-localization of enzymes on RNA scaffolds increases metabolic production in a geometrically dependent manner. *Nucleic acids research* **42,** 9493–9503; 10.1093/nar/gku617 (2014).

147. Bashor, C. J., Helman, N. C., Yan, S. & Lim, W. A. Using engineered scaffold interactions to reshape MAP kinase pathway signaling dynamics. *Science (New York, N.Y.)* **319,** 1539–1543; 10.1126/science.1151153 (2008).

148. Dueber, J. E. *et al.* Synthetic protein scaffolds provide modular control over metabolic flux. *Nature biotechnology* **27,** 753–759; 10.1038/nbt.1557 (2009).

149. Xin, L., Zhou, C., Yang, Z. & Liu, D. Regulation of an enzyme cascade reaction by a DNA machine. *Small (Weinheim an der Bergstrasse, Germany)* **9,** 3088–3091; 10.1002/smll.201300019 (2013).

150. Perham, R. N. Swinging arms and swinging domains in multifunctional enzymes: catalytic machines for multistep reactions. *Annual review of biochemistry* **69,** 961–1004; 10.1146/annurev.biochem.69.1.961 (2000).

151. Yang, Y. R. *et al.* 2D Enzyme Cascade Network with Efficient Substrate Channeling by Swinging Arms. *Chembiochem : a European journal of chemical biology* **19,** 212–216; 10.1002/cbic.201700613 (2018).

152. Liu, M. *et al.* A DNA tweezer-actuated enzyme nanoreactor. *Nature communications* **4,** 2127; 10.1038/ncomms3127 (2013).

153. Chen, Y. *et al.* A Synthetic Light-Driven Substrate Channeling System for Precise Regulation of Enzyme Cascade Activity Based on DNA Origami. *Journal of the American Chemical Society* **140,** 8990–8996; 10.1021/jacs.8b05429 (2018).

154. Idan, O. & Hess, H. Origins of activity enhancement in enzyme cascades on scaffolds. *ACS nano* **7,** 8658–8665; 10.1021/nn402823k (2013).

155. Zhang, Y. & Hess, H. Toward Rational Design of High-efficiency Enzyme Cascades. *ACS Catal.* **7,** 6018–6027; 10.1021/acscatal.7b01766 (2017).

156. Dunn, M. F. *et al.* The tryptophan synthase bienzyme complex transfers indole between the alpha- and beta-sites via a 25-30 A long tunnel. *Biochemistry* **29,** 8598–8607; 10.1021/bi00489a015 (1990).

157. Korasick, D. A. *et al.* Structure and characterization of a class 3B proline utilization A: Ligand-induced dimerization and importance of the C-terminal domain for catalysis. *The Journal of biological chemistry* **292,** 9652–9665; 10.1074/jbc.M117.786855 (2017).

158. Jaekel, A., Stegemann, P. & Saccà, B. Manipulating Enzymes Properties with DNA Nanostructures. *Molecules (Basel, Switzerland)* **24**; 10.3390/molecules24203694 (2019).

159. SantaLucia, J. & Hicks, D. The thermodynamics of DNA structural motifs. *Annual review of biophysics and biomolecular structure* **33,** 415–440; 10.1146/annurev.biophys.32.110601.141800 (2004).

160. Howard, K. P. Thermodynamics of DNA Duplex Formation: A Biophysical Chemistry Laboratory Experiment. *J. Chem. Educ.* **77,** 1469; 10.1021/ed077p1469 (2000).

161. Hou, M. H. *et al.* Effects of polyamines on the thermal stability and formation kinetics of DNA duplexes with abnormal structure. *Nucleic acids research* **29,** 5121–5128; 10.1093/nar/29.24.5121 (2001).

162. Arbona, J. M., Elezgaray, J. & Aimé, J. P. Modelling the folding of DNA origami. *EPL* **100,** 28006; 10.1209/0295-5075/100/28006 (2012).

163. Arbona, J.-M., Aimé, J.-P. & Elezgaray, J. Cooperativity in the annealing of DNA origamis. *The Journal of chemical physics* **138,** 15105; 10.1063/1.4773405 (2013).

164. Anfinsen, C. B. Principles that govern the folding of protein chains. *Science (New York, N.Y.)* **181,** 223–230; 10.1126/science.181.4096.223 (1973).

165. Dunn, K. E. *et al.* Guiding the folding pathway of DNA origami. *Nature* **525,** 82–86; 10.1038/nature14860 (2015).

166. Wei, X., Nangreave, J., Jiang, S., Yan, H. & Liu, Y. Mapping the thermal behavior of DNA origami nanostructures. *J. Am. Chem. Soc.* **135,** 6165–6176; 10.1021/ja4000728 (2013).

167. Wei, X., Nangreave, J. & Liu, Y. Uncovering the self-assembly of DNA nanostructures by thermodynamics and kinetics. *Accounts of chemical research* **47,** 1861–1870; 10.1021/ar5000665 (2014).

168. Sobczak, J.-P. J., Martin, T. G., Gerling, T. & Dietz, H. Rapid folding of DNA into nanoscale shapes at constant temperature. *Science (New York, N.Y.)* **338,** 1458–1461; 10.1126/science.1229919 (2012).

169. Bae, W. *et al.* Programmed folding of DNA origami structures through single-molecule force control. *Nature communications* **5,** 5654; 10.1038/ncomms6654 (2014).

170. Endo, M. *et al.* Helical DNA origami tubular structures with various sizes and arrangements. *Angewandte Chemie (International ed. in English)* **53,** 7484–7490; 10.1002/anie.201402973 (2014).

171. Shrestha, P. *et al.* Mechanical properties of DNA origami nanoassemblies are determined by Holliday junction mechanophores. *Nucleic acids research* **44,** 6574–6582; 10.1093/nar/gkw610 (2016).

172. Hohng, S. *et al.* Fluorescence-force spectroscopy maps two-dimensional reaction landscape of the holliday junction. *Science (New York, N.Y.)* **318,** 279–283; 10.1126/science.1146113 (2007).

173. McKinney, S. A., Déclais, A.-C., Lilley, D. M. J. & Ha, T. Structural dynamics of individual Holliday junctions. *Nature structural biology* **10,** 93–97; 10.1038/nsb883 (2003).

174. Liu, Y. *et al.* Modular Reconfigurable DNA Origami: From Two-Dimensional to Three-Dimensional Structures. *Angewandte Chemie (International ed. in English)* **59,** 23277–23282; 10.1002/anie.202010433 (2020).

175. Cui, Y. *et al.* Versatile DNA Origami Nanostructures in Simplified and Modular Designing Framework. *ACS nano* **11,** 8199–8206; 10.1021/acsnano.7b03187 (2017).

176. Fan, S. *et al.* Spatiotemporal Control of Molecular Cascade Reactions by a Reconfigurable DNA Origami Domino Array. *Angewandte Chemie (International ed. in English)*, e202116324; 10.1002/anie.202116324 (2021).

177. Song, J. *et al.* Reconfiguration of DNA molecular arrays driven by information relay. *Science (New York, N.Y.)* **357**; 10.1126/science.aan3377 (2017).

178. Kosinski, R. *et al.* Sites of high local frustration in DNA origami. *Nature communications* **10,** 1061; 10.1038/s41467-019-09002-6 (2019).

179. Schlücker, S. Surface-enhanced Raman spectroscopy: concepts and chemical applications. *Angewandte Chemie (International ed. in English)* **53,** 4756–4795; 10.1002/anie.201205748 (2014).

180. Albrecht, M. G. & Creighton, J. A. Anomalously intense Raman spectra of pyridine at a silver electrode. *J. Am. Chem. Soc.* **99,** 5215–5217; 10.1021/ja00457a071 (1977).

181. Pérez-Jiménez, A. I., Lyu, D., Lu, Z., Liu, G. & Ren, B. Surface-enhanced Raman spectroscopy: benefits, trade-offs and future developments. *Chemical science* **11,** 4563–4577; 10.1039/d0sc00809e (2020).

182. Gardiner, D. J. Introduction to Raman Scattering. In *Practical Raman Spectroscopy*, edited by D. J. Gardiner & P. R. Graves (Springer Berlin Heidelberg, Berlin, Heidelberg, 1989), pp. 1–12.

183. Ding, S.-Y. *et al.* Nanostructure-based plasmon-enhanced Raman spectroscopy for surface analysis of materials. *Nat Rev Mater* **1**; 10.1038/natrevmats.2016.21 (2016).

184. Amendola, V., Pilot, R., Frasconi, M., Maragò, O. M. & Iatì, M. A. Surface plasmon resonance in gold nanoparticles: a review. *Journal of physics. Condensed matter : an Institute of Physics journal* **29,** 203002; 10.1088/1361-648X/aa60f3 (2017).

185. Yoon, J. H., Selbach, F., Langolf, L. & Schlücker, S. Ideal Dimers of Gold Nanospheres for Precision Plasmonics: Synthesis and Characterization at the Single-Particle Level for Identification of Higher Order Modes. *Small (Weinheim an der Bergstrasse, Germany)* **14**; 10.1002/smll.201702754 (2018).

186. Mirkin, C. A., Letsinger, R. L., Mucic, R. C. & Storhoff, J. J. A DNA-based method for rationally assembling nanoparticles into macroscopic materials. *Nature* **382,** 607–609; 10.1038/382607a0 (1996).

187. Zheng, J. *et al.* Two-dimensional nanoparticle arrays show the organizational power of robust DNA motifs. *Nano letters* **6,** 1502–1504; 10.1021/nl060994c (2006).

188. Sharma, J. *et al.* Control of self-assembly of DNA tubules through integration of gold nanoparticles. *Science (New York, N.Y.)* **323,** 112–116; 10.1126/science.1165831 (2009).

189. Aldaye, F. A., Palmer, A. L. & Sleiman, H. F. Assembling materials with DNA as the guide. *Science (New York, N.Y.)* **321,** 1795–1799; 10.1126/science.1154533 (2008).

190. Thacker, V. V. *et al.* DNA origami based assembly of gold nanoparticle dimers for surface-enhanced Raman scattering. *Nature communications* **5,** 3448; 10.1038/ncomms4448 (2014).

191. Tanwar, S., Haldar, K. K. & Sen, T. DNA Origami Directed Au Nanostar Dimers for Single-Molecule Surface-Enhanced Raman Scattering. *J. Am. Chem. Soc.* **139,** 17639–17648; 10.1021/jacs.7b10410 (2017).

192. Zhang, T., Gao, N., Li, S., Lang, M. J. & Xu, Q.-H. Single-Particle Spectroscopic Study on Fluorescence Enhancement by Plasmon Coupled Gold Nanorod Dimers Assembled on DNA Origami. *The journal of physical chemistry letters* **6,** 2043–2049; 10.1021/acs.jpclett.5b00747 (2015).

193. Tapio, K. *et al.* A Versatile DNA Origami-Based Plasmonic Nanoantenna for Label-Free Single-Molecule Surface-Enhanced Raman Spectroscopy. *ACS nano* **15,** 7065–7077; 10.1021/acsnano.1c00188 (2021).

194. Lan, X. *et al.* Au nanorod helical superstructures with designed chirality. *J. Am. Chem. Soc.* **137,** 457–462; 10.1021/ja511333q (2015).

195. Kuzyk, A. *et al.* Reconfigurable 3D plasmonic metamolecules. *Nature materials* **13,** 862–866; 10.1038/nmat4031 (2014).

196. Kuzyk, A. *et al.* DNA-based self-assembly of chiral plasmonic nanostructures with tailored optical response. *Nature* **483,** 311–314; 10.1038/nature10889 (2012).

197. Bayrak, T. *et al.* DNA-Mold Templated Assembly of Conductive Gold Nanowires. *Nano letters* **18,** 2116–2123; 10.1021/acs.nanolett.8b00344 (2018).

198. Zhou, C., Duan, X. & Liu, N. A plasmonic nanorod that walks on DNA origami. *Nature communications* **6,** 8102; 10.1038/ncomms9102 (2015).

199. Funck, T., Nicoli, F., Kuzyk, A. & Liedl, T. Sensing Picomolar Concentrations of RNA Using Switchable Plasmonic Chirality. *Angewandte Chemie (International ed. in English)* **57,** 13495–13498; 10.1002/anie.201807029 (2018).

200. Kosinski, R. *et al.* The role of DNA nanostructures in the catalytic properties of an allosterically regulated protease. *Science advances* **8,** eabk0425; 10.1126/sciadv.abk0425 (2022).

201. Schopf, J. W., Kudryavtsev, A. B., Czaja, A. D. & Tripathi, A. B. Evidence of Archean life: Stromatolites and microfossils. *Precambrian Research* **158,** 141–155; 10.1016/j.precamres.2007.04.009 (2007).

202. Bianconi, E. *et al.* An estimation of the number of cells in the human body. *Annals of human biology* **40,** 463–471; 10.3109/03014460.2013.807878 (2013).

203. Sender, R., Fuchs, S. & Milo, R. Revised Estimates for the Number of Human and Bacteria Cells in the Body. *PLoS biology* **14,** e1002533; 10.1371/journal.pbio.1002533 (2016).

204. Ellis, J. R. Macromolecular crowding: obvious but underappreciated. *Trends in Biochemical Sciences* **26,** 597–604; 10.1016/s0968-0004(01)01938-7 (2001).

205. Grossi, G., Dalgaard Ebbesen Jepsen, M., Kjems, J. & Andersen, E. S. Control of enzyme reactions by a reconfigurable DNA nanovault. *Nature communications* **8,** 992; 10.1038/s41467-017-01072-8 (2017).

206. Hahn, J., Chou, L. Y. T., Sørensen, R. S., Guerra, R. M. & Shih, W. M. Extrusion of RNA from a DNA-Origami-Based Nanofactory. *ACS nano* **14,** 1550–1559; 10.1021/acsnano.9b06466 (2020).

207. Rabe, K. S., Müller, J., Skoupi, M. & Niemeyer, C. M. Cascades in Compartments: En Route to Machine-Assisted Biotechnology. *Angewandte Chemie (International ed. in English)* **56,** 13574–13589; 10.1002/anie.201703806 (2017).

208. Tasset & D. M. et al. Oligonucleotide Inhibitors of Human Thrombin that Bind Distinct Epitopes. *J. Mol. Biol.,* 688–698; 10.1006/jmbi.1997.1275 (1997).

209. Di Cera, E. *et al.* The Na+ binding site of thrombin. *The Journal of biological chemistry* **270,** 22089–22092; 10.1074/jbc.270.38.22089 (1995).

210. Christina M. Wells and Enrico Di Cera. Thrombin Is a Na+-Activated Enzyme. *Biochemistry* **31,** 11721–11730; 10.1021/bi00162a008 (1992).

211. Alan Fersht. *Structure and mechanism in protein science: a guide to enzyme catalysis and protein folding* (World Scientific Publishing Co. Pte. Ltd., 2017).

212. W. John Albery/Jeremy R. Knowles. Effizienz und Evolution der Enzymkatalyse. *Angewandte Chemie* (1977).

213. W. John Albery/Jeremy R. Knowles. Evolution of enzyme function and the development of catalytic efficiency. *Biochemistry* (1976).

214. Huntington, J. A. Thrombin plasticity. *Biochim Biophys Acta.*; 10.1016/j.bbapap.2011.07.005 (2012).

215. Chahal, G., Thorpe, M. & Hellman, L. The Importance of Exosite Interactions for Substrate Cleavage by Human Thrombin. *PloS one* **10,** e0129511; 10.1371/journal.pone.0129511 (2015).

216. Di Cera, E. Thrombin. *Mol Aspects Med.,* 203–254; 10.1016/j.mam.2008.01.001 (2008).

217. Bode, W. *et al.* The refined 1.9 A crystal structure of human a-thrombin: interaction with D-Phe-Pro-Arg chloromethylketone and significance of the Tyr-Pro-Pro-Trp insertion segment. *EMBO Journal* **8,** 3467–3475 (1989).

218. Carter, W. J., Cama, E. & Huntington, J. A. Crystal structure of thrombin bound to heparin. *The Journal of biological chemistry* **280,** 2745–2749; 10.1074/jbc.M411606200 (2005).

219. Kim, D.-N., Kilchherr, F., Dietz, H. & Bathe, M. Quantitative prediction of 3D solution shape and flexibility of nucleic acid nanostructures. *Nucleic acids research* **40,** 2862–2868; 10.1093/nar/gkr1173 (2012).

220. Neet, K. E. & Ainslie, G. R. Hysteretic enzymes **64,** 192–226; 10.1016/S0076-6879(80)64010-5 (1980).

221. Frieden, C. Slow Transitions and Hysteretic Behavior in Enzymes. *Ann. Rev. Biochem.* **48,** 471–489 (1979).

222. Cristofaro, R. de & Di Cera, E. Effect of protons on the amidase activity of human α-thrombin. *Journal of molecular biology* **216,** 1077–1085; 10.1016/S0022-2836(99)80021-7 (1990).

223. Macaya, R. F., Schultze, P., Smith, F. W., Roe, J. A. & Feigon, J. Thrombin-binding DNA aptamer forms a unimolecular quadruplex structure in solution. *Proceedings of the National Academy of Sciences of the United States of America* **90,** 3745–3749; 10.1073/pnas.90.8.3745 (1993).

224. Di Cera, E., Cristofaro, R. de, Albright, D. J. & Fenton, J. W. Linkage between Proton Binding and Amidase Activity in Human a-Thrombin: Effect of Ions and Temperature **30,** 7913–7924 (1991).

225. Douglas, S. M. *et al.* Rapid prototyping of 3D DNA-origami shapes with caDNAno. *Nucleic acids research* **37,** 5001–5006; 10.1093/nar/gkp436 (2009).

226. Castro, C. E. *et al.* A primer to scaffolded DNA origami. *Nature methods* **8,** 221–229; 10.1038/nmeth.1570 (2011).

227. Zuker, M. Mfold web server for nucleic acid folding and hybridization prediction. *Nucleic acids research* **31,** 3406–3415; 10.1093/nar/gkg595 (2003).

228. Saccà, B. *et al.* Reversible reconfiguration of DNA origami nanochambers monitored by single-molecule FRET. *Angewandte Chemie (International ed. in English)* **54,** 3592–3597; 10.1002/anie.201408941 (2015).

229. Schöneweiß, E.-C. & Saccà, B. The collective behavior of spring-like motifs tethered to a DNA origami nanostructure. *Nanoscale* **9,** 4486–4496; 10.1039/c6nr08314e (2017).

230. Peters, J. P. & Maher, L. J. DNA curvature and flexibility in vitro and in vivo. *Quarterly reviews of biophysics* **43,** 23–63; 10.1017/S0033583510000077 (2010).

231. Erkelenz, M. *et al.* Site-specific facet protection of gold nanoparticles inside a 3D DNA origami box: a tool for molecular plasmonics. *Chemical communications (Cambridge, England)* **57,** 3151–3153; 10.1039/d0cc07712g (2021).

232. Douglas, S. M., Chou, J. J. & Shih, W. M. DNA-nanotube-induced alignment of membrane proteins for NMR structure determination, 6644–6648 (2007).

233. Stahl, E., Martin, T. G., Praetorius, F. & Dietz, H. Facile and scalable preparation of pure and dense DNA origami solutions. *Angewandte Chemie (International ed. in English)* **53,** 12735–12740; 10.1002/anie.201405991 (2014).

234. Machado, M. R. *et al.* The SIRAH 2.0 Force Field: Altius, Fortius, Citius. *Journal of chemical theory and computation* **15,** 2719–2733; 10.1021/acs.jctc.9b00006 (2019).

235. Abraham, M. J. *et al.* GROMACS: High performance molecular simulations through multi-level parallelism from laptops to supercomputers. *SoftwareX* **1-2,** 19–25; 10.1016/j.softx.2015.06.001 (2015).

236. Jorgensen, W. L., Chandrasekhar, J., Madura, J. D., Impey, R. W. & Klein, M. L. Comparison of simple potential functions for simulating liquid water. *The Journal of chemical physics* **79,** 926–935; 10.1063/1.445869 (1983).

237. Pang, Y. T., Miao, Y., Wang, Y. & McCammon, J. A. Gaussian Accelerated Molecular Dynamics in NAMD. *Journal of chemical theory and computation* **13,** 9–19; 10.1021/acs.jctc.6b00931 (2017).

238. Darden, T., York, D. & Pedersen, L. Particle mesh Ewald: An N ·log(N) method for Ewald sums in large systems. *The Journal of chemical physics* **98,** 10089–10092; 10.1063/1.464397 (1993).

239. Phillips, J. C. *et al.* Scalable molecular dynamics on CPU and GPU architectures with NAMD. *The Journal of chemical physics* **153,** 44130; 10.1063/5.0014475 (2020).

240. Phillips, J. C. *et al.* Scalable molecular dynamics with NAMD. *Journal of computational chemistry* **26,** 1781–1802; 10.1002/jcc.20289 (2005).

241. Vanommeslaeghe, K. & MacKerell, A. D. CHARMM additive and polarizable force fields for biophysics and computer-aided drug design. *Biochimica et biophysica acta* **1850,** 861–871; 10.1016/j.bbagen.2014.08.004 (2015).

242. Klauda, J. B. *et al.* Update of the CHARMM all-atom additive force field for lipids: validation on six lipid types. *The journal of physical chemistry. B* **114,** 7830–7843; 10.1021/jp101759q (2010).

243. Zoete, V., Cuendet, M. A., Grosdidier, A. & Michielin, O. SwissParam: a fast force field generation tool for small organic molecules. *Journal of computational chemistry* **32,** 2359–2368; 10.1002/jcc.21816 (2011).

244. Yesselman, J. D., Price, D. J., Knight, J. L. & Brooks, C. L. MATCH: an atom-typing toolset for molecular mechanics force fields. *Journal of computational chemistry* **33,** 189–202; 10.1002/jcc.21963 (2012).

245. Krol, M. *et al.* Force-field parametrization and molecular dynamics simulations of Congo red. *Journal of Computer-Aided Molecular Design*, 41–53 (2003).

246. Humphrey, W., Dalke, A. & Schulten, K. VMD: Visual Molecular Dynamics. *Journal of Molecular Graphics*, 33–38 (1996).

247. A. Cornish-Bowden. *Fundamentals of Enzyme Kinetics* (Wiley-Blackwell, 2012).

248. Pace, C. N., Shirley, B. A., McNutt, M. & Gajiwala, K. Forces contributing to the conformational stability of proteins. *FASEB journal : official publication of the Federation of American Societies for Experimental Biology* **10,** 75–83; 10.1096/fasebj.10.1.8566551 (1996).

249. Wagenbauer, K. F., Wachauf, C. H. & Dietz, H. Quantifying quality in DNA self-assembly. *Nature communications* **5,** 3691; 10.1038/ncomms4691 (2014).

250. Schneider, F., Möritz, N. & Dietz, H. The sequence of events during folding of a DNA origami. *Science advances* **5,** eaaw1412; 10.1126/sciadv.aaw1412 (2019).

251. Wah, J. L. T., David, C., Rudiuk, S., Baigl, D. & Estevez-Torres, A. Observing and Controlling the Folding Pathway of DNA Origami at the Nanoscale. *ACS nano* **10,** 1978–1987; 10.1021/acsnano.5b05972 (2016).

252. Song, J. *et al.* Direct visualization of transient thermal response of a DNA origami. *J. Am. Chem. Soc.* **134,** 9844–9847; 10.1021/ja3017939 (2012).

253. Protozanova, E., Yakovchuk, P. & Frank-Kamenetskii, M. D. Stacked-unstacked equilibrium at the nick site of DNA. *Journal of molecular biology* **342,** 775–785; 10.1016/j.jmb.2004.07.075 (2004).

254. Criado, J. M., Sánchez-Jiménez, P. E. & Pérez-Maqueda, L. A. Critical study of the isoconversional methods of kinetic analysis. *J Therm Anal Calorim* **92,** 199–203; 10.1007/s10973-007-8763-7 (2008).

255. Friedman, H. L. Kinetics of thermal degradation of char-forming plastics from thermogravimetry. Application to a phenolic plastic. *J. polym. sci., C Polym. symp.* **6,** 183–195; 10.1002/polc.5070060121 (1964).

256. Ozawa, T. Kinetic analysis by repeated temperature scanning. Part 1. Theory and methods. *Thermochimica Acta* **356,** 173–180; 10.1016/S0040-6031(00)00517-7 (2000).

257. Šesták, J. & Berggren, G. Study of the kinetics of the mechanism of solid-state reactions at increasing temperatures. *Thermochimica Acta* **3,** 1–12; 10.1016/0040-6031(71)85051-7 (1971).

258. Chen, G. *et al.* Regioselective surface encoding of nanoparticles for programmable self-assembly. *Nature materials* **18,** 169–174; 10.1038/s41563-018-0231-1 (2019).

259. Lermusiaux, L., Sereda, A., Portier, B., Larquet, E. & Bidault, S. Reversible switching of the interparticle distance in DNA-templated gold nanoparticle dimers. *ACS nano* **6,** 10992–10998; 10.1021/nn304599d (2012).

260. Edwardson, T. G. W., Lau, K. L., Bousmail, D., Serpell, C. J. & Sleiman, H. F. Transfer of molecular recognition information from DNA nanostructures to gold nanoparticles. *Nature chemistry* **8,** 162–170; 10.1038/nchem.2420 (2016).

261. Kühler, P. *et al.* Plasmonic DNA-origami nanoantennas for surface-enhanced Raman spectroscopy. *Nano letters* **14,** 2914–2919; 10.1021/nl5009635 (2014).

262. Kaminska, I., Bohlen, J., Mackowski, S., Tinnefeld, P. & Acuna, G. P. Strong Plasmonic Enhancement of a Single Peridinin-Chlorophyll a-Protein Complex on DNA Origami-Based Optical Antennas. *ACS nano* **12,** 1650–1655; 10.1021/acsnano.7b08233 (2018).

263. Simoncelli, S. *et al.* Quantitative Single-Molecule Surface-Enhanced Raman Scattering by Optothermal Tuning of DNA Origami-Assembled Plasmonic Nanoantennas. *ACS nano* **10,** 9809–9815; 10.1021/acsnano.6b05276 (2016).

264. Bordley, J. A., Hooshmand, N. & El-Sayed, M. A. The Coupling between Gold or Silver Nanocubes in Their Homo-Dimers: A New Coupling Mechanism at Short Separation Distances. *Nano letters* **15,** 3391–3397; 10.1021/acs.nanolett.5b00734 (2015).

265. Park, J.-E., Lee, Y. & Nam, J.-M. Precisely Shaped, Uniformly Formed Gold Nanocubes with Ultrahigh Reproducibility in Single-Particle Scattering and Surface-Enhanced Raman Scattering. *Nano letters* **18,** 6475–6482; 10.1021/acs.nanolett.8b02973 (2018).

266. Ke, Y., Voigt, N. V., Gothelf, K. V. & Shih, W. M. Multilayer DNA origami packed on hexagonal and hybrid lattices. *J. Am. Chem. Soc.* **134,** 1770–1774; 10.1021/ja209719k (2012).

267. Pamies, R. *et al.* Aggregation behaviour of gold nanoparticles in saline aqueous media. *J Nanopart Res* **16**; 10.1007/s11051-014-2376-4 (2014).

268. Zhao, Z., Jacovetty, E. L., Liu, Y. & Yan, H. Encapsulation of Gold Nanoparticles in a DNA Origami Cage. *Angew. Chem.* **123,** 2089–2092; 10.1002/ange.201006818 (2011).

6 Supplementary Materials

6.1 Supplementary Texts

Supplementary Text 1: Substrate inhibition

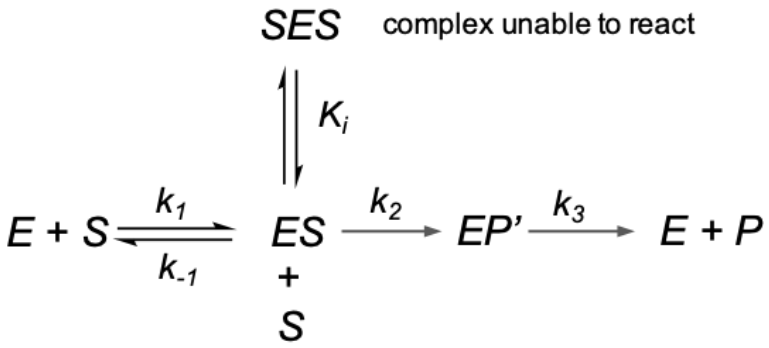

In conditions of excessive substrate concentrations (S >> E), an additional substrate molecule can bind to the ES complex, generating an unproductive SES complex. This complex is a dead-end in the reaction and is in equilibrium with ES + S, described by the equilibrium constant K_i. Substrate inhibition is therefore similar to non-productive inhibition in the sense that no competition occurs for the formation of ES, however, progression from ES to EP' is slowed down. The expression for the velocity obeys the following equation[247]:

$$v = \frac{v'_{max}[S]}{K'_M+[S]\left(1+\frac{[S]}{K_i}\right)} = \frac{v'_{max}[S]}{K'_M+S+\frac{[S]^2}{K_i}} \qquad \textbf{Eq. 12}$$

From this formula it is apparent that for high [S], the lower term containing $[S]^2$ becomes dominant and *v* will run towards zero. Reprinted and adapted from reference [200].

Supplementary Text 2: Kinetic linkage of thrombin in presence of DNA

This text was reprinted and adapted from reference [200].

In these simulations the condition $k_{-4}\ k_2 = k_{-1}\ k_5$ is always satisfied, as k_{-4} = A k_{-1} and k_5= A k_{-1}, with A = multiplicative factor (100, 1 or 0.01). This ensures that the kinetic linkage scheme always results into an apparent MM kinetics, independently of the pseudo-equilibrium regime between the enzyme species. In this way, the experimental conditions can be better simulated, even in case the two species, i.e. the free E and the DNA-bound form E_{DNA}, are not effectively in equilibrium. The results of the simulations are reported in Figure 25, Figure S 35 and Figure S 36.

The conditions for our simulations are reported below:

<u>Simulation conditions (valid for all simulations #1 to #12):</u>

- two initial enzyme species in solution, E and E_{DNA}
- each enzyme species can perform a catalytic cycle
- initial concentrations of enzyme and "DNA ligand" are
  $[E]_0$ = 1.2 nM
  $[DNA]_0$ = 1 nM
  to simulate our experimental conditions.
- all enzyme intermediates are in a pseudo-equilibrium regime according to a K_D, which is identical (but variable) between the two kinetic pathways.
- for the free-thrombin (E) pathway, we chose the rate coefficients reported in the literature for similar buffer conditions[210,224]
  k_1 = 6.000 min^{-1} μM^{-1}

  k_{-1} = 16.000 min^{-1}

  k_2 = 100 min^{-1}

  k_3 = 500 min^{-1}

  this would result in a k_{cat} = ca. 80 min^{-1} and a K_M = 2 μM, which well resemble the values obtained in our assays for thrombin-only samples.

- the dissociation constant for the E_{DNA} species is set to
  K_D = 1.0 nM (simulations #1 to #3)
  K_D = 10 nM (simulations #4 to #6)
  K_D = 0.1 nM (simulations #7 to #9)
  K_D = 1 μM (simulations #10 to #12)

to test how the pseudo-equilibrium between the species affects the velocity of the reaction.

for the reaction of the E_{DNA} species with the substrate (E_{DNA} pathway), we proceeded as follows:

simulation #1 to #3

- $k_7 = k_8 = k_9 = 10.000\ min^{-1}\ \mu M^{-1}$
  $k_{-7} = k_{-9} = 10\ min^{-1}$

  $k_{-8} = (k_1\ k_8\ k_{-4}\ k_{-7}) / (k_{-1}\ k_7\ k_4) = 3\ min^{-1}$ to satisfy the thermodynamic cycle

  In these conditions, $K_D = 1$ nM (valid for simulation #1, #2 and #3).

  at the equilibrium, [E] = 64% and [E_{DNA}] = 36%

- k_4 to k_6 are identical to their corresponding analogs (k_1 to k_3) in the E cycle, thus both enzyme species perform equally (simulation #1)
- k_4 to k_6 are 100-fold their corresponding analogs in the E cycle, meaning that the E_{DNA} pathway is faster (simulation #2).
- k_4 to k_6 are 0.01-fold their corresponding analogs in the E cycle, meaning that the E_{DNA} pathway is slower (simulation #3).

simulation #4 to #6

- $k_7 = k_8 = k_9 = 10.000\ min^{-1}\ \mu M^{-1}$
  $k_{-7} = k_{-9} = 100\ min^{-1}$

  $k_{-8} = (k_1\ k_8\ k_{-4}\ k_{-7}) / (k_{-1}\ k_7\ k_4)$ to satisfy the thermodynamic cycle

  In these conditions, $K_D = 10$ nM (valid for simulation #4, #5 and #6).

  at the equilibrium, [E] = 92% and [E_{DNA}] = 8%

- k_4 to k_6 equal to k_1 to k_3 (equal rates for both kinetic pathways).
- k_4 to k_6 100-fold the values of k_1 to k_3 (E_{DNA} pathway is faster)
- k_4 to k_6 0.01-fold the values of k_1 to k_3 (E_{DNA} pathway is slower)

simulation #7 to #9

- $k_7 = k_8 = k_9 = 10.000\ min^{-1}\ \mu M^{-1}$
  $k_{-7} = k_{-9} = 1\ min^{-1}$

  $k_{-8} = (k_1\ k_8\ k_{-4}\ k_{-7}) / (k_{-1}\ k_7\ k_4)$ to satisfy the thermodynamic cycle

  In these conditions, $K_D = 0.1$ nM (valid for simulation #7, #8 and #9).

  at the equilibrium, [E] = 33% and [E_{DNA}] = 67%

- k_4 to k_6 equal to k_1 to k_3 (equal rates for both kinetic pathways).
- k_4 to k_6 100-fold the values of k_1 to k_3 (E_{DNA} pathway is faster)
- k_4 to k_6 0.01-fold the values of k_1 to k_3 (E_{DNA} pathway is slower)

simulation #10 to #12

- $k_7 = k_8 = k_9 = 10.000\ min^{-1}\ \mu M^{-1}$
  $k_{-7} = k_{-9} = 10.000\ min^{-1}$

  $k_{-8} = (k_1\ k_8\ k_{-4}\ k_{-7}) / (k_{-1}\ k_7\ k_4)$ to satisfy the thermodynamic cycle

  In these conditions, $K_D = 1\ \mu M$ (valid for simulation #10, #11 and #12).

  at the equilibrium, [E] = 100% and [E_{DNA}] = 0%

- k_4 to k_6 equal to k_1 to k_3 (equal rates for both kinetic pathways).
- k_4 to k_6 100-fold the values of k_1 to k_3 (E_{DNA} pathway is faster)
- k_4 to k_6 0.01-fold the values of k_1 to k_3 (E_{DNA} pathway is slower)

All kinetic simulations were performed using the DynaFit program available free-of-charge at (http://www.biokin.com/dynafit/suite). A representative script for simulation #1 is reported below. The script has been accordingly changed to run the other simulations.

SIMULATION SCRIPT

simulate a family of initial rate vs. substrate curves for the kinetic linkage of thrombin (1 effector) according to reference [210]

```
[task]
  task = simulate
  data = rates
  approximation = king-altman

[mechanism]
  reaction S  --> P
  modifiers DNA
```

```
  E + S  <==> ES                 : k1 k-1
  ES --> EP                      : k2
  EP --> E + P                   : k3

  E(DNA) + S <==> ES(DNA)    : k4 k-4
  ES(DNA)--> EP(DNA)         : k5
  EP(DNA)--> E(DNA) + P      : k6

  E  + DNA <--> E(DNA)       : k7 k-7
  ES + DNA <--> ES(DNA)      : k8 k-8
  EP + DNA <--> EP(DNA)      : k9 k-9

;we suppose that at the beginning of the reaction the free enzyme species in solution is E
 [constants]
  k1 = 6000, k-1 = 16000
  k2 = 100
  k3 = 500

  k4 = 6000, k-4 = 16000
  k5 = 100
  k6 = 500

  k7 = 10000, k-7 = 10
  k8 = 10000, k-8 = (k1 k8 k-4 k-7) / (k-1 k7 k4),  ; thermodynamic cycle!
  k9 = 10000, k-9 = 10

[concentrations]
;concentrations are expressed in micromolar
;times are in minutes
  E = 0.0012

[responses]
  P = 1
```

[data]

variable S

mesh file

error constant 2 percent

directory ./THROMBIN/E-E(DNA)/data

extension txt

file f1 | conc DNA = 0.001 | label 1 nM

[output]

directory ./THROMBIN/E-E(DNA)/output_sim01

[end]

The expression of the steady-state rate has been derived upon application of the King-Altman method and is reported below:

Rate equation

$$v = [E]_0 \boldsymbol{N}/\boldsymbol{D} = d[P]/dt = + k_3 [EP] + k_6 [EP(DNA)]$$

$$\boldsymbol{N} = n_1 [S] + n_2 [S]^2 + n_3 [S][DNA] + n_4 [S][DNA]^2 + n_5 [S]^2[DNA] + n_6 [S][DNA]^3 + n_7 [S]^2[DNA]^2$$

$$\boldsymbol{D} = d_1 + d_2 [S] + d_3 [S]^2 + d_4 [DNA] + d_5 [DNA]^2 + d_6 [S][DNA] + d_7 [DNA]^3 + d_8 [S][DNA]^2 + d_9 [S]^2[DNA] + d_{10} [S][DNA]^3 + d_{11} [S]^2[DNA]^2$$

Coefficients

$n_1 = n_S =$ k_1 **(** $k_2 k_3 k_{-4} k_6 k_{-7} k_2 k_3 k_{-4} k_{-7} k_{-9} k_2 k_3 k_5 k_6 k_{-7} k_2 k_3 k_5 k_{-7} k_{-9} k_2 k_3 k_6 k_{-7} k_{-8} k_2 k_3 k_{-7} k_{-8} k_{-9}$ **)**

$n_2 = n_{SS} =$ $k_1 k_2 k_3 k_4$ **(** $k_5 k_{-9} k_6 k_{-8} k_{-8} k_{-9}$ **)**

$n_3 = n_{SDNA} =$ $k_1 k_2 k_{-4} k_6 k_{-7} k_9 k_1 k_2 k_5 k_6 k_{-7} k_9 k_1 k_2 k_6 k_{-7} k_{-8} k_9 k_1 k_3 k_5 k_6 k_{-7} k_8 k_1 k_3 k_5 k_{-7} k_8 k_{-9} k_{-1} k_3 k_4 k_5 k_6 k_7 k_{-1} k_3 k_4 k_5 k_7 k_{-9} k_2 k_3 k_4 k_5 k_6 k_7 k_2 k_3 k_4 k_5 k_7 k_{-9} k_2 k_3 k_4 k_6 k_7 k_{-8} k_2 k_3 k_4 k_7 k_{-8} k_{-9}$

$n_4 = n_{SDNADNA} =$ $k_1 k_5 k_6 k_{-7} k_8 k_9 k_{-1} k_4 k_5 k_6 k_7 k_9 k_2 k_4 k_5 k_6 k_7 k_9 k_2 k_4 k_6 k_7 k_{-8} k_9 k_3 k_4 k_5 k_6 k_7 k_8 k_3 k_4 k_5 k_7 k_8 k_{-9}$

$n_5 = n_{SSDNA} =$ $k_1\ k_4\ (\ k_2\ k_5\ k_6\ k_9\ k_2\ k_6\ k_{-8}\ k_9\ k_3\ k_5\ k_6\ k_8\ k_3\ k_5\ k_8\ k_{-9}\ )$

$n_6 = n_{SDNADNADNA} =$ $k_4\ k_5\ k_6\ k_7\ k_8\ k_9$

$n_7 = n_{SSDNADNA} =$ $k_1\ k_4\ k_5\ k_6\ k_8\ k_9$

$d_1 = d =$ $k_3\ k_{-7}\ (\ k_{-1}\ k_{-8}\ k_{-9} + k_{-1}\ k_6\ k_{-8} + k_{-1}\ k_{-4}\ k_{-9} + k_{-1}\ k_{-4}\ k_6 + k_{-1}\ k_5\ k_{-9} + k_{-1}\ k_5\ k_6 + k_2\ k_{-8}\ k_{-9} + k_2\ k_6\ k_{-8} + k_2\ k_{-4}\ k_{-9} + k_2\ k_{-4}\ k_6 + k_2\ k_5\ k_{-9} + k_2\ k_5\ k_6\ )$

$d_2 = d_S =$ $k_{-1}\ k_3\ k_4\ k_{-8}\ k_{-9} + k_{-1}\ k_3\ k_4\ k_6\ k_{-8} + k_{-1}\ k_3\ k_4\ k_5\ k_{-9} + k_2\ k_3\ k_4\ k_{-8}\ k_{-9} + k_2\ k_3\ k_4\ k_6\ k_{-8} + k_2\ k_3\ k_4\ k_5\ k_{-9} + k_1\ k_3\ k_{-7}\ k_{-8}\ k_{-9} + k_1\ k_3\ k_6\ k_{-7}\ k_{-8} + k_1\ k_3\ k_{-4}\ k_{-7}\ k_{-9} + k_1\ k_3\ k_{-4}\ k_6\ k_{-7} + k_1\ k_3\ k_5\ k_{-7}\ k_{-9} + k_1\ k_3\ k_5\ k_6\ k_{-7} + k_1\ k_2\ k_{-7}\ k_{-8}\ k_{-9} + k_1\ k_2\ k_6\ k_{-7}\ k_{-8} + k_1\ k_2\ k_{-4}\ k_{-7}\ k_{-9} + k_1\ k_2\ k_{-4}\ k_6\ k_{-7} + k_1\ k_2\ k_5\ k_{-7}\ k_{-9} + k_1\ k_2\ k_5\ k_6\ k_{-7}$

$d_3 = d_{SS} =$ $k_1\ k_4\ (\ k_3\ k_{-8}\ k_{-9} + k_3\ k_6\ k_{-8} + k_3\ k_5\ k_{-9} + k_2\ k_{-8}\ k_{-9} + k_2\ k_6\ k_{-8} + k_2\ k_5\ k_{-9}\ )$

$d_4 = d_{DNA} =$ $k_{-1}\ k_6\ k_{-7}\ k_{-8}\ k_9 + k_{-1}\ k_{-4}\ k_6\ k_{-7}\ k_9 + k_{-1}\ k_5\ k_6\ k_{-7}\ k_9 + k_2\ k_6\ k_{-7}\ k_{-8}\ k_9 + k_2\ k_{-4}\ k_6\ k_{-7}\ k_9 + k_2\ k_5\ k_6\ k_{-7}\ k_9 + k_3\ k_{-4}\ k_{-7}\ k_8\ k_{-9} + k_3\ k_{-4}\ k_6\ k_{-7}\ k_8 + k_3\ k_5\ k_{-7}\ k_8\ k_{-9} + k_3\ k_5\ k_6\ k_{-7}\ k_8 + k_{-1}\ k_3\ k_7\ k_{-8}\ k_{-9} + k_{-1}\ k_3\ k_6\ k_7\ k_{-8} + k_{-1}\ k_3\ k_{-4}\ k_7\ k_{-9} + k_{-1}\ k_3\ k_{-4}\ k_6\ k_7 + k_{-1}\ k_3\ k_5\ k_7\ k_{-9} + k_{-1}\ k_3\ k_5\ k_6\ k_7 + k_2\ k_3\ k_7\ k_{-8}\ k_{-9} + k_2\ k_3\ k_6\ k_7\ k_{-8} + k_2\ k_3\ k_{-4}\ k_7\ k_{-9} + k_2\ k_3\ k_{-4}\ k_6\ k_7 + k_2\ k_3\ k_5\ k_7\ k_{-9} + k_2\ k_3\ k_5\ k_6\ k_7$

$d_5 = d_{DNADNA} =$ $k_{-4}\ k_6\ k_{-7}\ k_8\ k_9 + k_5\ k_6\ k_{-7}\ k_8\ k_9 + k_{-1}\ k_6\ k_7\ k_{-8}\ k_9 + k_{-1}\ k_{-4}\ k_6\ k_7\ k_9 + k_{-1}\ k_5\ k_6\ k_7\ k_9 + k_2\ k_6\ k_7\ k_{-8}\ k_9 + k_2\ k_{-4}\ k_6\ k_7\ k_9 + k_2\ k_5\ k_6\ k_7\ k_9 + k_3\ k_{-4}\ k_7\ k_8\ k_{-9} + k_3\ k_{-4}\ k_6\ k_7\ k_8 + k_3\ k_5\ k_7\ k_8\ k_{-9} + k_3\ k_5\ k_6\ k_7\ k_8$

$d_6 = d_{SDNA} =$ $k_{-1}\ k_4\ k_6\ k_{-8}\ k_9 + k_3\ k_4\ k_5\ k_8\ k_{-9} + k_1\ k_6\ k_{-7}\ k_{-8}\ k_9 + k_1\ k_{-4}\ k_6\ k_{-7}\ k_9 + k_1\ k_5\ k_6\ k_{-7}\ k_9 + k_3\ k_4\ k_7\ k_{-8}\ k_{-9} + k_3\ k_4\ k_6\ k_7\ k_{-8} + k_1\ k_5\ k_{-7}\ k_8\ k_{-9} + k_{-1}\ k_4\ k_5\ k_7\ k_{-9} + k_2\ k_4\ k_7\ k_{-8}\ k_{-9} + k_2\ k_4\ k_6\ k_7\ k_{-8} + k_2\ k_4\ k_5\ k_7\ k_{-9} + k_1\ k_2\ k_6\ k_{-8}\ k_9 + k_1\ k_2\ k_{-4}\ k_6\ k_9 + k_1\ k_2\ k_5\ k_6\ k_9 + k_1\ k_3\ k_{-4}\ k_8\ k_{-9} + k_1\ k_3\ k_{-4}\ k_6\ k_8 + k_1\ k_3\ k_5\ k_6\ k_8 + k_1\ k_3\ k_{-7}\ k_8\ k_{-9} + k_1\ k_3\ k_6\ k_{-7}\ k_8 + k_{-1}\ k_3\ k_4\ k_7\ k_{-9} + k_{-1}\ k_3\ k_4\ k_6\ k_7 + k_2\ k_3\ k_4\ k_7\ k_{-9} + k_2\ k_3\ k_4\ k_6\ k_7 + k_1\ k_2\ k_{-7}\ k_{-8}\ k_9 + k_1\ k_2\ k_{-4}\ k_{-7}\ k_9 + k_1\ k_2\ k_5\ k_{-7}\ k_9 + k_1\ k_3\ k_5\ k_{-7}\ k_8 + k_{-1}\ k_3\ k_4\ k_5\ k_7 + k_2\ k_3\ k_4\ k_5\ k_7$

$d_7 = d_{DNADNADNA} =$ $k_6\ k_7\ k_8\ k_9\ (\ k_{-4} + k_5\ )$

$d_8 = d_{SDNADNA} =$ $k_4\ k_6\ k_7\ k_{-8}\ k_9 + k_4\ k_5\ k_7\ k_8\ k_{-9} + k_1\ k_{-4}\ k_6\ k_8\ k_9 + k_1\ k_5\ k_6\ k_8\ k_9 + k_1\ k_6\ k_{-7}\ k_8\ k_9 + k_{-1}\ k_4\ k_6\ k_7\ k_9 + k_2\ k_4\ k_6\ k_7\ k_9 + k_3\ k_4\ k_7\ k_8\ k_{-9} + k_3\ k_4\ k_6\ k_7\ k_8 + k_1\ k_5\ k_{-7}\ k_8\ k_9 + k_{-1}\ k_4\ k_5\ k_7\ k_9 + k_2\ k_4\ k_7\ k_{-8}\ k_9 + k_2\ k_4\ k_5\ k_7\ k_9 + k_3\ k_4\ k_5\ k_7\ k_8$

$d_9 = d_{SSDNA} =$ $k_1\ k_4\ (\ k_6\ k_{-8}\ k_9 + k_5\ k_8\ k_{-9} + k_2\ k_6\ k_9 + k_3\ k_8\ k_{-9} + k_3\ k_6\ k_8 + k_2\ k_{-8}\ k_9 + k_2\ k_5\ k_9 + k_3\ k_5\ k_8\ )$

$d_{10} = d_{SDNADNADNA} =$ $k_4\ k_7\ k_8\ k_9\ (\ k_6 + k_5\ )$

$d_{11} = d_{SSDNADNA} =$ $k_1\ k_4\ k_8\ k_9\ (\ k_6 + k_5\ )$

6.2 Data

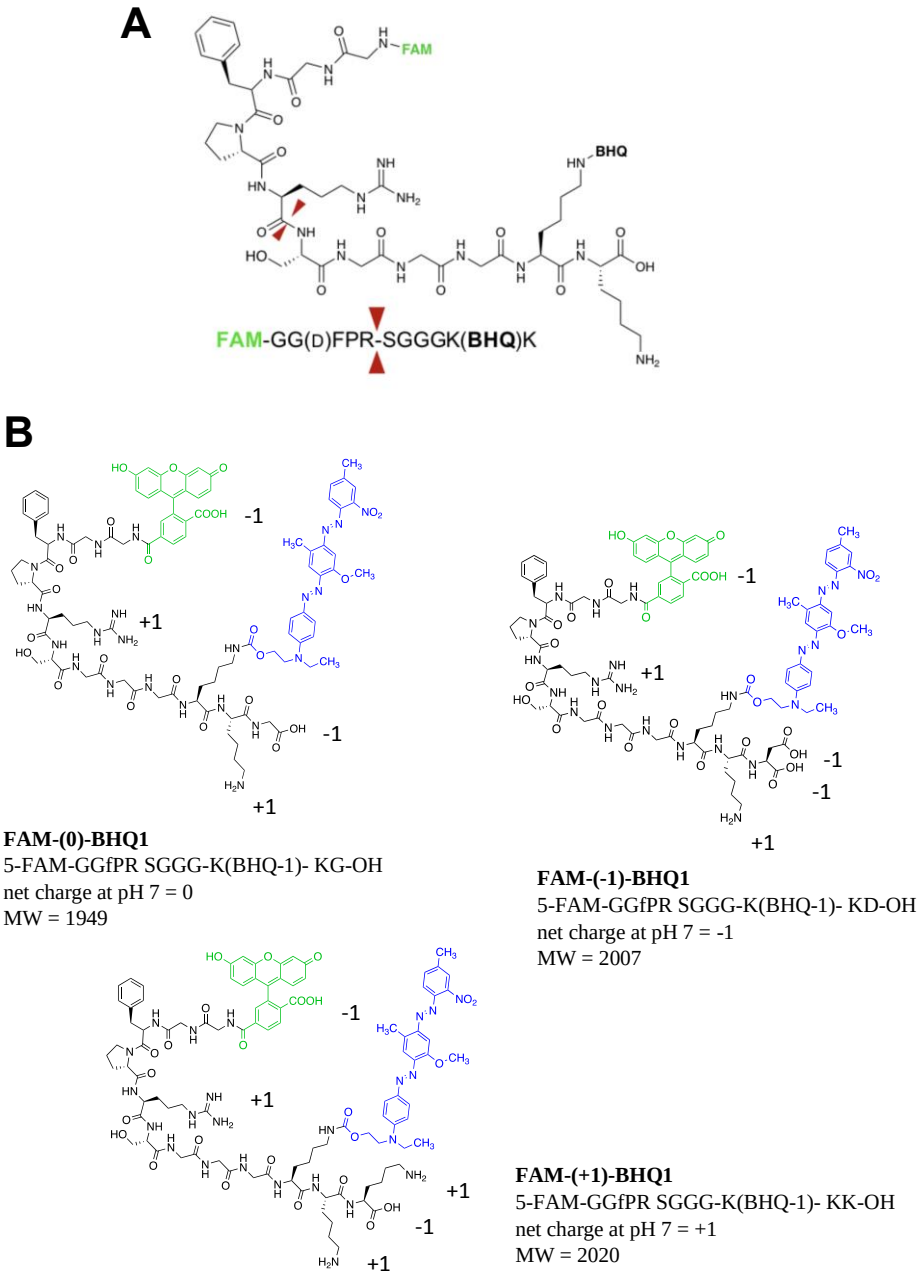

Figure S 1: Stereochemical view of thrombin substrates. (**A**) "Blank" substrate without terminal amino acid (Aaa). Red arrows indicate the cutting site. (**B**) Substrates (0), (-1) and (+1) with net charges at pH 7.00 indicated.

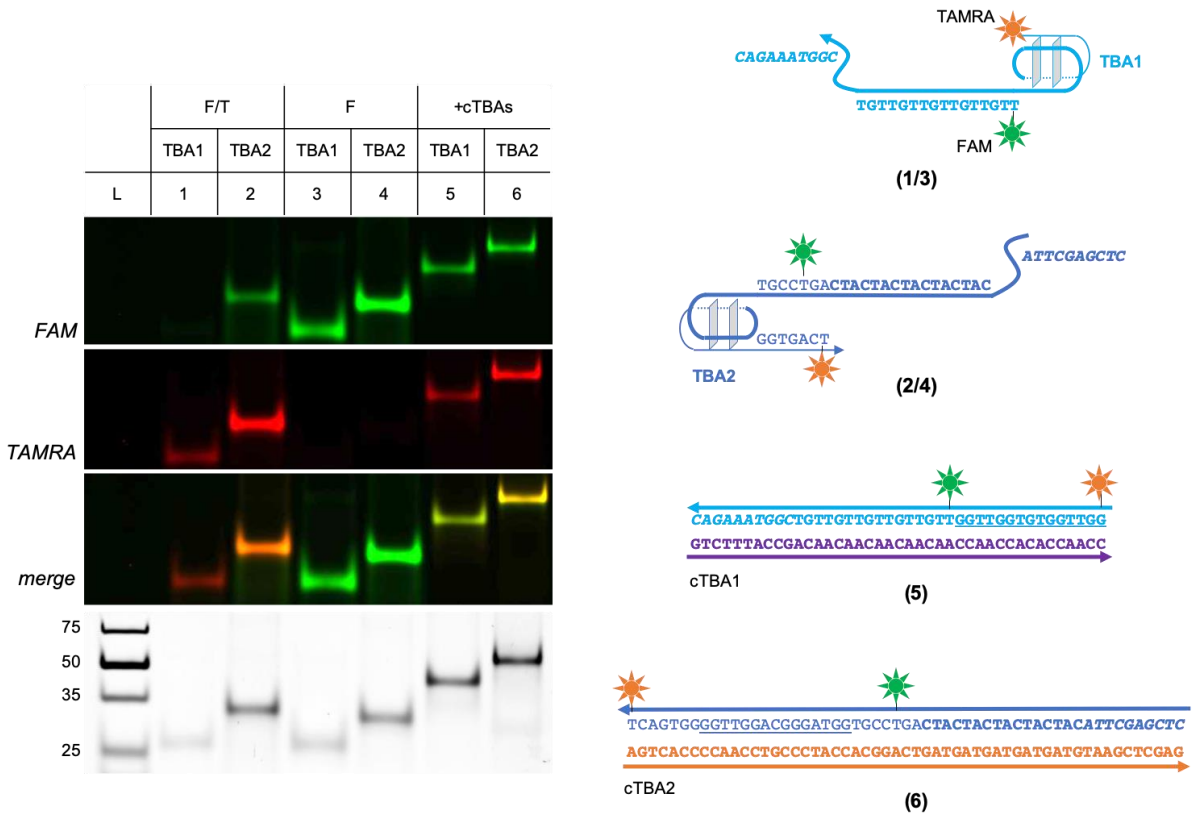

Figure S 2: Analysis of aptamer formation by native PAGE: Oligonucleotides containing the aptamer sequences (light and dark blue) were labeled with a donor-acceptor fluorescence pair (FAM/TAMRA) in the direct vicinity of the G4-motifs. Correct formation of the aptamers results in a decreased FAM signal since donor and acceptor are in proximity (Lane 1 and 2, F/T). Positive controls show maximum FAM signal in absence of the acceptor (Lane 3 and 4, F). Binding of a fully complementary oligonucleotide (cTBA) to TBA1 and TBA2 results in the linearization of the oligos, causing the distance between donor and acceptor to increase and thus increasing the FAM signal (Lane 5 and 6, +cTBAs). Gel running conditions: 25% acrylamide in 1X TBEMg buffer at 80 V, for 2h at 4°C. The gel was scanned with a Typhoon FLA 9000 at different wavelengths to monitor the presence of fluorescein (green) and TAMRA (orange) modified oligonucleotides and finally stained in ethidium bromide. Lane L contains a 10 bp ladder. Gel images were recorded by Dr. Elisa Schöneweiß, former member of the group of Prof. Saccà, University of Duisburg-Essen. Reprinted and adapted from reference [200].

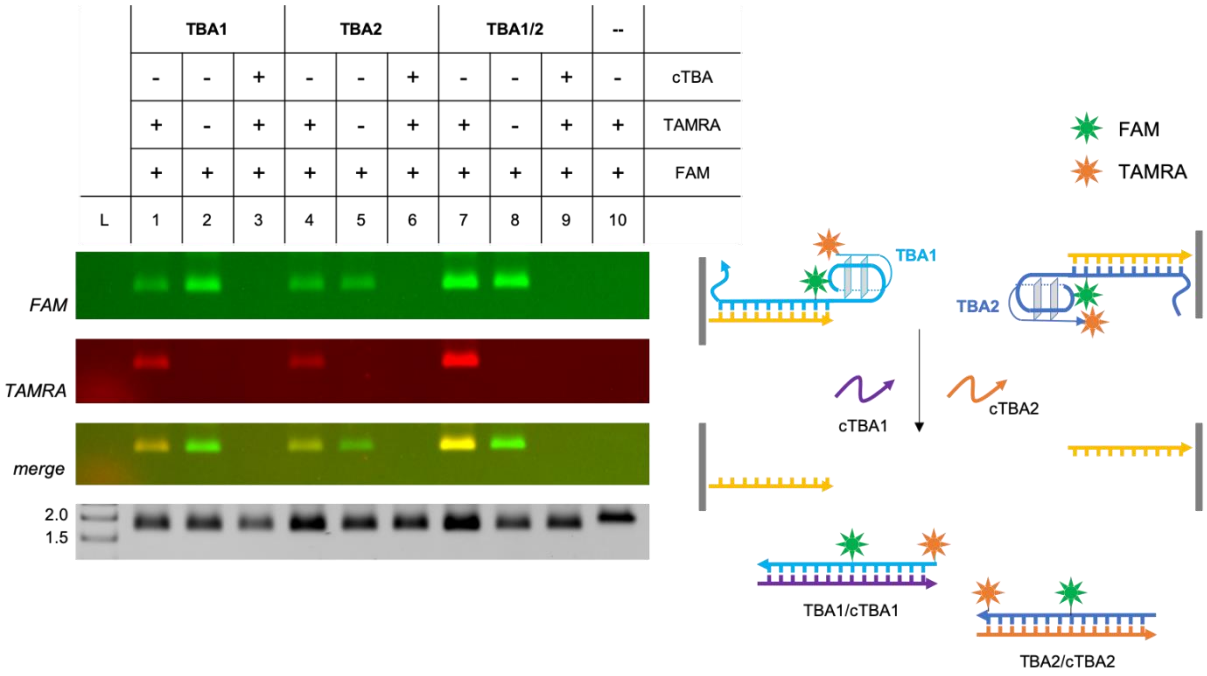

Figure S 3: Incorporation of TBAs into the DNA-origami cage. Both aptamers (TBA1 and TBA2, light and dark blue strands) contain a donor-acceptor fluorescence pair (FAM/TAMRA) in the vicinity of the G4-motif. Furthermore, a binding region enable hybridization and integration of the TBAs into the DNA origami structure (rect, yellow strands). Successful incorporation was proven by colocalization of fluorescence signal and the DNA origami bands (last panel, EtBr staining) (lanes 1, 2, 4, 5, 7 and 8). Addition of a fully complementary oligonucleotide (cTBA1 and cTBA2, purple and orange) let to a toehold-mediated strand displacement and detachment of TBAs from the origami structure (lanes 3, 6 and 9). Specificity of TBA binding was verified by absence of fluorescence signal for origami samples without handles (lane 10). Gel running parameters: 0.75% agarose in 1X TBEMg at 80 V, for 2.5 h at 4°C. Lane L contains a 1 kbp DNA ladder. DNA origami samples migrate between 1.5 kbp and 2.0 kbp. Gel images were recorded by Dr. Elisa Schöneweiß, former member of the group of Prof. Saccà, University of Duisburg-Essen. Reprinted and adapted from reference [200].

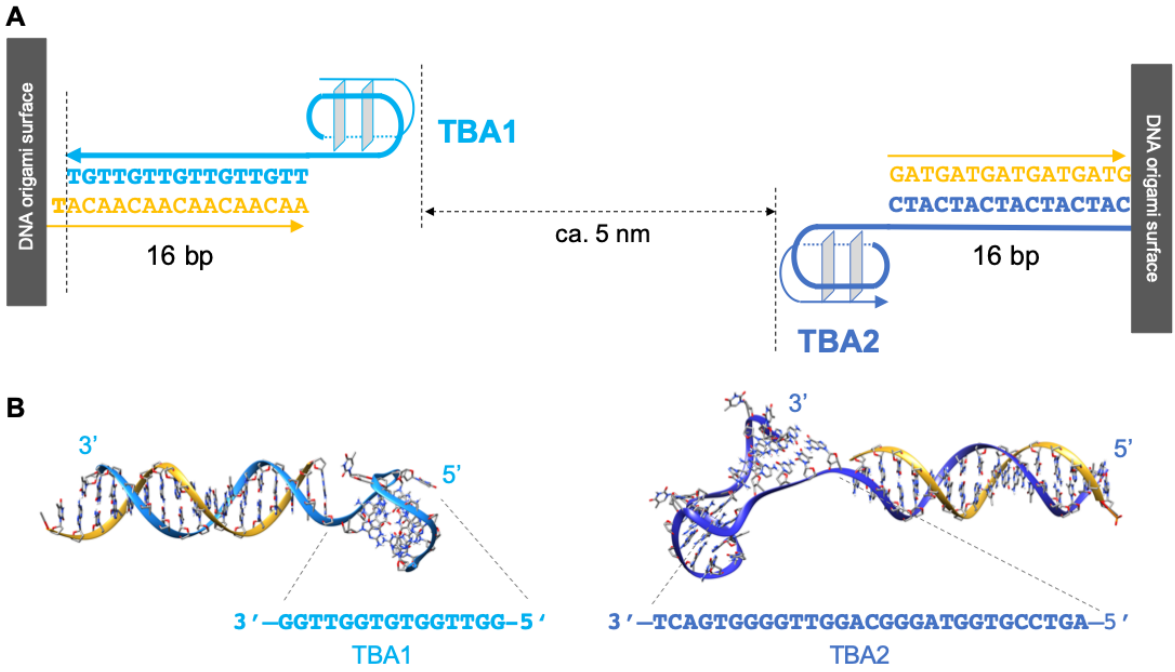

Figure S 4: Detailed view of TBAs within the DNA origami cavity. (**A**) Aptamers TBA1 (light blue) and TBA2 (dark blue) bind to protruding staples (yellow), facing inwards into the DNA origami cavity. Binding sequences are 16 bp long. Calculating with a helical pitch of 0.34 nm/bp and an approximated size of about 2 nm height for the G-quadruplexes, the distance between both aptamers is estimated to be about 5 nm, large enough to accommodate thrombin. (**B**) Molecular model of both aptamers and their respective sequences. The TBA1 and TBA2 structures are taken from previously reported crystallographic data (PDB codes are, respectively, 4DIH and 4I7Y). Reprinted and adapted from reference [200].

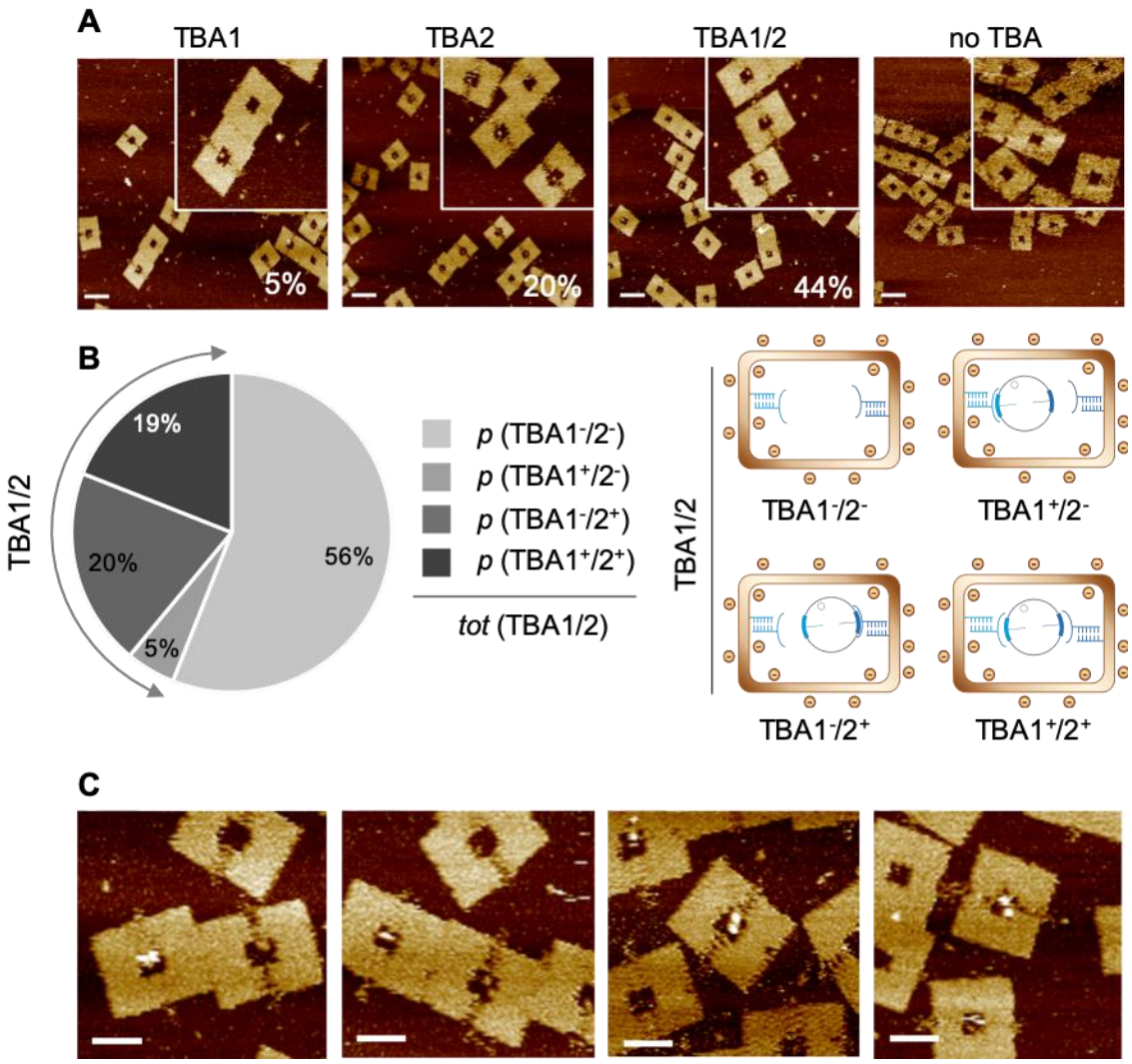

Figure S 5: Analysis of thrombin binding to the rectangular DNA origami by AFM. (**A**) Representative AFM images of DNA origamis featuring one (TBA1 or TBA2) or both (TBA1/2) aptamers in presence of thrombin. The enzyme is added in a 5 equimolar excess, incubated for 1h at room temperature and finally excess protein is removed by PEG purification (resuspension overnight). Percentages of bound structures are given as numerical values at the bottom of each picture. Scale bars are 100 nm. A sample featuring no TBAs was used as a control for the specificity of binding. (**B**) Chart diagram illustrating the distribution of different structures within the TBA1/2 sample. Assuming that the binding affinity of each aptamer is independent of the presence of the other aptamer, the total amount of bound structures (44 %, n = 2859) in the doubly-modified design (TBA1/2) can be split into four populations: 5 % (n = 1988) in the $TBA1^{+}/2^{-}$ state, 20 % in the $TBA1^{-}/2^{+}$ state (*n* = 2039) and the remaining 19 % is related to the simultaneous binding of both aptamers ($TBA1^{+}/2^{+}$), leaving 56 % of unbound structures ($TBA1^{-}/2^{-}$). (**C**) Representative AFM images of instances where two thrombin molecules were bound in the central cavity of the DNA origami structure. Scale bars are 100 nm. The amount of double-loaded origamis was almost negligible (ca. 1.5 %). AFM images were recorded by Dr. Elisa Schöneweiß, former member of the group of Prof. Saccà, University of Duisburg-Essen. Reprinted and adapted from reference [200].

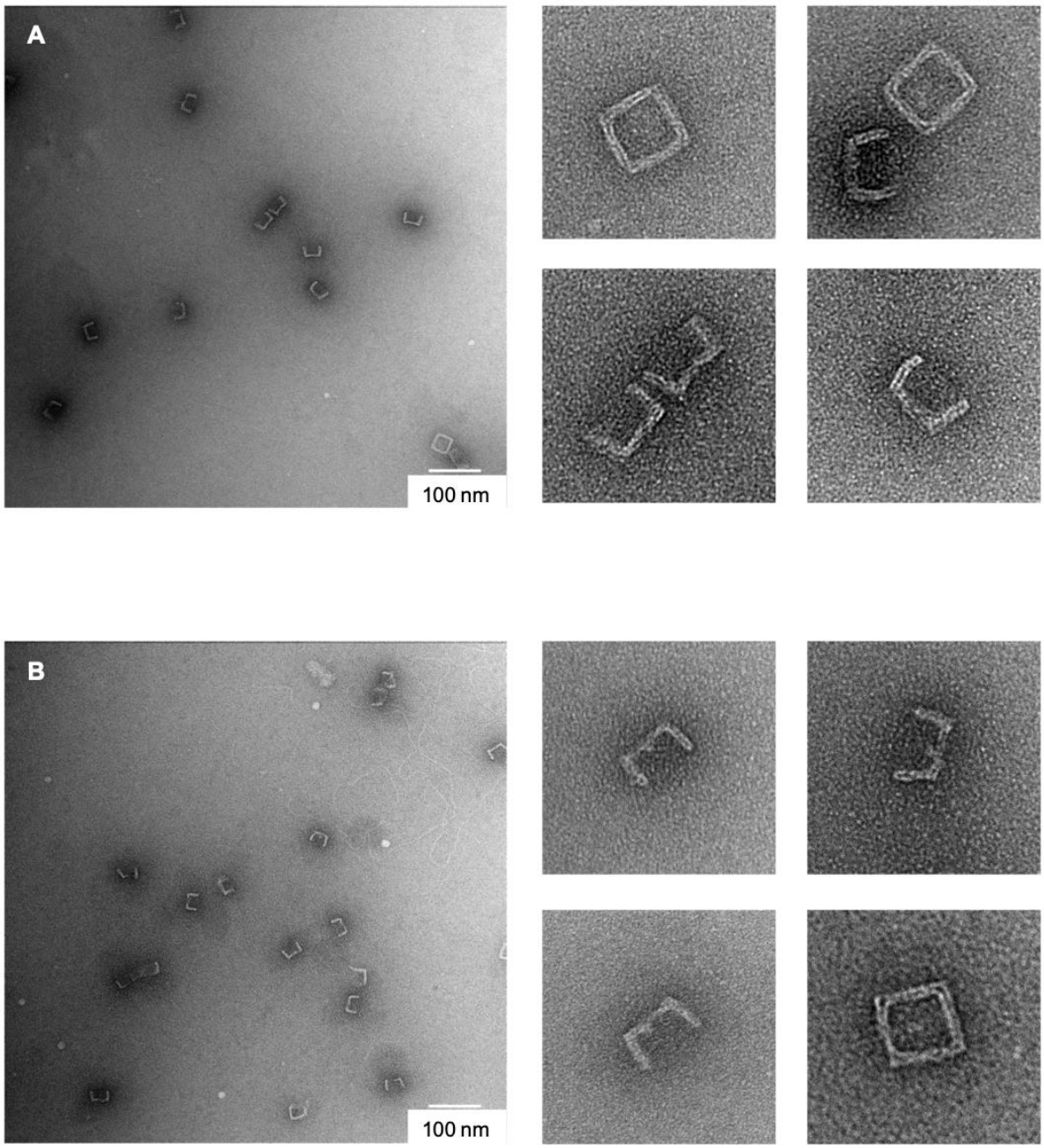

Figure S 6: Analysis of thrombin binding to the DNA-origami box structure by TEM. DNA boxes were incubated with a 5-fold equimolar excess of thrombin and incubated for 1 h at room temperature. Excess thrombin was removed by PEG purification (resuspension overnight at room temperature). (**A**) A control sample without addition of thrombin. (**B**) DNA boxes carrying both aptamers show the presence of thrombin within the center of its cavity. Right side shows zoom-in images of single structures. Estimating the amount of bound structures was not applicable, since the size of the protein is small and makes it in many instances difficult to judge true binding events. Scale bars are 100 nm. TEM images were recorded by Dr. Michael Erkelenz from the group of Prof. Schlücker, University of Duisburg-Essen. Reprinted and adapted from reference [200].

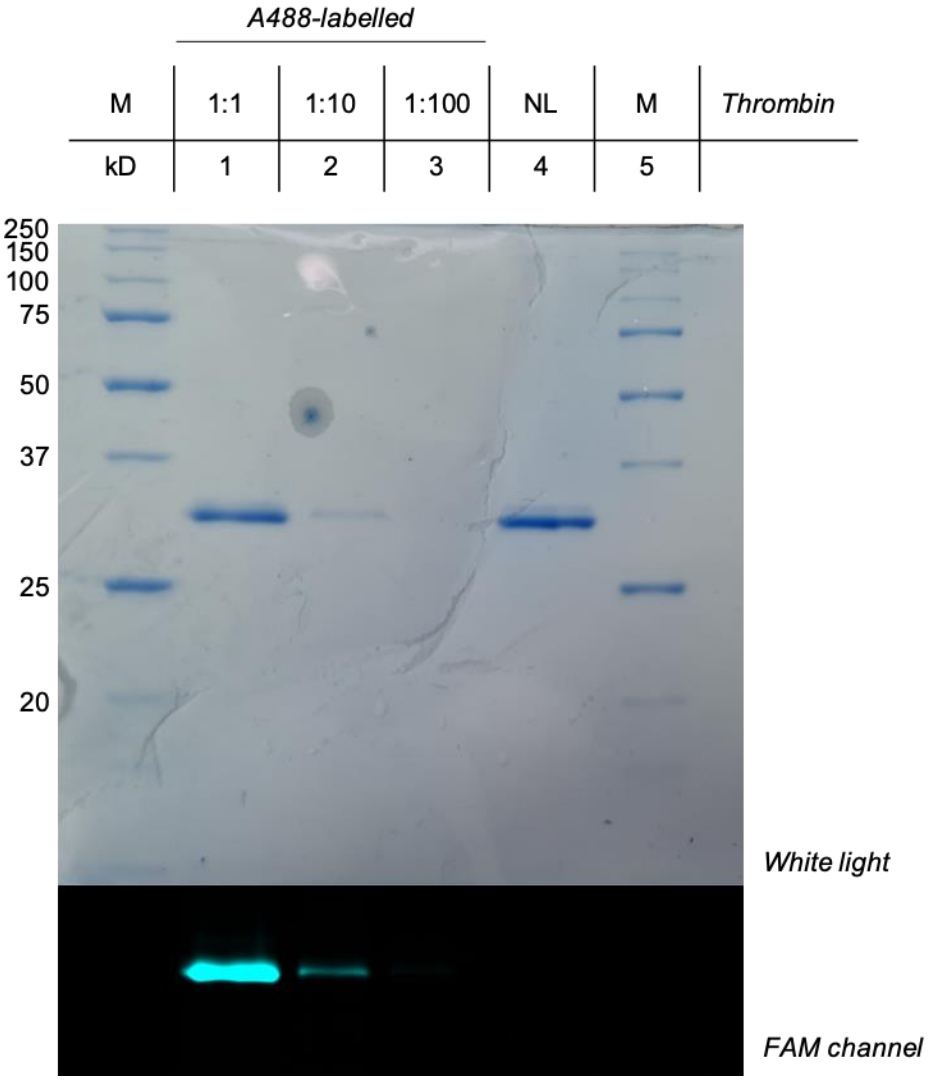

Figure S 7: Fluorescence labeling of thrombin. Successful labelling of thrombin was verified by SDS PAGE. Bands between the 25 kDa and 37 kDa marker likely correspond to the B-chain fragment of the alpha-human thrombin (MW ~ 31 kDa). The A-chain fragment (MW ca 6 kDa) is probably too small to be efficiently retained within the gel. Three dilution were applied to the gel, clearly showing fluorescent signal (FAM channel). A control sample containing unlabeled thrombin shows no fluorescence. For the labelling reaction 150 µL of thrombin stock solution (≈ 8.7 µM) were mixed with 1 µL NHS-A488 dye (ThermoFisher) in thrombin storage buffer solution. The samples were incubated at room temperature for 1h, protected from light irradiation and the excess of dye was removed using dye-removal columns (ThermoFisher) according to the manufacturer instructions. 2 µL sample were mixed with 2 µL of SDS loading buffer (containing DTT) and 6 µL thrombin storage buffer and heated for 10 min at 70°C. 10 µL of sample was loaded on the gel Gel and running conditions: 12 % SDS PAGE with 4.5% stacking gel, 60 min at 200 V, ice cooled in 1x SDS running buffer. Lane M contains a protein marker (BioRad #161-0363). Reprinted and adapted from reference [200].

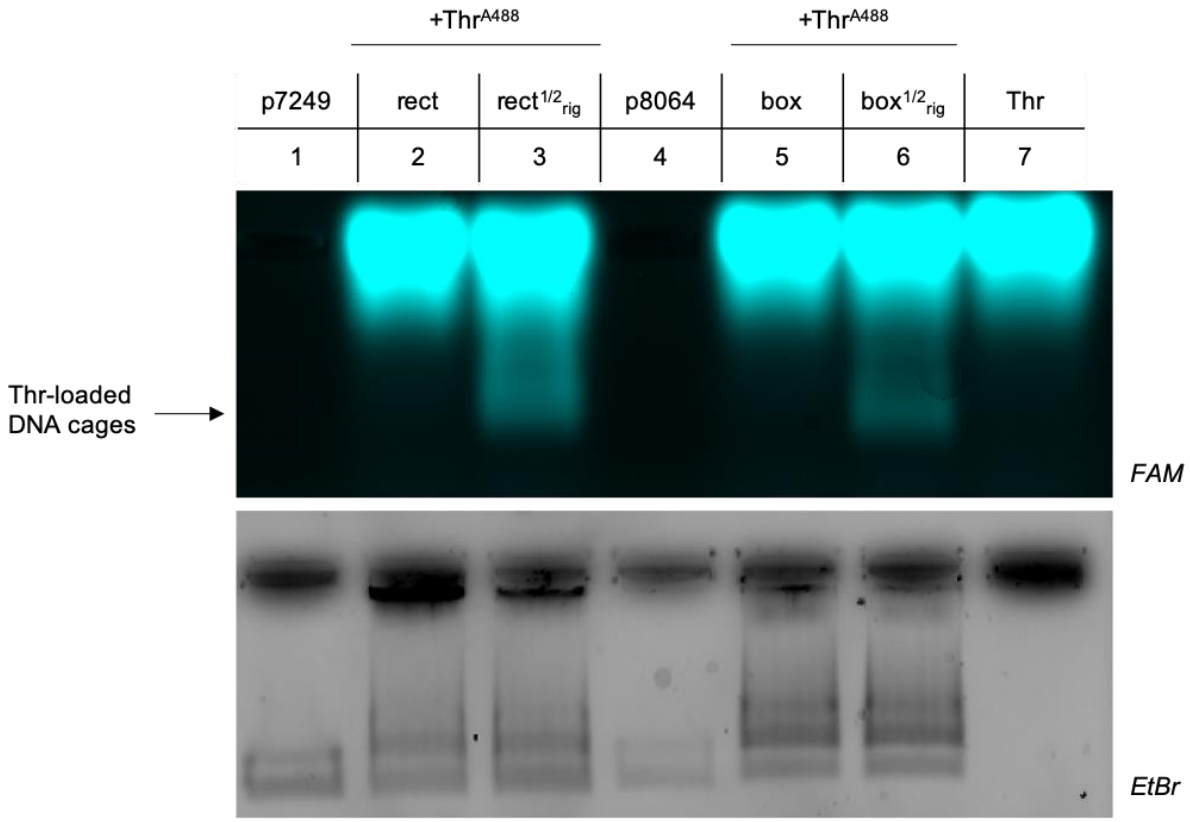

Figure S 8: Binding of labelled thrombin to DNA origami structures. Rect and box origamis, containing both TBAs were loaded with labelled thrombin. Successful binding was verified by the appearance of fluorescent bands (lanes 3 and 6, FAM channel) that are co-localized with the DNA origami bands (EtBr channel). Control samples that lack TBAs (Lanes 2 and 5) show no fluorescent bands, suggesting specificity of thrombin binding. Lane 1 and 4 contain the scaffolds used for the DNA origami assembly. Lane 7 contains labelled thrombin alone. For the binding reaction 20 μL of DNA origami cages, either with or without inner TBA modifications, were treated with 2.2 μL of A488-modified thrombin for 2 hours at room temperature. Gel running parameters: 1% agarose in 1X TBEMg at 80 V, for 2 h at 4°C. Lane L contains a 1 kbp DNA ladder. DNA origami samples migrate between 1.5 kbp and 2.0 kbp. Reprinted and adapted from reference [200].

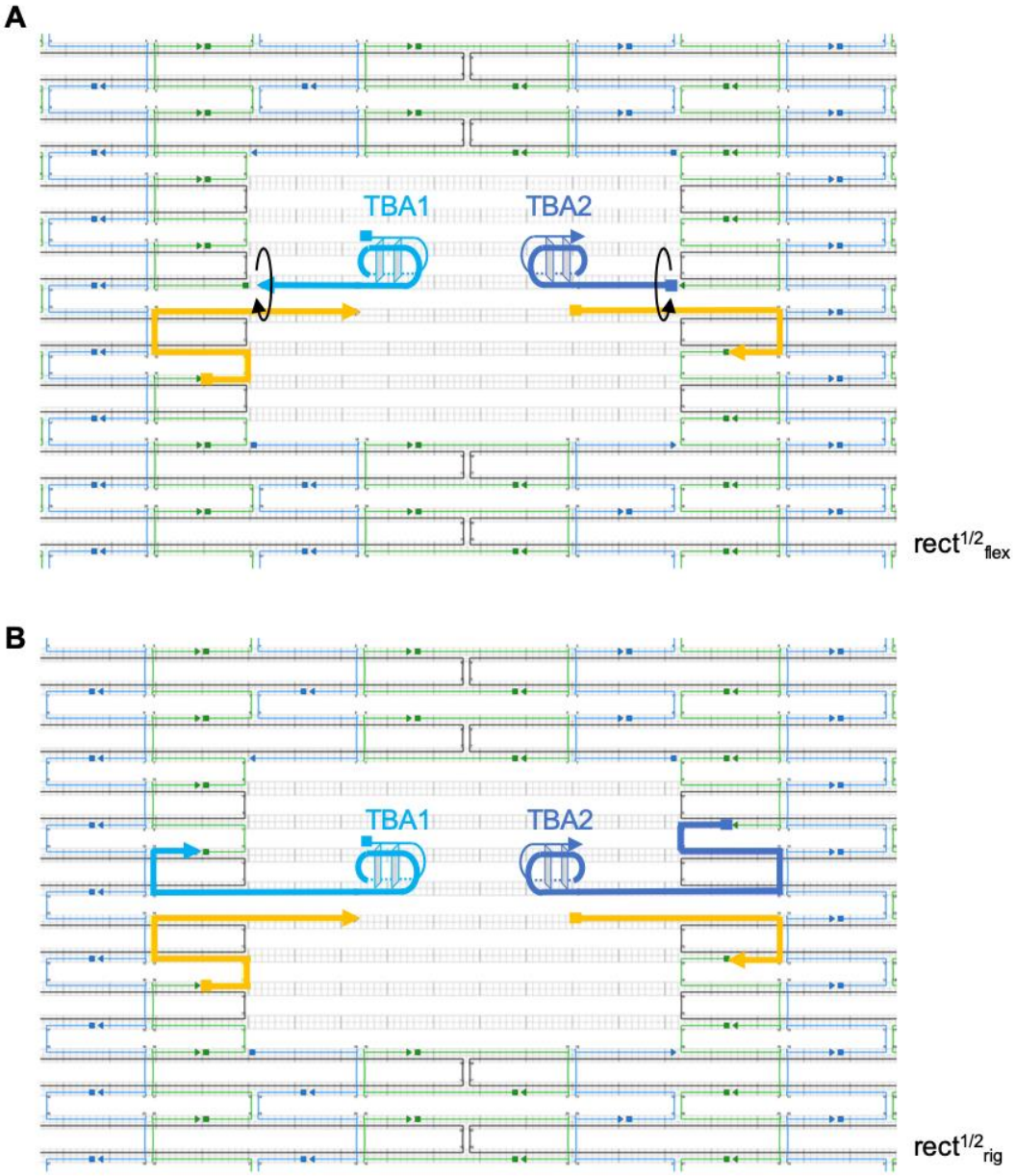

Figure S 9: Difference between the flex and rigid design within the rect DNA origami. (**A**) In the flex configuration, TBAs (light and dark blue) are bound to protruding staples (yellow) within the DNA origami that point into the cavity of the structure. The presence of a nick at the origami "wall" allows for some rotational freedom of the aptamer. (**B**) In the rigid design, aptamers are anchored within the DNA origami. The fully intact double stranded protrusion result in a more rigid design. Reprinted and adapted from reference [200].

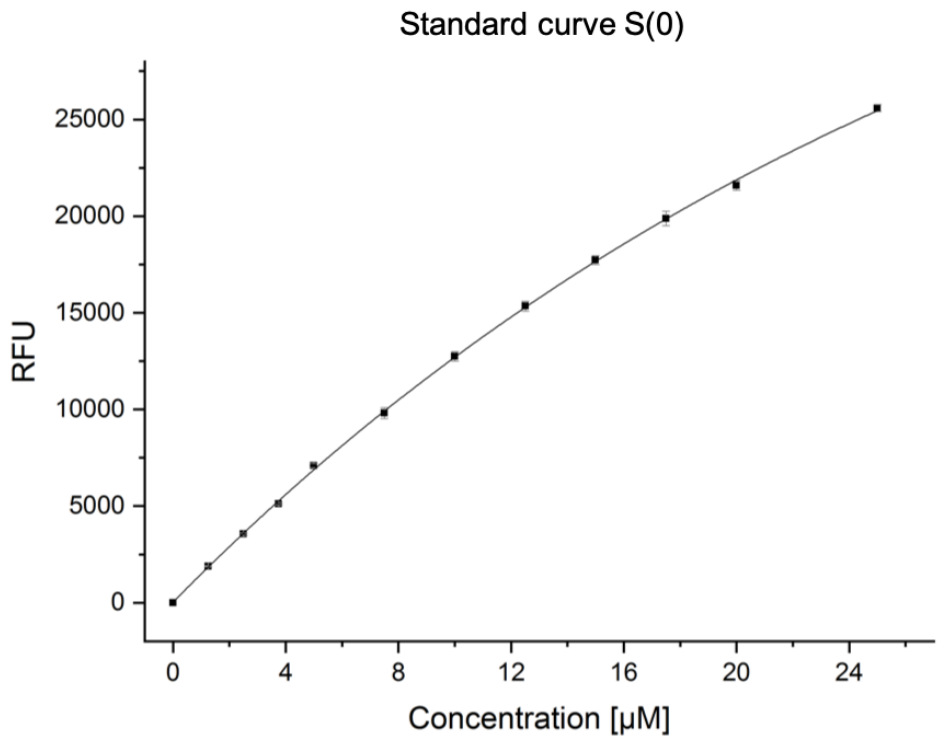

Figure S 10: Standard curve for the substrate S(0). Standard curves were obtained by measuring the fluorescence signal of varying concentrations (0 – 25 µM) of substrates that lack the quencher unit (FAM-only) in 1X TEMg buffer. Excitation wavelength was 482 nm, emission signal was recorded at 527 nm. The numerical values were plotted against substrate concentration and fitted with a non-linear function. The fit allows the quantification of product formation since FAM signals can now be converted to product concentrations. Reprinted and adapted from reference [200].

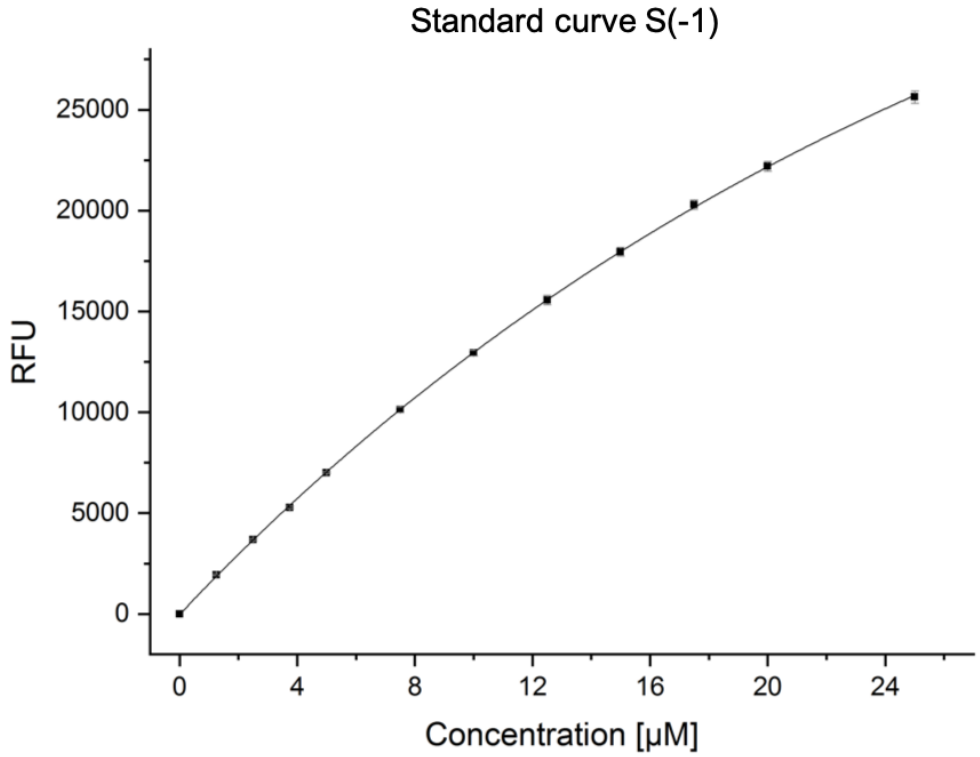

Figure S 11: Standard curve for the substrate S(-1). Standard curves were obtained by measuring the fluorescence signal of varying concentrations (0 – 25 µM) of substrates that lack the quencher unit (FAM-only) in 1X TEMg buffer. Excitation wavelength was 482 nm, emission signal was recorded at 527 nm. The numerical values were plotted against substrate concentration and fitted with a non-linear function. The fit allows the quantification of product formation since FAM signals can now be converted to product concentrations. Reprinted and adapted from reference [200].

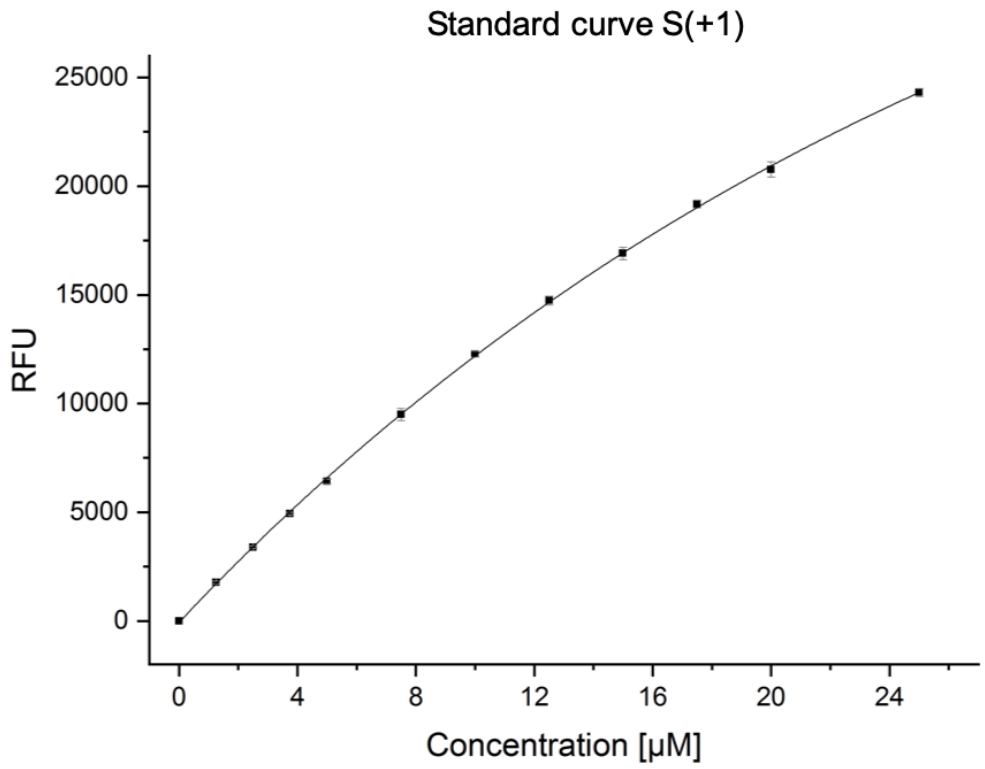

Figure S 12: Standard curve for the substrate S(+1). Standard curves were obtained by measuring the fluorescence signal of varying concentrations (0 – 25 µM) of substrates that lack the quencher unit (FAM-only) in 1X TEMg buffer. Excitation wavelength was 482 nm, emission signal was recorded at 527 nm. The numerical values were plotted against substrate concentration and fitted with a non-linear function. The fit allows the quantification of product formation since FAM signals can now be converted to product concentrations. Reprinted and adapted from reference [200].

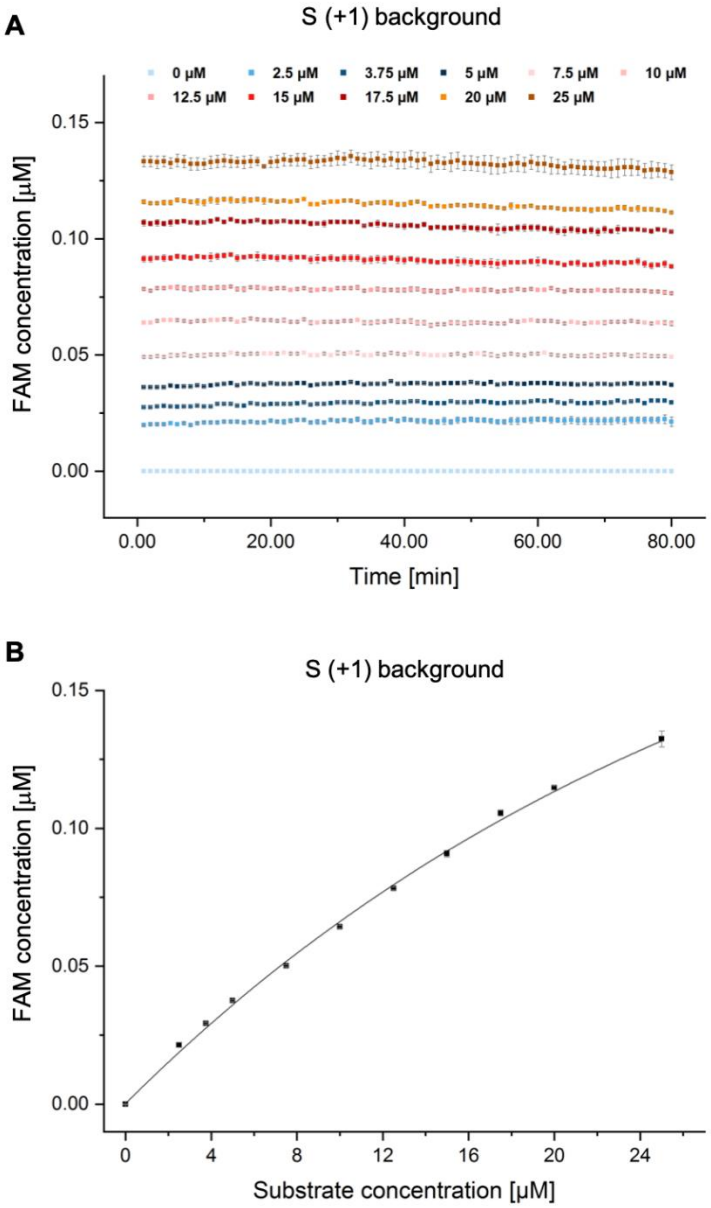

Figure S 13: Background fluorescence control. (**A**) To estimate the amount of background signal from the substrates, varying amounts of substrate (0 – 25 µM) were measured in 1x TEMg buffer in absence of any enzyme. Excitation wavelength was 482 nm, emission was recorded at 527 nm. Although fluorophore and quencher (FAM and BHQ1) are in close proximity, not all fluorescence signal is extinguished. Background signal increases with increasing substrate concentration (**B**). Importantly, the signal is relatively constant over time. Since in the actual enzyme assays, fluorescence changes are recorded, the background signal does not affect the determination of the reaction rates. Furthermore, the background signal is typically less than 1% of the FAM intensity recorded during peptide hydrolysis and can be therefore neglected, keeping the validity of the standard curve unaltered. Reprinted and adapted from reference [200].

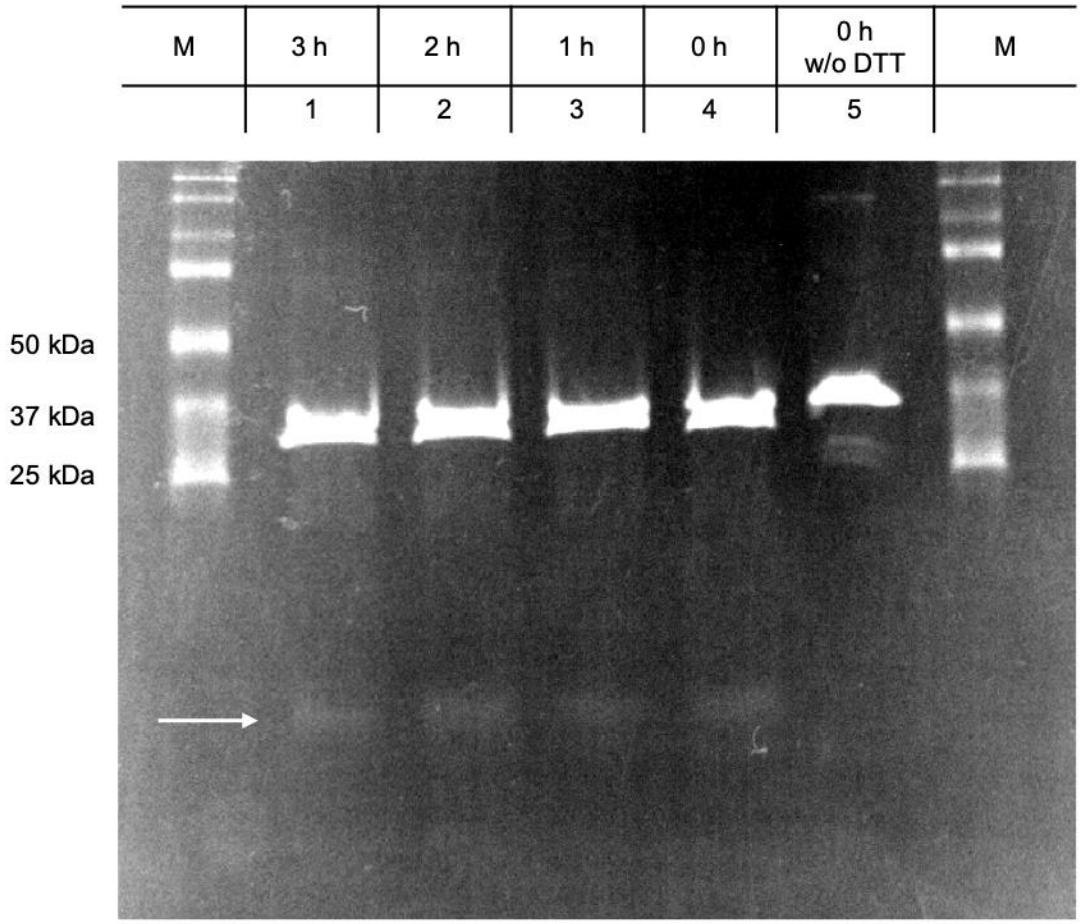

Figure S 14: Analysis of thrombin stability by SDS-PAGE. Thrombin was diluted in 1x TEMg buffer and incubated for the indicated time (Lanes 1-4). Expected band patterns emerge for all time intervals (Upper band ~ 31-32 kDa and lower band ~ 6 kDa, indicated by arrow). No additional bands appear, suggesting that no significant degradation takes place over the time course of the experiment. A control sample (no DTT, lane 5) shows the expected MW of about 38 kDa of the native protein. In detail: 10 µL of thrombin stock solution (≈ 8.5 µM) were mixed with 2 µL 10X TEMg12.5 and 8 µL of ddH_2O. Gel and running conditions: 12 % SDS PAGE with 4.5% stacking gel, 60 min at 200 V, ice cooled in 1x SDS running buffer. Lane M contains a protein marker (BioRad #161-0363). Samples were heated for 5 minutes at 95°C prior to loading. Reprinted and adapted from reference [200].

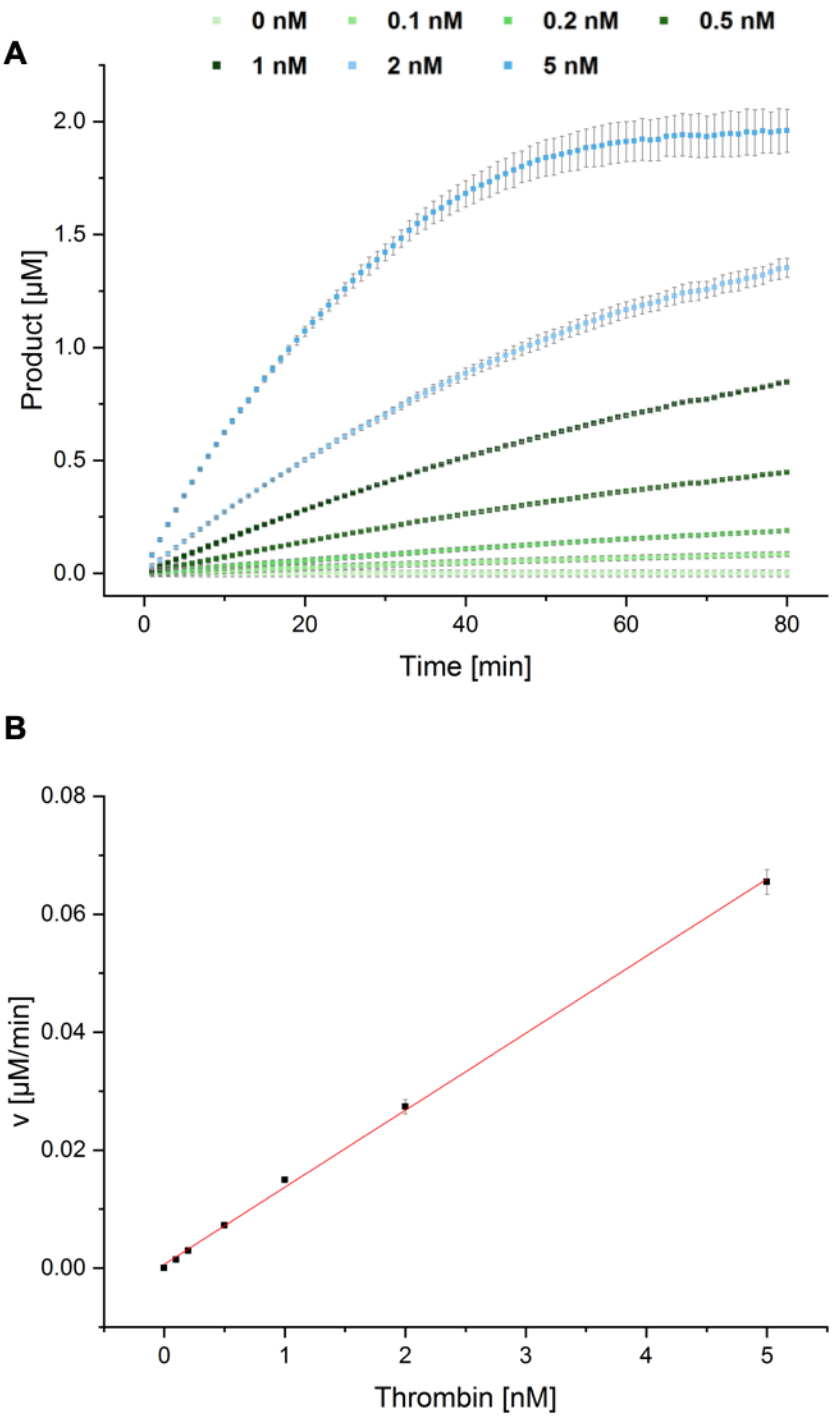

Figure S 15: Thrombin linearity test. To test whether protein aggregation of degradation takes place, varying concentrations of thrombin were used for enzymatic assays with a fixed concentration of substrate S(0). (**A**) Product formation over time. (**B**) Initial rates of (**A**) plotted against thrombin concentrations. Linearity of the fit ensures that no aggregation or degradation takes place in the experimental conditions used for the assay. Substrate concentration: 2.5 µM. Cleavage of the substrate was recorded at 37°C by measuring the fluorescence signal at 527 nm for a period of 80 min. Reprinted and adapted from reference [200].

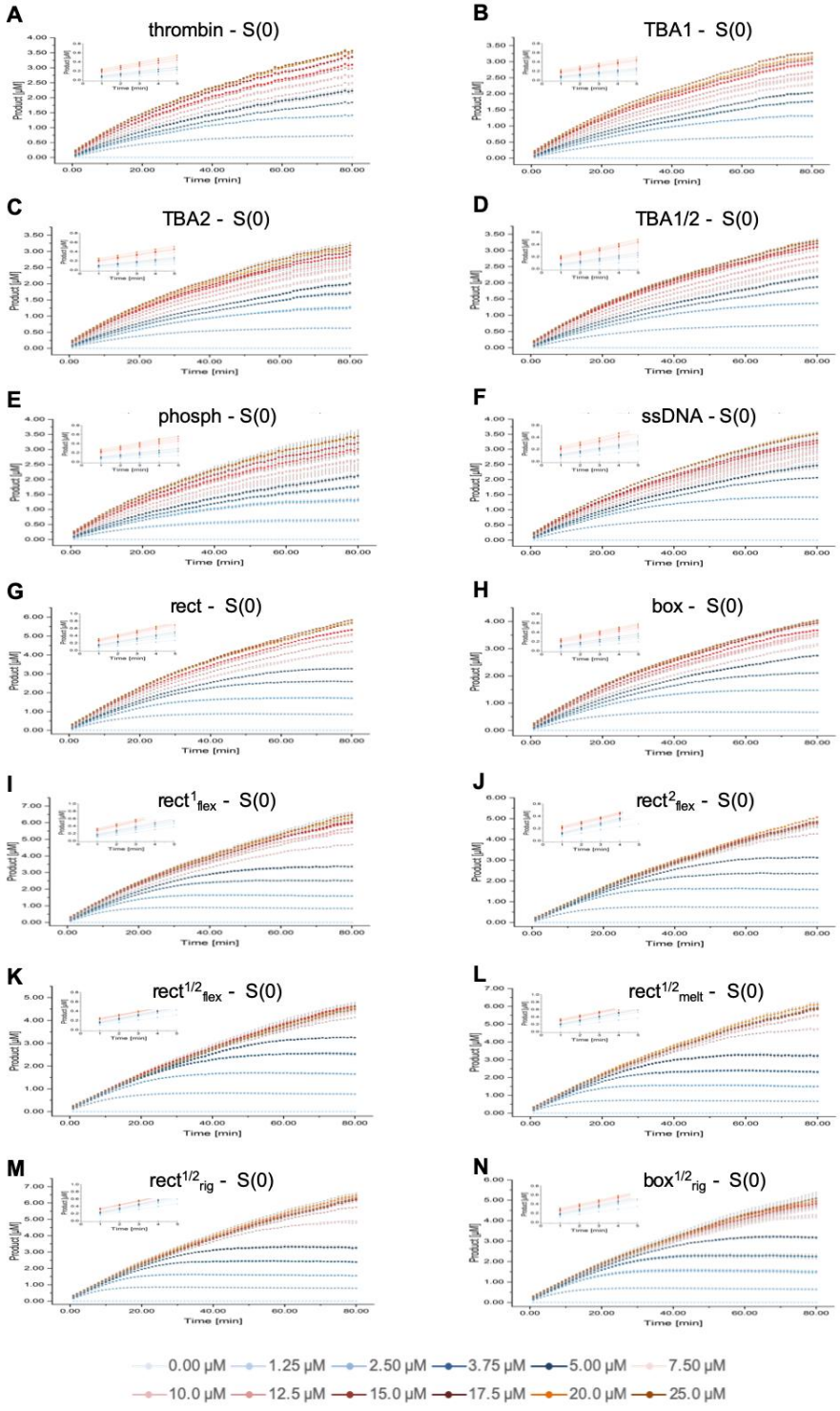

Figure S 16: Exemplary curves of product formation for S(0). Summary of substrate hydrolysis for all different constructs (as described in the main text) used in this work. Enzymatic assays were performed as described in the Materials & Methods section (see 4.2.11). Insets show zoom-ins of the initial phase of the reaction. Here, the substrate used was FAM-GGfPR|SGGGK(BHQ1)KG-OH (where "|" indicates the position of peptide cleavage). The calculated net charge of the FRET peptide S(0) at pH 7 is 0. Reprinted and adapted from reference [200].

Enlarged version of this figure is given below for convenience.

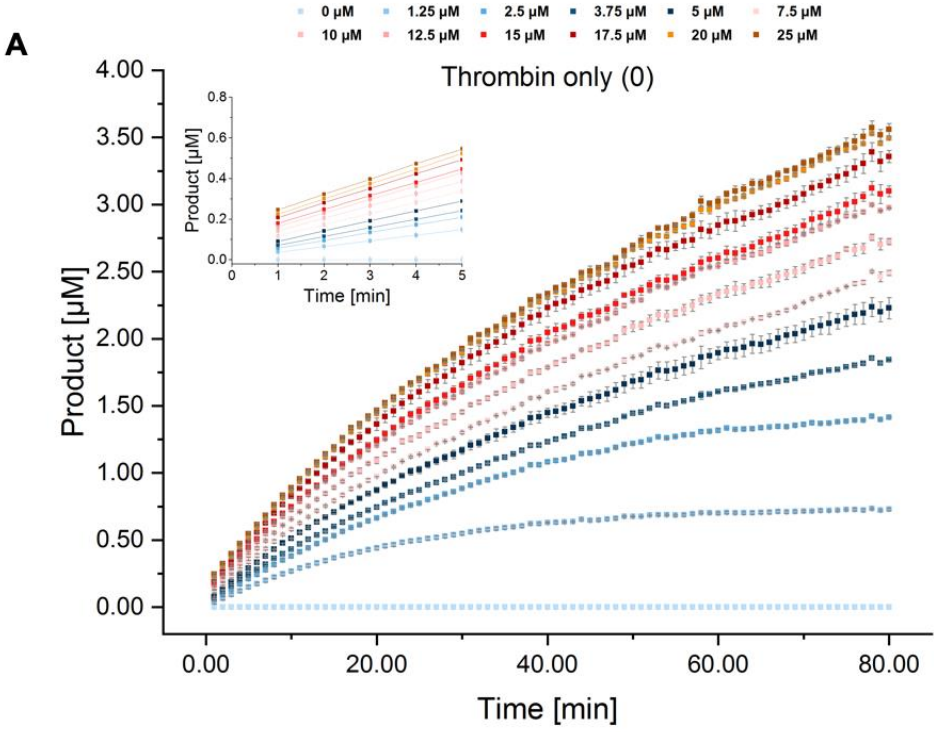
A
0 µM
1.25 µM
2.5 µM
3.75 µM
5 µM
7.5 µM
10 µM
12.5 µM
15 µM
17.5 µM
20 µM
25 µM
Thrombin only (0)
Product [µM]
Time [min]
0.00
20.00
40.00
60.00
80.00
0.00
0.50
1.00
1.50
2.00
2.50
3.00
3.50
4.00

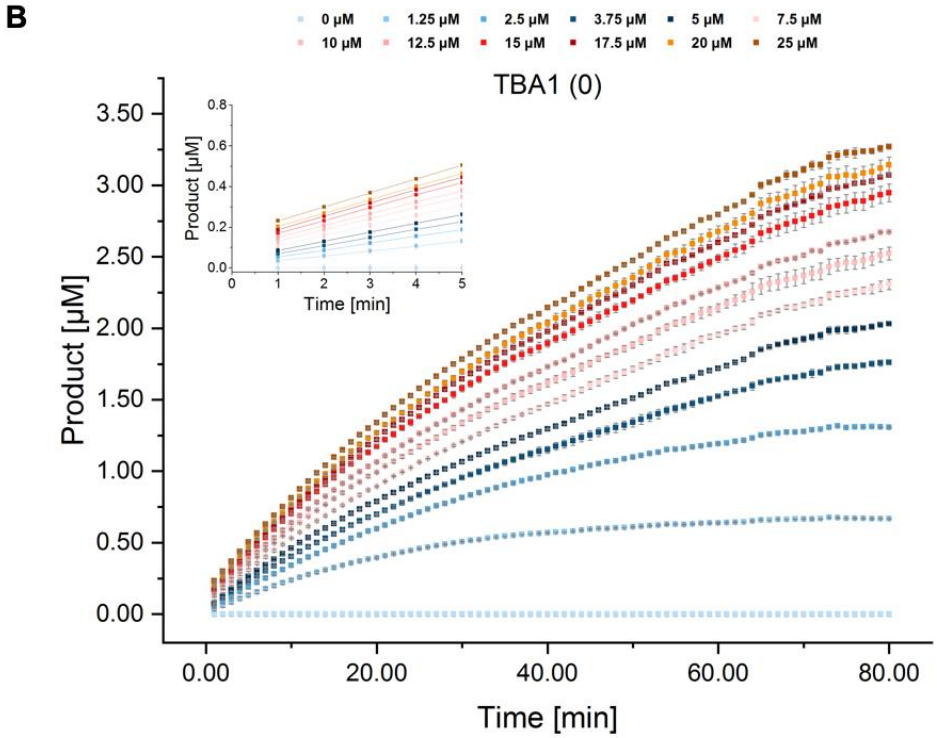
B
0 µM
1.25 µM
2.5 µM
3.75 µM
5 µM
7.5 µM
10 µM
12.5 µM
15 µM
17.5 µM
20 µM
25 µM
TBA1 (0)
Product [µM]
Time [min]
0.00
20.00
40.00
60.00
80.00
0.00
0.50
1.00
1.50
2.00
2.50
3.00
3.50

C

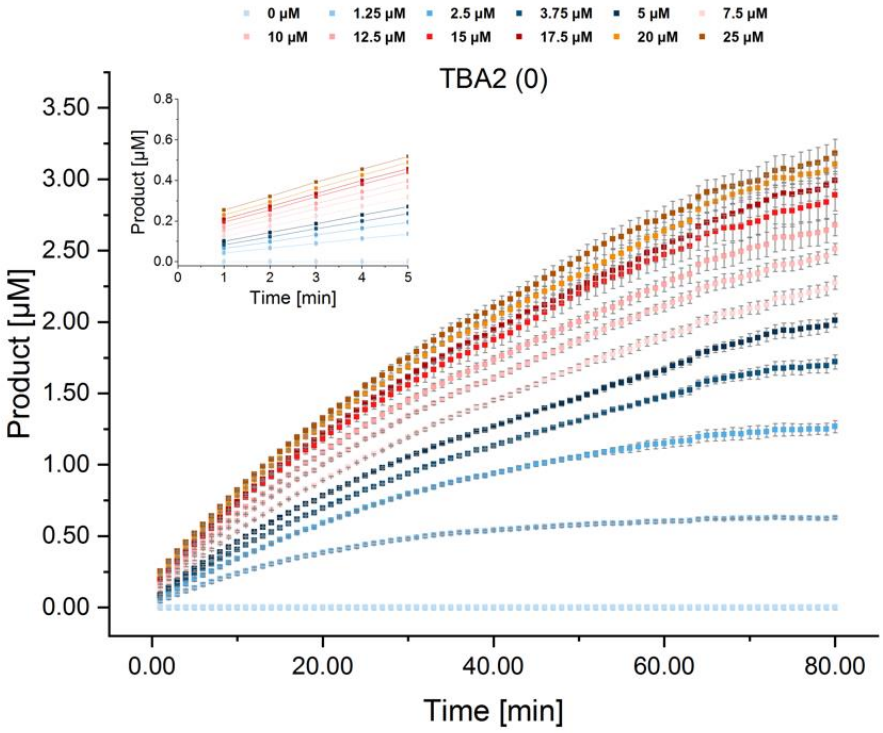
0 µM
1.25 µM
2.5 µM
3.75 µM
5 µM
7.5 µM
10 µM
12.5 µM
15 µM
17.5 µM
20 µM
25 µM
TBA2 (0)
Product [µM]
Time [min]
0.00
0.50
1.00
1.50
2.00
2.50
3.00
3.50
0.00
20.00
40.00
60.00
80.00

D

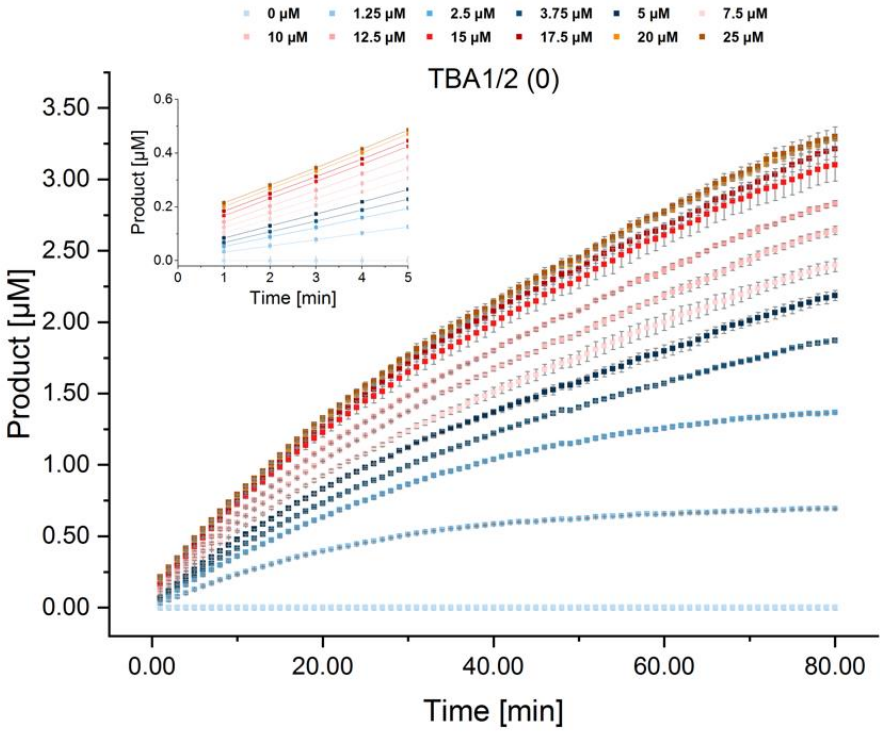
0 µM
1.25 µM
2.5 µM
3.75 µM
5 µM
7.5 µM
10 µM
12.5 µM
15 µM
17.5 µM
20 µM
25 µM
TBA1/2 (0)
Product [µM]
Time [min]
0.00
0.50
1.00
1.50
2.00
2.50
3.00
3.50
0.00
20.00
40.00
60.00
80.00

E

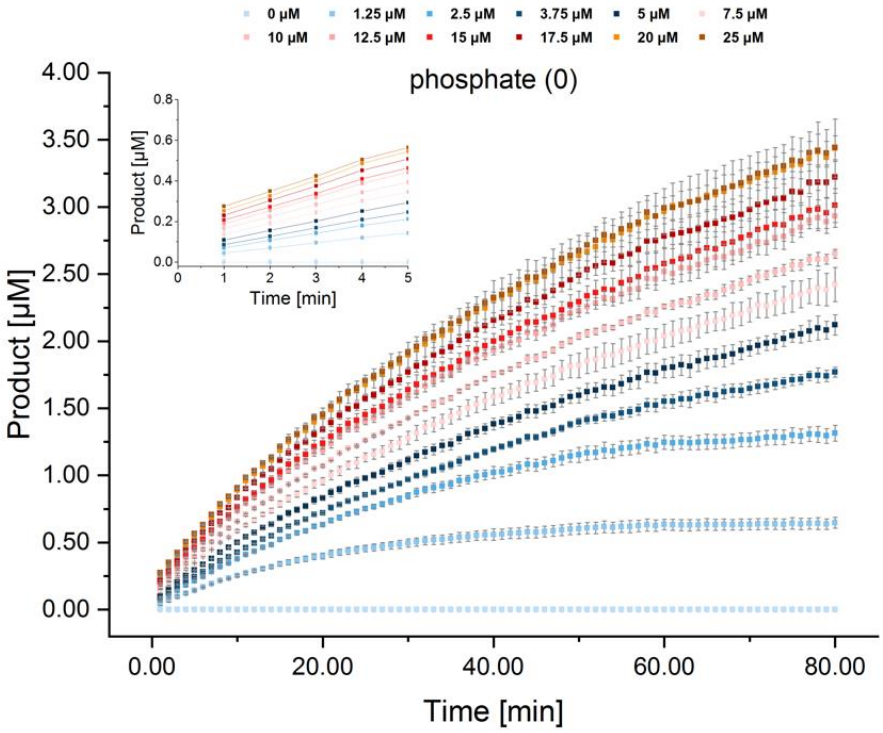
0 µM
1.25 µM
2.5 µM
3.75 µM
5 µM
7.5 µM
10 µM
12.5 µM
15 µM
17.5 µM
20 µM
25 µM
phosphate (0)
Product [µM]
Time [min]
0.00
0.50
1.00
1.50
2.00
2.50
3.00
3.50
4.00
0.00
20.00
40.00
60.00
80.00
0.0
0.2
0.4
0.6
0.8
0
1
2
3
4
5

F

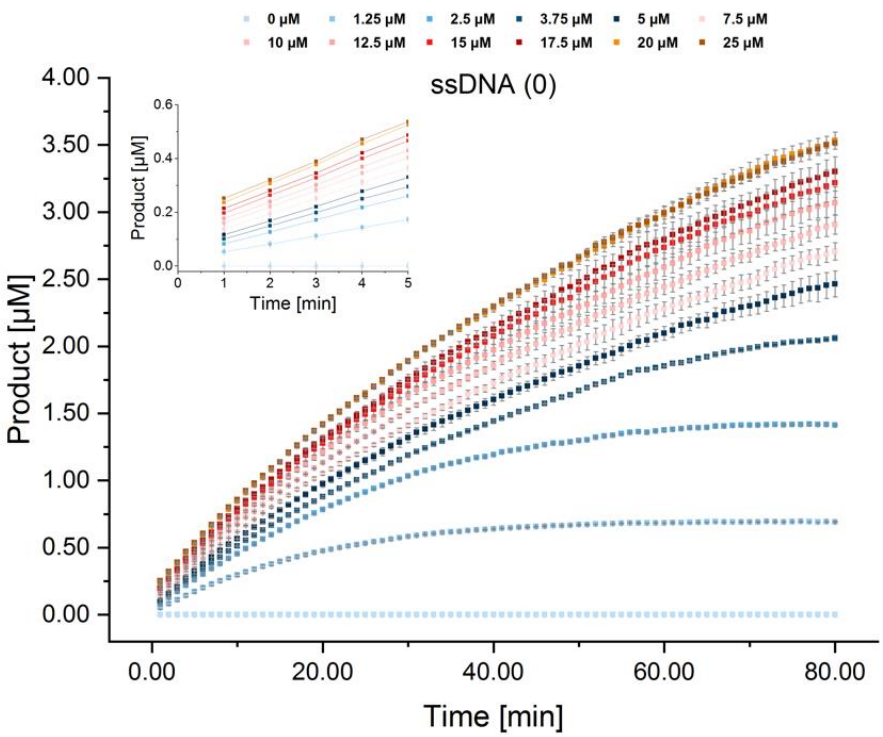
0 µM
1.25 µM
2.5 µM
3.75 µM
5 µM
7.5 µM
10 µM
12.5 µM
15 µM
17.5 µM
20 µM
25 µM
ssDNA (0)
Product [µM]
Time [min]
0.00
0.50
1.00
1.50
2.00
2.50
3.00
3.50
4.00
0.00
20.00
40.00
60.00
80.00
0.0
0.2
0.4
0.6
0
1
2
3
4
5

G

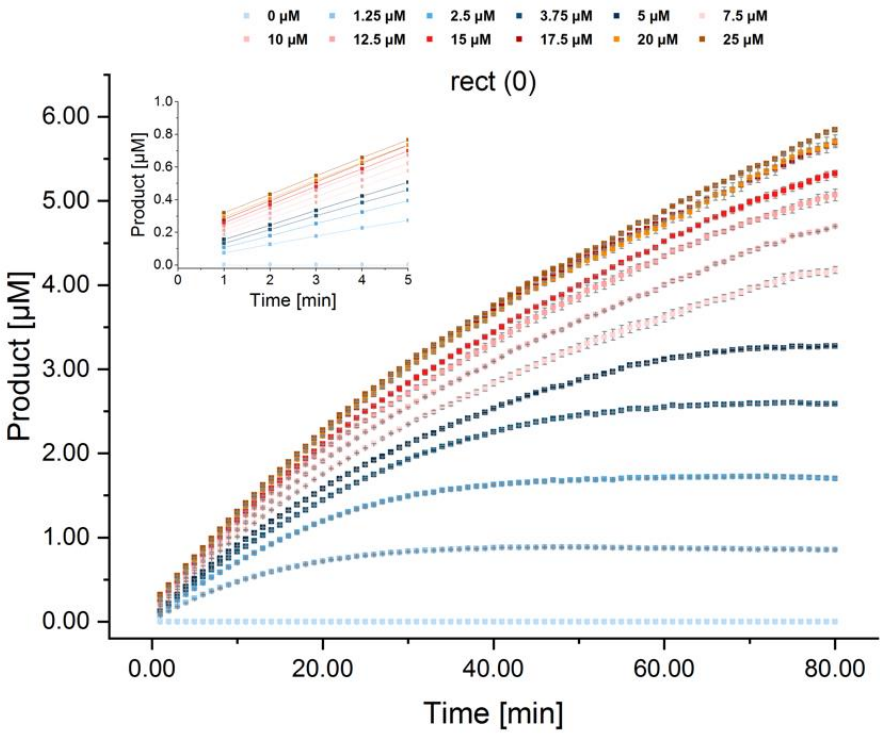
0 µM
1.25 µM
2.5 µM
3.75 µM
5 µM
7.5 µM
10 µM
12.5 µM
15 µM
17.5 µM
20 µM
25 µM
rect (0)
Product [µM]
Time [min]
0.00
1.00
2.00
3.00
4.00
5.00
6.00
0.00
20.00
40.00
60.00
80.00

H

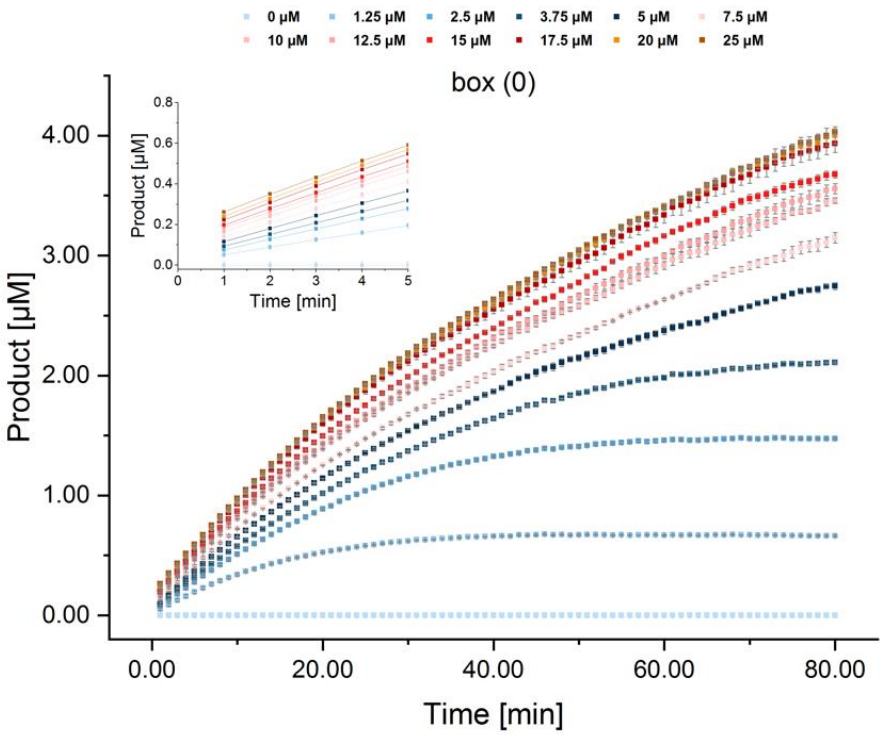
0 µM
1.25 µM
2.5 µM
3.75 µM
5 µM
7.5 µM
10 µM
12.5 µM
15 µM
17.5 µM
20 µM
25 µM
box (0)
Product [µM]
Time [min]
0.00
1.00
2.00
3.00
4.00
0.00
20.00
40.00
60.00
80.00

I

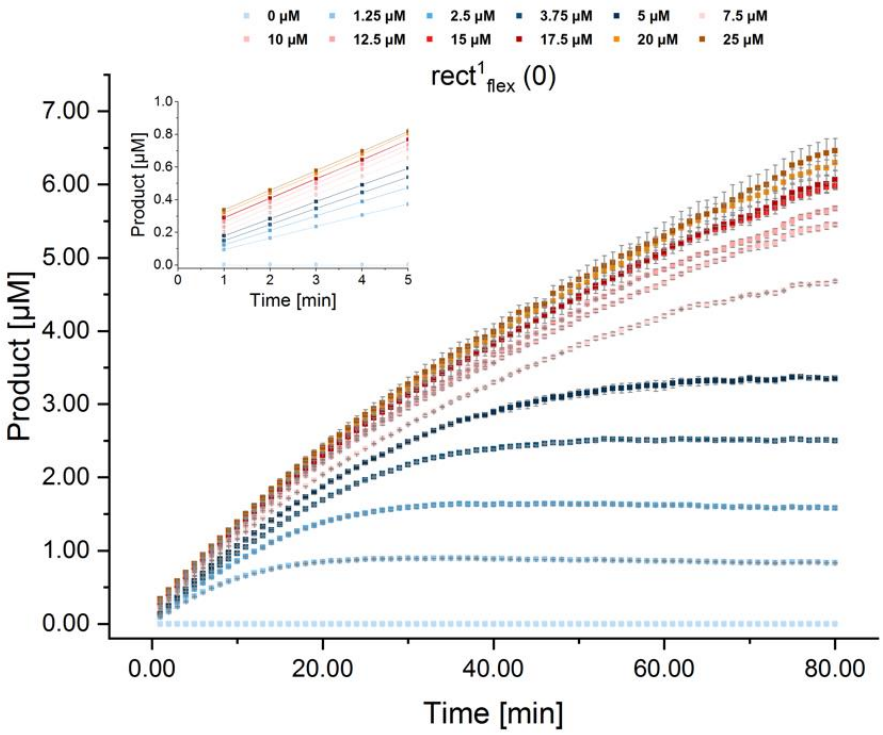
0 µM
1.25 µM
2.5 µM
3.75 µM
5 µM
7.5 µM
10 µM
12.5 µM
15 µM
17.5 µM
20 µM
25 µM
rect1flex (0)
Product [µM]
Time [min]
0.00
20.00
40.00
60.00
80.00
1.00
2.00
3.00
4.00
5.00
6.00
7.00

J

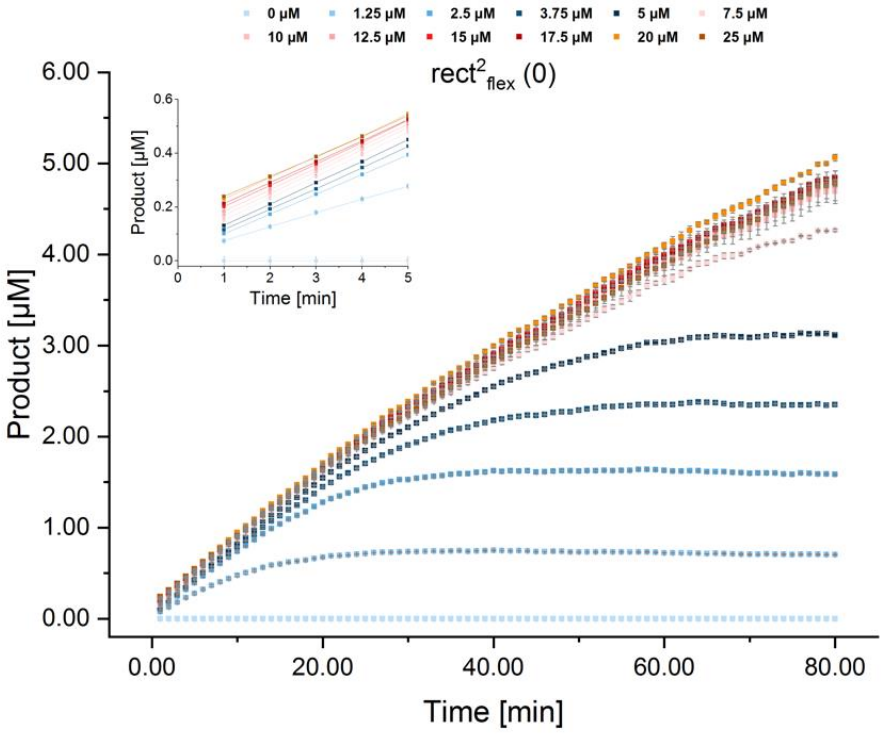
0 µM
1.25 µM
2.5 µM
3.75 µM
5 µM
7.5 µM
10 µM
12.5 µM
15 µM
17.5 µM
20 µM
25 µM
rect2flex (0)
Product [µM]
Time [min]
0.00
20.00
40.00
60.00
80.00
1.00
2.00
3.00
4.00
5.00
6.00

K

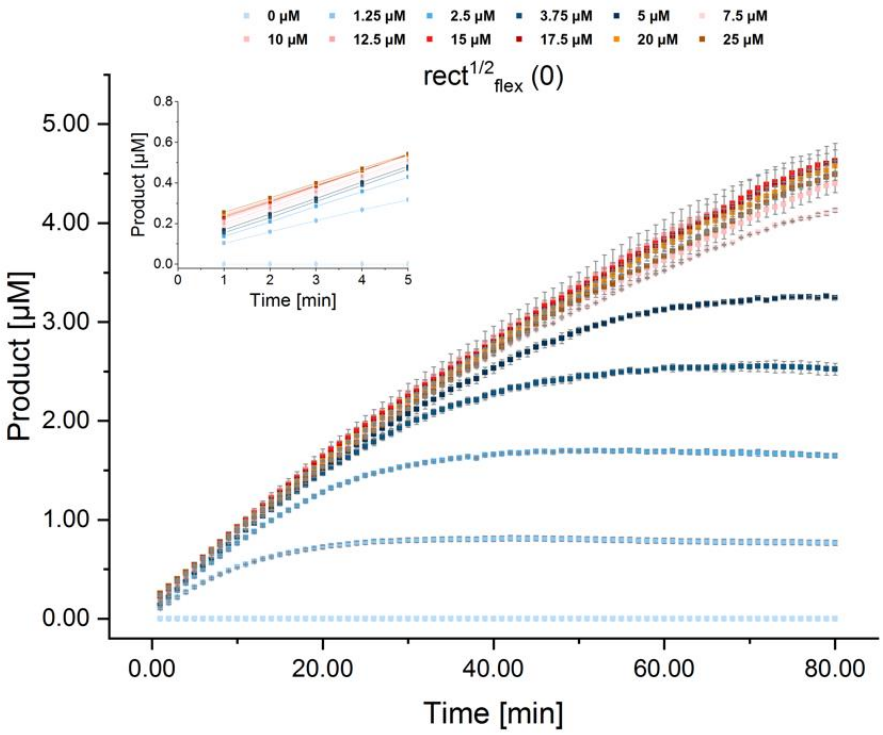
0 µM
1.25 µM
2.5 µM
3.75 µM
5 µM
7.5 µM
10 µM
12.5 µM
15 µM
17.5 µM
20 µM
25 µM
rect1/2flex (0)
Product [µM]
Time [min]
0.00
1.00
2.00
3.00
4.00
5.00
0.00
20.00
40.00
60.00
80.00

L

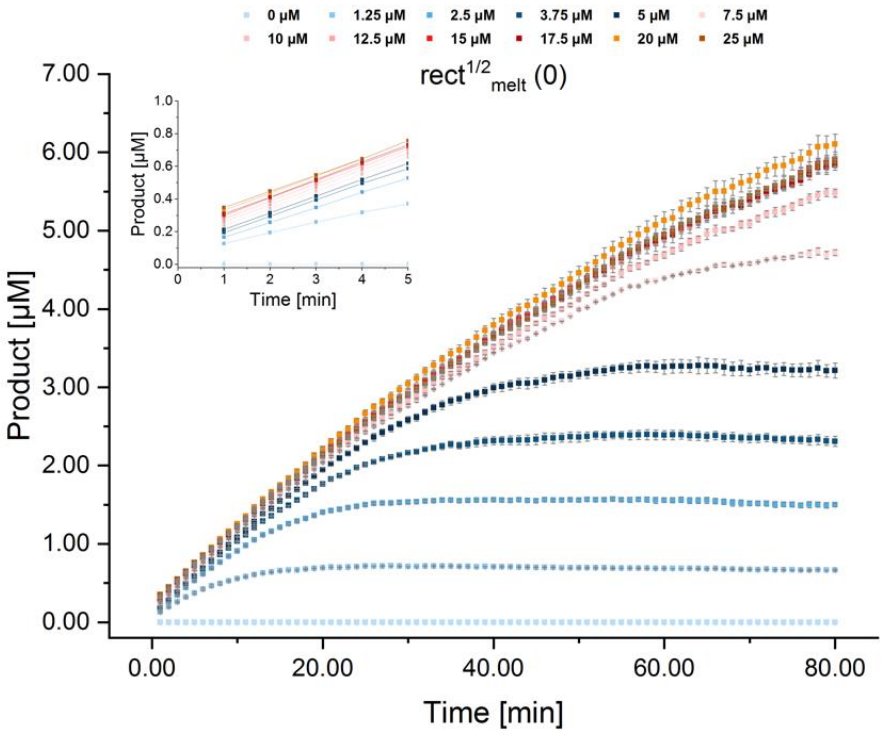
0 µM
1.25 µM
2.5 µM
3.75 µM
5 µM
7.5 µM
10 µM
12.5 µM
15 µM
17.5 µM
20 µM
25 µM
rect1/2melt (0)
Product [µM]
Time [min]
0.00
1.00
2.00
3.00
4.00
5.00
6.00
7.00
0.00
20.00
40.00
60.00
80.00

M

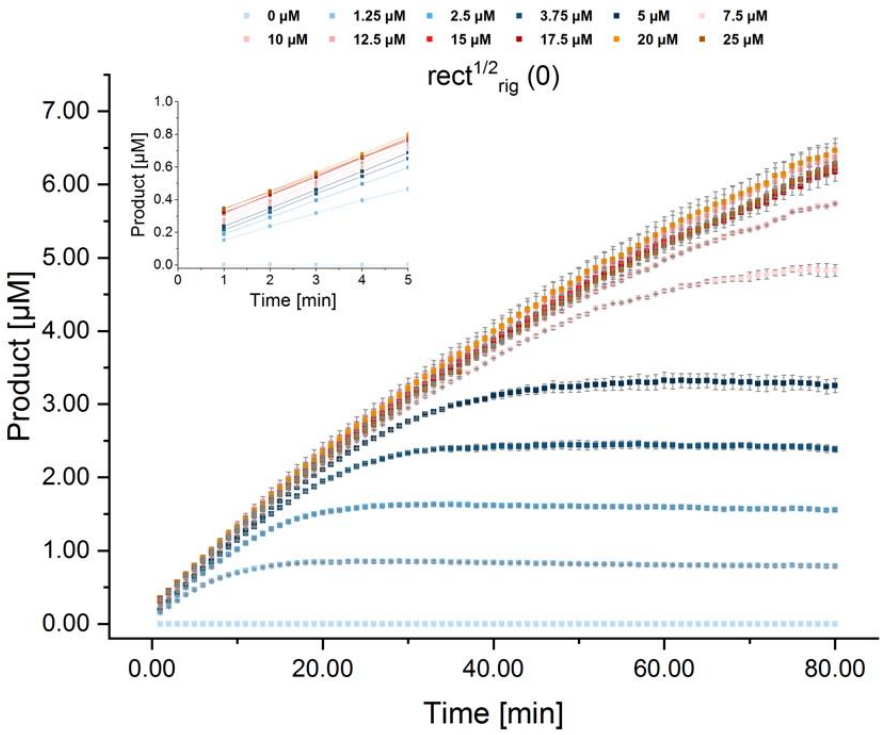
0 µM
1.25 µM
2.5 µM
3.75 µM
5 µM
7.5 µM
10 µM
12.5 µM
15 µM
17.5 µM
20 µM
25 µM
rect1/2rig (0)
Product [µM]
Time [min]
0.00
1.00
2.00
3.00
4.00
5.00
6.00
7.00
0.00
20.00
40.00
60.00
80.00

N

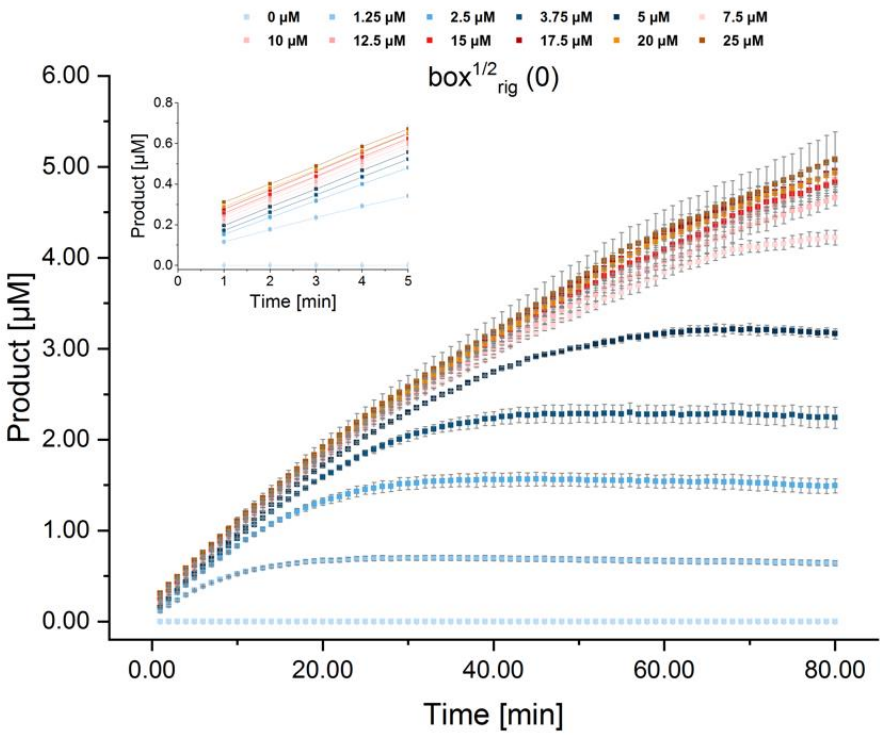
0 µM
1.25 µM
2.5 µM
3.75 µM
5 µM
7.5 µM
10 µM
12.5 µM
15 µM
17.5 µM
20 µM
25 µM
box1/2rig (0)
Product [µM]
Time [min]
0.00
1.00
2.00
3.00
4.00
5.00
6.00
0.00
20.00
40.00
60.00
80.00

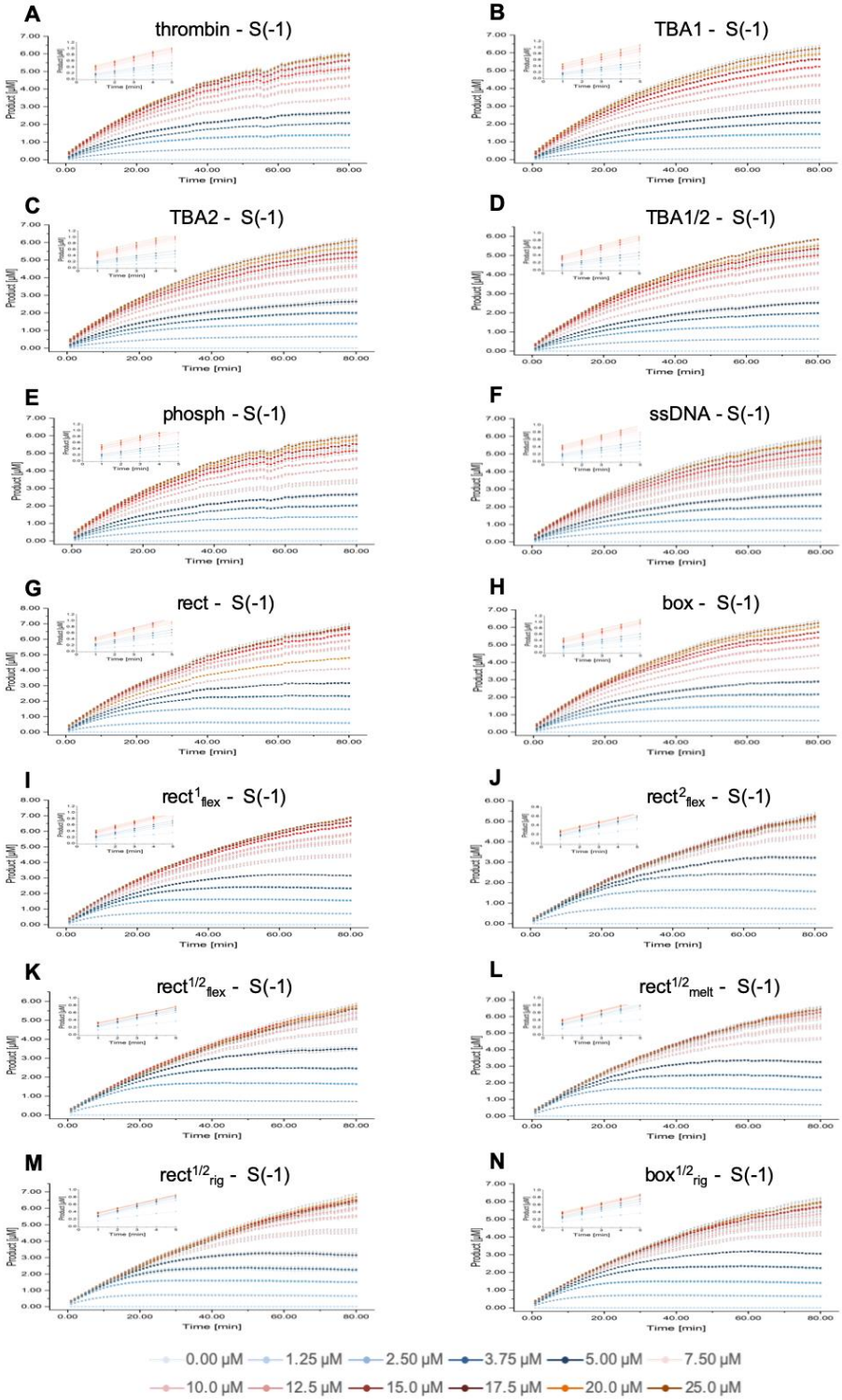

Figure S 17: Exemplary curves of product formation for S(-1). Same legend as in Figure S 16. Here, the substrate used was FAM-GGfPR|SGGGK(BHQ1)KD-OH (where "|" indicates the position of peptide cleavage). The calculated net charge of the FRET peptide S(-1) at pH 7 is -1. Reprinted and adapted from reference [200].

Enlarged version of this figure is given below for convenience.

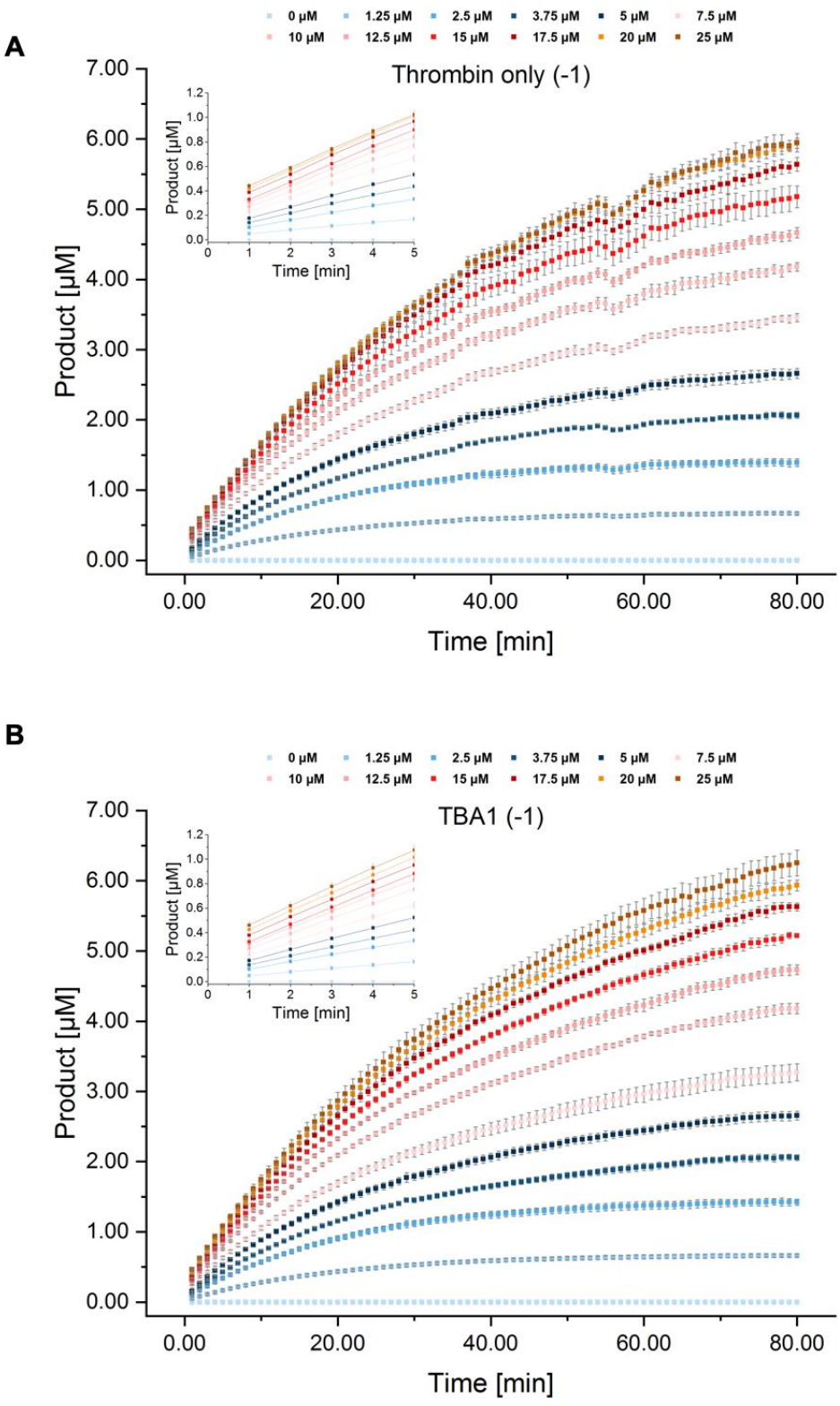
A
0 µM
1.25 µM
2.5 µM
3.75 µM
5 µM
7.5 µM
10 µM
12.5 µM
15 µM
17.5 µM
20 µM
25 µM
Thrombin only (-1)
Product [µM]
Time [min]
B
TBA1 (-1)
Product [µM]
Time [min]

C

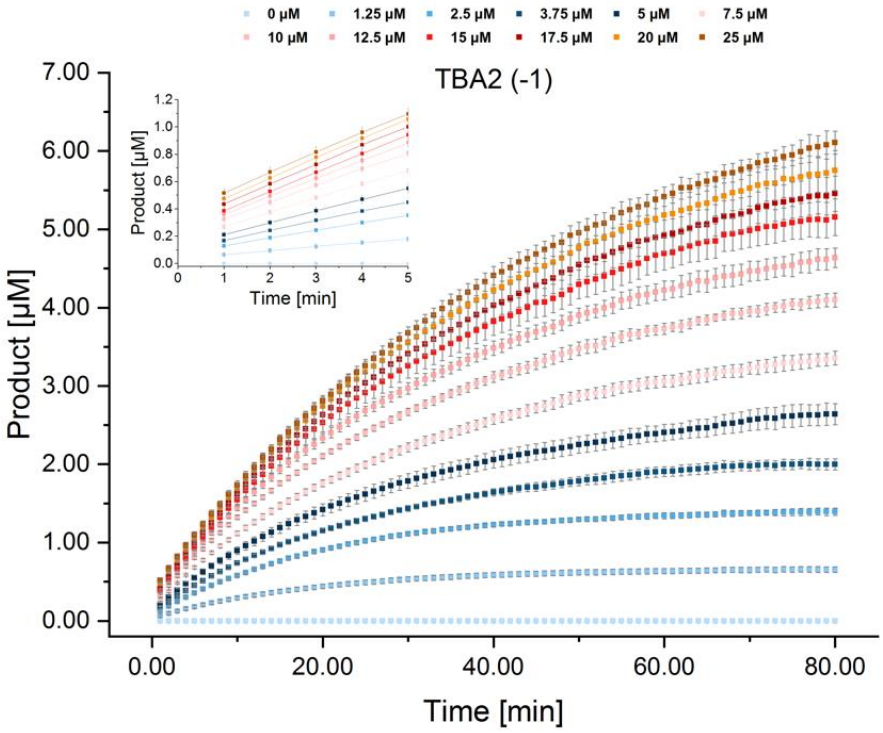
0 µM
1.25 µM
2.5 µM
3.75 µM
5 µM
7.5 µM
10 µM
12.5 µM
15 µM
17.5 µM
20 µM
25 µM
TBA2 (-1)
Product [µM]
Time [min]

D

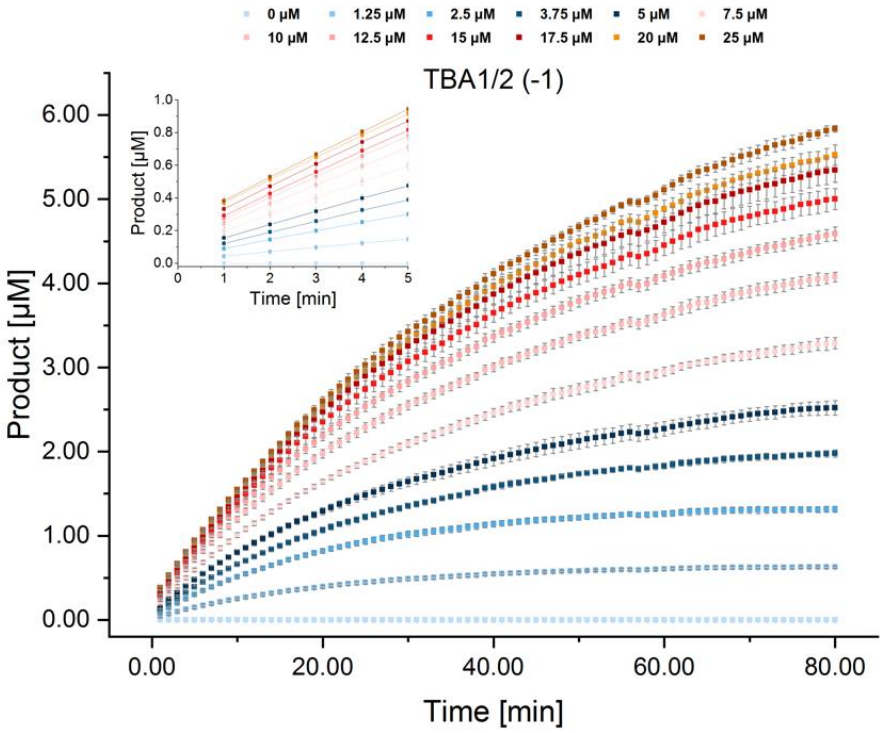
0 µM
1.25 µM
2.5 µM
3.75 µM
5 µM
7.5 µM
10 µM
12.5 µM
15 µM
17.5 µM
20 µM
25 µM
TBA1/2 (-1)
Product [µM]
Time [min]

E

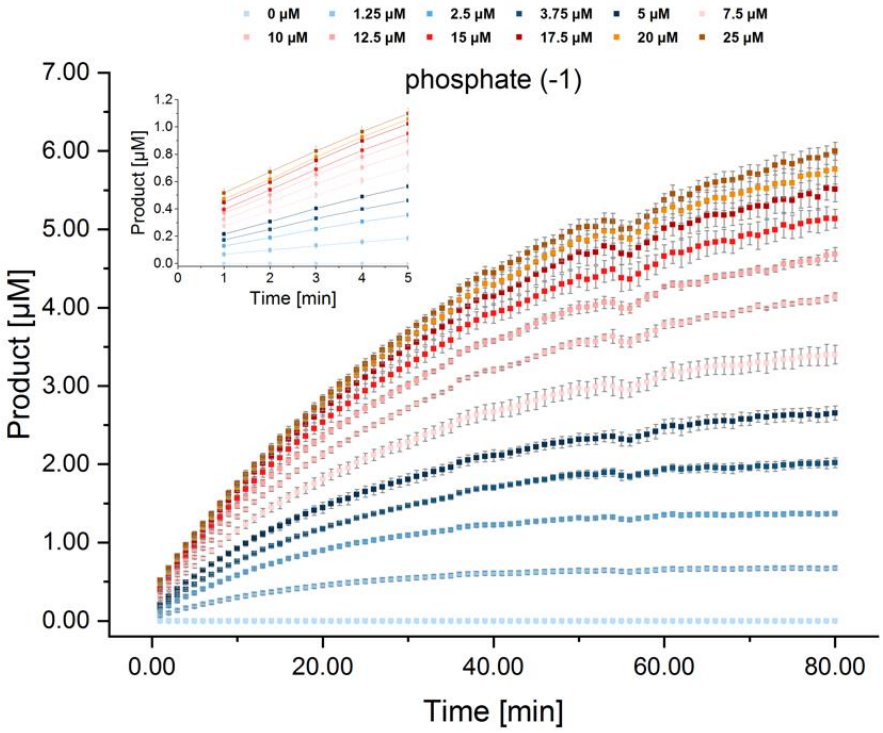
0 µM
1.25 µM
2.5 µM
3.75 µM
5 µM
7.5 µM
10 µM
12.5 µM
15 µM
17.5 µM
20 µM
25 µM
phosphate (-1)
Product [µM]
Time [min]
0.00
1.00
2.00
3.00
4.00
5.00
6.00
7.00
0.00
20.00
40.00
60.00
80.00
0.0
0.2
0.4
0.6
0.8
1.0
1.2
0
1
2
3
4
5

F

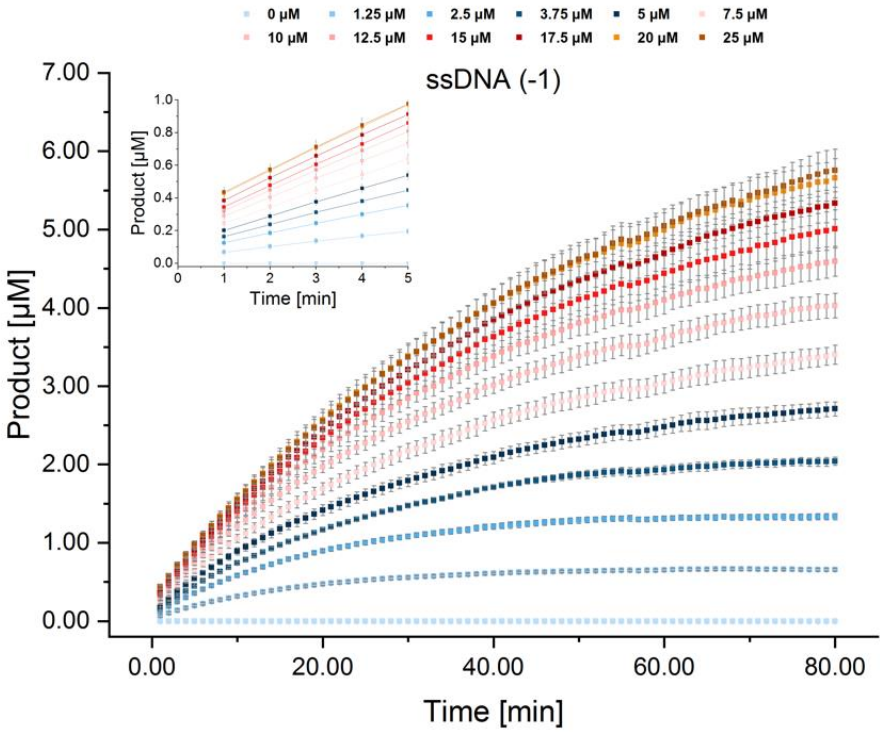
0 µM
1.25 µM
2.5 µM
3.75 µM
5 µM
7.5 µM
10 µM
12.5 µM
15 µM
17.5 µM
20 µM
25 µM
ssDNA (-1)
Product [µM]
Time [min]
0.00
1.00
2.00
3.00
4.00
5.00
6.00
7.00
0.00
20.00
40.00
60.00
80.00
0.0
0.2
0.4
0.6
0.8
1.0
0
1
2
3
4
5

G

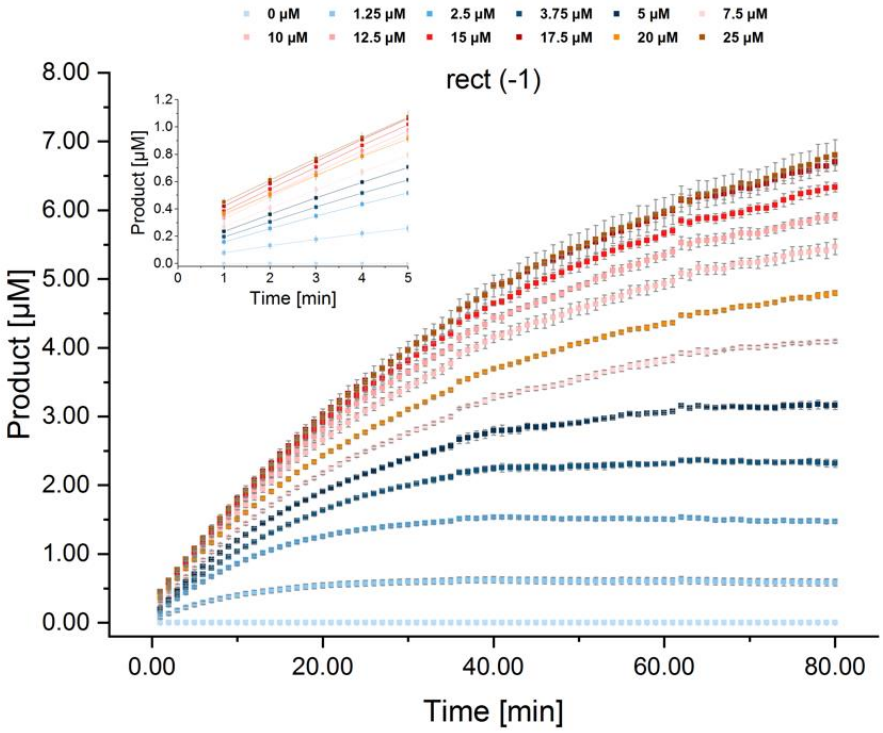
0 µM
1.25 µM
2.5 µM
3.75 µM
5 µM
7.5 µM
10 µM
12.5 µM
15 µM
17.5 µM
20 µM
25 µM
rect (-1)
Product [µM]
Time [min]
0.00
1.00
2.00
3.00
4.00
5.00
6.00
7.00
8.00
0.00
20.00
40.00
60.00
80.00

H

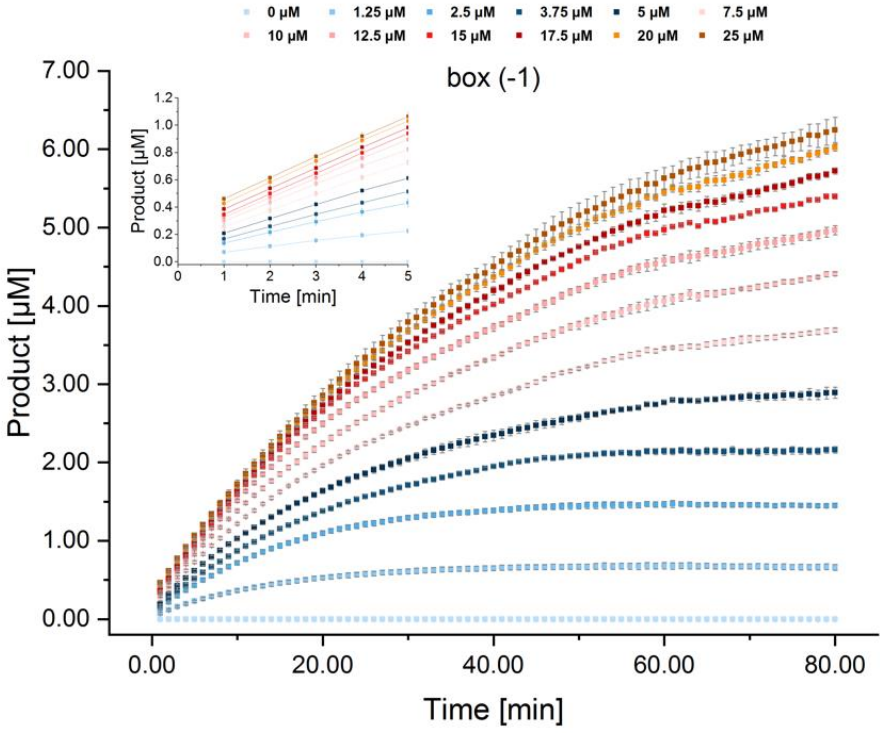
0 µM
1.25 µM
2.5 µM
3.75 µM
5 µM
7.5 µM
10 µM
12.5 µM
15 µM
17.5 µM
20 µM
25 µM
box (-1)
Product [µM]
Time [min]
0.00
1.00
2.00
3.00
4.00
5.00
6.00
7.00
0.00
20.00
40.00
60.00
80.00

I

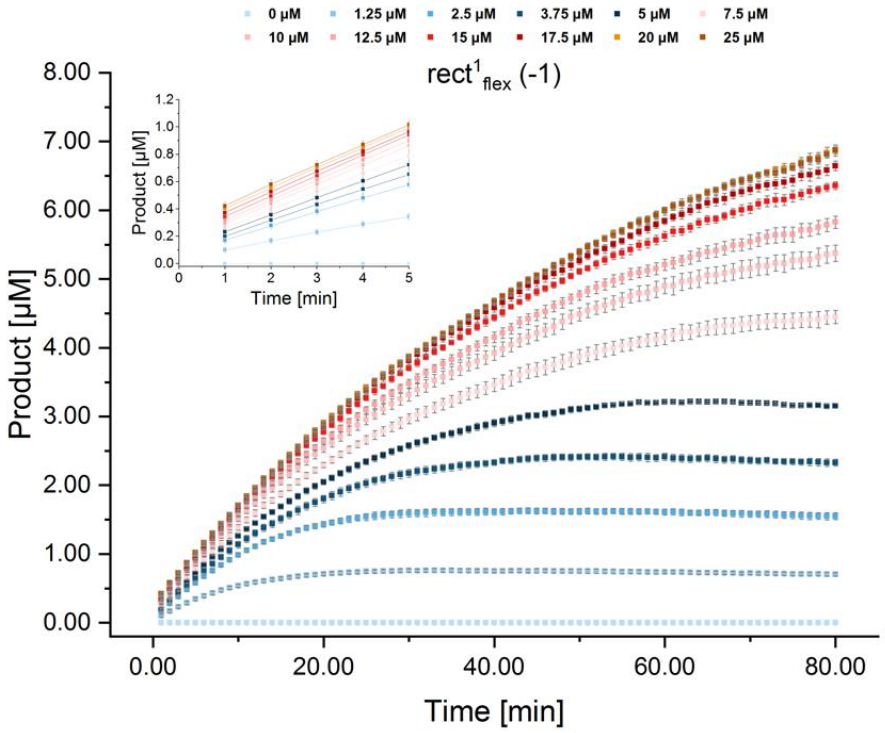
0 µM
1.25 µM
2.5 µM
3.75 µM
5 µM
7.5 µM
10 µM
12.5 µM
15 µM
17.5 µM
20 µM
25 µM
rect1flex (-1)
Product [µM]
Time [min]
0.00
1.00
2.00
3.00
4.00
5.00
6.00
7.00
8.00
0.00
20.00
40.00
60.00
80.00

J

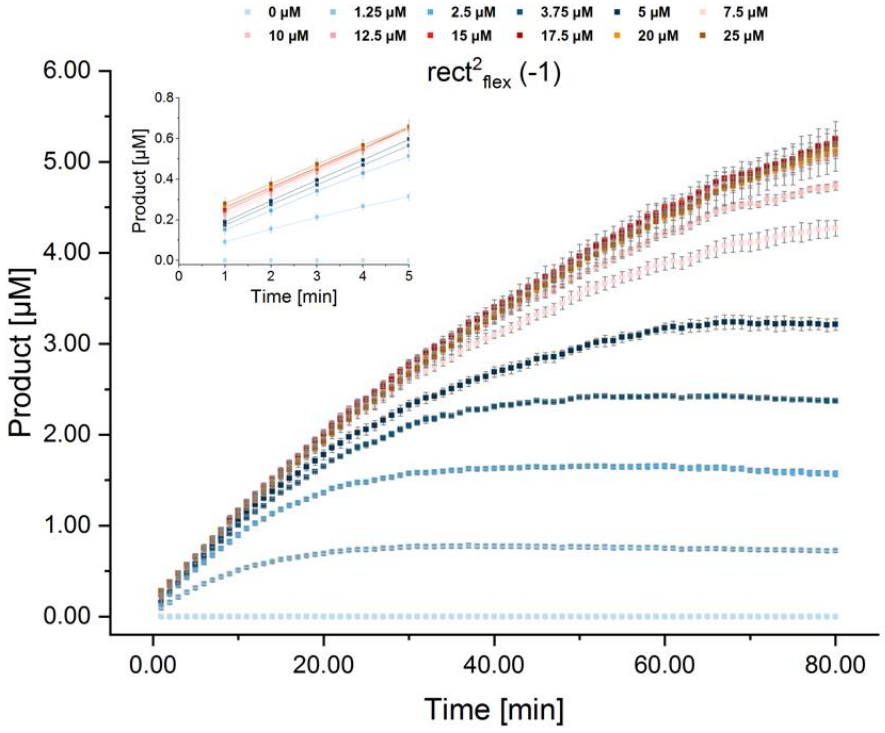
0 µM
1.25 µM
2.5 µM
3.75 µM
5 µM
7.5 µM
10 µM
12.5 µM
15 µM
17.5 µM
20 µM
25 µM
rect2flex (-1)
Product [µM]
Time [min]
0.00
1.00
2.00
3.00
4.00
5.00
6.00
0.00
20.00
40.00
60.00
80.00

K

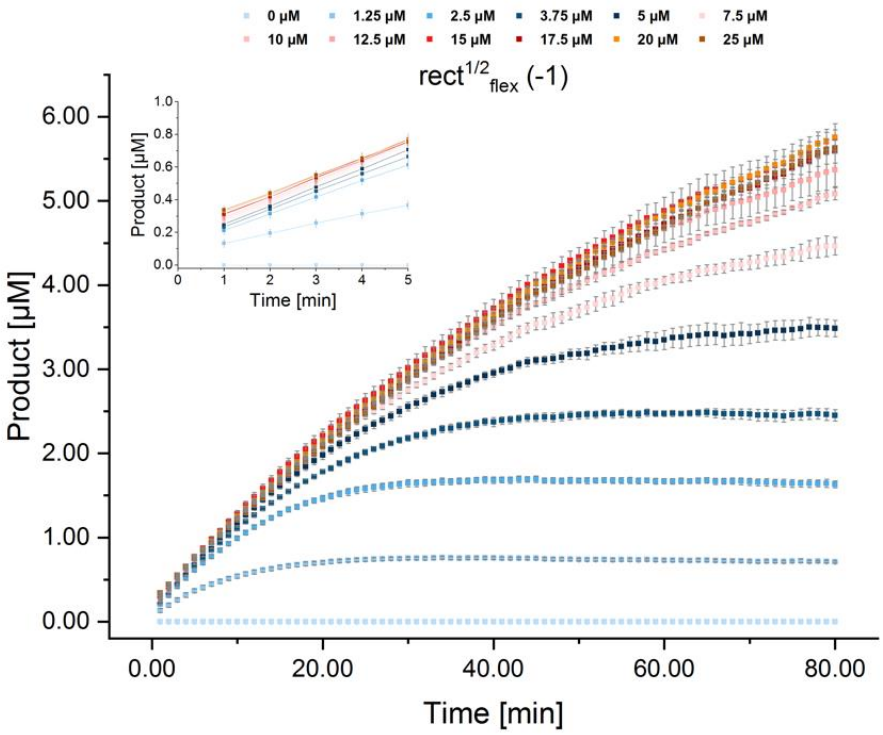
0 µM
1.25 µM
2.5 µM
3.75 µM
5 µM
7.5 µM
10 µM
12.5 µM
15 µM
17.5 µM
20 µM
25 µM
rect1/2flex (-1)
Product [µM]
Time [min]
0.00
1.00
2.00
3.00
4.00
5.00
6.00
0.00
20.00
40.00
60.00
80.00

L

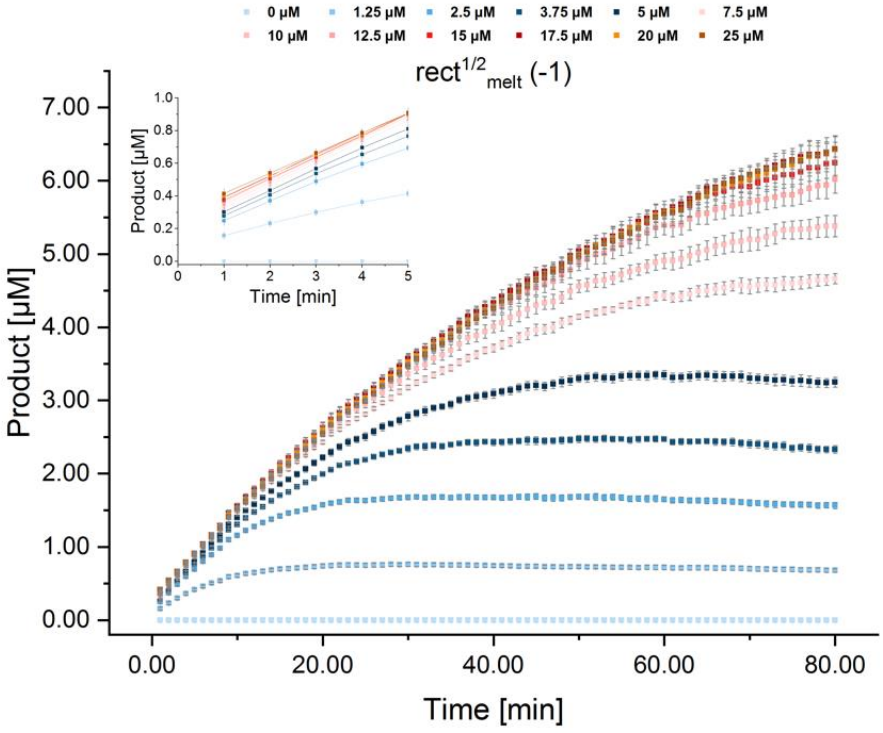
0 µM
1.25 µM
2.5 µM
3.75 µM
5 µM
7.5 µM
10 µM
12.5 µM
15 µM
17.5 µM
20 µM
25 µM
rect1/2melt (-1)
Product [µM]
Time [min]
0.00
1.00
2.00
3.00
4.00
5.00
6.00
7.00
0.00
20.00
40.00
60.00
80.00

M

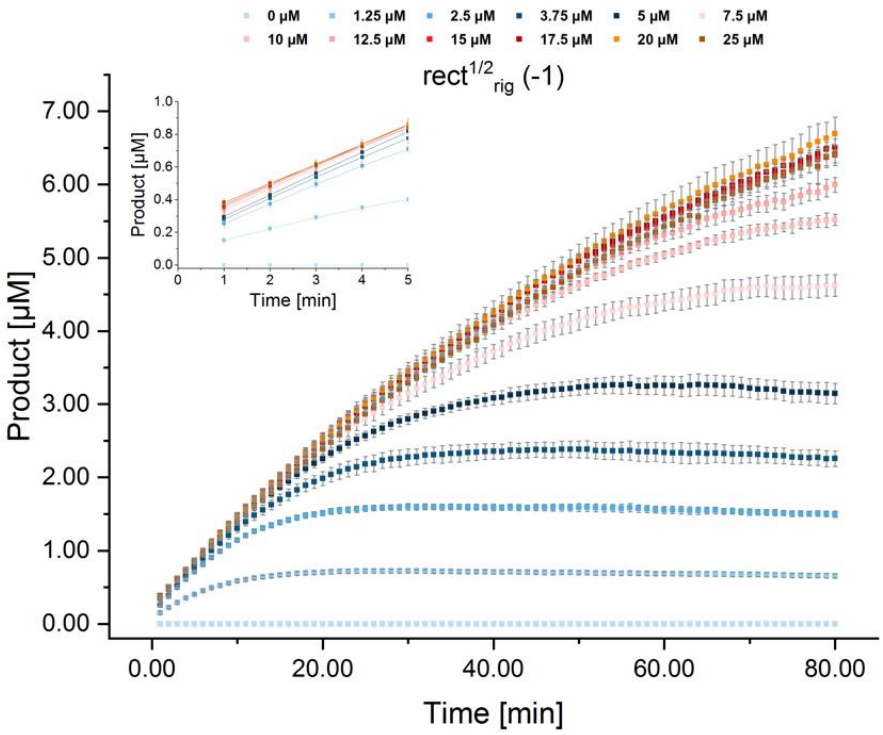
0 µM
1.25 µM
2.5 µM
3.75 µM
5 µM
7.5 µM
10 µM
12.5 µM
15 µM
17.5 µM
20 µM
25 µM
rect1/2rig (-1)
Product [µM]
Time [min]
0.00
1.00
2.00
3.00
4.00
5.00
6.00
7.00
0.00
20.00
40.00
60.00
80.00
0.0
0.2
0.4
0.6
0.8
1.0
0
1
2
3
4
5

N

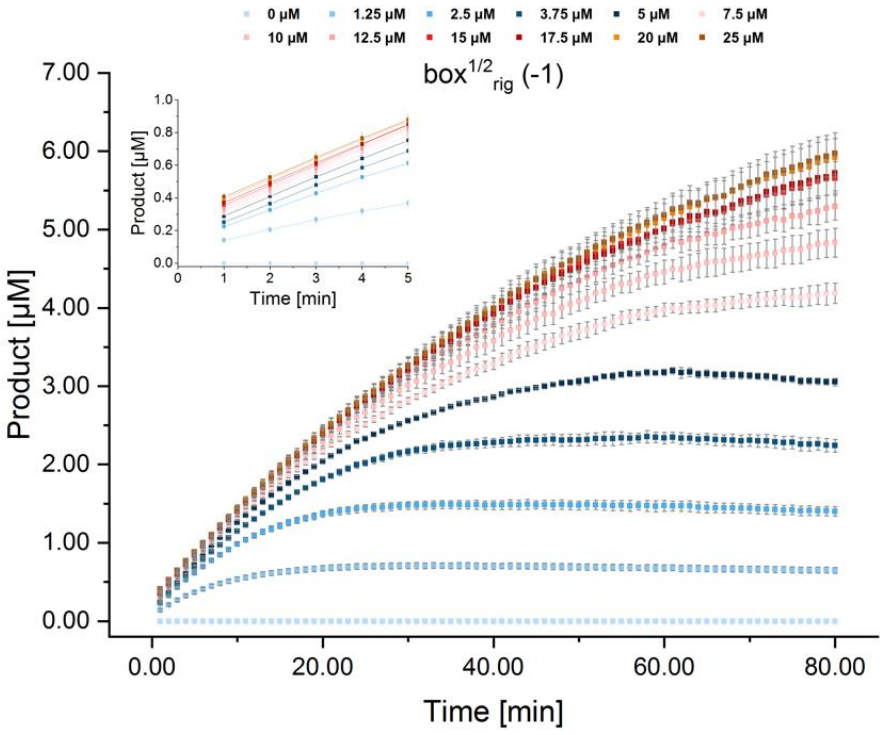
0 µM
1.25 µM
2.5 µM
3.75 µM
5 µM
7.5 µM
10 µM
12.5 µM
15 µM
17.5 µM
20 µM
25 µM
box1/2rig (-1)
Product [µM]
Time [min]
0.00
1.00
2.00
3.00
4.00
5.00
6.00
7.00
0.00
20.00
40.00
60.00
80.00
0.0
0.2
0.4
0.6
0.8
1.0
0
1
2
3
4
5

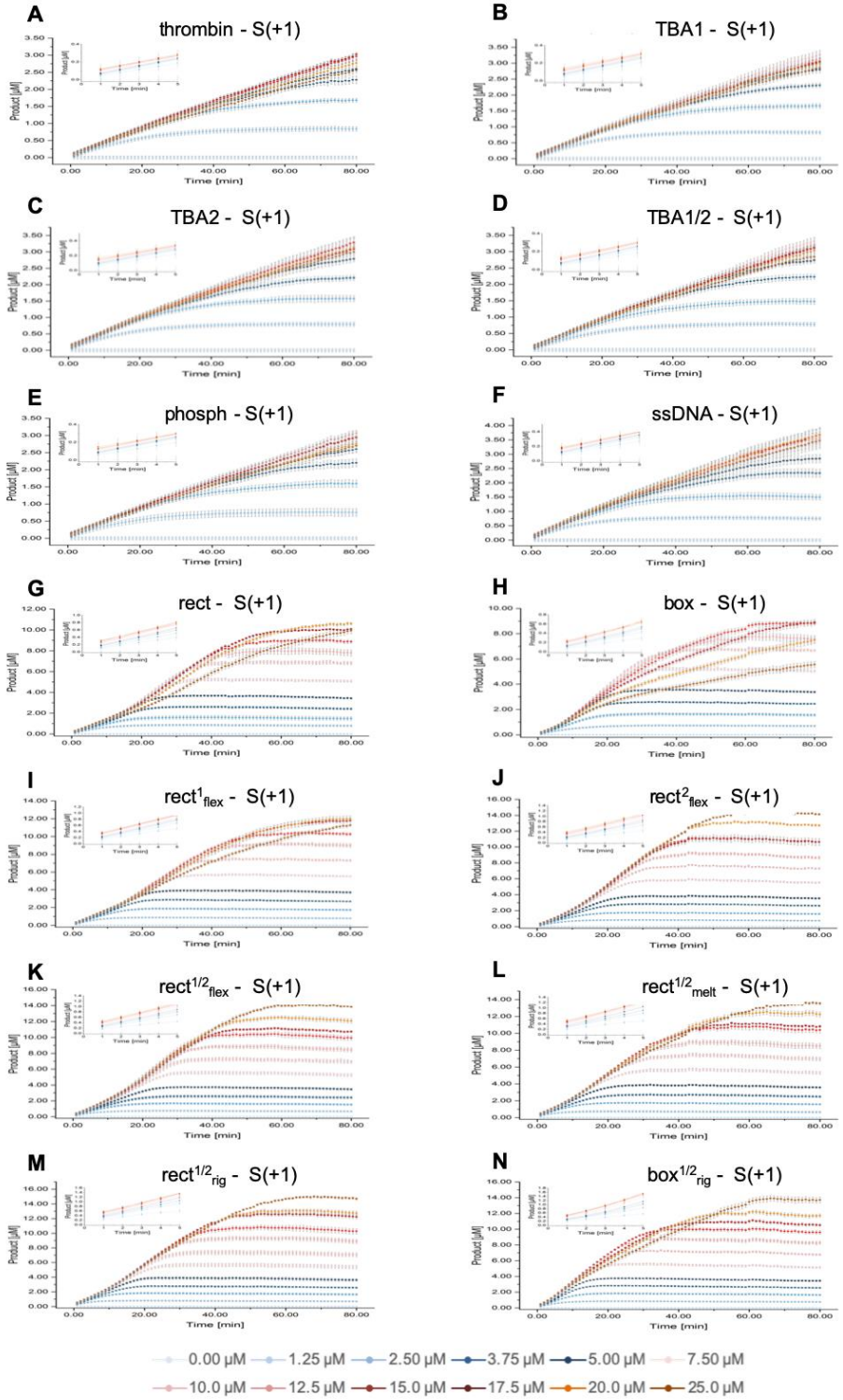

Figure S 18: Exemplary curves of product formation for S(+1). Same legend as in Figure S 16. Here, the substrate used was FAM-GGfPR|SGGGK(BHQ1)KK-OH (where "|" indicates the position of peptide cleavage). The calculated net charge of the FRET peptide S(+1) at pH 7 is +1. Reprinted and adapted from reference [200].

Enlarged version of this figure is given below for convenience.

A

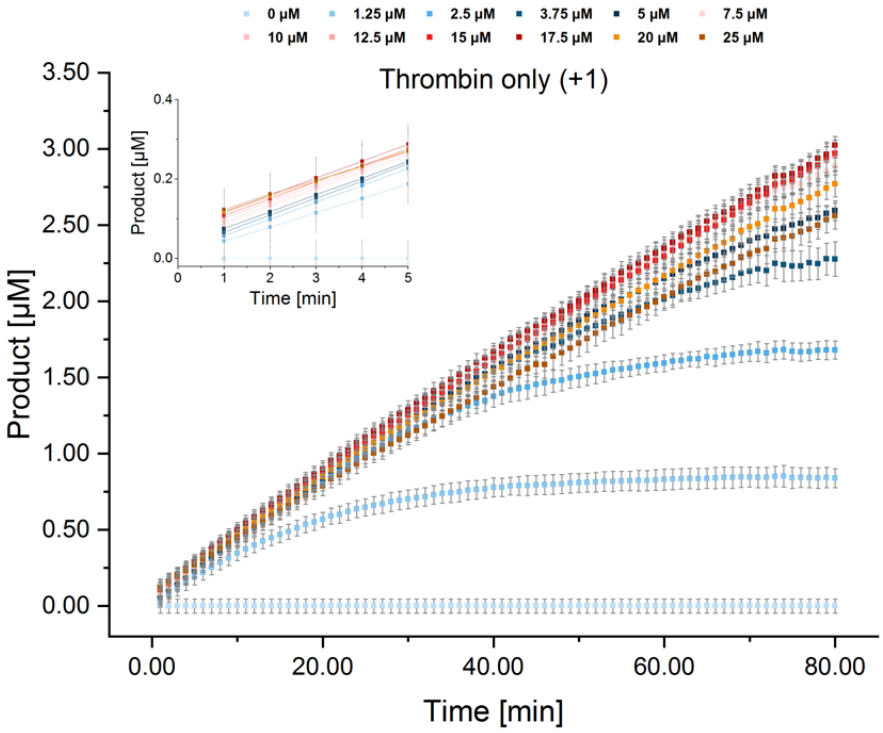
0 µM
1.25 µM
2.5 µM
3.75 µM
5 µM
7.5 µM
10 µM
12.5 µM
15 µM
17.5 µM
20 µM
25 µM
Thrombin only (+1)
Product [µM]
Time [min]
0.00
0.50
1.00
1.50
2.00
2.50
3.00
3.50
0.00
20.00
40.00
60.00
80.00
0.0
0.2
0.4
0
1
2
3
4
5

B

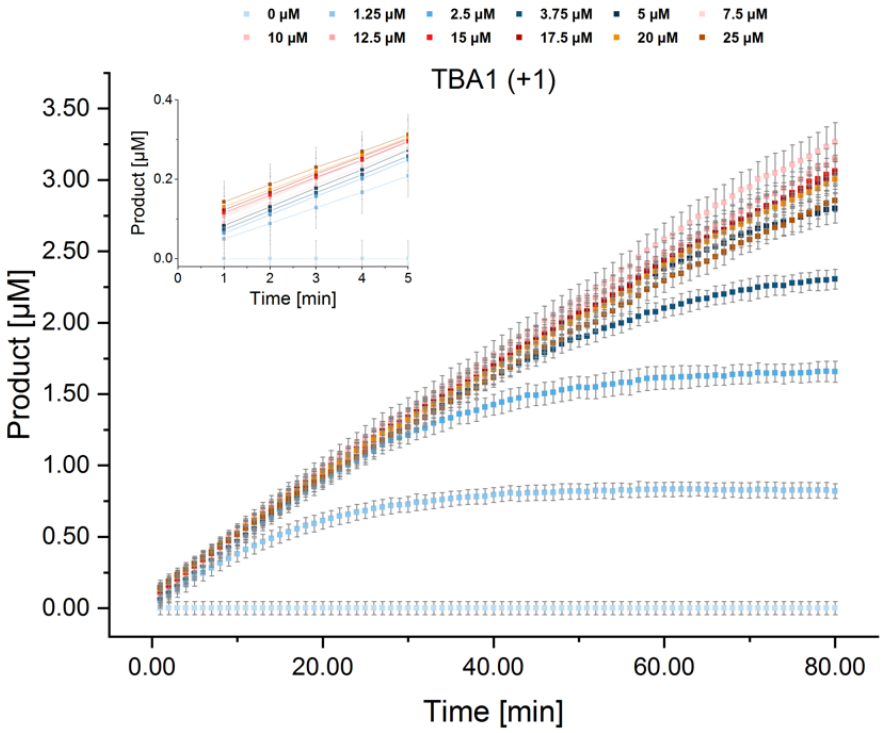
0 µM
1.25 µM
2.5 µM
3.75 µM
5 µM
7.5 µM
10 µM
12.5 µM
15 µM
17.5 µM
20 µM
25 µM
TBA1 (+1)
Product [µM]
Time [min]
0.00
0.50
1.00
1.50
2.00
2.50
3.00
3.50
0.00
20.00
40.00
60.00
80.00
0.0
0.2
0.4
0
1
2
3
4
5

C

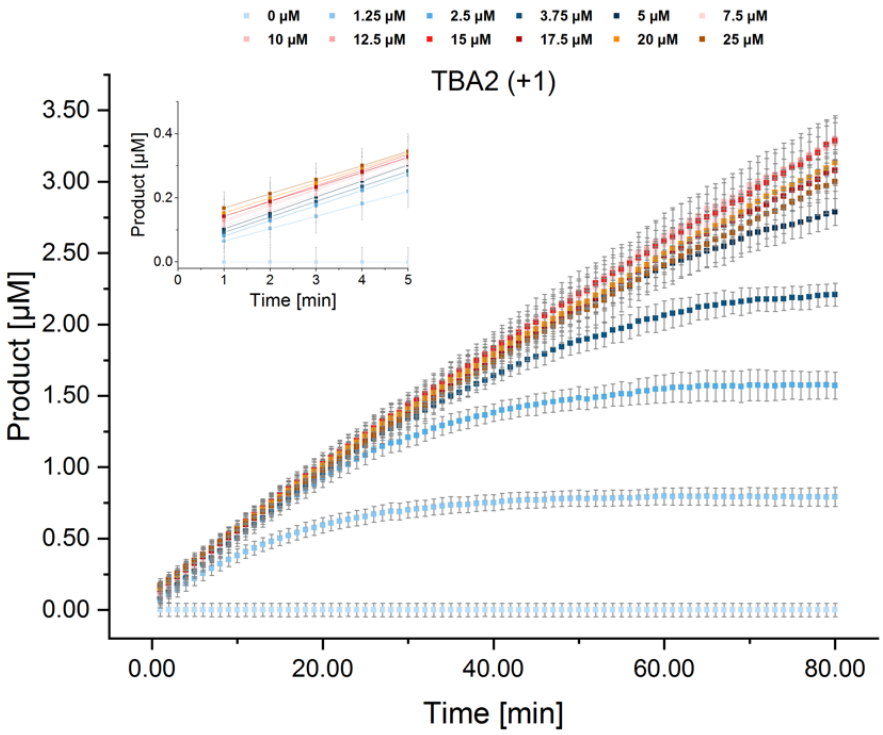
0 µM
1.25 µM
2.5 µM
3.75 µM
5 µM
7.5 µM
10 µM
12.5 µM
15 µM
17.5 µM
20 µM
25 µM
TBA2 (+1)
Product [µM]
Time [min]
0.00
0.50
1.00
1.50
2.00
2.50
3.00
3.50
0.0
0.2
0.4
0
1
2
3
4
5
0.00
20.00
40.00
60.00
80.00

D

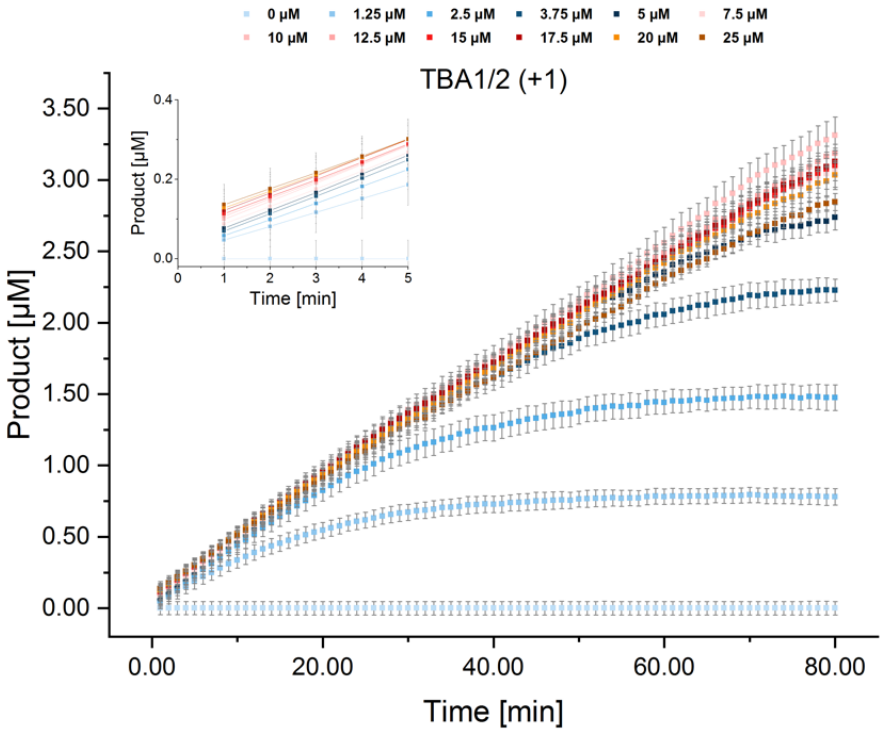
0 µM
1.25 µM
2.5 µM
3.75 µM
5 µM
7.5 µM
10 µM
12.5 µM
15 µM
17.5 µM
20 µM
25 µM
TBA1/2 (+1)
Product [µM]
Time [min]
0.00
0.50
1.00
1.50
2.00
2.50
3.00
3.50
0.0
0.2
0.4
0
1
2
3
4
5
0.00
20.00
40.00
60.00
80.00

E

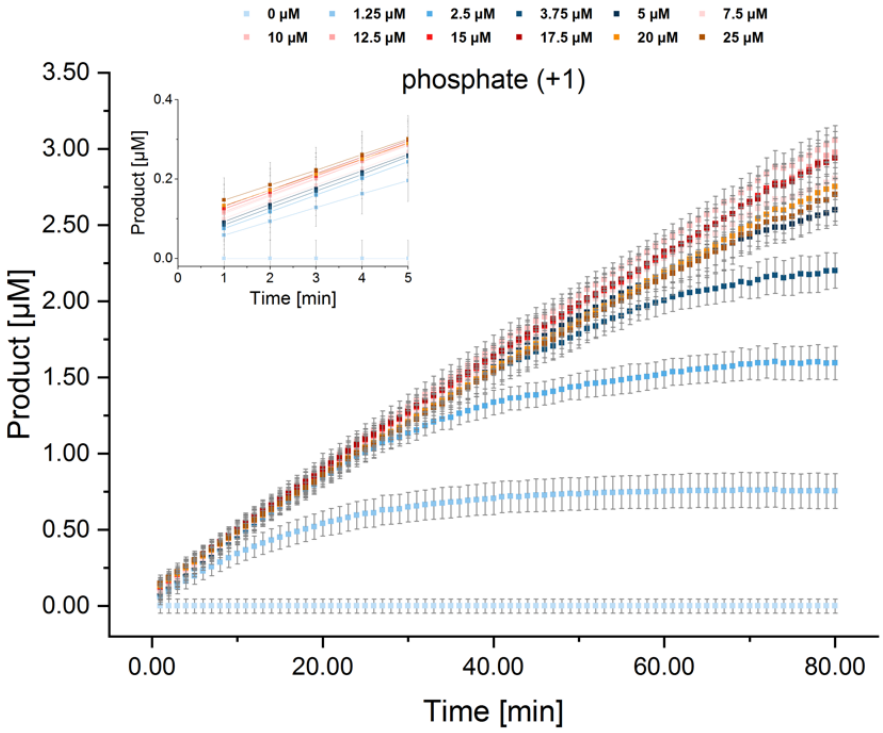
0 µM
1.25 µM
2.5 µM
3.75 µM
5 µM
7.5 µM
10 µM
12.5 µM
15 µM
17.5 µM
20 µM
25 µM
phosphate (+1)
Product [µM]
Time [min]
0.00
0.50
1.00
1.50
2.00
2.50
3.00
3.50
0.00
20.00
40.00
60.00
80.00
0.0
0.2
0.4
0
1
2
3
4
5

F

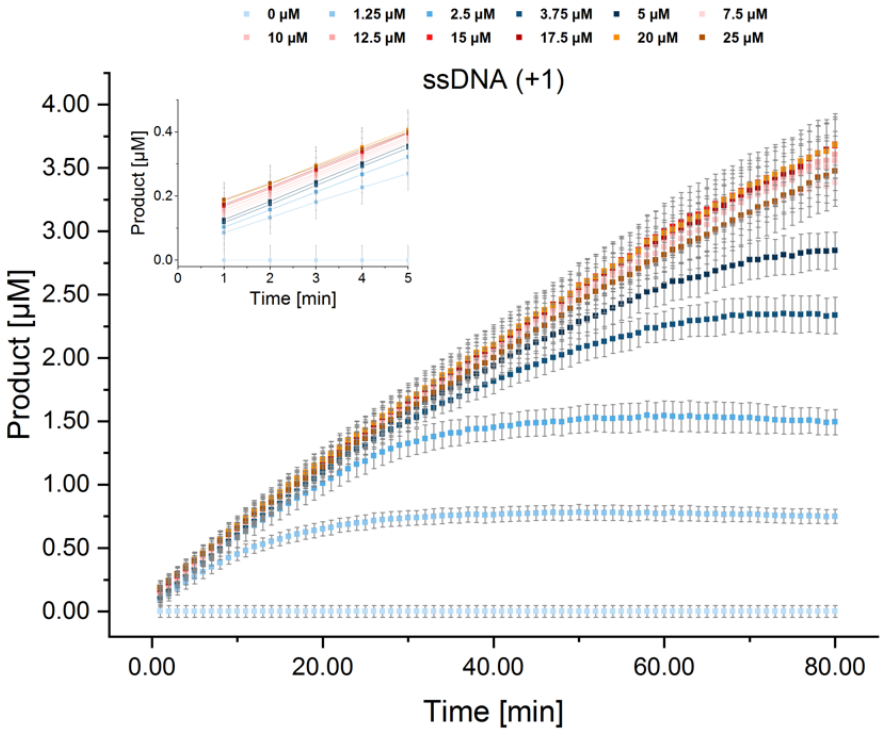
0 µM
1.25 µM
2.5 µM
3.75 µM
5 µM
7.5 µM
10 µM
12.5 µM
15 µM
17.5 µM
20 µM
25 µM
ssDNA (+1)
Product [µM]
Time [min]
0.00
0.50
1.00
1.50
2.00
2.50
3.00
3.50
4.00
0.00
20.00
40.00
60.00
80.00
0.0
0.2
0.4
0
1
2
3
4
5

G

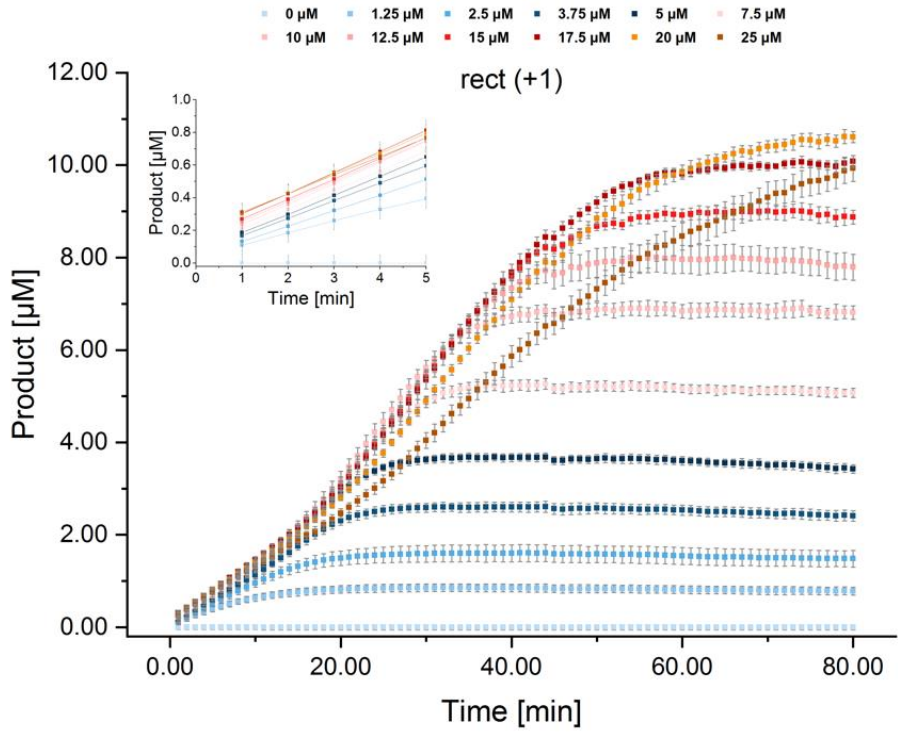
0 µM
1.25 µM
2.5 µM
3.75 µM
5 µM
7.5 µM
10 µM
12.5 µM
15 µM
17.5 µM
20 µM
25 µM
rect (+1)
Product [µM]
Time [min]
0.00
2.00
4.00
6.00
8.00
10.00
12.00
0.00
20.00
40.00
60.00
80.00

H

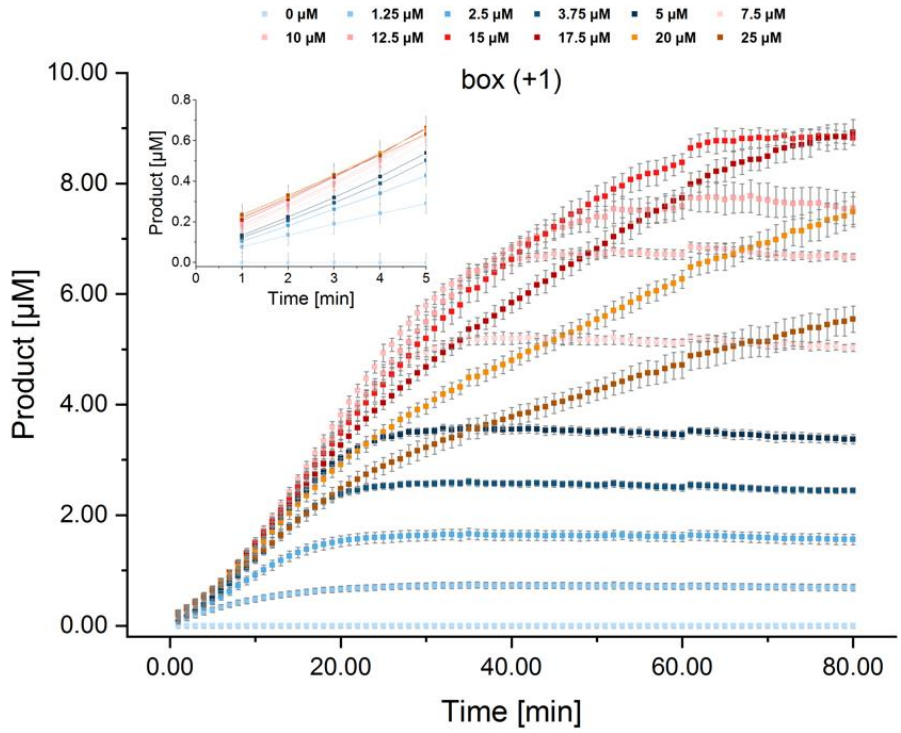
0 µM
1.25 µM
2.5 µM
3.75 µM
5 µM
7.5 µM
10 µM
12.5 µM
15 µM
17.5 µM
20 µM
25 µM
box (+1)
Product [µM]
Time [min]
0.00
2.00
4.00
6.00
8.00
10.00
0.00
20.00
40.00
60.00
80.00

I

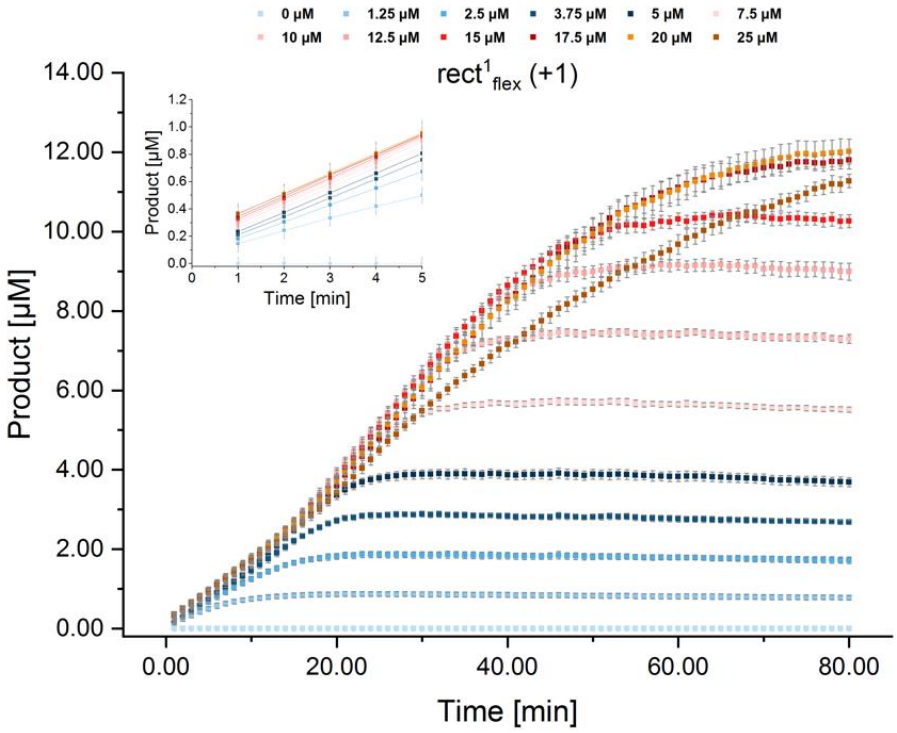
0 µM
1.25 µM
2.5 µM
3.75 µM
5 µM
7.5 µM
10 µM
12.5 µM
15 µM
17.5 µM
20 µM
25 µM
rect1flex (+1)
Product [µM]
Time [min]
0.00
2.00
4.00
6.00
8.00
10.00
12.00
14.00
0.00
20.00
40.00
60.00
80.00

J

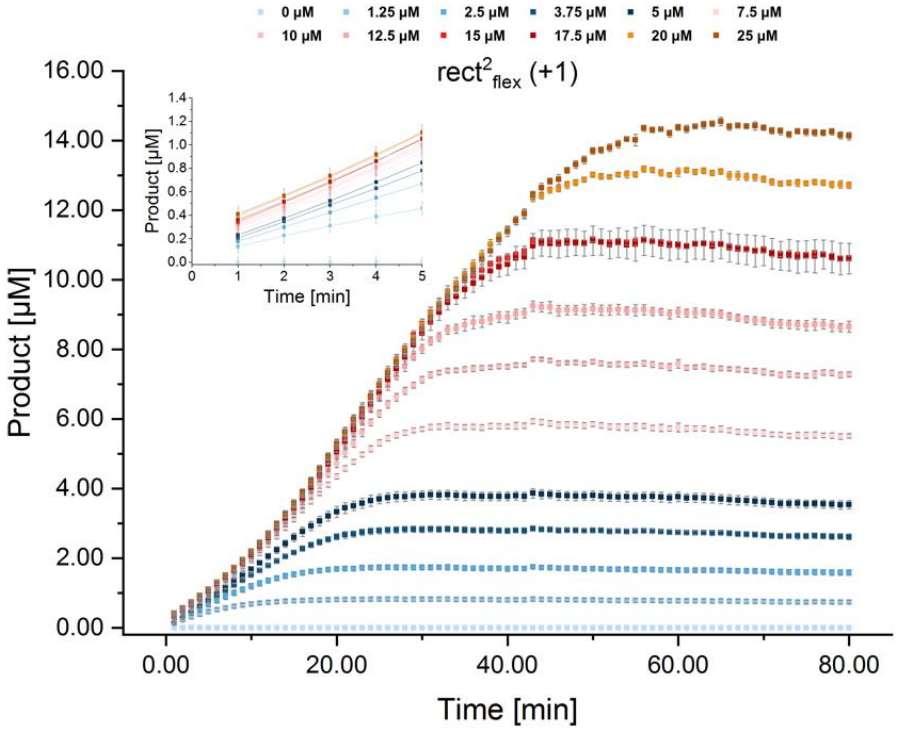
0 µM
1.25 µM
2.5 µM
3.75 µM
5 µM
7.5 µM
10 µM
12.5 µM
15 µM
17.5 µM
20 µM
25 µM
rect2flex (+1)
Product [µM]
Time [min]
0.00
2.00
4.00
6.00
8.00
10.00
12.00
14.00
16.00
0.00
20.00
40.00
60.00
80.00

K

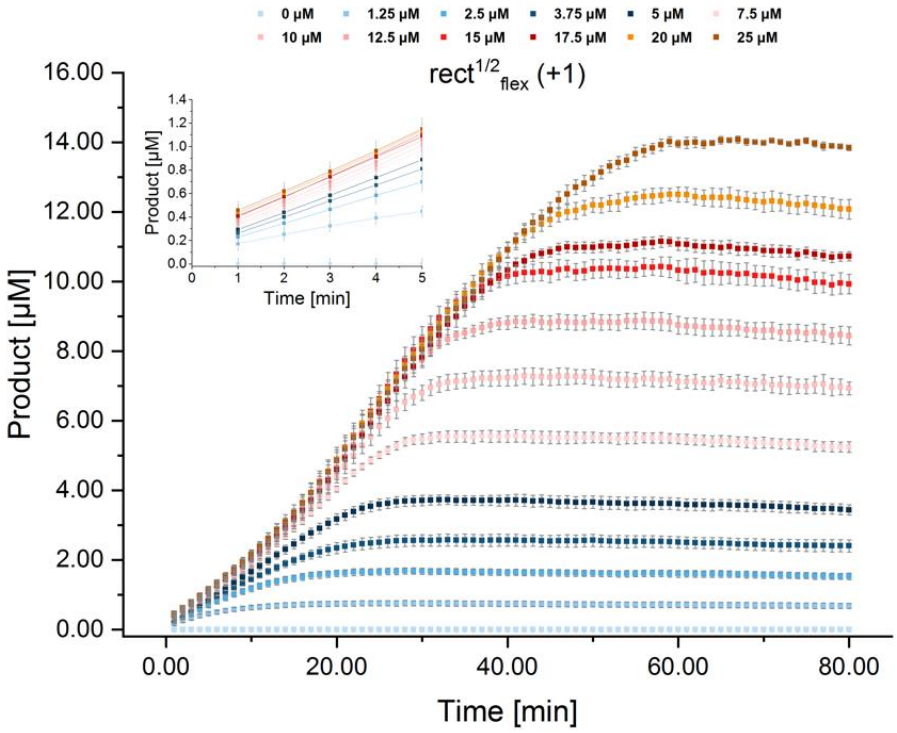
0 µM
1.25 µM
2.5 µM
3.75 µM
5 µM
7.5 µM
10 µM
12.5 µM
15 µM
17.5 µM
20 µM
25 µM
rect1/2flex (+1)
Product [µM]
Time [min]
0.00
2.00
4.00
6.00
8.00
10.00
12.00
14.00
16.00
0.00
20.00
40.00
60.00
80.00

L

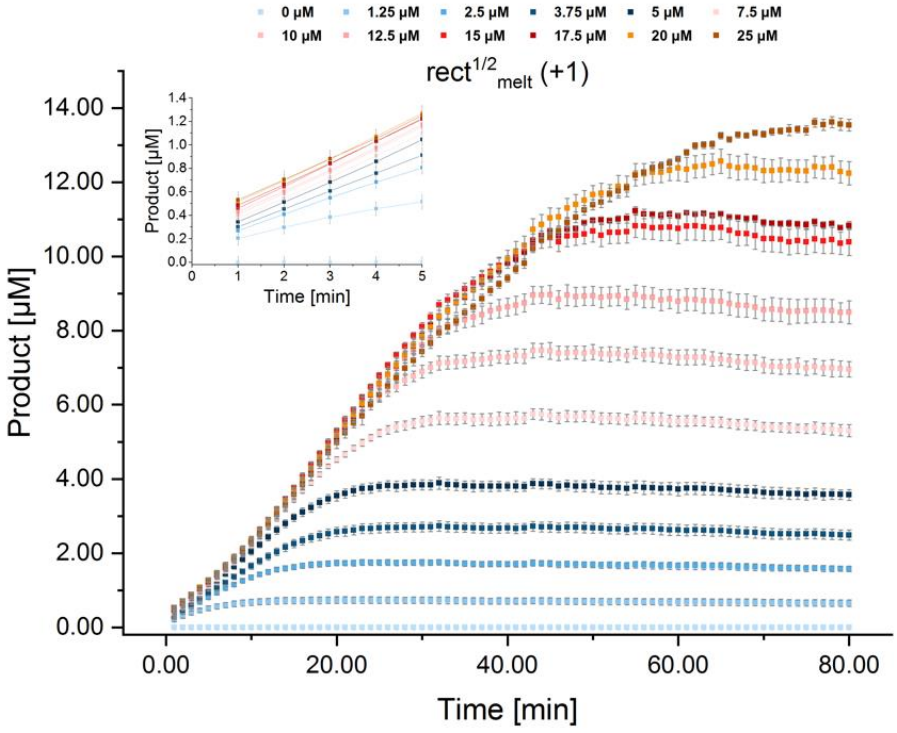
0 µM
1.25 µM
2.5 µM
3.75 µM
5 µM
7.5 µM
10 µM
12.5 µM
15 µM
17.5 µM
20 µM
25 µM
rect1/2melt (+1)
Product [µM]
Time [min]
0.00
2.00
4.00
6.00
8.00
10.00
12.00
14.00
0.00
20.00
40.00
60.00
80.00

M

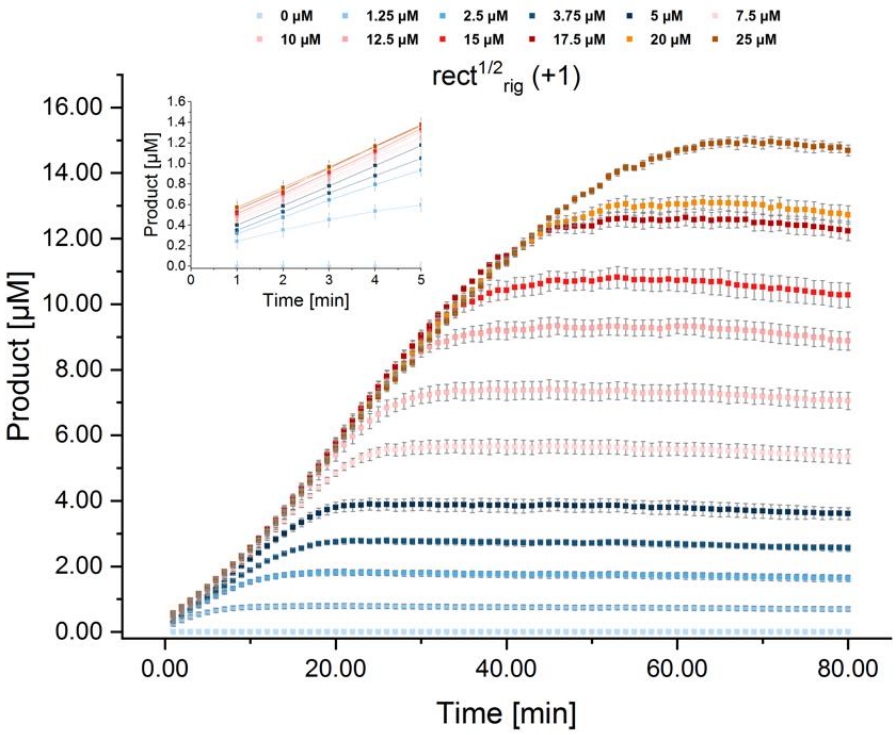
0 µM
1.25 µM
2.5 µM
3.75 µM
5 µM
7.5 µM
10 µM
12.5 µM
15 µM
17.5 µM
20 µM
25 µM
rect1/2rig (+1)
Product [µM]
Time [min]
0.00
2.00
4.00
6.00
8.00
10.00
12.00
14.00
16.00
0.00
20.00
40.00
60.00
80.00

N

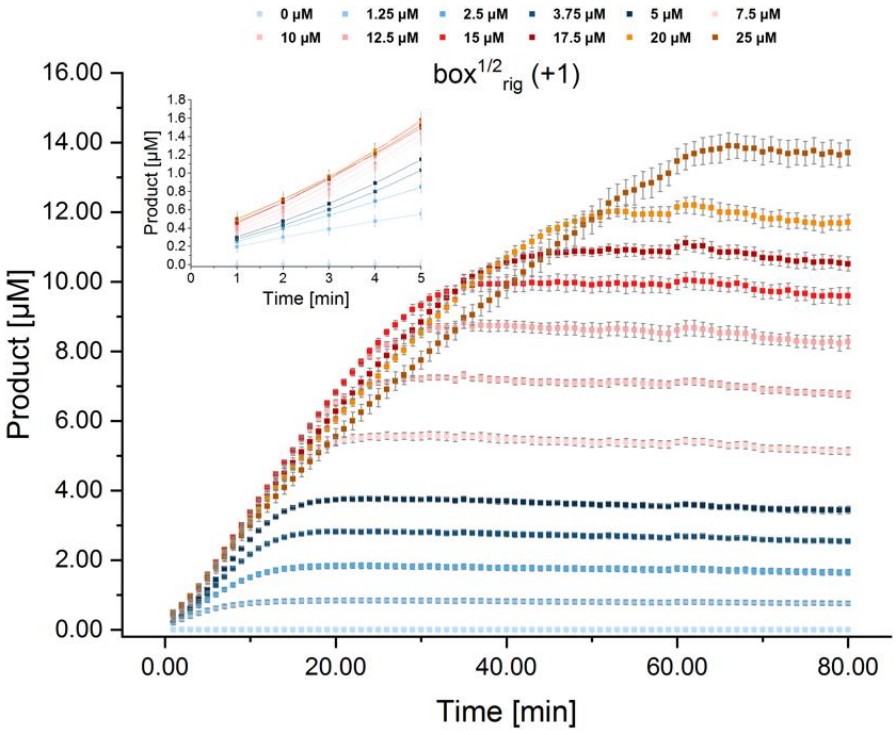
0 µM
1.25 µM
2.5 µM
3.75 µM
5 µM
7.5 µM
10 µM
12.5 µM
15 µM
17.5 µM
20 µM
25 µM
box1/2rig (+1)
Product [µM]
Time [min]
0.00
2.00
4.00
6.00
8.00
10.00
12.00
14.00
16.00
0.00
20.00
40.00
60.00
80.00

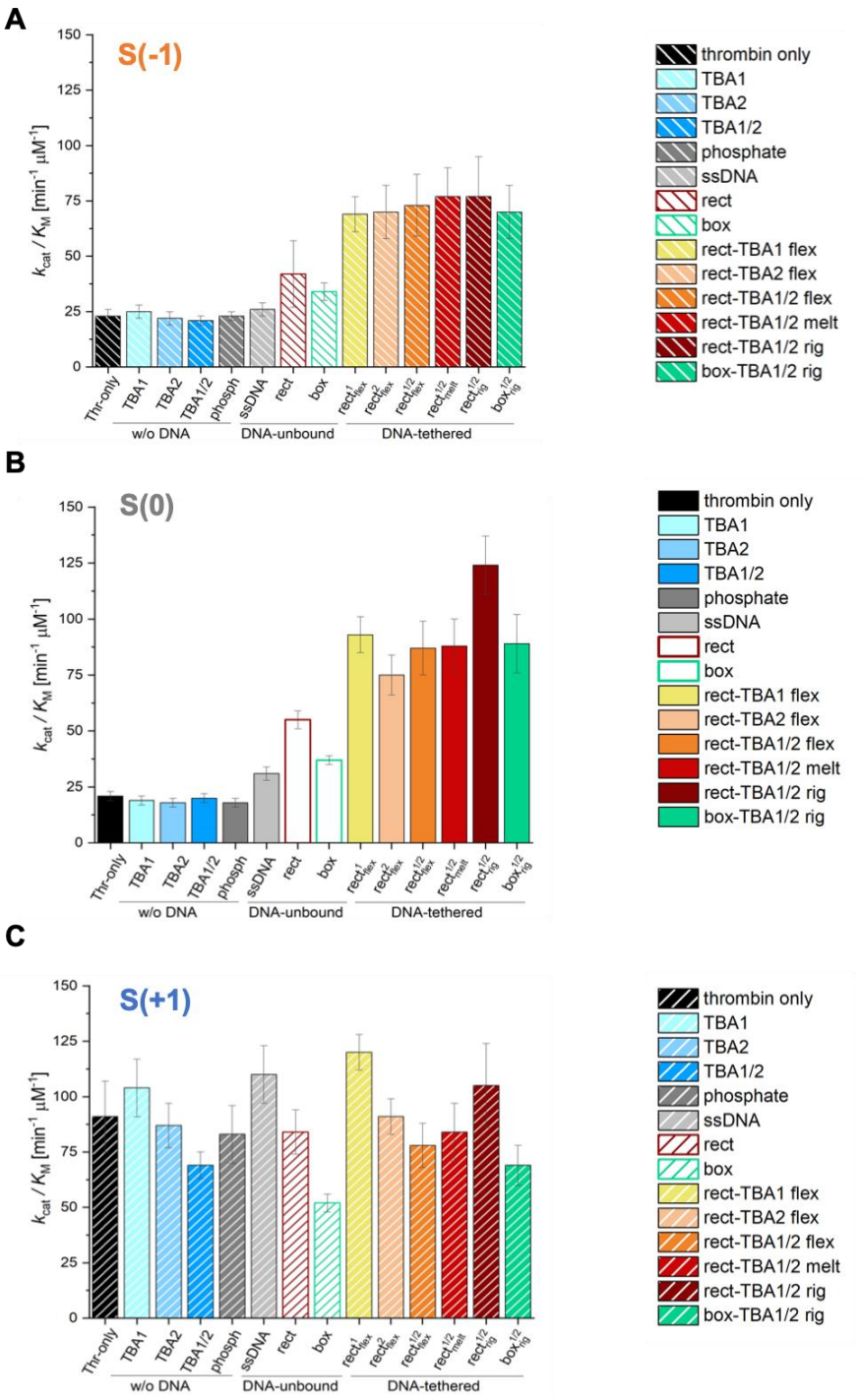

Figure S 19: Specificity constants (k_{cat}/K_M) of thrombin for all the three substrates. The specificity constants were calculated by application of the extracted MM parameters. S(-1) and S(0) behave fairly similar, with increased values for increased DNA scaffolding. S(+1) on the other hand is largely unaffected by the DNA surrounding and no pattern emerges. Reprinted and adapted from reference [200].

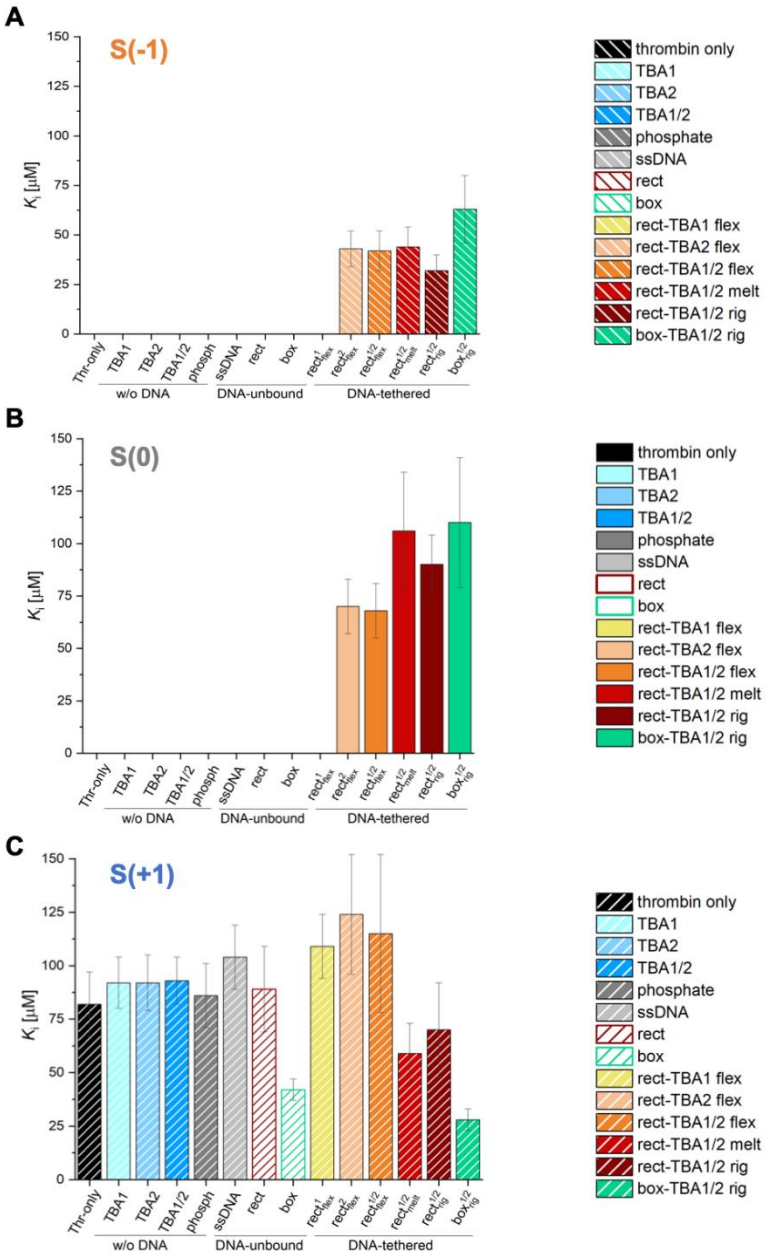

Figure S 20: Dissociation constants (K_i) of thrombin for all three substrates. Substrate inhibition was observed for all three substrates and extracted from the progress curves. While S(-1) and S(0) behave fairly similar, with substrate inhibition taking place especially for DNA scaffolded enzymes, S(+1) is different in that inhibition is observed throughout all samples. Reprinted and adapted from reference [200].

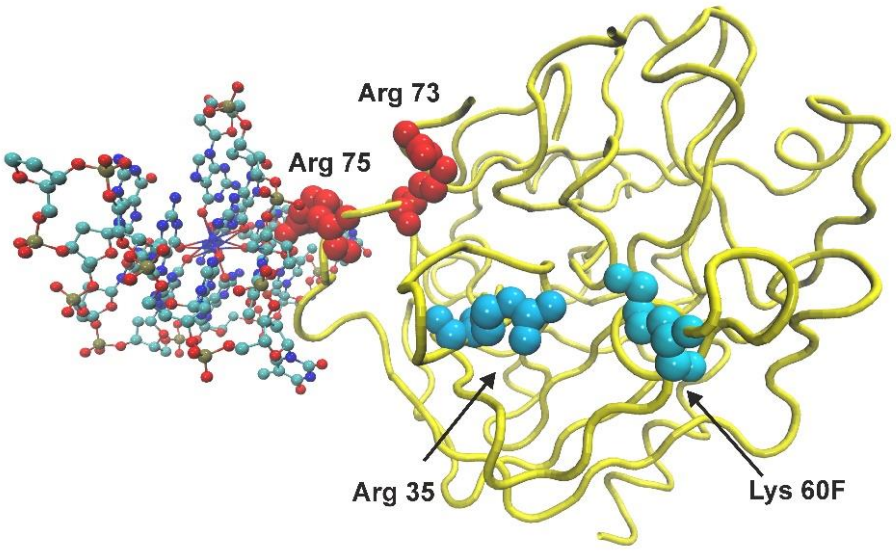

Figure S 21: Structure of thrombin interacting with the aptamer at the exosite I. The crystal structure of thrombin with the TBA1 aptamer bound to exosite I is shown {Russo Krauss, 2012 #17}. The protein is colored in yellow, Arg 73 and Arg 75 are in red. Lys 60F and Arg 35 at the vicinity of the exosite I are colored in light blue. The aptamer is shown in CPK representation. The residues involved in the interactions with the two most populated clusters for peptide S(-1) and in the most populated cluster for peptide S(0) are not involved in the interaction with the aptamer (Figure S 25, Figure S 26). The only residue from the ones mentioned above that is compromised in the interaction with the aptamer is residue Arg 75, which is interacting with S(0) in the second most populated cluster as shown in Figure S 26. Therefore, since most of the main interactions of the peptides with the region involving exosite I and its vicinity are not inhibited by the presence of the aptamer, it is believed that the peptides can still interact with that region in the scenario where the aptamers are used. Substrate S(+1) instead does not interact with the exosite I of thrombin and is therefore not expected to hinder aptamer interaction at this region of the protein (Figure S 24).

This paragraph was reprinted and adapted from reference [200]. All MD simulations were performed by the group of Prof. Sánchez-García, university of Duisburg-Essen.

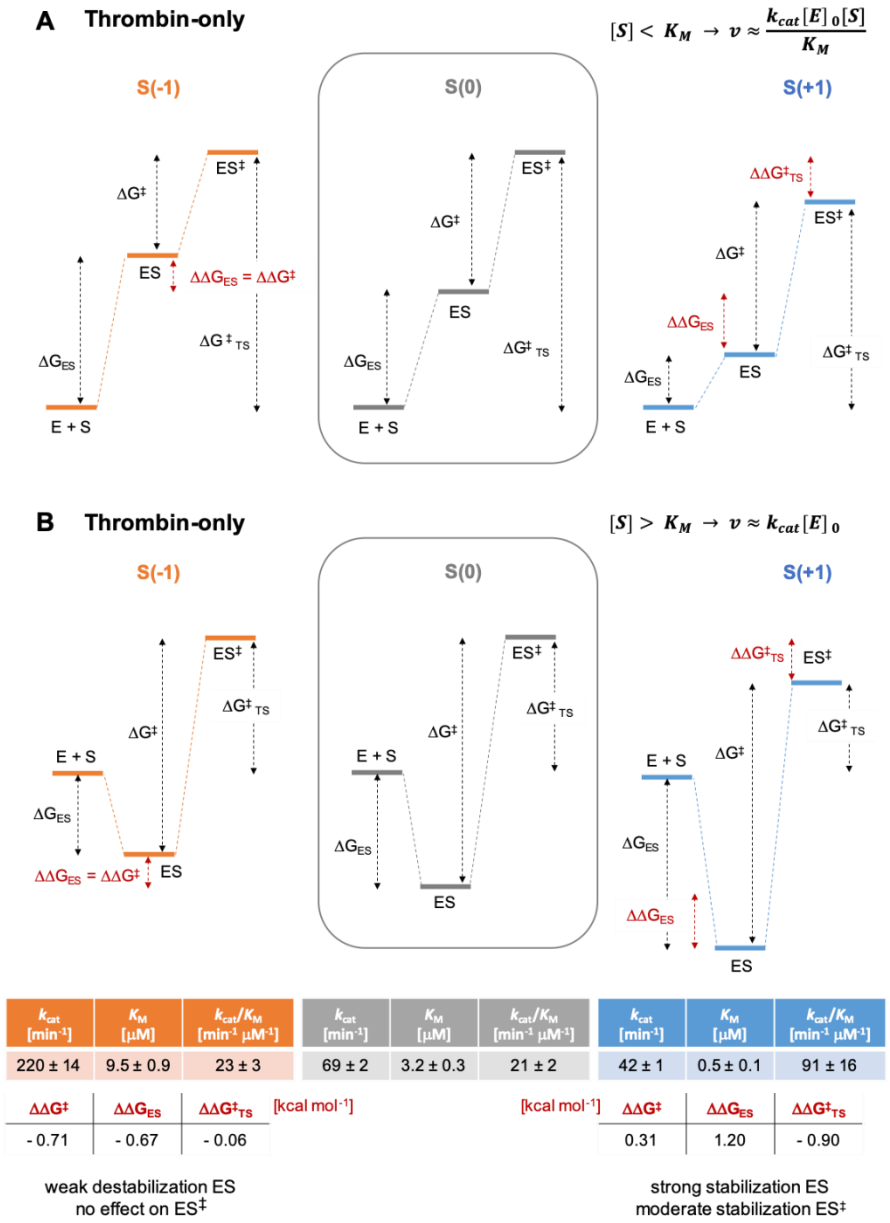

k_{cat} [min^{-1}]	K_M [μM]	k_{cat}/K_M [min^{-1} μM^{-1}]	k_{cat} [min^{-1}]	K_M [μM]	k_{cat}/K_M [min^{-1} μM^{-1}]	k_{cat} [min^{-1}]	K_M [μM]	k_{cat}/K_M [min^{-1} μM^{-1}]
220 ± 14	9.5 ± 0.9	23 ± 3	69 ± 2	3.2 ± 0.3	21 ± 2	42 ± 1	0.5 ± 0.1	91 ± 16

ΔΔG‡	ΔΔG$_{ES}$	ΔΔG‡$_{TS}$	[kcal mol^{-1}]
- 0.71	- 0.67	- 0.06	

[kcal mol^{-1}]	ΔΔG‡	ΔΔG$_{ES}$	ΔΔG‡$_{TS}$
	0.31	1.20	- 0.90

weak destabilization ES
no effect on ES‡

strong stabilization ES
moderate stabilization ES‡

Figure S 22: Application of the transition state theory on the thrombin catalyzed hydrolysis of S(-1) and S(+1) with respect to S(0) for thrombin-only. Assuming a simple MM mechanism, the transition state theory allows to depict changes in the energy barriers of an enzymatic reaction that progresses from the unreacted E + S through the ES complex to the transition state ES‡ and finally to the products. It enables comparisons between the same enzymatic reaction within different conditions (e.g. different substrates). Two substrate regimes are considered, S < K_M (**A**) and S > K_M (**B**). The variation in the free energy changes between each enzyme species were calculated respectively from the K_M, k_{cat} and k_{cat}/K_M values of the thr/S(-1) or thr/S(+1) reaction with respect to the thr/S(0) reference. For all reactions it was assumed that the unbound state E + S is energetically identical. Numerical values of the differences in the energy barriers are given in the table below. Reprinted and adapted from reference [200].

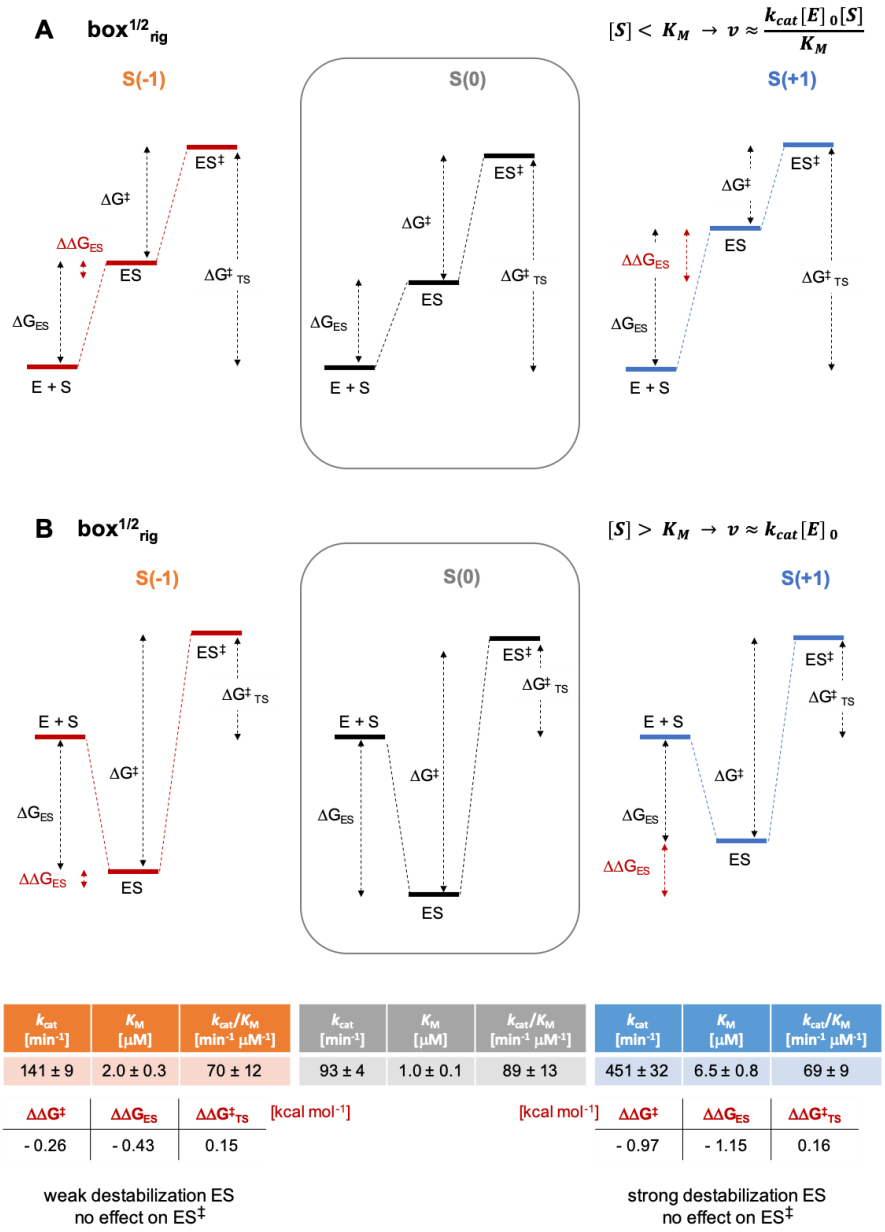

Figure S 23: Application of the transition state theory on the thrombin catalyzed hydrolysis of S(-1) and S(+1) with respect to S(0) for box$^{1/2}_{rig}$. Assuming a simple MM mechanism, the transition state theory allows to depict changes in the energy barriers of an enzymatic reaction that progresses from the unreacted E + S through the ES complex to the transition state ES‡ and finally to the products. It enables comparisons between the same enzymatic reaction within different conditions (e.g. different substrates). Two substrate regimes are considered, S < K_M (**A**) and S > K_M (**B**). The variation in the free energy changes between each enzyme species were calculated respectively from the K_M, k_{cat} and k_{cat}/K_M values of the thr/S(-1) or thr/S(+1) reaction with respect to the thr/S(0) reference. For all reactions it was assumed that the unbound state E + S is energetically identical. Numerical values of the differences in the energy barriers are given in the table below. Reprinted and adapted from reference [200].

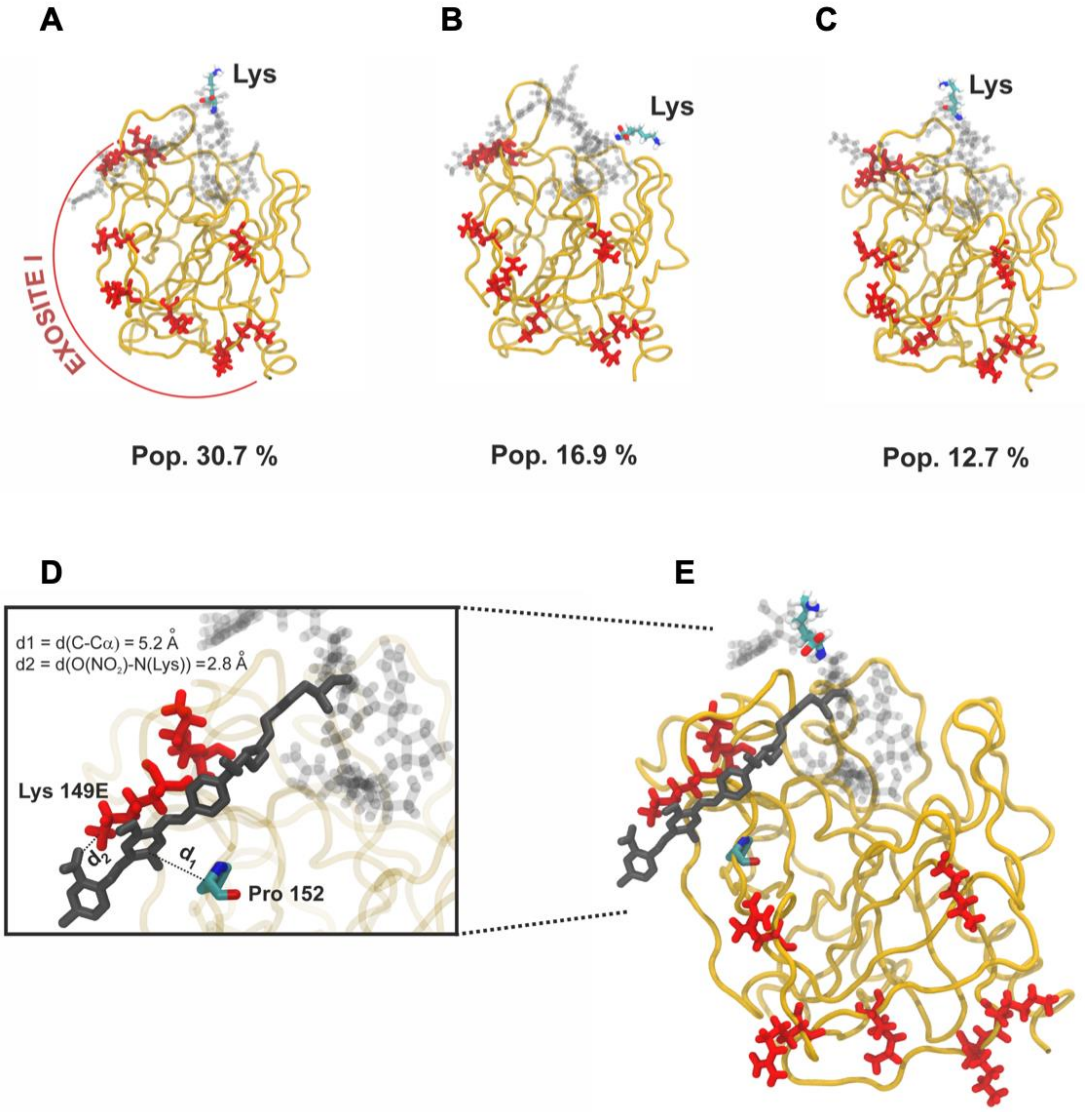

Figure S 24: MD simulations of the S(+1) peptide/thrombin complex. (**A**-**C**) Representative structures extracted from the three main clusters observed during the GaMD simulations. The relative populations of the most abundant clusters are shown. The protein is colored in yellow, the peptide, except the terminal amino acid, is colored in gray and rendered as transparent. The positively charged amino acids at the exosite I are colored in red. The terminal Lys of the peptide is highlighted and labelled. (**D**) S(+1) establishes conserved interactions with the exosite I through one of the fluorophores, HBQ1. This interaction is probably driven by the combination of the electrostatic attraction between the positive region at the exosite I and the partial negative charges at the nitro group in the fluorophore as well as hydrophobic interactions between the aromatic rings of HBQ1 and the hydrophobic residues of the exosite I. The close proximity of the nitro group on the HBQ1 fluorophore to Lys 149E at the exosite I (2.8 Å) indicates electrostatic interactions. Additionally, the hydrophobic interaction is facilitated by Pro 152 near the phenyl rings of the HBQ1 fluorophore. The values shown for the distances correspond to the most populated cluster observed during the GaMD (**E**). The HBQ1 fluorophore is depicted in gray, while the rest of the peptide is rendered as gray and transparent, the protein is shown in yellow (transparent in panel **D**). The positively charged residues of the exosite I are shown in red. Hydrogen atoms of Pro 152 and HBQ1 are omitted for simplicity.

This paragraph was reprinted and adapted from reference [200]. All MD simulations were performed by the group of Prof. Sánchez-García, University of Duisburg-Essen.

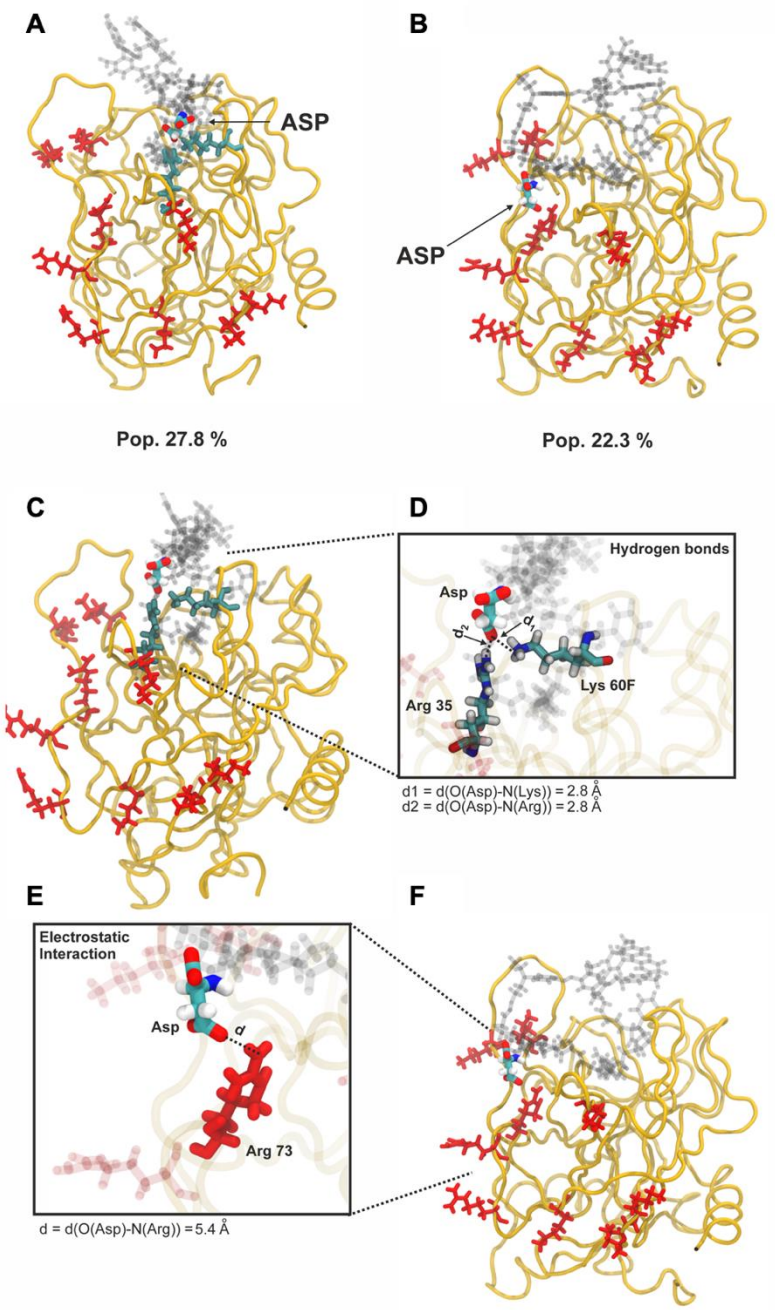

Figure S 25: MD simulations of the S(-1) peptide/thrombin complex. (**A**-**B**) The relative populations of the most abundant clusters are shown. The protein is colored in yellow, the peptide, except for the terminal amino acid, is shown in transparent gray. The positively charged amino acids at the exosite I are indicated in red. Two residues interacting with the C-terminal Asp are colored in green. These are better visible in the enlarged views below, which depict the interactions occurring in the main (**C**, **D**) and second (**E**, **F**) most populated clusters. The main interactions established between S(-1) and the exosite I of thrombin are of electrostatic nature and involve the negatively charged carboxylate group of the C-terminal Asp of S(-1) and the positively charged side chains of Lys 60F and Arg 35, with interaction distances of 2.8 Å and angles of 146° and 156° (**D**). To a less extent, Arg 73 at the exosite I also interacts with the C-terminal Asp of the peptide (**E**). The peptide is shown in transparent gray, the protein in yellow (transparent in panels **D** and **E**). The positively charged residues of the exosite I are shown in red (transparent in panels **D** and **E**).

This paragraph was reprinted and adapted from reference [200]. All MD simulations were performed by the group of Prof. Sánchez-García, University of Duisburg-Essen.

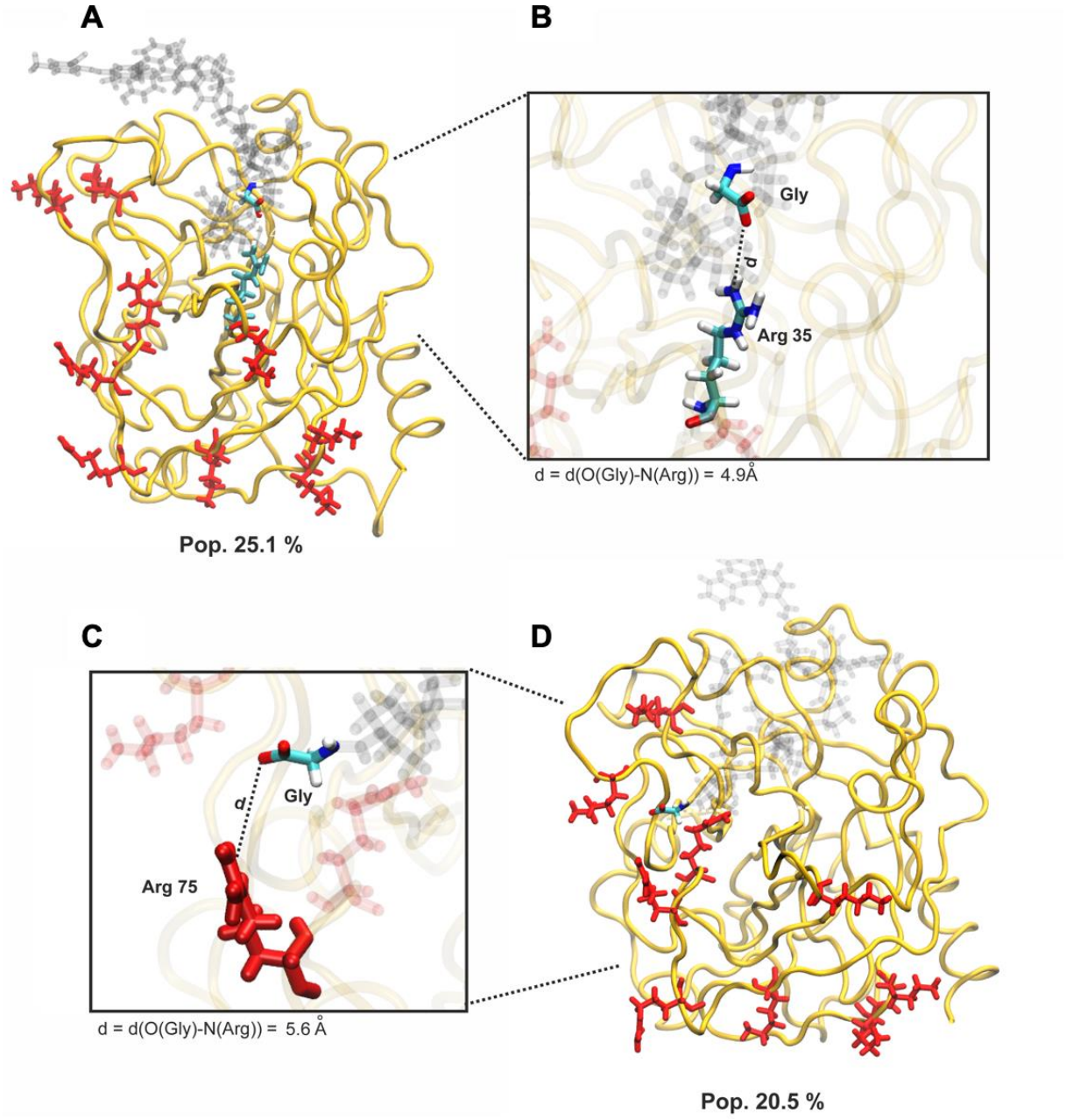

Figure S 26: MD simulations of the S(0) peptide/thrombin complex. (**A**-**B**) The relative populations of the most abundant clusters (**A** and **D**) are shown. (**B**) Like S(-1), S(0) interacts with Arg 35; however, at a larger distance (4.9 Å). Similar to S(-1), the neutral peptide also exhibits interactions with other residues of the exosite I, as shown for the second most populated cluster (**D**) where the C-terminal Gly residue of the peptide interacts with Arg 75 (**C**). The protein is shown in yellow, the peptide, except for the terminal amino acid, is depicted in transparent gray. The positive amino acids at the exosite I are indicated in red.

This paragraph was reprinted and adapted from reference [200]. All MD simulations were performed by the group of Prof. Sánchez-García, University of Duisburg-Essen.

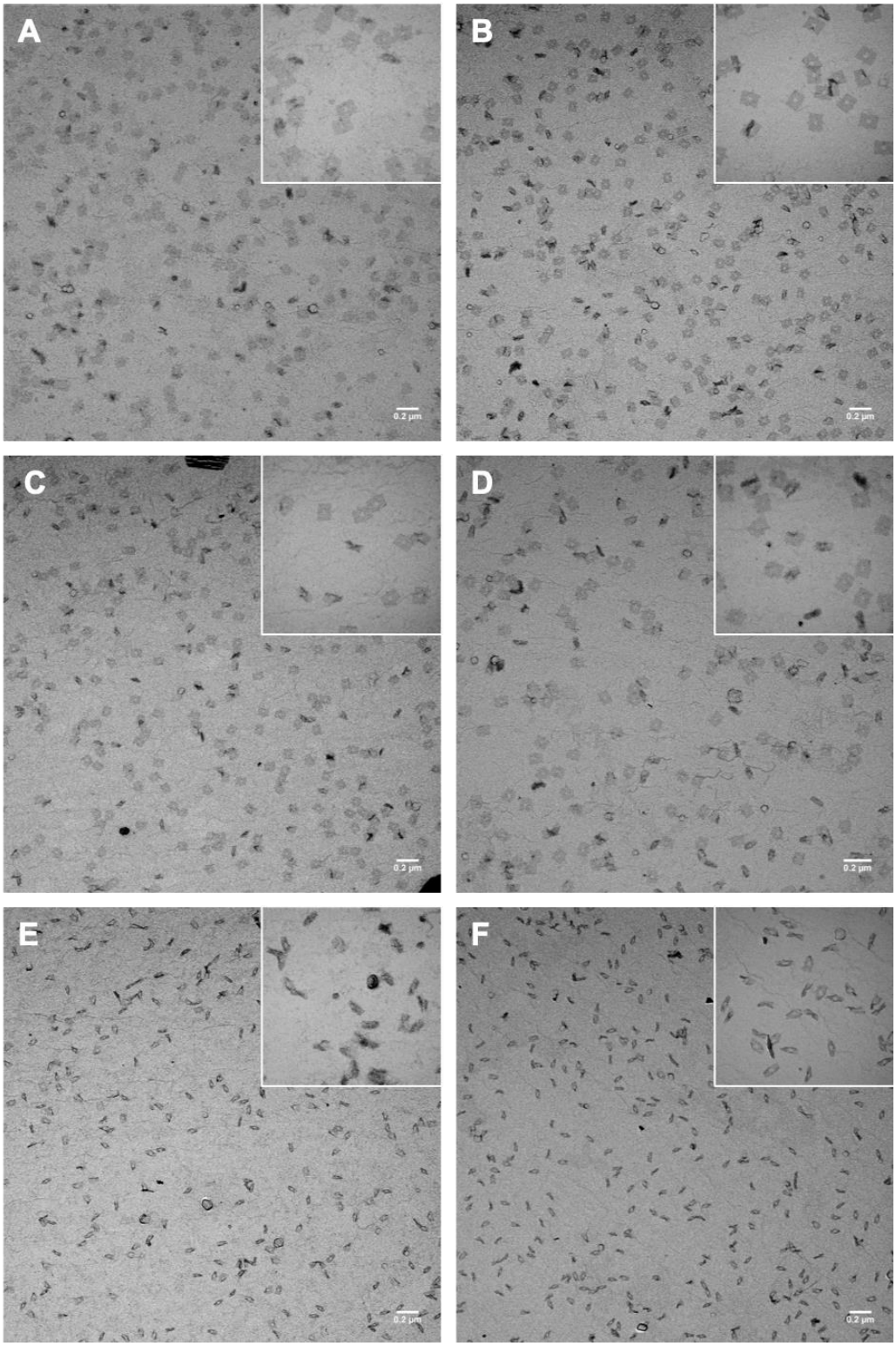

cont. on the following page

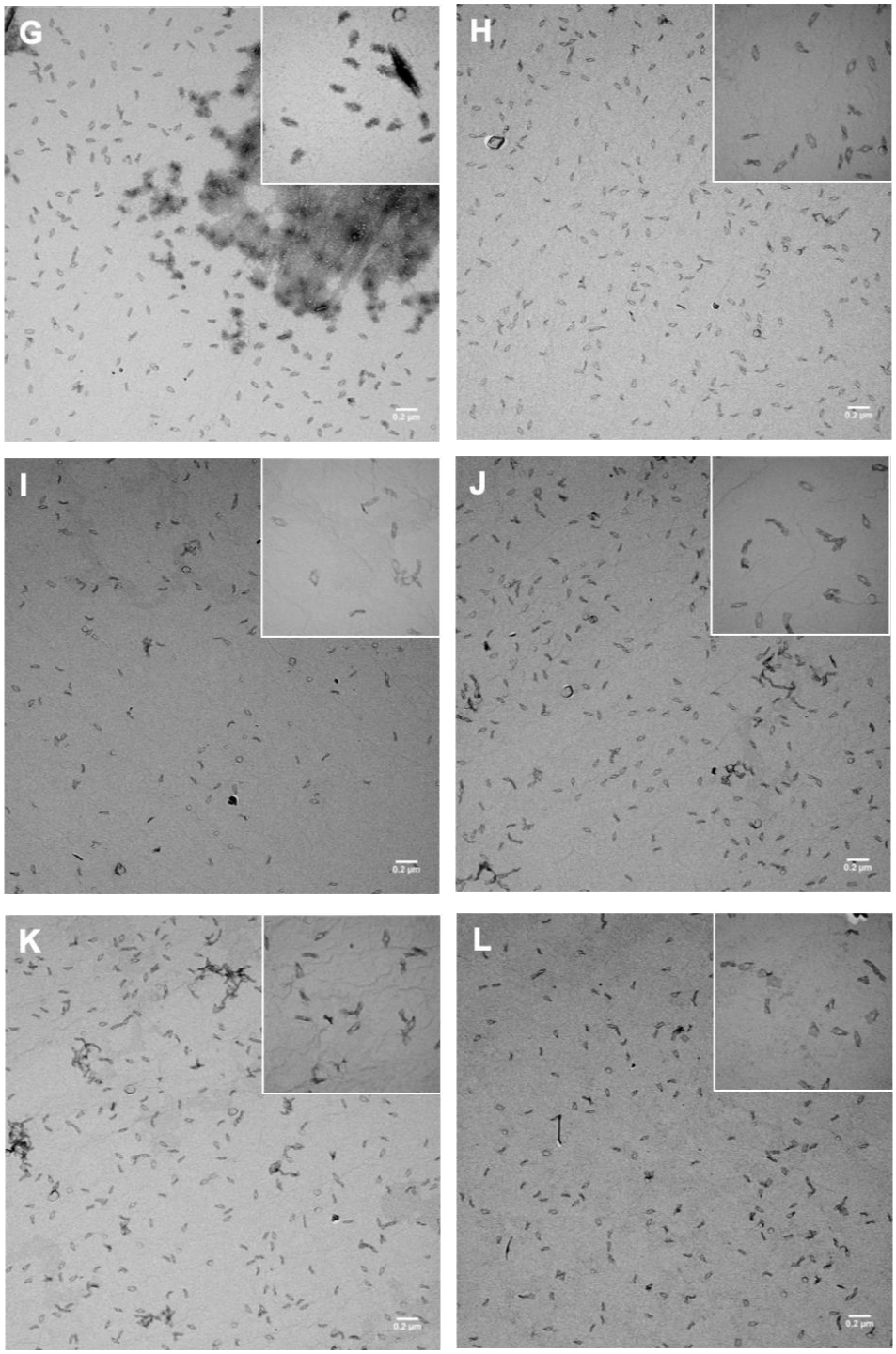

Figure S 27: TEM analysis of thrombin/S(-1) samples in presence of rect DNA origami structures after the enzymatic assay. After the enzymatic assay (as described in 4.2.11) a small aliquot of each reaction (**A-L**: 0, 1.25, 2.5, 3.75, 5, 7.5, 10, 12.5, 15, 17.5, 20, 25 µM) was analyzed by TEM. Images show no visible aggregation and intact structures for all substrate concentrations. Insets show zoomed-in regions of the micrograph. Scale bars are 200 nm. Reprinted and adapted from reference [200]. TEM images were recorded by Dr. Michael Erkelenz from the group of Prof. Schlücker, University of Duisburg-Essen.

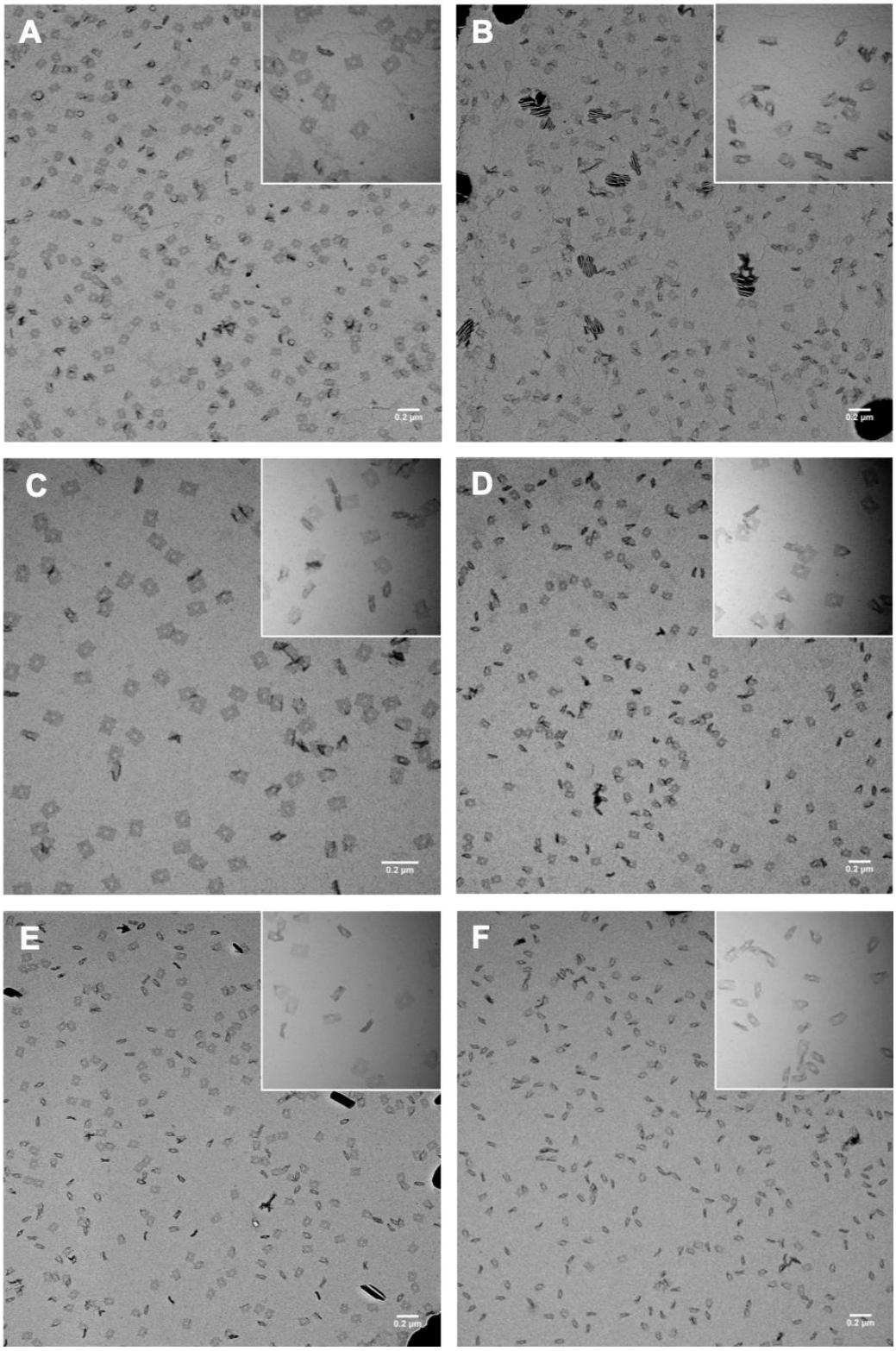

cont. on the following page

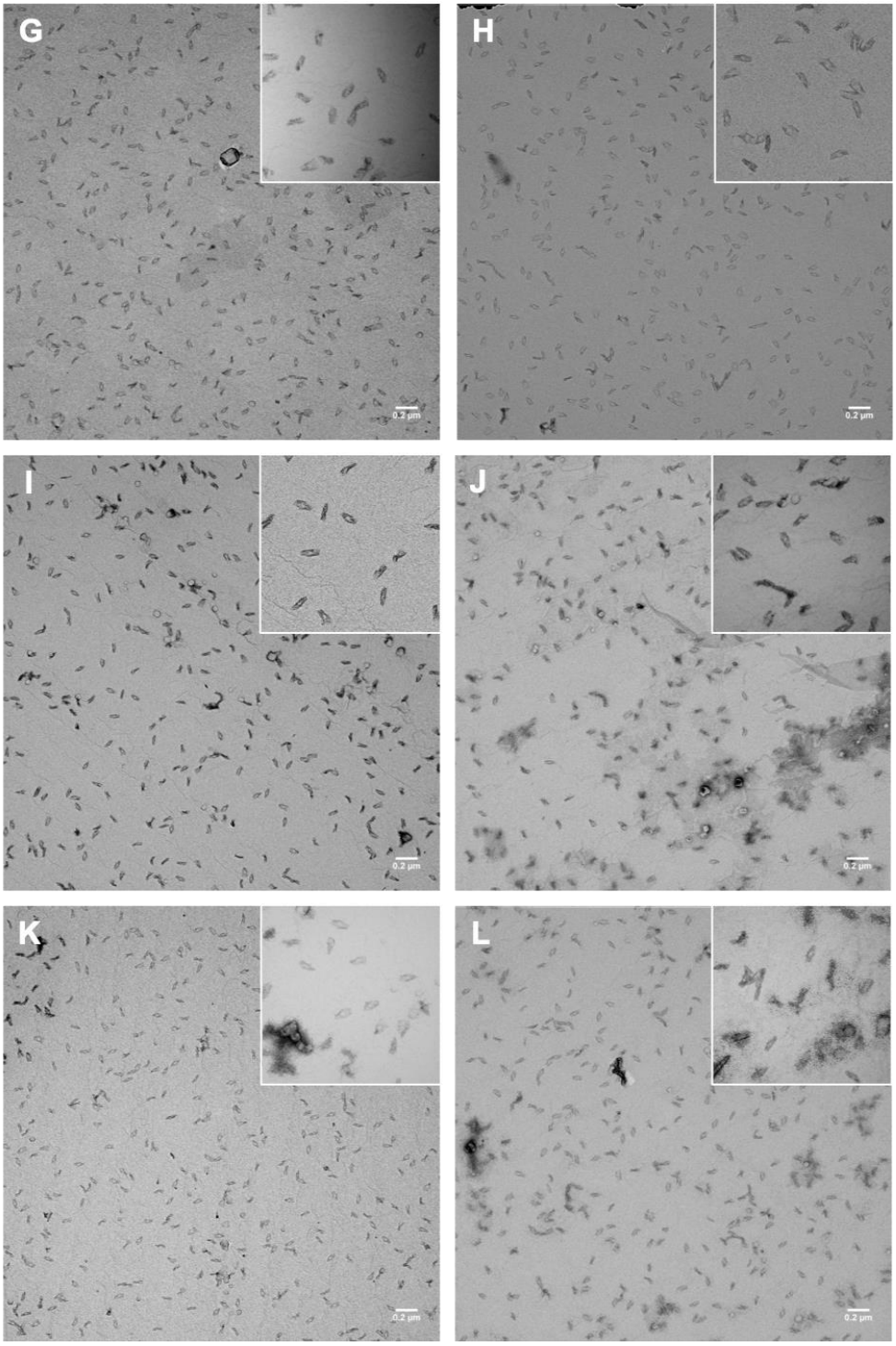

Figure S 28: TEM analysis of thrombin/S(0) samples in presence of rect DNA origami structures after the enzymatic assay. After the enzymatic assay (as described in 4.2.11) a small aliquot of each reaction (**A-L**: 0, 1.25, 2.5, 3.75, 5, 7.5, 10, 12.5, 15, 17.5, 20, 25 µM) was analyzed by TEM. Images show no visible aggregation and intact structures for all substrate concentrations. Insets show zoomed-in regions of the micrograph. Scale bars are 200 nm. Reprinted and adapted from reference [200]. TEM images were recorded by Dr. Michael Erkelenz from the group of Prof. Schlücker, University of Duisburg-Essen.

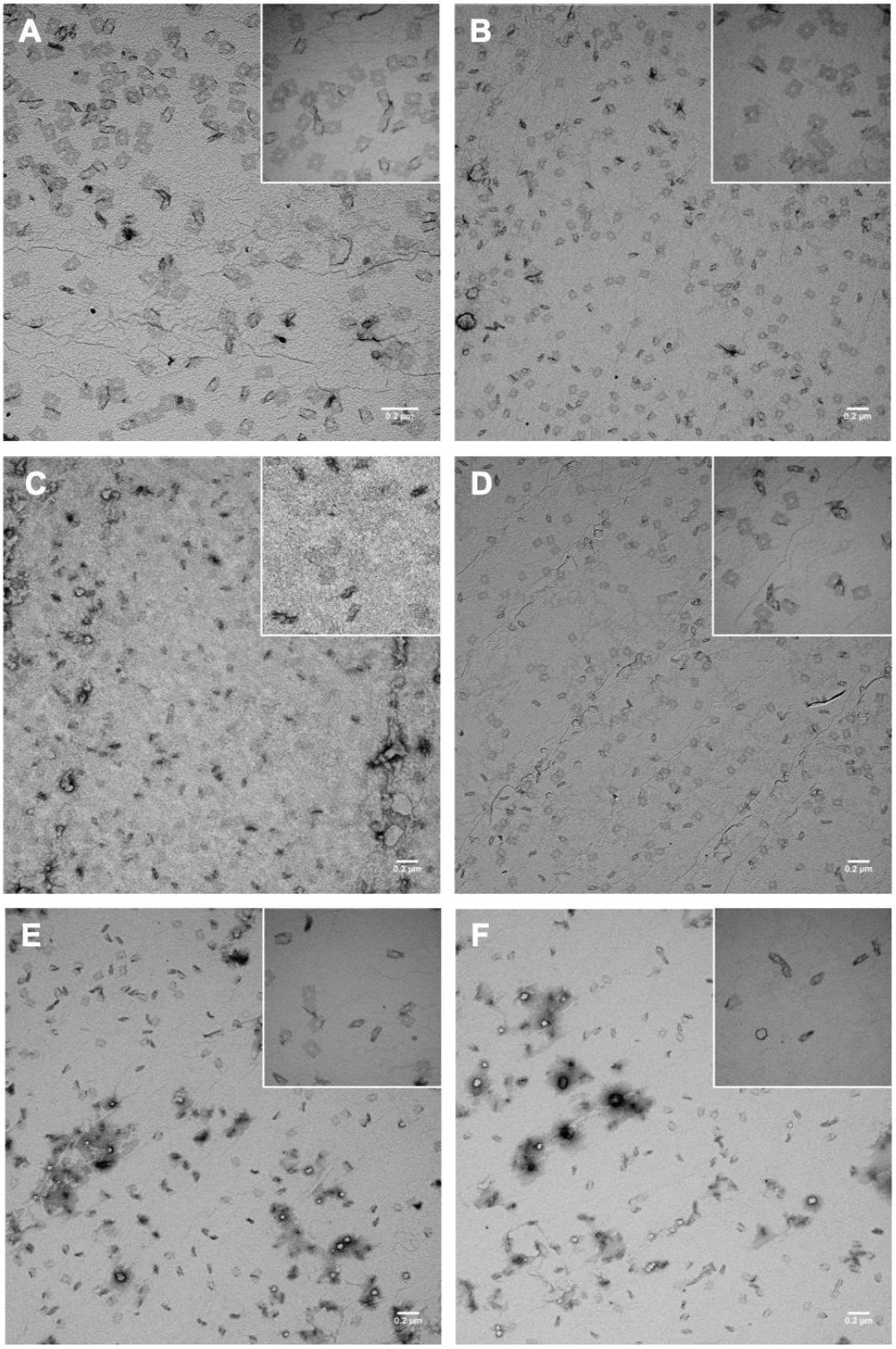

cont. on the following page

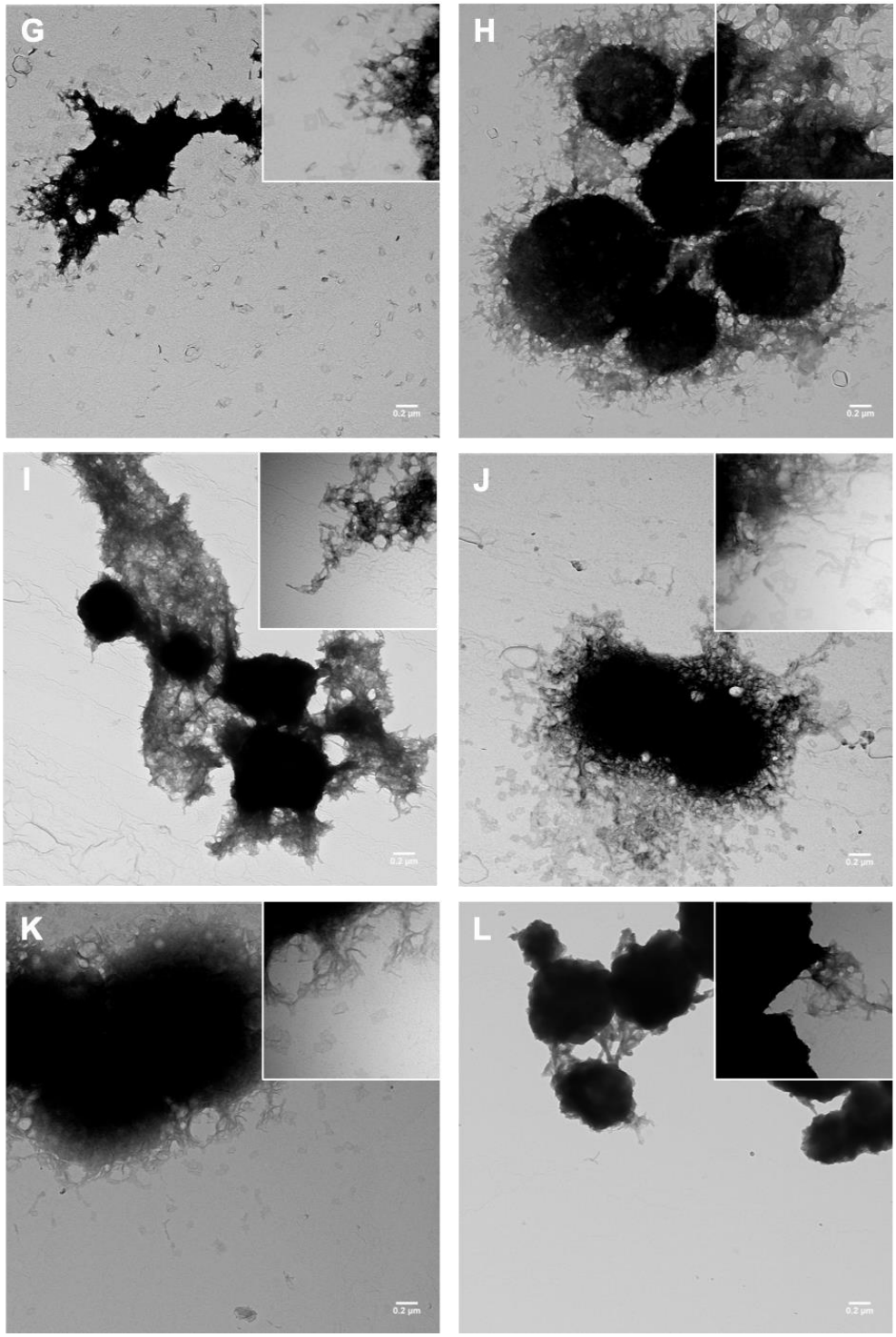

Figure S 29: TEM analysis of thrombin/S(+1) samples in presence of rect DNA origami structures after the enzymatic assay. After the enzymatic assay (as described in 4.2.11) a small aliquot of each reaction (**A-L**: 0, 1.25, 2.5, 3.75, 5, 7.5, 10, 12.5, 15, 17.5, 20, 25 µM) was analyzed by TEM. Images show visible aggregation above a substrate concentration of 10 µM. Insets show zoomed-in regions of the edges of the aggregates, where occasionally single structure are visible. Scale bars are 200 nm. Reprinted and adapted from reference [200]. TEM images were recorded by Dr. Michael Erkelenz from the group of Prof. Schlücker, University of Duisburg-Essen.

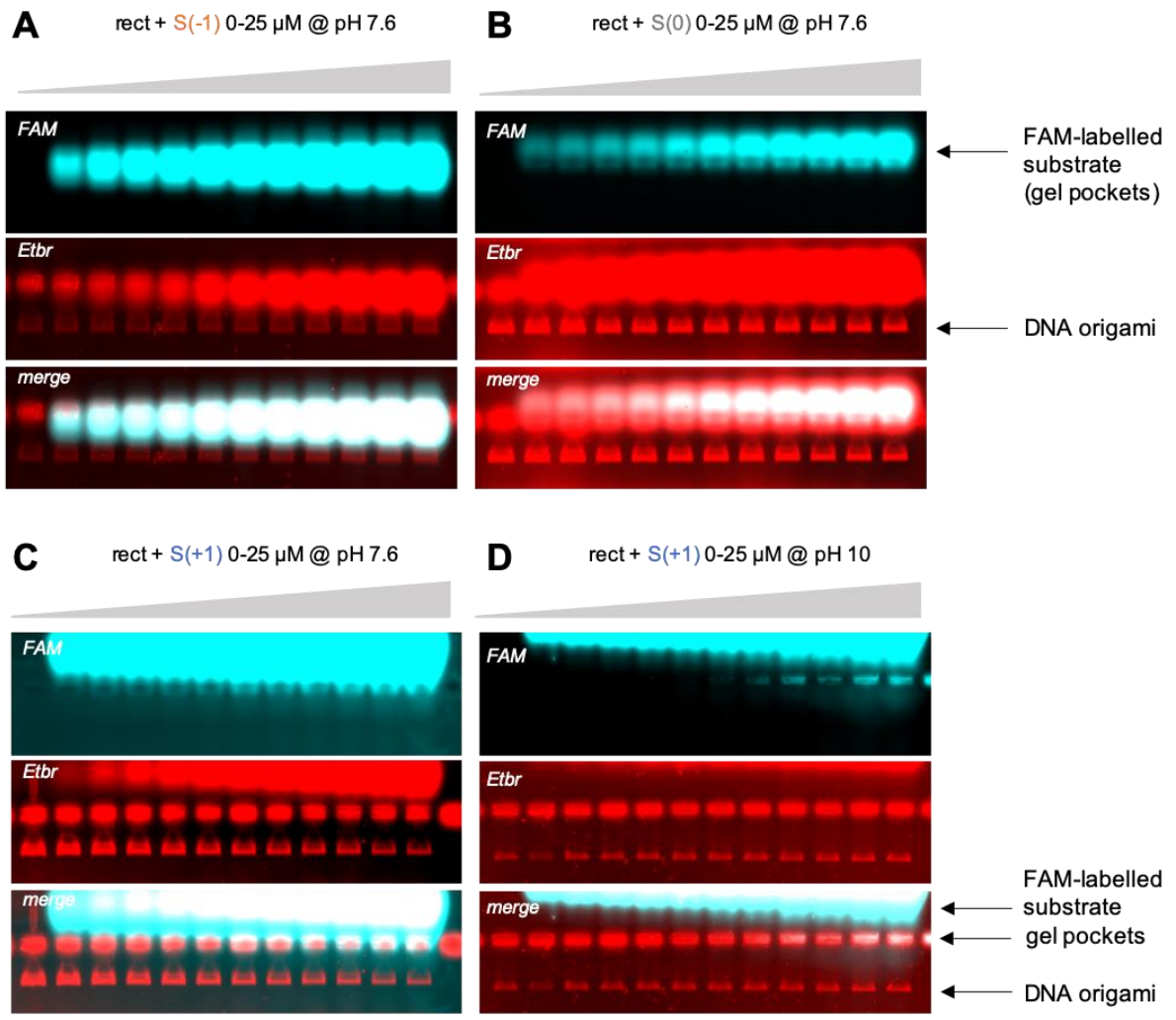

Figure S 30: Unspecific DNA origami/substrate interactions analyzed via AGE. 20 µL of DNA origami rect cages (lacking the inner TBAs) were incubated with varying concentrations of FAM-only substrates (0 – 25 µM) for 1 h at 37 °C. Depending on the net charge, substrates migrate towards the positive (S(-1)) or negative pole (S(+1)), or basically stay within the wells (S(0)). In all cases migration is rather slow (FAM channel) While the intensity of DNA origami bands stays comparable among all substrate concentrations for S(-1) (**A**) and S(0) (**B**) (EtBr channel), band intensity significantly decreases for S(+1), especially at high substrate concentration regimes (**C**), suggesting aggregation events as observed by TEM. Interestingly, when the pH was adjusted to 10 (**D**), this trend is reversed, and origami bands show similar intensities again, likely due to a lower or almost neutral net charge of the substrate at these conditions. Gel running parameters: 1% agarose in 1X TBEMg at 80 V, for 1 h at 4°C. Reprinted and adapted from reference [200].

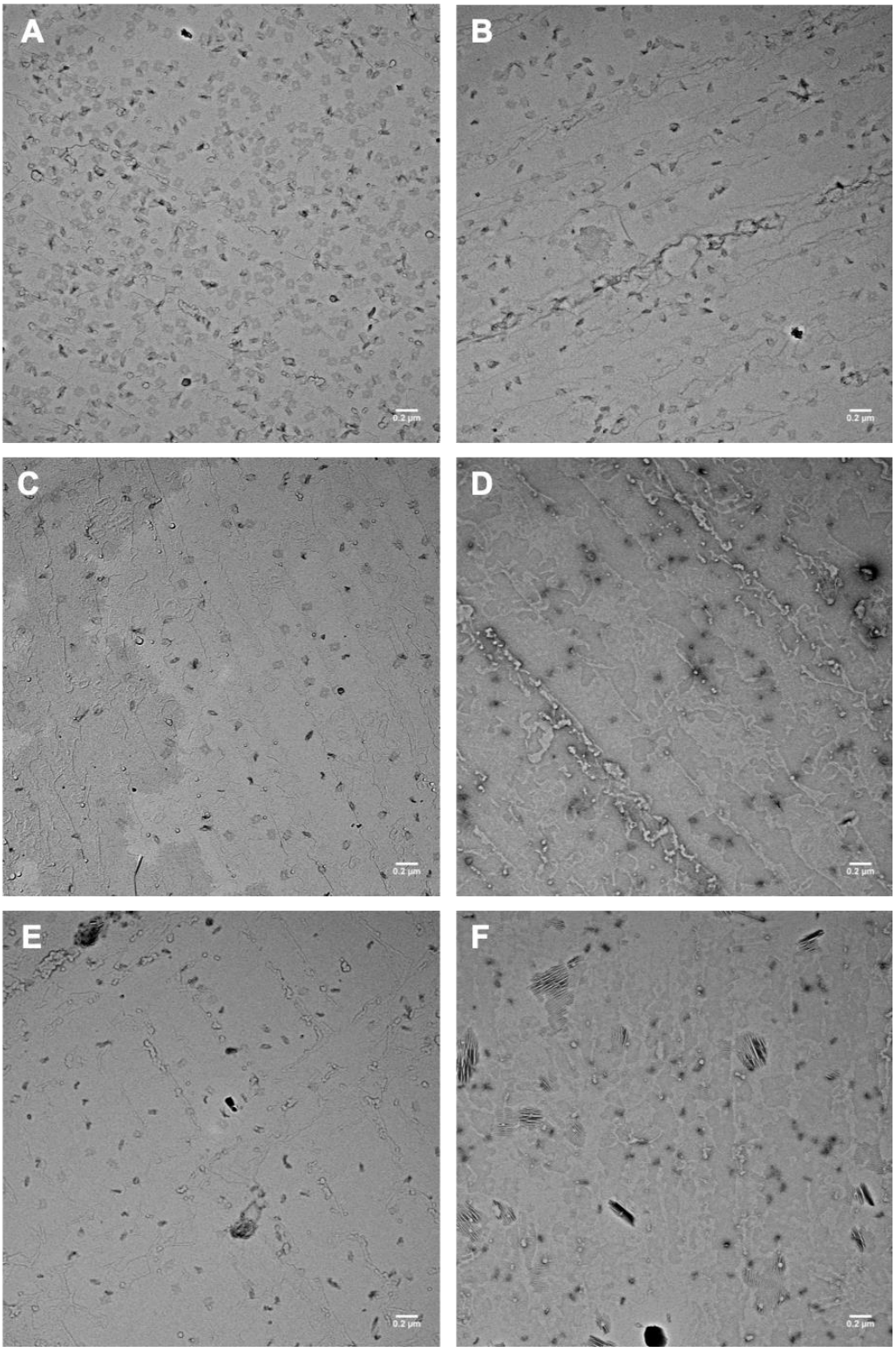

cont. on the following page

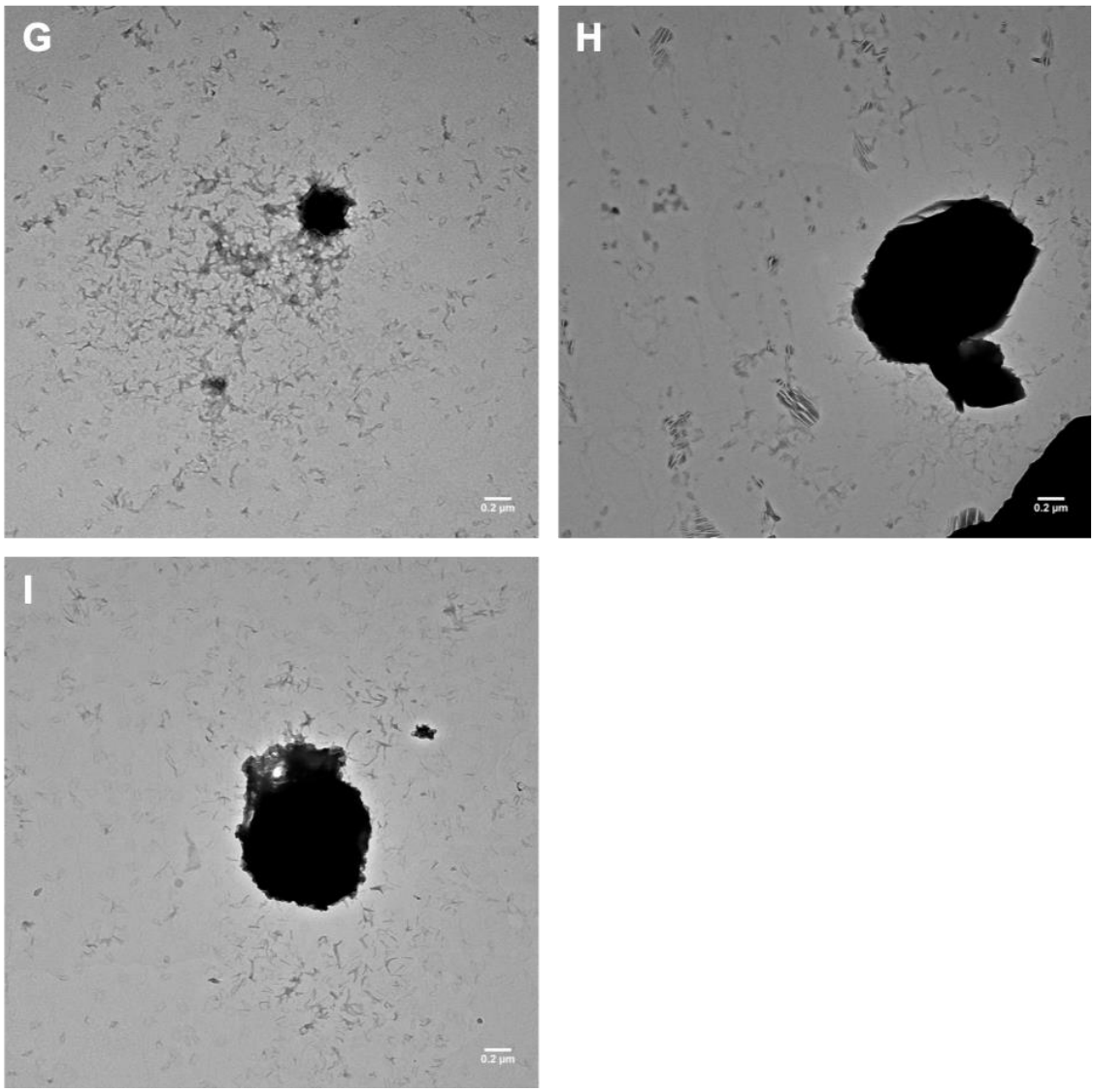

Figure S 31: TEM analysis of thrombin/S(+1) samples in presence of rect DNA origami structures at different time points. During the time course of the enzymatic reaction (as described in 4.2.11) of rect/thrombin with 15 µM S(+1), small aliquotes were taken and analyzed by TEM. Time points were: **A**-**I**: 0 min [before addition of substrate], 0 min [after addition of substrate], 2 min, 5 min, 10 min, 20 min, 40 min, 60 min and 80 min. The images show visible aggregation of the origami structures taking place already during the reaction (starting from ca. minute 40). Since the kinetic parameters are extracted from the very first minutes of the reaction, the observed aggregation does not falsify the initial reaction rates. Scale bars are 200 nm. TEM images were recorded by Dr. Michael Erkelenz from the group of Prof. Schlücker, University of Duisburg-Essen. Reprinted and adapted from reference [200].

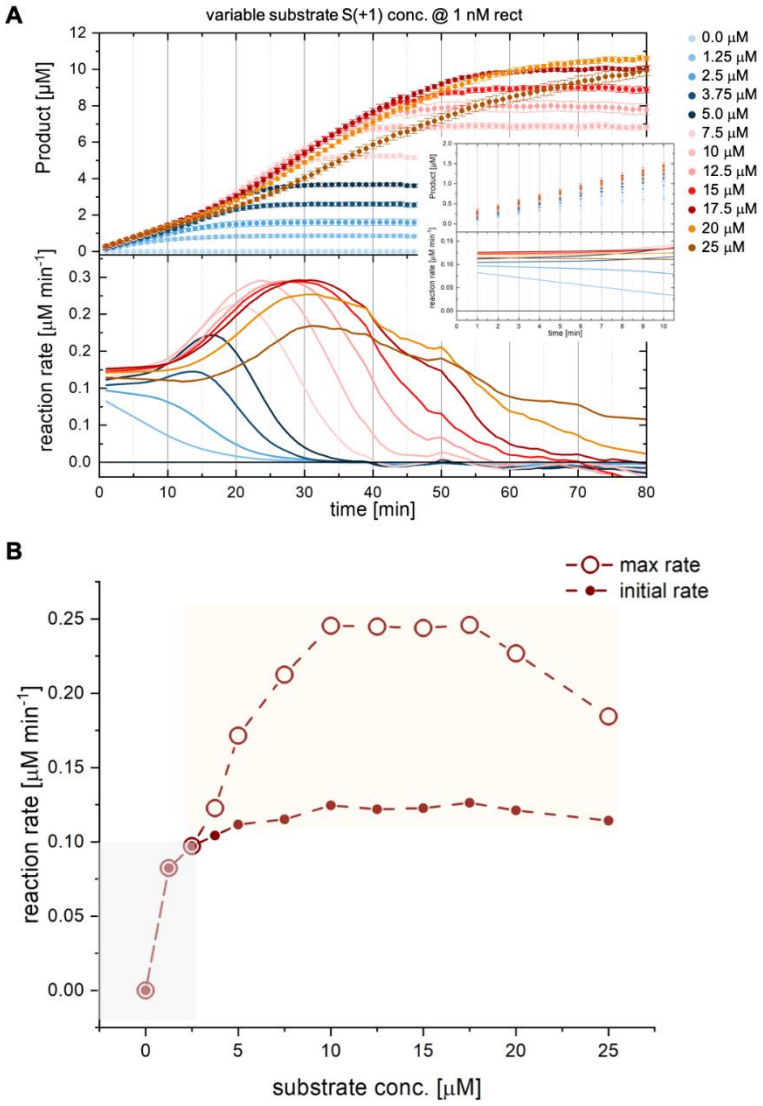

Figure S 32: Initial *vs.* maximum reaction rates of rect for S(+1). Progress curves of the enzymatic reaction of rect/thrombin sample for S(+1) show a sigmoidal shape above a substrate concentration of ca. 3 µM (**A**, top panel), starting at about 10 min. Plotting the reaction rates for the whole time period of the reaction (**A**, bottom panel) illustrates that at these substrate concentration regimes, maximum reaction rates are not within the initial phase of the reaction but are reached much later. Insets show the initial linear phase, which was used for the analysis and extraction of the MM parameters. Initial reaction rate and maximum reaction rates hence diverge at this concentration (**B**), with the latter assuming much higher values (0.24 µM min^{-1} vs 0.11 µM min^{-1} for substrate concentrations of about 10-15 µm). Above that concentrations the trend reverses, approximating a typical MM progress curve again. Maximal rates are also reached proportionally later in time for higher substrate concentrations (**A**, bottom panel). Enzymatic assay conditions: 1.2 nM thrombin, S(+1) from 0 to 25 µM, 1nM DNA origami without aptamers (rect) in 1X TEMg at 37°C. The data shown are the average result of three replicates. Reprinted and adapted from reference [200].

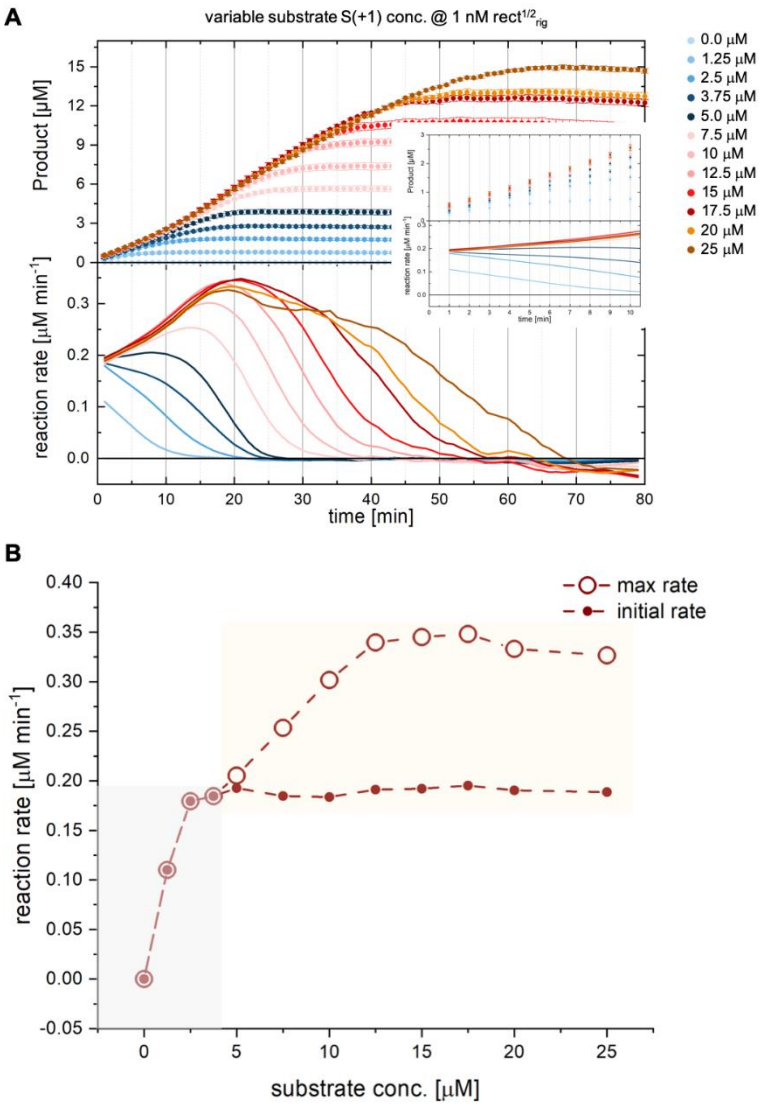

Figure S 33: Initial *vs*. maximum reaction rates of rect$^{1/2}_{rig}$ for S(+1). Non-MM behaviour observed for high concentrations of S(+1) in presence of rect$^{1/2}_{rig}$. Similar conclusions as in Figure S 32. Enzymatic assay conditions: 1.2 nM thrombin, S(+1) from 0 to 25 µM, 1nM DNA origami with aptamers (rect$^{1/2}_{rig}$) in 1X TEMg at 37°C. The data shown are the average result of three replicates. Reprinted and adapted from reference [200].

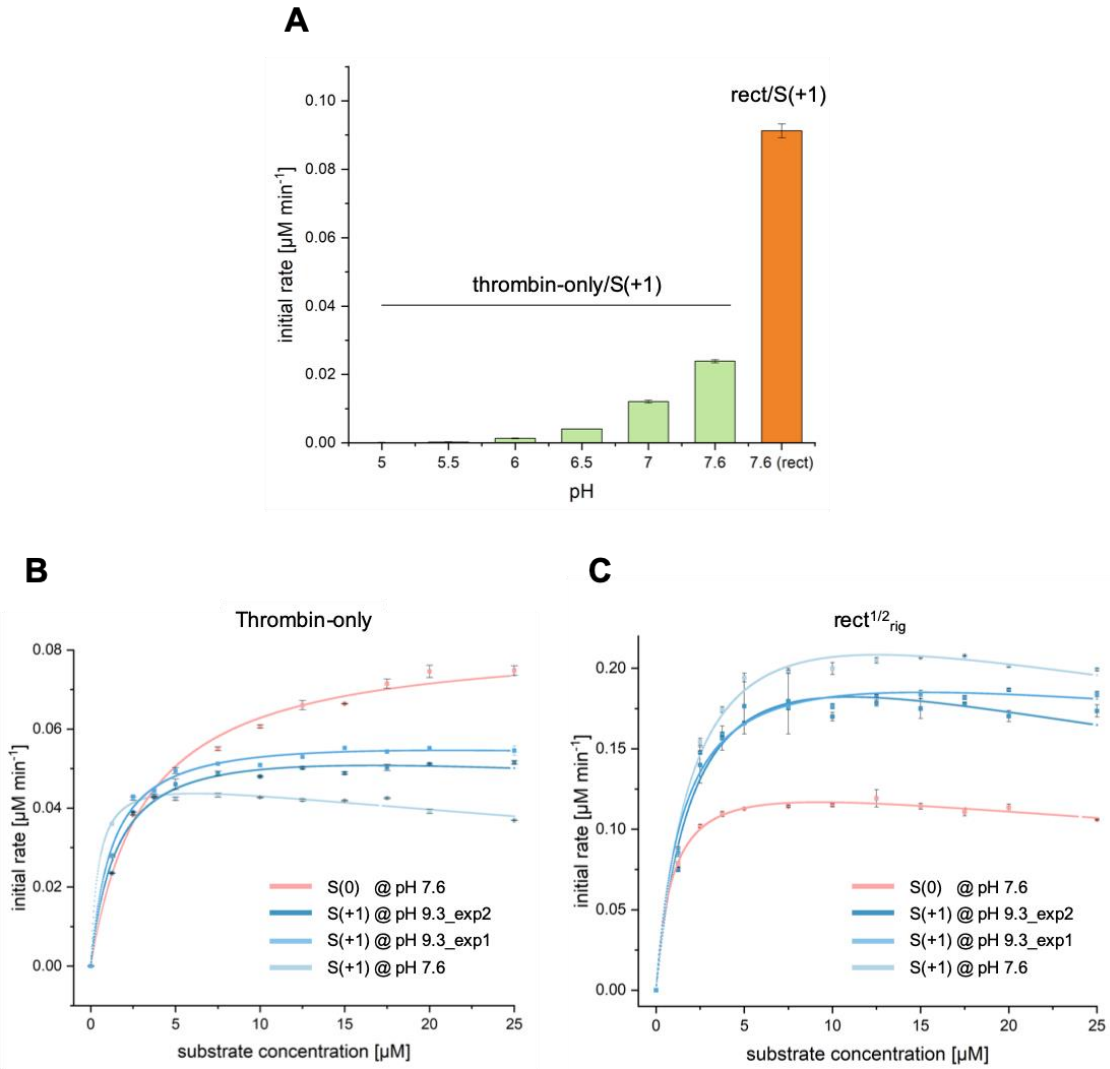

Figure S 34: Performance of thrombin-catalyzed cleavage of S(+1) in varying pH environments. (**A**) Enzymatic reactions of thrombin-only were performed as described in the Methods section (4.2.11) at a substrate concentration of 15 µM within a range of pH values (5 – 7.6, green bars). Enzyme performance significantly drops for lower pH values until almost no activity is present (pH 5). For comparison, a thrombin/rect sample (orange bars) was monitored in standard buffer. If lower pH regimes would be present in proximity of the DNA origami structure, lower reaction rates should be observed. Since the presence of DNA origamis clearly increases the reaction rates, this hypothesis cannot be considered to be a possible reason for increased enzymatic performance in this system. (**B, C**) The enzymatic cleavage of S(+1) was recorded for increased pH values for thrombin-only (**B**) and $rect^{1/2}_{rig}$ samples (**C**). For comparison, reaction rates of S(0) and S(+1) in standard buffer are depicted as well. Interestingly, reactions taking place at elevated pH values show reaction curve profiles that resemble an intermediate of both, S(0) and S(+1) reactions, likely due to the altered substrate net charge of S(+1) at these conditions. Enzymatic assays at higher pH values could not be performed due to the occurrence of salt precipitates (presumably derived by the magnesium ions contained in the buffer and that are however necessary for the stability of the DNA origami structures). Reprinted and adapted from reference [200].

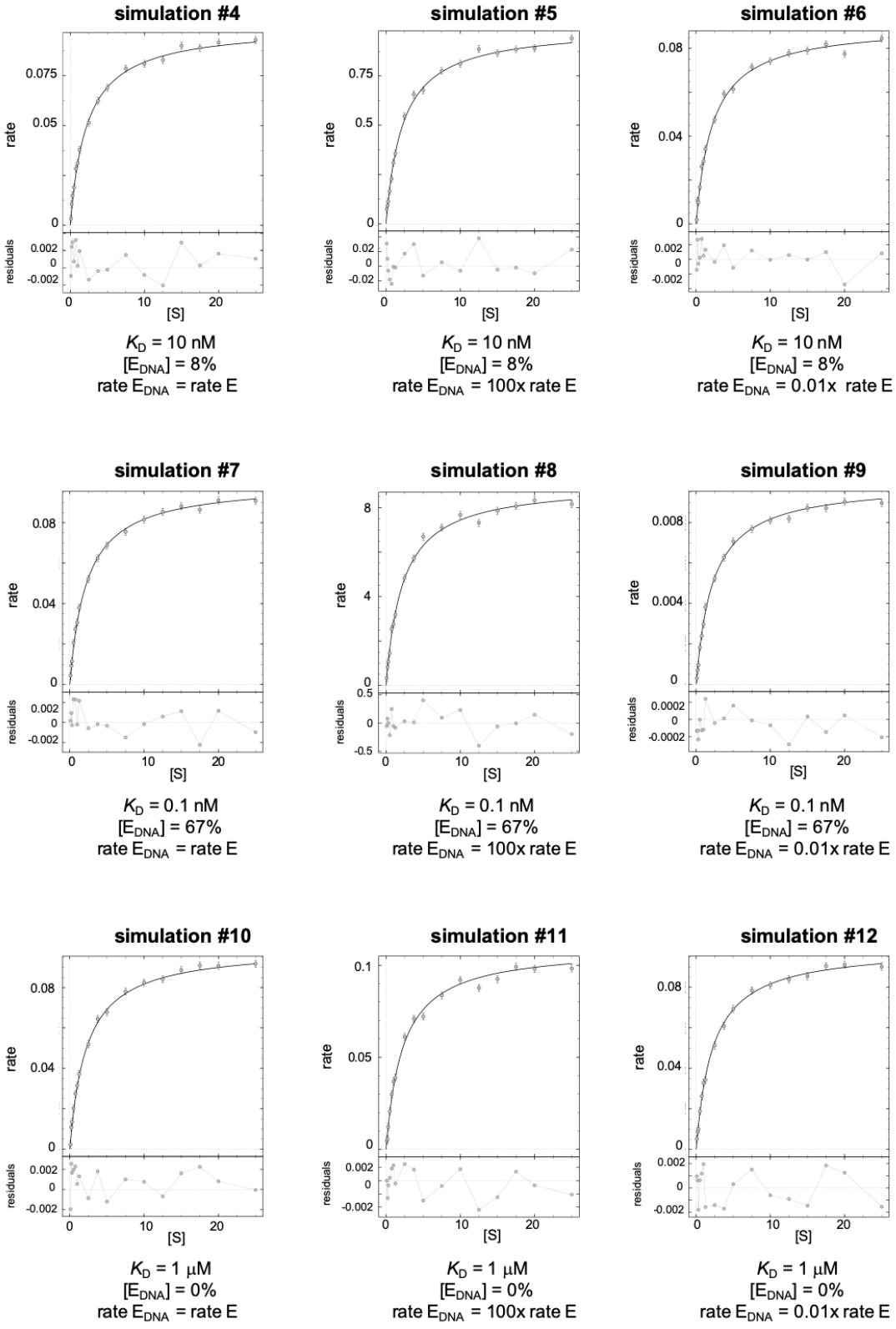

Figure S 35: Simulations of thrombin catalyzed hydrolysis for varying parameters (KD = 10 nM, 0.1 nM and 1 µM). Same legend as in Figure 25, using different sets of rate coefficients for the association/dissociation of the E_{DNA} complex (k_7 to k_9) and for the reaction catalyzed by E_{DNA} (k_4 to k_6). The steady-state rate of the reaction is dominated by the faster enzyme, even if this is not the most abundant species. See Supplementary Text 2 for the details of the simulations. Reprinted and adapted from reference [200].

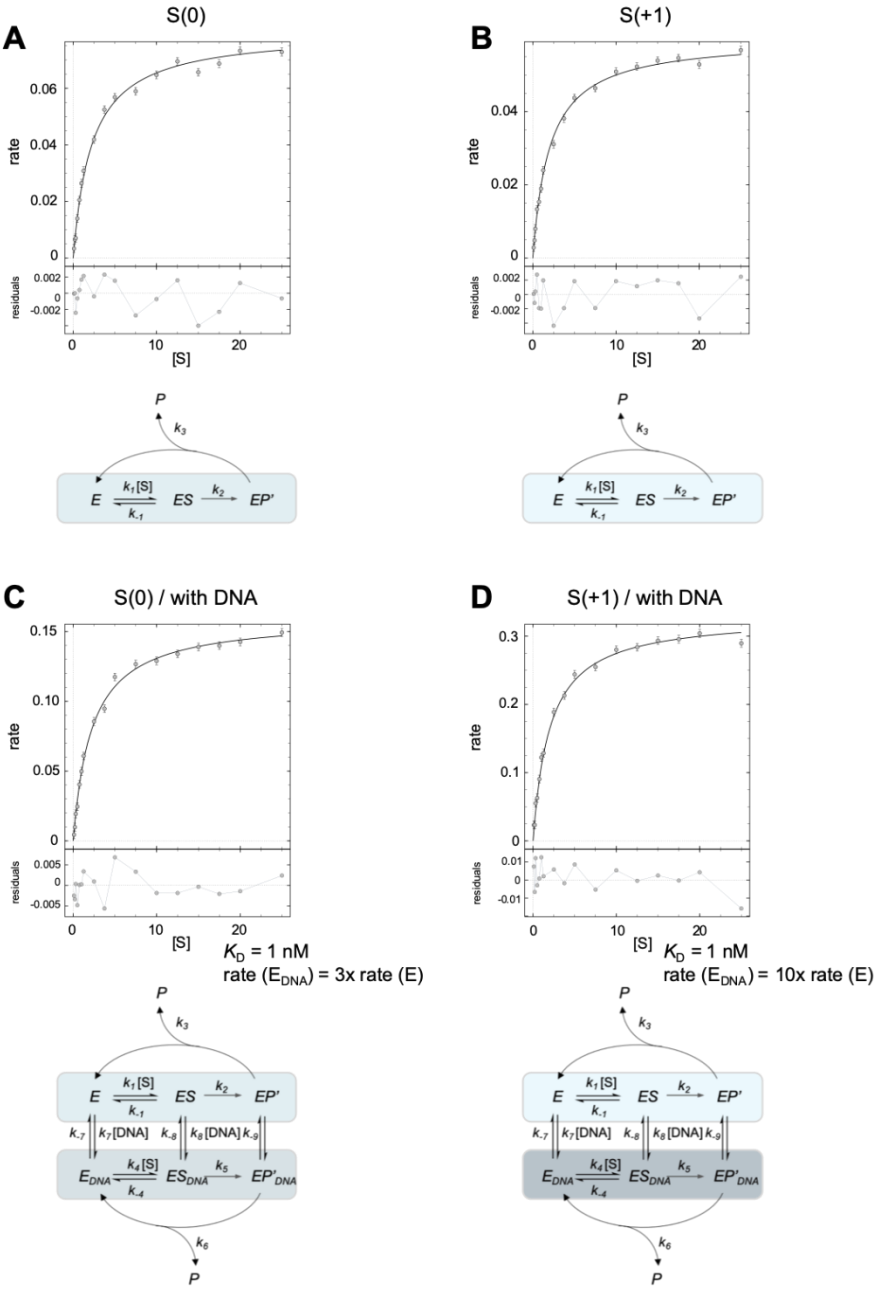

Figure S 36: Simulations of thrombin catalyzed hydrolysis of different substrates in absence and presence of DNA. Simulations were run as described in Supplementary Text 2. Rate coefficients for thrombin-only pathways (**A** and **B**) were k_1 = 6.000 min^{-1} µM^{-1}; k_{-1} = 16.000 min^{-1}; k_2 = 80 min^{-1} and k_3 = 400 min^{-1} for S(0) and, respectively, 5.000 min^{-1} µM^{-1}, 12.000 min^{-1}; 60 min^{-1}and 300 min^{-1} for S(+1). Simulations in presence of DNA (**C** and **D**) were done by imposing a K_D = 1 nM. Although E_{DNA} species will be the minority in these conditions, their presence clearly accelerates the total reaction rates since their substrate turnover is faster (Note: darker boxes correspond to increased reaction rates). Rate coefficients for the E_{DNA} pathway were chosen so that the total reaction rates approximate the ones observed in the enzymatic assays. Specifically, the rate coefficients of the E_{DNA} path increased of a 3-fold factor for substrate S(0), leading to k_4 = 18.000 min^{-1} µM^{-1}; k_{-4} = 48.000 min^{-1}; k_5 = 240 min^{-1} and k_6 = 1200 min^{-1} and a 10-fold factor for substrate S(+1), leading respectively to 50.000 min^{-1} µM^{-1}; k_{-1} = 120.000 min^{-1}; k_2 = 600 min^{-1} and k_3 = 3000 min^{-1}. These values are only for indicative purposes and are not meant to resemble the true values of rate coefficients examined. Reprinted and adapted from reference [200].

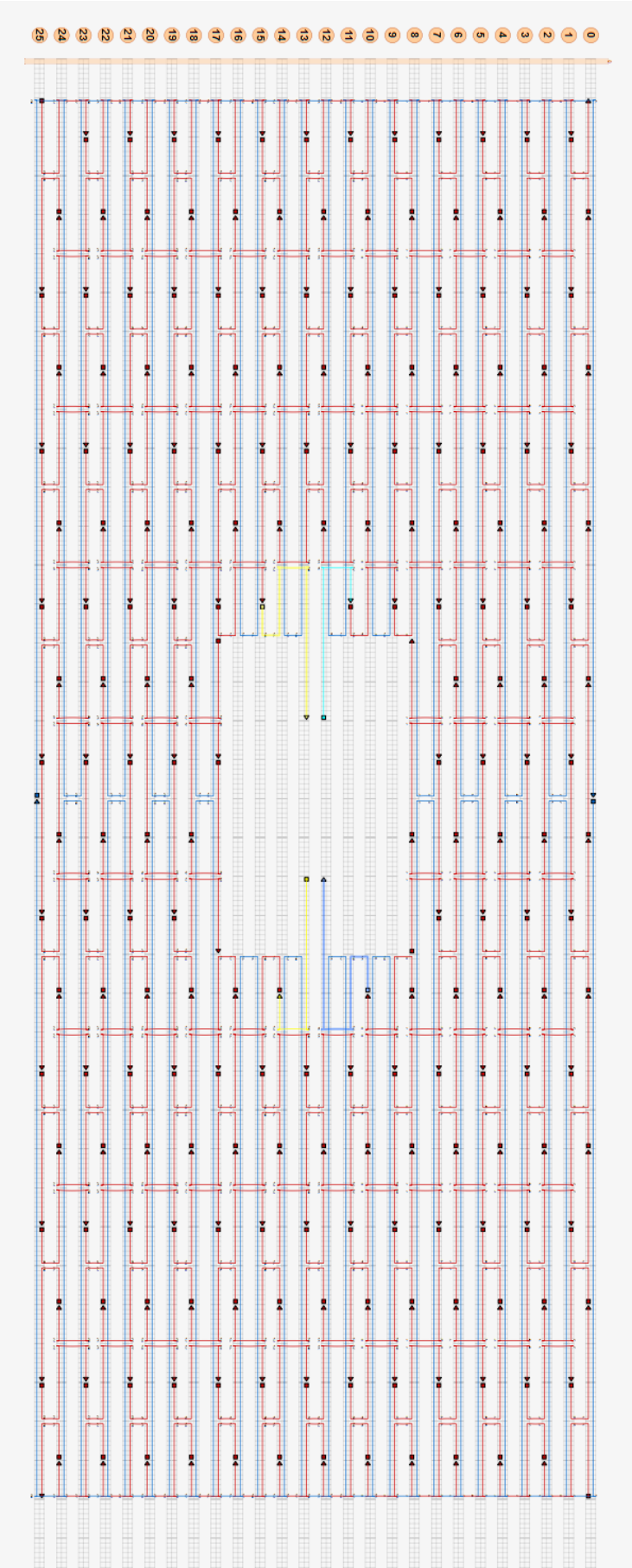

Figure S 37: caDNAno design of rect. Single stranded scaffold p7249 was folded into a rectangular DNA structure. Unpaired scaffold loops and 5T-overhangs at the edges are not shown. Protruding arms and TBA-carrying oligonucleotides are colored in yellow and light/dark blue respectively. For a detailed view on thrombin binding see Figure S 4 and Figure S 9.

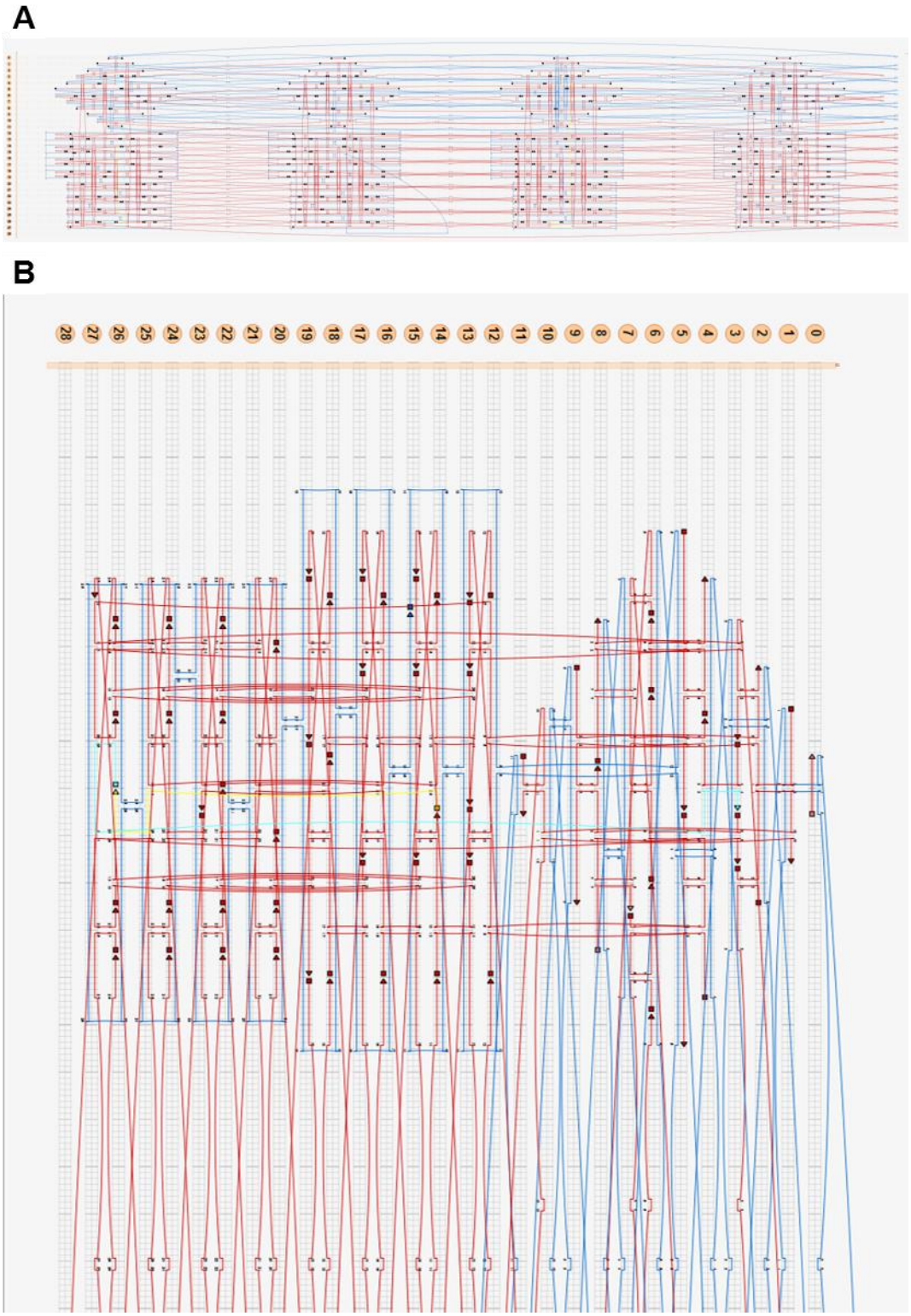

cont. on the following page

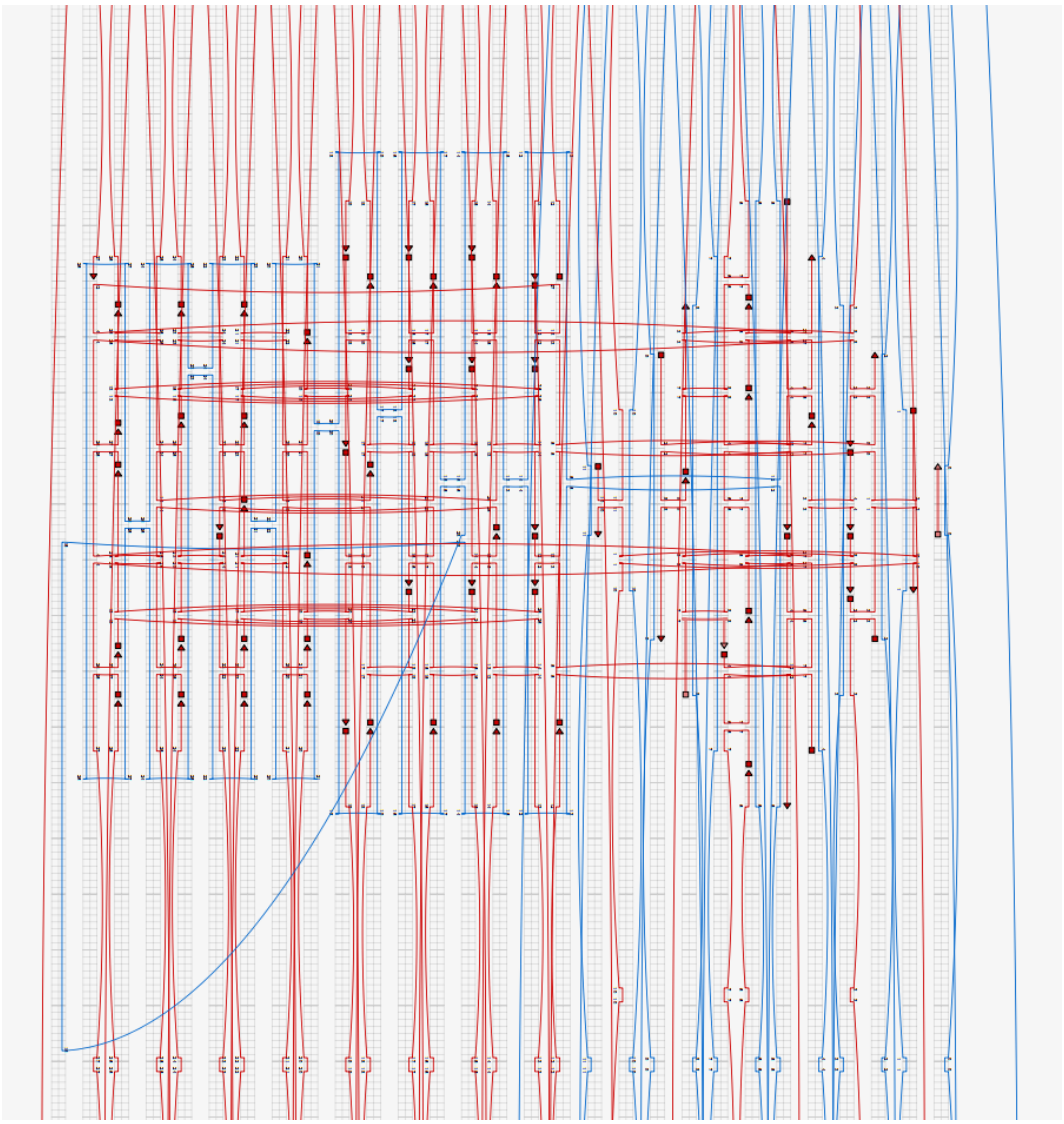

cont. on the following page

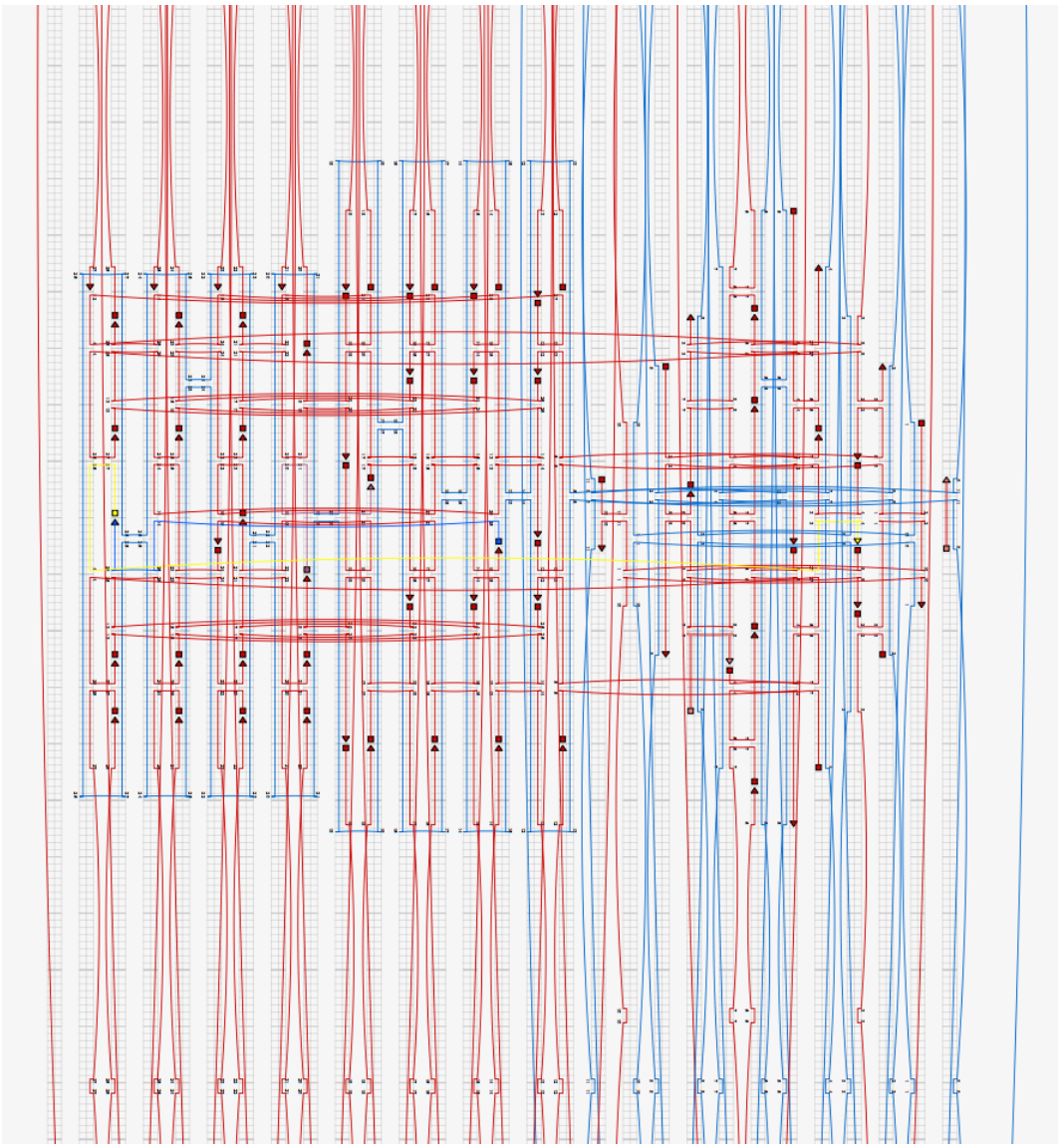

cont. on the following page

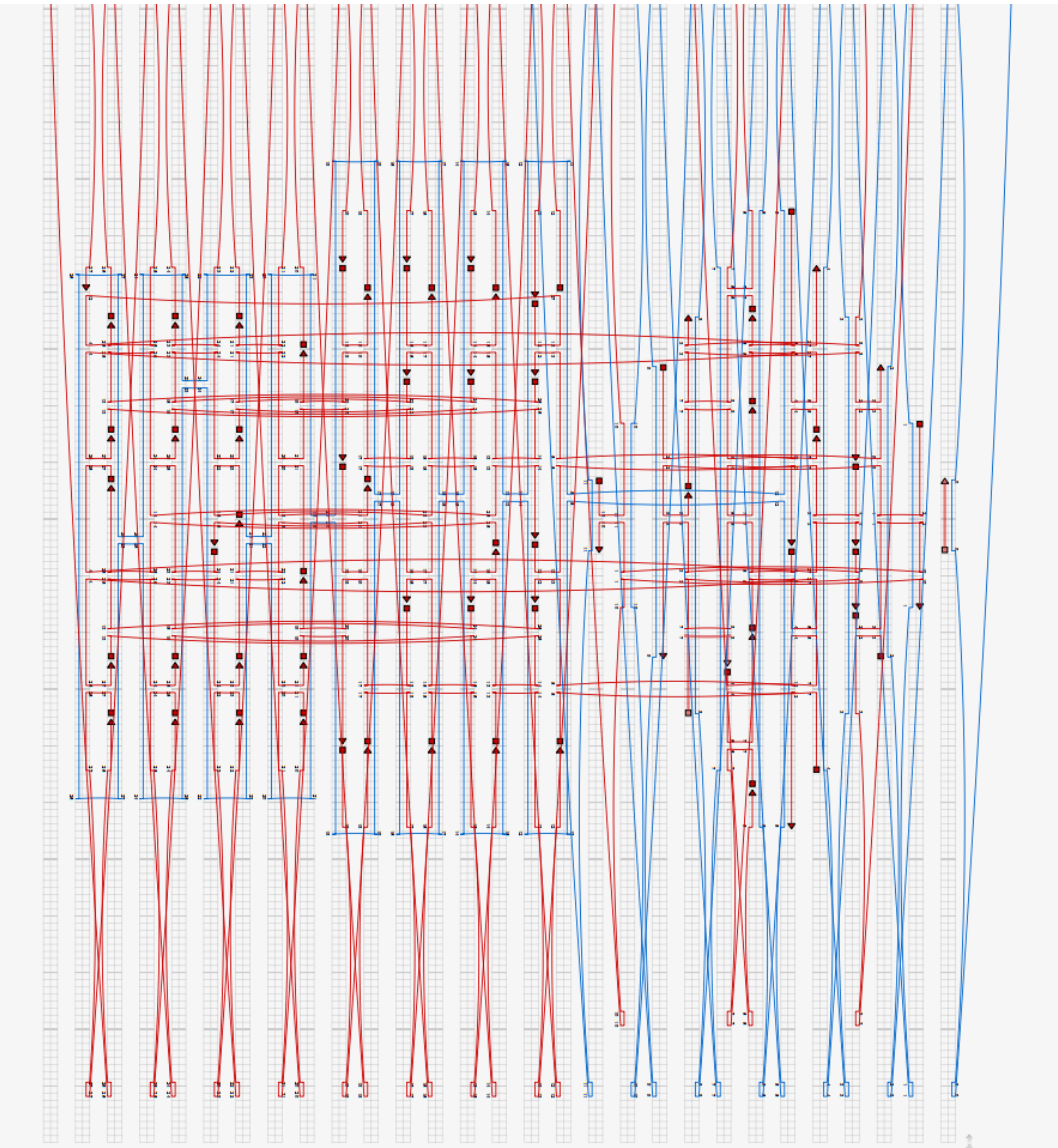

Figure S 38: caDNAno design of box. (**A**) overview of box design. (**B**) Zoom-In of the design of box. The structure is designed in square lattice and is dual-layered. Each picture displays one side of the 3D box, including the bottom plate. Connections between each side are interspersed with unpaired scaffold or staple parts to allow the structure to relax. Protruding arms and TBA-carrying oligonucleotides are colored yellow and light/dark blue respectively. Protruding parts of these staples are not shown. For detailed view on thrombin binding see Figure S 4.

Table S 6: Kinetic parameters of the hydrolysis of S(-1) by thrombin. Application of the MM equation corrected for substrate inhibition (when necessary) on the recorded kinetic profiles allowed for the extraction of the kinetic parameters of the reaction, namely, the catalytic efficiency or turnover number (k_{cat}), the MM constant (K_M), the specificity constant (k_{cat}/K_M), and, when relevant, the inhibition constant (K_I). Reported values are the result of at least three replicates. Software used for the plotting was OriginPro 2017G. Nomenclature of the samples as described in the main text. Reprinted and adapted from reference [200].

	Thr/S(-1)	k_{cat} [min^{-1}]	K_M [μM]	k_{cat}/K_M [$min^{-1}\mu M^{-1}$]	K_i [μM]
thrombin only	-	220 ± 14	9.5 ± 0.9	23 ± 3	-
w/o DNA	TBA1	176 ± 11	7.1 ± 0.7	25 ± 3	-
	TBA2	204 ± 15	9 ± 1	22 ± 3	-
	TBA1/2	200 ± 13	9.5 ± 0.9	21 ± 2	-
	phosph	210 ± 11	9.1 ± 0.7	23 ± 2	-
DNA-unbound	ssDNA	155 ± 8	6.0 ± 0.5	26 ± 3	-
	rect	208 ± 37	5 ± 1	42 ± 15	-
	box	176 ± 11	5.2 ± 0.6	34 ± 4	-
DNA-bound	$rect^1_{flex}$	150 ± 6	2.2 ± 0.2	69 ± 8	-
	$rect^2_{flex}$	125 ± 8	1.8 ± 0.3	70 ± 12	43 ± 9
	$rect^{1/2}_{flex}$	142 ± 10	1.9 ± 0.3	73 ± 14	42 ± 10
	$rect^{1/2}_{melt}$	164 ± 11	2.1 ± 0.3	77 ± 13	44 ± 10
	$rect^{1/2}_{rig}$	172 ± 16	2.2 ± 0.5	77 ± 18	32 ± 8
	$box^{1/2}_{rig}$	141 ± 9	2.0 ± 0.3	70 ± 12	63 ± 17

Table S 7: Kinetic parameters of the hydrolysis of S(+1) by thrombin. Application of the MM equation corrected for substrate inhibition (when necessary) on the recorded kinetic profiles allowed for the extraction of the kinetic parameters of the reaction, namely, the catalytic efficiency or turnover number (k_{cat}), the MM constant (K_M), the specificity constant (k_{cat}/K_M), and, when relevant, the inhibition constant (K_I). Reported values are the result of at least three replicates. Software used for the plotting was OriginPro 2017G. Nomenclature of the samples as described in the main text. Reprinted and adapted from reference [200].

	Thr/S(+1)	k_{cat} [min^{-1}]	K_M [μM]	k_{cat}/K_M [min^{-1}μM^{-1}]	K_I [μM]
thrombin only	-	42 ± 1	0.46 ± 0.08	91 ± 16	82 ± 15
w/o DNA	TBA1	45 ± 1	0.44 ± 0.06	104 ± 13	92 ± 12
	TBA2	48 ± 1	0.55 ± 0.07	87 ± 10	92 ± 13
	TBA1/2	45 ± 1	0.65 ± 0.06	69 ± 6	93 ± 11
	phosph	42 ± 1	0.5 ± 0.08	83 ± 13	86 ± 15
DNA-unbound	ssDNA	56 ± 1	0.51 ± 0.06	110 ± 13	104 ± 15
	rect	132 ± 5	1.6 ± 0.2	84 ± 10	89 ± 20
	box	144 ± 1	2.8 ± 0.2	52 ± 4	42 ± 5
DNA-bound	$rect^1_{flex}$	154 ± 3	1.28 ± 0.08	120 ± 8	109 ± 15
	$rect^2_{flex}$	184 ± 6	2.0 ± 0.2	91 ± 8	124 ± 28
	$rect^{1/2}_{flex}$	187 ± 9	2.4 ± 0.3	78 ± 10	115 ± 37
	$rect^{1/2}_{melt}$	227 ± 14	2.7 ± 0.4	84 ± 13	59 ± 14
	$rect^{1/2}_{rig}$	236 ± 16	2.2 ± 0.4	105 ± 19	70 ± 22
	$box^{1/2}_{rig}$	451 ± 32	6.5 ± 0.8	69 ± 9	28 ± 5

6.3 Sequences

Oligonucleotides were purchased from Sigma-Aldrich as desalted, lyophilized product in 96-well plates at 15 nmol scale. Olgionucleotides were resuspended in 150 µL ddH_2O and stored at -20 °C. Primers were resuspended in adequate amounts of ddH_2O to reach a concentration of 100 µM and stored at -20 °C.

THERMAL FOLDING OF A THREE-DOMAINS DNA ORIGAMI STRUCTURE

Sequence (5´- 3 ´)	**Comment**
ACCCAAATCGATGGCCCACTACGTCGGGCAAC	**Right side core staple (faceA)**
GAACGTGGCGAGATAGGGTTGAGTTGGTGGTT	**Core staple**
CCCCGATTACAAGAGTCCACTATTGGTTTGCC	**Core staple**
GTAAAGCAAACGTCAAAGGGCGAACCCTGAGA	**Core staple**
GTAGGTAAATTTTTAGAACCCTCATCGCAAAT	**Right side core staple (faceA)**
AGGGTAGCAGCCTCAGAGCATAAACAATAAAT	**Core staple**
CAACCGTTCAAAAACATTATGACCTCAATTCT	**Core staple**
GGAGACAGGGAGAAGCCTTTATTTTTTCATTT	**Core staple**
GGATAAAAAGATTCAAAAGGGTGAGTTGATAA	**Core staple**
GGTTGTACCTAGCTGATAAATTAAGGAGCAAA	**Core staple**
CTTTTGCGTCAAATCACCATCAATGTAAAACT	**Core staple**
GGTCAATATGCGAACGAGTAGATTCCGAAAGA	**Right side core staple (faceA)**
CATACAGGTGCTGAATATAATGCTTGCTCCTT	**Core staple**
ACTAATAGTAAATATGCAACTAAACCAACAGG	**Core staple**
GGGGCGCGTTTCATTCCATATAACAGCTTCAA	**Core staple**
CCCAATTCACCTGTTTAGCTATATCAACGCAA	**Core staple**
ACATGTTTTAGTAGCATTAACATCGCTAAATC	**Core staple**
TCTGGAAGAGCTGAAAAGGTGGCACTGTAATA	**Core staple**
CTTCAAATAAGATTAAGAGGAAGCGTTTACCA	**Right side core staple (faceA)**
TTGATAAGTGCTTTAAACAGTTCAGTCCAATA	**Core staple**
TCAGGATTATAAATCAAAAATCAGGGGGTAAT	**Core staple**
AGCGAACCTTATAGTCAGAAGCAAGAGAGGCT	**Core staple / substituted in optical tweezer exp.**
GCATCAAAATCGCGTTTTAATTCGAGTTGATT	**Core staple**

GAATGACCAGAGAGTACCTTTAATGTAGCTCA	**Core staple**
CCTGACTAAGACCGGAAGCAAACTGTACGGTG	**Core staple**
AAGAGCAATAAAAACCAAAATAGCAGCGGATT	**Core staple**
ATTTAGGAGTTTAGACTGGATAGCGAAAACGA	**Core staple**
ACATAACGAGAAGTTTTGCCAGAGGTCTTTAC	**Core staple**
GCTTGAGAACACCAGAACGAGTAGAAATTGTG	**Right side core staple (faceB)**
AATCTACGTCATCAAGAGTAATCTGAGGACAG	**Core staple**
CTCATTATTTCATTACCCAAATCATCATAAGG	**Core staple**
TGTGAATTCATTCAGTGAATAAGGTTACTTAG	**Core staple**
AGCTGATTCTTTTCACCAGTGAGAAATCATGG	**Right side core staple (faceA)**
CCGAAATCCTTTCCAGTCGGGAAACCTAATGA	**Core staple**
CCAGCAGGCATTAATGAATCGGCCAGCCGGAA	**Core staple**
GAGTTGCACGGTTTGCGTATTGGGTGTTATCC	**Core staple**
TCGAAATCTGTATCATCGCCTGATCTTTTGCG	**Right side core staple (faceB)**
ATGAACGGCCAACCTAAAACGAAAGGAAGTTT	**Core staple**
GAACCGAACTAAAACACTCATCTTAGAGGCTT	**Core staple**
CCGGAACGTACCAAGCGCGAAACAGACAGCAT	**Core staple**
CGGAGATTCGCGACCTGCTCCATGCTTGCCCT	**Core staple**
AGAATACACTGACCAACTTTGAAATGACAAGA	**Core staple**
AGCGATTAAGGCGCAGACGGTCAAACGTAACA	**Core staple**
GGATCGTCATATTCGGTCGCTGAGTCTGTATG	**Right side core staple (faceB)**
CCATTAAAGGTTTATCAGCTTGCTTTGAAAAT	**Core staple**
TGAGGACTTAAACAGCTTGATACCCTAAAGGA	**Core staple**
CGGAACGAATGACAACAACCATCGAGTTTCAG	**Core staple**
TAACCGATACCCTCAGCAGCGAAAAAGTACAA	**Core staple**
GAATTTCTAAAGACTTTTTCATGAGAGGCAAA	**Core staple**
CGCCGACAGGGTAGCAACGGCTACTGACCCCC	**Core staple**
GGATTTTGAAGTTTTGTCGTCTTTCGAGAGGG	**Right side core staple (faceB)**
CTCCAAAAGAACCCATGTACCGTACACCCTCA	**Core staple**
ATTGCGAACCAGTACAAACTACAAGCCACCCT	**Core staple**
CGGAGTGACAGACAGCCCTCATAGGGTGTATC	**Core staple**
ACGATCTACTAAACAACTTTCAACCCCACGCA	**Core staple**
TTTCGTCATAATAATTTTTTCACGTTCGAGGT	**Core staple**

GCATTCCAGAATAGAAAGGAACAAGATAGTTG	**Core staple**
TTGATATAAGCGGGGTTTTGCTCAAAATAAAT	**Right side core staple (faceB)**
GAGCCACCATAAACAGTTAATGCCCTGGTAAT	**Core staple**
CAGAACCGACCTATTATTCTGAAATCATACAT	**Core staple**
ACCGTACTGGCTGAGACTCCTCAACGCAGTCT	**Core staple**
TTAGGATTAGTATAGCCCGGAATATTAGCGTA	**Core staple**
ATTTCGGACCACCCTCAGAACCGCACACTGAG	**Core staple**
TATTAAGACAGGAGGTTTAGTACCCGCCTGTA	**Core staple**
CCTCATTATGAGGCAGGTCAGACGGCGACAGA	**Right side core staple (faceB)**
AAGTTTTAGAGCCGCCACCCTCAGTAATCAAA	**Core staple**
GGCTTTTGGCCACCACCCTCAGAGTAGCCCCC	**Core staple**
CTGAATTTCACCAGAGCCGCCGCCCTGTAGCG	**Core staple**
CAGGAGGTAAGCCAGAATGGAAAGGAGAAGGA	**Core staple**
CCCTCAGAATGATACAGGAGTGTACCCTGCCT	**Core staple**
AGAACCACACCGTTCCAGTAAGCGCATGAAAG	**Core staple**
TGGTTTTTGCCCTTCACCGCCTGGAAACCGTC	**Core staple**
GCCAGCTGCGAAAATCCTGTTTGAGTTGTTCC	**Core staple / substituted in optical tweezer exp.**
GGGAGAGGGCAAGCGGTCCACGCTAAAGAACG	**Core staple**
ATCAAGTTCACCAATGAAACCATCAAAGAAAC	**Right side core staple (faceB)**
ATCACCGGAAGGTGAATTATCACCCAACCGAT	**Core staple**
TTATTAGCATTTGGGAATTAGAGCTTTACCAG	**Core staple**
CGTTTTCAAGCACCATTACCATTAATTTTGTC	**Core staple**
GGAAACGTTGCCTTTAGCGTCAGAAGCATTGA	**Core staple**
CTTGAGCCGTTTGCCATCTTTTCAAACCGCCA	**Core staple**
TCACCAGTTCGGCATTTTCGGTCACCGCCACC	**Core staple**
GCAAAGACAAGGTGGCAACATATAGCTAATAT	**Right side core staple (faceB)**
TGAGGGAGGAGGAAACGCAATAATTTTAAGAA	**Core staple**
CGCCAAAGGAACTGGCATGATTAAGAAATAGC	**Core staple**
ACAATCAAGTATGTTAGCAAACGTAGTTAAGC	**Core staple**
CATACATAACCACGGAATAAGTTTGCAAGGCC	**Core staple**
ACCCAAAAACAAAAGGGCGACATTGTCACCGA	**Core staple**
ATTACGCATAGAAAATTCATATGGCAGCAAAA	**Core staple**
AACAAAGTTAACCCACAAGAATTGAGAAAATA	**Core staple**

TTACAGAGTCTTACCGAAGCCCTTAACGGAAT	**Core staple**
GCATTAGAAAGAGCAAGAAACAATGACTCCTT	**Core staple**
TATTTTGCAAGCCTTAAATCAAGAATCCCATC	**Right side core staple (faceC)**
ATTATTTAGCGCCCAATAGCAAGCATCGAGAA	**Core staple**
CCTAATTTGCTTATCCGGTATTCTCAAGAACG	**Core staple**
TCTTACCATTAGCGAACCTCCCGAAATCAATA	**Core staple**
CTAATTTAGAACAAGAAAAATAATTATCATAT	**Right side core staple (faceC)**
CAAGCAAGCGACAAAAGGTAAAGTATTTAGGC	**Core staple**
GGTATTAACGACAATAAACAACATAGAATCGC	**Core staple**
ATCGGCTGACGCGCCTGTTTATCATAAAGCCA	**Core staple**
TAAGTCCTCGAGCATGTAGAAACCCTTGCGGG	**Core staple**
CCAGACGAACCAAGTACCGCACTCAAATCAGA	**Core staple**
AATGCAGATCTTTCCTTATCATTCAAGAACGC	**Core staple**
TCATAGCTGACTCTAGAGGATCCCAGATCGCA	**Right side core staple (faceA)**
GTGAGCTATGTGCTGCAAGGCGATCGATCGGT	**Core staple**
GCATAAAGAGGGTTTTCCCAGTCACGCCATTC	**Core staple / substituted in FRET experiments**
GCTCACAACGGCCAGTGCCAAGCTTTCTGGTG	**Core staple**
GCGTTATAAACACCGGAATCATAAAAGACGCT	**Right side core staple (faceC)**
AGAGGCATCTTTTTCAAATATATTTGTAAATG	**Core staple**
CATATTTATCTGACCTAAATTTAAACCTCCGG	**Core staple**
ACGCTCAACCGTGTGATAAATAAGCAAAATCA	**Core staple**
TAAGAATACAAATTCTTACCAGTAACAATAGA	**Core staple**
TTTCATCTACAACGCCAACATGTAAATTCTGT	**Core staple**
AATACCGACAGTAGGGCTTAATTGGTTCAGCT	**Core staple**
GAGAAGAGCCCTTAGAATCCTTGAGAGAAACA	**Right side core staple (faceC)**
CTGATGCATCATTTGAATTACCTTATGATGAA	**Core staple**
CTTAGGTTACATAAATCAATATATATTATTCA	**Core staple**
TAGGTCTGGCTTCTGTAAATCGTCGAATACCA	**Core staple**
TTAATTTTTCAATAGTGAATTTATGCGTTAAA	**Core staple**
GAAACAGTGGGTTATATAACTATATTAGTTAA	**Core staple**
ATAACCTTAGAGACTACCTTTTTATGGTTTGA	**Core staple**
ATAACGGAGTCAGATGAATATACATGCCCGAA	**Right side core staple (faceC)**
ACAAACATATACTTCTGAATAATGATTATCAG	**Core staple**

TTTCAATTCCATATCAAAATTATTCCAGAAGG	**Core staple**
AGTTACAAATAAAGAAATTGCGTATAACATTA	**Core staple**
GGTTTAACTTCGCCTGATTGCTTTGCTATTAA	**Core staple**
AGAACCTAACCTGAGCAAAAGAAGTTTTAATG	**Core staple**
AAACAGAAAATCGCGCAGAGGCGAGTGAGTGA	**Core staple**
CGTTATTAGACTTTACAAACAATTAGGCGGTC	**Right side core staple (faceC)**
ATGATGGCAATTGAGGAAGGTTATAAACCCTC	**Core staple**
AGCGGAATAGCACTAACAACTAATCTAAAGCA	**Core staple**
TCATTTTGTAGATAATACATTTGAGCCACGCT	**Core staple**
AAGTATTAATTTTAAAAGTTTGAGGATTTTCA	**Core staple**
TCTTTAGGTATCATCATATTCCTGGAAGGGTT	**Core staple**
GCCGTCAACGGAACAAAGAAACCATGCACGTA	**Core staple**
AGTATTAATACCGAACGAACCACCTTGCAACA	**Right side core staple (faceC)**
AATCAATACTGAAAGCGTAAGAATCAGTAATA	**Core staple**
TCACCTTGATTTTTGAATGGCTATATTTACAT	**Core staple**
GAGAGCCAAACTGATAGCCCTAAAACATTTTG	**Core staple**
ATTAAAAACACCGCCTGCAACAGTGGATTTAG	**Core staple**
CAGACAATCTGAACCTCAAATATCCTAAAATA	**Core staple**
AATGCGCGGCAGCAAATGAAAAATAGATTAGA	**Core staple**
TGCAGGTCGTTTCCTGTGTGAAATCGCCAGGG	**Core staple**
GTAACGCCTGTAAAGCCTGGGGTGCCTGTCGT	**Core staple / substituted in FRET experiments**
TAAAACGATTCCACACAACATACGAACGCGCG	**Core staple**
GGAAAAACATATTACCGCCAGCCAGTGCTTTC	**Right side core staple (faceC)**
AAAGGGACTTAACCGTTGTAGCAATTATAATC	**Core staple**
TGGCAGATAATAACATCACTTGCCGGAACGGT	**Core staple**
ACGCTCAAAACTATCGGCCTTGCTAAACAGGA	**Core staple**
CCAGAACAGCTCATGGAAATACCTACATCGCC	**Core staple**
TGATTAGTTCACCAGTCACACGACACGTGGCA	**Core staple**
AGAACTCATCGTCTGAAATGGATTTAGTCTTT	**Core staple**
GTTGCTTTAATCAGAGCGGGAGCTGGTAATAT	**Core staple**
GTCACGCTATCCTGAGAAGTGTTTTACTTCTT	**Core staple**
GCTTAATGAAAGGGATTTTAGACATGAGTAGA	**Core staple**
CTCCAGCCGCCAGTTTGAGGGGACATTGTAAA	**Right side core staple (faceA)**

GCGGGCCTAACAACCCGTCGGATTTCTGGCCT	**Core staple**
AGGCTGCGGGCGGATTGACCGTAAACCAATAG	**Core staple / substituted in FRET experiments**
CCGGAAACGGTGTAGATGGGCGCAATTAAATT	**Core staple**
GTGCATCTAGCTTTCCGGCACCGCTGCATGCC	**Core staple**
GAACAAACCAACTGTTGGGAAGGGTAAGTTGG	**Core staple / substituted in FRET experiments**
GTCACGTTCAGGCAAAGCGCCATTCGACGTTG	**Core staple**
CGTTAATAGCCCCAAAAACAGGAAAGTAATGT	**Right side core staple (faceA)**
TCCTGTAGCATTGCCTGAGAGTCTTGCCGGAG	**Core staple**
GAACGCCATCGATGAACGGTAATCATGATATT	**Core staple / substituted in FRET experiments**
TTTGTTAAAATCATATGTACCCCGGAAAGGCC	**Core staple**
TCAGAAAATTTTGTTAAAATTCGCTCGTAACC	**Core staple**
CAAGAGAATCAAAAATAATTCGCGCTCCGTGG	**Core staple**
AGCATGTCATCAGCTCATTTTTTATGGGATAG	**Core staple**
TTAATCAAAAGAATAGCCCGAGAAAGGAAGGGAA**TT**	**Edge type 0**
TTCAAAATTAAGCAATAATATTTTTGAGAGATCT**TT**	**Edge type 0**
TTTGGCTTAGAGCTTAATCAAGGCAAAGAATTAG**TT**	**Edge type 0**
TTTTGAATCCCCCTCAAAAGGTCATTTTTGCGGA**TT**	**Edge type 0**
TTGGAACAACATTATTACTCGTCATAAATATTCA**TT**	**Edge type 0**
TTATAGGCTGGCTGACCTTTAATAAAACGAACTA**TT**	**Edge type 0**
TTTGCCACTACGAAGGCATGTACAGACCAGGCGC**TT**	**Edge type 0**
TTAGCCTTTAATTGTATCCGGGTAAAATACGTAA**TT**	**Edge type 0**
TTATAGCAAGCCCAATAGAAAAGGCTCCAAAAGG**TT**	**Edge type 0**
TTGAGTAACAGTGCCCGTACCCTCATTTTCAGGG**TT**	**Edge type 0**
TTGGAACCGCCTCCCTCAACGGGGTCAGTGCCTT**TT**	**Edge type 0**
TTTTGCGCTCACTGCCCGGGCAAAATCCCTTATA**TT**	**Edge type 0**
TTCGGAAATTATTCATTAAACCAGAGCCACCACC**TT**	**Edge type 0**
TTTTACCAGAAGGAAACCGGAAGGTAAATATTGA**TT**	**Edge type 0**
TTACGATTTTTTGTTTAAAGATAGCCGAACAAAG**TT**	**Edge type 0**
TTCGTAGGAATCATTACCTCCCAATCCAAATAAG**TT**	**Edge type 0**
TTAGAGAATATAAAGTACCCGTTTTTATTTTCAT**TT**	**Edge type 0**
TTAAAGAACGCGAGAAAATTTCGAGCCAGTAATA**TT**	**Edge type 0**
TTATTACATTTAACAATTAATCCAATCGCAAGAC**TT**	**Edge type 0**

TTCCTGATTGTTTGGATTCAAGAAAACAAAATTA**TT**	**Edge type 0**
TTATCAACAGTTGAAAGGAATTCATCAATATAAT**TT**	**Edge type 0**
TTATAGAACCCTTCTGACTCTGGTCAGTTGGCAA**TT**	**Edge type 0**
TTGCTGGCGAAAGGGGGAACTCACATTAATTGCG**TT**	**Edge type 0**
TTCTGTCCATCACGCAAAATTCTGGCCAACAGAG**TT**	**Edge type 0**
TTAGCGAAAGGAGCGGGCCACCGAGTAAAAGAGT**TT**	**Edge type 0**
TTTTAAATGTGAGCGAGTCTTCGCTATTACGCCA**TT**	**Edge type 0**
TTACAAAGGCTATCAGGTCCAGCTTTCATCAACA**TT**	**Edge type 0**
TTTGCAATGCCTGGATTGTATAAG**TT**	**Edge type 0**
TTTTAGATACATTTATATTTTAAA**TT**	**Edge type 0**
TTTAAATGAATTTGCTTGCAGGGA**TT**	**Edge type 0**
TTATAAGTGCCGTCCAGACGTTAG**TT**	**Edge type 0**
TTTATTCACAAACGTACCAGGCGG**TT**	**Edge type 0**
TTCGTAATCAGTAATTGGCCTTGA**TT**	**Edge type 0**
TTTAGCTTAGATTTTACTAGAAAA**TT**	**Edge type 0**
TTTTTTACATCGGAAACATAGCGA**TT**	**Edge type 0**
TTATTAAATCCTTGTAACAGTACC**TT**	**Edge type 0**
TTAAACAGAGGTGCGACAACTCGT**TT**	**Edge type 0**
TTCGGCCTCAGGACGGGTACCGAG**TT**	**Edge type 0**
TTCAAATATTTAAGACGACAGTAT**TT**	**Edge type 0**
TAGTTTGACCA**TT**	**Edge type 0**
TTGTTAAAGGCCG	**Edge type 0**
GATAGCAGCAC**TT**	**Edge type 0**
TTCTCGAATTCGT	**Edge type 0**
TTAGCCTGTTTAG	**Edge type 0**
AGCAGAAGATA**TT**	**Edge type 0**
GAATAGCCCGAGAAAGGAAGGGAA**TTTTT**AGCGAAAG	**Edge type 1**
AGCAATAATATTTTTGAGAGATCT**TTTTT**ACAAAGGC	**Edge type 1**
AGCTTAATCAAGGCAAAGAATTAG**TTTTT**CAAAATTA	**Edge type 1**
CCCTCAAAAGGTCATTTTTGCGGA**TTTTT**TGGCTTAG	**Edge type 1**
ATTATTACTCGTCATAAATATTCA**TTTTT**TTGAATCC	**Edge type 1**
GCTGACCTTTAATAAAACGAACTA**TTTTT**GGAACAAC	**Edge type 1**

CGAAGGCATGTACAGACCAGGCGC**TTTTT**ATAGGCTG	**Edge type 1**
ATTGTATCCGGGTAAAATACGTAA**TTTTT**TGCCACTA	**Edge type 1**
CCCAATAGAAAAGGCTCCAAAAGG**TTTTT**AGCCTTTA	**Edge type 1**
GTGCCCGTACCCTCATTTTCAGGG**TTTTT**ATAGCAAG	**Edge type 1**
CTCCCTCAACGGGGTCAGTGCCTT**TTTTT**GAGTAACA	**Edge type 1**
ACTGCCCGGGCAAAATCCCTTATA**TTTTT**AATCAAAA	**Edge type 1**
ATTCATTAAACCAGAGCCACCACC**TTTTT**GGAACCGC	**Edge type 1**
AGGAAACCGGAAGGTAAATATTGA**TTTTT**CGGAAATT	**Edge type 1**
TTGTTTAAAGATAGCCGAACAAAG**TTTTT**TTACCAGA	**Edge type 1**
TCATTACCTCCCAATCCAAATAAG**TTTTT**ACGATTTT	**Edge type 1**
TAAAGTACCCGTTTTTATTTTCAT**TTTTT**CGTAGGAA	**Edge type 1**
CGAGAAAATTTCGAGCCAGTAATA**TTTTT**AGAGAATA	**Edge type 1**
TAACAATTAATCCAATCGCAAGAC**TTTTT**AAAGAACG	**Edge type 1**
TTTGGATTCAAGAAAACAAAATTA**TTTTT**ATTACATT	**Edge type 1**
TTGAAAGGAATTCATCAATATAAT**TTTTT**CCTGATTG	**Edge type 1**
CTTCTGACTCTGGTCAGTTGGCAA**TTTTT**ATCAACAG	**Edge type 1**
AAGGGGGAACTCACATTAATTGCG**TTTTT**TTGCGCTC	**Edge type 1**
CACGCAAAATTCTGGCCAACAGAG**TTTTT**ATAGAACC	**Edge type 1**
GAGCGGGCCACCGAGTAAAAGAGT**TTTTT**CTGTCCAT	**Edge type 1**
GAGCGAGTCTTCGCTATTACGCCA**TTTTT**GCTGGCGA	**Edge type 1**
TATCAGGTCCAGCTTTCATCAACA**TTTTT**TTAAATGT	**Edge type 1**
AATTTGCTTGCAGGGA**TTTTT**GTTAAAGGCCG	**Edge type 1**
AGATTTTACTAGAAAA**TTTTT**AGCCTGTTTAG	**Edge type 1**
CAGGACGGGTACCGAG**TTTTT**CTCGAATTCGT	**Edge type 1**
GCCTGGATTGTATAAG**TTTTT**CAAATA	**Edge type 1**
ACATTTATATTTTAAA**TTTTT**TGCAAT	**Edge type 1**
GCCGTCCAGACGTTAG**TTTTT**TAAATG	**Edge type 1**
CAAACGTACCAGGCGG**TTTTT**ATAAGT	**Edge type 1**
CAGTAATTGGCCTTGA**TTTTT**TATTCA	**Edge type 1**
ATCGGAAACATAGCGA**TTTTT**TAGCTT	**Edge type 1**
TCCTTGTAACAGTACC**TTTTT**TTTTAC	**Edge type 1**
AGGTGCGACAACTCGT**TTTTT**ATTAAA	**Edge type 1**
TTTAAGACGACAGTAT**TTTTT**CGGCCT	**Edge type 1**

TAGTTTGACCA**TTTTTT**TTAGAT	**Edge type 1**
GATAGCAGCAC**TTTTTT**CGTAAT	**Edge type 1**
AGCAGAAGATA**TTTTTT**AAACAG	**Edge type 1**
GAATAGCCCGAGAAAGGAAGGGAA**TTTTTT**AATCAAAA	**Edge type 2**
AGCAATAATATTTTTGAGAGATCT**TTTTTT**CAAAATTA	**Edge type 2**
AGCTTAATCAAGGCAAAGAATTAG**TTTTTT**TGGCTTAG	**Edge type 2**
CCCTCAAAAGGTCATTTTTGCGGA**TTTTTT**TTGAATCC	**Edge type 2**
ATTATTACTCGTCATAAATATTCA**TTTTTT**GGAACAAC	**Edge type 2**
GCTGACCTTTAATAAAACGAACTA**TTTTTT**ATAGGCTG	**Edge type 2**
CGAAGGCATGTACAGACCAGGCGC**TTTTTT**TGCCACTA	**Edge type 2**
ATTGTATCCGGGTAAAATACGTAA**TTTTTT**AGCCTTTA	**Edge type 2**
CCCAATAGAAAAGGCTCCAAAAGG**TTTTTT**ATAGCAAG	**Edge type 2**
GTGCCCGTACCCTCATTTTCAGGG**TTTTTT**GAGTAACA	**Edge type 2**
CTCCCTCAACGGGGTCAGTGCCTT**TTTTTT**GGAACCGC	**Edge type 2**
ACTGCCCGGGCAAAATCCCTTATA**TTTTTT**TTGCGCTC	**Edge type 2**
ATTCATTAAACCAGAGCCACCACC**TTTTTT**CGGAAATT	**Edge type 2**
AGGAAACCGGAAGGTAAATATTGA**TTTTTT**TTACCAGA	**Edge type 2**
TTGTTTAAAGATAGCCGAACAAAG**TTTTTT**ACGATTTT	**Edge type 2**
TCATTACCTCCCAATCCAAATAAG**TTTTTT**CGTAGGAA	**Edge type 2**
TAAAGTACCCGTTTTTATTTTCAT**TTTTTT**AGAGAATA	**Edge type 2**
CGAGAAAATTTCGAGCCAGTAATA**TTTTTT**AAAGAACG	**Edge type 2**
TAACAATTAATCCAATCGCAAGAC**TTTTTT**ATTACATT	**Edge type 2**
TTTGGATTCAAGAAAACAAAATTA**TTTTTT**CCTGATTG	**Edge type 2**
TTGAAAGGAATTCATCAATATAAT**TTTTTT**ATCAACAG	**Edge type 2**
CTTCTGACTCTGGTCAGTTGGCAA**TTTTTT**ATAGAACC	**Edge type 2**
AAGGGGGAACTCACATTAATTGCG**TTTTTT**GCTGGCGA	**Edge type 2**
CACGCAAAATTCTGGCCAACAGAG**TTTTTT**CTGTCCAT	**Edge type 2**
GAGCGGGCCACCGAGTAAAAGAGT**TTTTTT**AGCGAAAG	**Edge type 2**
GAGCGAGTCTTCGCTATTACGCCA**TTTTTT**TTAAATGT	**Edge type 2**
TATCAGGTCCAGCTTTCATCAACA**TTTTTT**ACAAAGGC	**Edge type 2**
TTTAAA**TTTTTT**TTAGATACATTTATAT	**Edge type 2**
CAGGGA**TTTTTT**TAAATGAATTTGCTTG	**Edge type 2**

CGTTAG**TTTTT**ATAAGTGCCGTCCAGA	**Edge type 2**
AGGCGG**TTTTT**TATTCACAAACGTACC	**Edge type 2**
CCTTGA**TTTTT**CGTAATCAGTAATTGG	**Edge type 2**
AGAAAA**TTTTT**TAGCTTAGATTTTACT	**Edge type 2**
TAGCGA**TTTTT**TTTTACATCGGAAACA	**Edge type 2**
AGTACC**TTTTT**ATTAAATCCTTGTAAC	**Edge type 2**
ACTCGT**TTTTT**AAACAGAGGTGCGACA	**Edge type 2**
ACCGAG**TTTTT**CGGCCTCAGGACGGGT	**Edge type 2**
CAGTAT**TTTTT**CAAATATTTAAGACGA	**Edge type 2**
TATAAG**TTTTT**TGCAATGCCTGGATTG	**Edge type 2**
TAGTTTGACCA**TT**	**Edge type 2**
TTGTTAAAGGCCG	**Edge type 2**
GATAGCAGCAC**TT**	**Edge type 2**
TTCTCGAATTCGT	**Edge type 2**
TTAGCCTGTTTAG	**Edge type 2**
AGCAGAAGATA**TT**	**Edge type 2**
TATCAGGGCAAGTTTTTTGGGGTCGTACTATG	**Planar connections**
AGTTTGGATAGAGCTTGACGGGGAGTGTAGCG	**Planar connections**
TGGACTCCCTAAATCGGAACCCTACCCGCCGC	**Planar connections**
GACGACGACACTATCATAACCCTCTAAATTGG	**Planar connections**
CTGCGGAAAGGTAGAAAGATTCATGGAAGAAA	**Planar connections**
AGTAAAATATACCACATTCAACTAAGAACTGG	**Planar connections**
TTTGCAAACCAAAAGGAATTACGATTAATCAT	**Planar connections**
GACGAGAATGGTTTAATTTCAACTGGCATAGT	**Planar connections**
ACCGGATAACCAGTCAGGACGTTGCAGTTGAG	**Planar connections**
AAGCTGCTACCTTATGCGATTTTAATGCAGAT	**Planar connections**
CAGAGAGACAGAGGGTAATTGAGCTTAGTTGC	**Planar connections**
AAGTAAGCCGTCAAAAATGAAAATACAGCCAT	**Planar connections**
AATAGCTAAGAATAACATAAAAACTTCCAGAG	**Planar connections**
CCAATAATCGGGAGAATTAACTGAATCCTGAA	**Planar connections**
AGGTTTTGACCCAGCTACAATTTTACACCCTG	**Planar connections**
TATAGAAGGCCAGTTACAAAATAAAGCAGCCT	**Planar connections**

GAGGCGTTACGCTAACGAGCGTCTAGGGAAGC	**Planar connections**
CTCGTTAGGACGAGCACGTATAACGAACCATC	**Planar connections**
AGTGAGGCGCTAGGGCGCTGGCAAAAGCCGGC	**Planar connections**
ACGCCAGAGCGCGTAACCACCACAAAGGGAGC	**Planar connections**
GGCCGATTCGCCGCTACAGGGCGCGAGGTGCC	**Planar connections**
TATCAGGGCAAGTTTTTTGGGGTC**TT**GTACTATG	**TT-connections**
AGTTTGGATAGAGCTTGACGGGGA**TT**GTGTAGCG	**TT-connections**
TGGACTCCCTAAATCGGAACCCTA**TT**CCCGCCGC	**TT-connections**
GACGACGACACTATCATAACCCTC**TT**TAAATTGG	**TT-connections**
CTGCGGAAAGGTAGAAAGATTCAT**TT**GGAAGAAA	**TT-connections**
AGTAAAATATACCACATTCAACTA**TT**AGAACTGG	**TT-connections**
TTTGCAAACCAAAAGGAATTACGA**TT**TTAATCAT	**TT-connections**
GACGAGAATGGTTTAATTTCAACT**TT**GGCATAGT	**TT-connections**
ACCGGATAACCAGTCAGGACGTTG**TT**CAGTTGAG	**TT-connections**
AAGCTGCTACCTTATGCGATTTTA**TT**ATGCAGAT	**TT-connections**
CAGAGAGACAGAGGGTAATTGAGC**TT**TTAGTTGC	**TT-connections**
AAGTAAGCCGTCAAAAATGAAAAT**TT**ACAGCCAT	**TT-connections**
AATAGCTAAGAATAACATAAAAAC**TT**TTCCAGAG	**TT-connections**
CCAATAATCGGGAGAATTAACTGA**TT**ATCCTGAA	**TT-connections**
AGGTTTTGACCCAGCTACAATTTT**TT**ACACCCTG	**TT-connections**
TATAGAAGGCCAGTTACAAAATAA**TT**AGCAGCCT	**TT-connections**
GAGGCGTTACGCTAACGAGCGTCT**TT**AGGGAAGC	**TT-connections**
CTCGTTAGGACGAGCACGTATAAC**TT**GAACCATC	**TT-connections**
AGTGAGGCGCTAGGGCGCTGGCAA**TT**AAGCCGGC	**TT-connections**
ACGCCAGAGCGCGTAACCACCACA**TT**AAGGGAGC	**TT-connections**
GGCCGATTCGCCGCTACAGGGCGC**TT**GAGGTGCC	**TT-connections**
CAGGCTGCGGGCGGATTGACC	**FRET design 2**
GCATAAAGAGGGTTTTCCCAGTCACGCCATT	**FRET design 2**
[**6FAM**]GTAAACCAATAGGAACGCCATCGATGAACGGTAATCATGATATT	**FRET design 2**
GCATAAAGAGGGTTTTCCCAGTCACGCCATT[**TAM**]	**FRET design 2**
GCATAAAGAGGGTTTTCCCAG	**FRET design 3**

GAACAAACCAACTGTTGGGAAGGG	**FRET design 3**
[**6FAM**]-TAAGTTGGGTAACGCCTGTAAAGCCTGGGGTGCCTGTCGT	**FRET design 3**
[**TAM**]-TCACGCCATTCAGGCTGCGGGCGGATTGACCGTAAACCAATAG	**FRET design 3**
GCCAGCTGCGAAAATCCTGTTTGAGTTGTTCC**[PEG9spacer]** GAGATCTCGATCCTCTACGCCGGACG	**Forward primer 1; 5'-origami sequence – spacer – plasmid sequence**
DIG-AAAGGCGGACAGGTATCCGGTAAGC	**Reverse primer 1**
AGCGAACCTTATAGTCAGAAGCAAGAGAGGCT**[PEG9spacer]** GAGATCTCGATCCTCTACGCCGGACG	**Forward primer 2; 5'-origami sequence – spacer – plasmid sequence**
Bt-AAAGGCGGACAGGTATCCGGTAAGC	**Reverse primer 2**

DNA ORIGAMI/THROMBIN ENZYME STUDIES

Sequence (5' - 3')	Comment
GAATTCGTTATTACGCCAGCTGGCGGACGACG	Core staple (rect)
ATAGCCGAGAATTGAGTTAAGCCCATTTGCCA	Core staple (rect)
AATTAATGTTGTATAAGCAAATATCGCGTCTG	Core staple (rect)
AAGGAATTTTACAAACAATTCGACTTATACTT	Core staple (rect)
TCCTTATCACTCATCGAGAACAAGTTGCACCC	Core staple (rect)
TGTATCATCTTTGAAAGAGGACAGGCTTGAGA	Core staple (rect)
GAATTGCGTGTAGCATTCCACAGACAGCCCTC	Core staple (rect)
CCACTATTGAGGTGCCGTAAAGCACTAAATCG	Core staple (rect)
ATCCTCATTTAGCGGGGTTTTGCTCAGTACCA	Core staple (rect)
AAAAGGTAATTGAGAATCGCCATAGTTTGAAA	Core staple (rect)
AGATCTACTGATAATCAGAAAAGCAACATTAA	Core staple (rect)
AAAAGGGCTATTGACGGAAATTATGCCATCTT	Core staple (rect)
TACCGACCTCCAATCGCAAGACAAATCCTTGA	Core staple (rect)
CTCTGAATGAGGCTGAGACTCCTCAAGAGAAG	Core staple (rect)
CACCGGAACAAAATCACCGGAACCTTTTTAGGGAGGG	Core staple (rect)
ACCAGTCACGATTTTAAGAACTGGTTTTTCCGGAACG	Core staple (rect)
GTTTTAAGTCAGAAGCAAAGCGACCCTGAC	Core staple (rect)
TTGGGGTCAAAGAACGTGGACTCCCTTTTCAC	Core staple (rect)
GATTAGGATAAAGCCAGAATGGAAAGAGCCGC	Core staple (rect)
TTACCGAAAACAATGAAATAGCAATTTTTACCAACGC	Core staple (rect)
CCATAAATCCAAAATAGCGAGAGGACATTATT	Core staple (rect)

TGGAAGTTCATCCAATAAATCATACAATAAAG	Core staple (rect)
GATAAAAACAAAAATCAGGTCTTTGATTGCAT	Core staple (rect)
CCTGAGTAATGACCCTGTAATACTCGCGAGCT	Core staple (rect)
ACCCACAAACAAAGTTACCAGAAGAATCAATA	Core staple (rect)
AATAAACAAGTATAAAGCCAACGCGTTAAATA	Core staple (rect)
GAAGAGTCTAACAATTTCATTTGATACATCGG	Core staple (rect)
GAATACCAGAATAAGGCTTGCCCTGCTGACCT	Core staple (rect)
ATGGCTTTGAACCTATTATTCTGAAACATGAA	Core staple (rect)
TTACATTGGCCTGCAACAGTGCCAAGCATCAC	Core staple (rect)
TCATCAAGCTCATCTTTGACCCCCCCATTAAA	Core staple (rect)
CAGTGAGACCTGTCGTGCCAGCTGCCTGCAGG	Core staple (rect)
AGCATTAATCATTCCATATAACAGTTAGAGCT	Core staple (rect)
GAAAATAGCAGCCTTTATTAGACG	Core staple (rect)
CTGGGGTGGGTTTGCCCCAGCAGGGGCAAAAT	Core staple (rect)
AGTATTAATTACCGTTCCAGTAAGCCACCCTC	Core staple (rect)
GACGGCCATTCCCAGTCACGACGTTTTTTGTAATGGG	Core staple (rect)
AGGCGCAGGCTCCATGTTACTTAGTTTTTGGATCGTC	Core staple (rect)
AGCGGAGTCGTAACGATCTAAAGTTTTGTCGT	Core staple (rect)
TATTATAATAACCCTCGTTTACAGATTTAG	Core staple (rect)
GGTGAATTATATGGTTTACCAGCGGTAAGCAG	Core staple (rect)
ATAATCAGAACTCAAACTATCGGCACAGAGAT	Core staple (rect)
GCTATTAAATAACCTTGCTTCTGTTTTTTAAATAAAG	Core staple (rect)
TCGGGAAACGGGCAACAGCTGATTACAAGAGT	Core staple (rect)
CCAATAGCTAATATCCCATCCTAAACGACGAC	Core staple (rect)
AAGCCTGTAGACTACCTTTTTAACAAATCATA	Core staple (rect)
GTCTTTAAGACAATATTTTTGAATTTTTTTAGCAATA	Core staple (rect)
ACCTTATGGGACGTTGGGAAGAAAATAGTAAA	Core staple (rect)
ATGTTTAGTAAATATTCATTGAATTCAAAGCG	Core staple (rect)
AAAGAAGTAAACAGTTCAGAAAACAAGACTTC	Core staple (rect)
AAACATAGGAAACAGTACATAAATACGTCAGA	Core staple (rect)
TAATTGCTTTAAGAGGAAGCCCGAGAGAATGA	Core staple (rect)
CATAACCGACGGCTACAGAGGCTTCGGAGATT	Core staple (rect)
TCAATATAATAACGGATTCGCCTGCAAAATTA	Core staple (rect)

TAGGAGCATAATACATTTGAGGATTACCATAT	Core staple (rect)
AGGGCGAAGAACCATCACCCAAATCAAGTTTT	Core staple (rect)
TCGACTCTGCAAGGCGATTAAGTTCGCATCGT	Core staple (rect)
GCAACAGGCCGATTAAAGGGATTTTAGACAGG	Core staple (rect)
GGGTAGCAATATATTCGGTCGCTGACAGTTTC	Core staple (rect)
GTGGGAACCGTTGGTGTAGATGGGGGGTAACG	Core staple (rect)
TACCAAGCCCAGGCGCATAGGCTGGACGAGAA	Core staple (rect)
AGTACCGCATTCCAAGAACGGGTATTTTTGCATTTTC	Core staple (rect)
GCAAAGAATATGCAACTAAAGTCTCAACAT	Core staple (rect) / omitted in case of TBA incorporation
GTAATCGTAGCAAACAAGAGAATCTTTTTATAAAAAT	Core staple (rect)
TGTGAAATTTGGGAAGGGCGATCGCACTCCAG	Core staple (rect)
TGTACAGAGCGAAACAAAGTACAATGAGGACT	Core staple (rect)
ATAAGTTTGTATAAACAGTTAATGCCCCCTGC	Core staple (rect)
AAGAAAAAAAGCAAATCAGATATACGTTTTAG	Core staple (rect)
CAATATGATTAGCAAAATTAAGCAGGCAAG	Core staple (rect) / omitted in case of TBA incorporation
TAATTGCGCCCTGAGAGAGTTGCACGAGATAG	Core staple (rect)
CTGAATAACAGTAACAGTACCTTTATTACCTT	Core staple (rect)
AAAGACTTCAATGACAACAACCATAACTAAAG	Core staple (rect)
AGAACCCTTAAAAATACCGAACGAACAGTTGA	Core staple (rect)
CCAGGGTTGTGCCAAGCTTGCATGCATTAATG	Core staple (rect)
CGCGACCTACGGTCAATCATAAGGTGTGAATT	Core staple (rect)
CATATTCCAGTTACAAAATCGCGCAAAAGAAGATGATGAA	Core staple (rect)
TAGGTTGGCACCGGAATCATAATTTATACAAA	Core staple (rect)
TTTTGAGTAACAGTGCCCTAACGGGGTCAGTGCCTTTTTAGAGCCAC	Core staple (rect)
AGAAAACTTGACCTAAATTTAATGTTTAACAA	Core staple (rect)
AAGGTAAAGACATTCAACCGATTGTTTTTTAGCTATC	Core staple (rect)
GGTTGAGTAAGGGAGCCCCCGATTTAGAGCTT	Core staple (rect)
GTTACAAAAAGATTAGTTGCTATTCAAGCCGT	Core staple (rect)
GTATTGGGAACGCGCGGGGAGAGGTTTTTTGTAAAAC	Core staple (rect)
CTAAAACAAGTAATCTTGACAAGAAAGCTGCT	Core staple (rect)
AAAGTTTGACCTCAAATATCAAACGGTCAGTA	Core staple (rect)
ACAGGTAGACGAGTAGTAAATTGGATGAACGG	Core staple (rect)

GATGTGCTAGAGGATCCCCGGGTACTTTCCAG	Core staple (rect)
GAACCCTAGTTGTTCCAGTTTGGAGCCCTTCA	Core staple (rect)
TAATATCCGCCAGAATCCTGAGAAGTGTTTTT	Core staple (rect)
GAGAAACAATCCTGATTGTTTGGAAACTCGTA	Core staple (rect)
GTGGCACATGCGCGAACTGATAGCAATATCTT	Core staple (rect)
TTGGGAATAAGTTTATTTTGTCACGAAACCGA	Core staple (rect)
TAATATTTTGTTAAAATTTTAACCA	Core staple (rect)
TTCATAATCCGCCTCCCTCAGAGCTACTGGTA	Core staple (rect)
TGAATATATGGAAGGGTTAGAACCTTAGAAGT	Core staple (rect)
GCCTTCCTGGCCTCAGGAAGATCGGTGCGGGC	Core staple (rect)
GTGAATTTATACGTAATGCCACTAAGAATACA	Core staple (rect)
CTGACCAACGCCTGATAAATTGTGCGGAACGA	Core staple (rect)
TTCTTACCACATGTTCAGCTAATGTCCTGAAC	Core staple (rect)
GATTAGAGCGGAAGCAAACTCCAATTTTTTACTGCGG	Core staple (rect)
AACCGTGCGAGTAACAACCCGTCGTCATATGT	Core staple (rect)
TTAACACCGCAGATTCACCAGTCACAGCCATT	Core staple (rect)
AAATTGCGTTTGCACGTAAAACAGTTTTTTAGAGCCG	Core staple (rect)
AGAATAAAGTTATATAACTATATGGACGCTGA	Core staple (rect)
ACAGGAGGAAAAACGCTCATGGAATGGATTAT	Core staple (rect)
GGTCTGAGACAAACATCAAGAAAAATTGCTTT	Core staple (rect)
GAAAATTCATCACCGTCACCGACTCATTTTCG	Core staple (rect)
AGAAGCCTCCCTCATATATTTTAATTGCCTGA	Core staple (rect)
ATTAGACTGAGGAAGGTTATCTAACCTAAAAC	Core staple (rect)
TTTTAGAATTATTTCAACGCAAGGTTTTTAATAACCT	Core staple (rect)
GGAAACGCTTGAGCGCTAATATCATTTATCCC	Core staple (rect)
TCATCTTCTTTTCAAATATATTTTTTTTTAAATCGTC	Core staple (rect)
ATCTCCAATGAGTTTCGTCACCAGTACAAACT	Core staple (rect)
CGCCAACAAATAAGAGAATATAAAGCTGTCTT	Core staple (rect)
CCCTTATAAAGCCGGCGAACGTGGCGAGAAAG	Core staple (rect)
CGTAACACAAAAAAGGCTCCAAAACTTTCGAG	Core staple (rect)
TCCACGCTCCTAATGAGTGAGCTAGTTTCCTG	Core staple (rect)
CGCCAGCACAGAATCAAGTTTGCCACCAGTAG	Core staple (rect)
CTTTCCAGTGCTAAACAACTTTCAAGGCTTGC	Core staple (rect)

ACCCTCAGAAAGGCCGCTTTTGCGTTTTTTTTCTGTA	Core staple (rect)
AATCGGCCCGCCAGGGTGGTTTTTAACGTCAA	Core staple (rect)
CTTAAATCATAAACAGCCATATTAGAGAGATA	Core staple (rect)
GACGGGGAAATCAAAAGAATAGCCGCAAGCGG	Core staple (rect)
ATTAGATAATATTTTCATTTGGGGTTTGCGGG	Core staple (rect)
GTCATAGCGCCACCCTCAGAGCCACGTCATAC	Core staple (rect)
CACGGAATTAGAGCCAGCAAAATCTTTAGCGT	Core staple (rect)
TTTTAATGCGATAGCTTAGATTAATAAATGCT	Core staple (rect)
CATGTAGATCATCGTAGGAATCATTTTGAAGC	Core staple (rect)
TGGGATTTACGTTAGTAAATGAATTT	Core staple (rect)
AGGGAGTTCAGCGAAAGACAGCATTCGAAATC	Core staple (rect)
TCAATAGACTAACAACTAATAGATTTTTTGGCTATTA	Core staple (rect)
GTGAGAAACATAAAGCTAAATCGGATAGTAGT	Core staple (rect)
GTTTAGCTCATTTCGCAAATGGTCTTTTTCAGGTCAG	Core staple (rect)
GAGGGTAAAATAATAACGGAATACAAAGACAC	Core staple (rect)
ATGTGAGCATCTGCCAGTTTGAGGGAAAGGGG	Core staple (rect)
CAGGAAGACCGGAGAGGGTAGCTATCAAAAGG	Core staple (rect)
AAATATCGCATTTTTGCGGATGGCTTGATTCC	Core staple (rect)
ATCGCCATTCTGACCTGAAAGCGTCTTGCCTG	Core staple (rect)
CCAGCTTTGCCATCAAAAATAATTTTAAATTG	Core staple (rect)
CATTCAGTCATTCAACTAATGCAGGTAAGAGCAACACTATC	Core staple (rect)
AGAGCCGCAGCGCGTTTTCATCGGTGAGCCAT	Core staple (rect)
TAAGAGGTCGTTTTAATTCGAGCTCCCCCTCA	Core staple (rect)
AGCTACAAGTCTTTCCAGAGCCTAAATAATAA	Core staple (rect)
TAAACGTATATTCAACCGTTCTATCACCAT	Core staple (rect)
CGGGTAAACTTAAACAGCTTGATACGTTGAAA	Core staple (rect)
AATCCAAACCGACTTGCGGGAGGTTACCGCGC	Core staple (rect)
GAGCAAGAGCCCTTTTTAAGAAAACCAAAGAC	Core staple (rect)
AATCGTCAACTGGATAGCGTCCAATTTTTCTCATTAT	Core staple (rect)
TAACGAGCTTTTATCCTGAATCTTTTTTTTTAAACCA	Core staple (rect)
AGTAGCGATTGACAGGAGGTTGAGACAAATAA	Core staple (rect)
ACAGTATCGTAGCCAGCTTTCATCCCCAAAAA	Core staple (rect)
GGAGAATTGATTAAGACTCCTTATTACATAAA	Core staple (rect)

ATAGGAACCCGGCACCGCTTCTGGTCAGGCTG	Core staple (rect)
AACGGTACAGAACAATATTACCGCCACGACCA	Core staple (rect)
CGAACCTCTAAGAAACGATTTTTTCAAAGTCA	Core staple (rect)
CTATTTCGTGATGATACAGGAGTGCGCCACCC	Core staple (rect)
GTGAGTGATTAATTTTCCCTTAGAAGAACGCG	Core staple (rect)
CCGCCTGGTTGCGCTCACTGCCCGCCGAGCTC	Core staple (rect)
ACAACGCCAATAATAATTTTTTCACCGATAGT	Core staple (rect)
GATGCAAAGTGTGATAAATAAGGCTCAACAGT	Core staple (rect)
CTCTTCGCAATCATGGTCATAGCTACTCACAT	Core staple (rect)
ACACCAGAAAAGATTCATCAGTTGCAGACGAC	Core staple (rect)
CGCAACTGTGTTATCCGCTCACAATGTAAAGC	Core staple (rect)
ATAGGTCAAAACGGCGGATTGACCTTTTTGATGAACG	Core staple (rect)
TTTTATTTAACCAATCAATAATCGGTACCGAC	Core staple (rect)
TGGTTTAAACGAACTAACGGAACACTTTTGCA	Core staple (rect)
GAATACCATGATTATCAGATGATGTAATTTTA	Core staple (rect)
TTAATAAATTTCAACTTTAATCATGAACCGAA	Core staple (rect)
CAATTCTGGGCATCAATTCTACTATTGTACCA	Core staple (rect)
GAGCCAGTTGTAATTTAGGCAGAGTTTTTAGTTAATT	Core staple (rect)
AGGGCTTAAAGTAATTCTGTCCAGTTTACGAG	Core staple (rect)
CTTCTTTGCGCAAATTAACCGTTGTT	Core staple (rect)
CAAAATTATAGATTTTCAGGTTTACAATATAT	Core staple (rect)
AATGCTTTTTTGCCAGAGGGGGTAAATCTACG	Core staple (rect)
GTAATAAAAAAACAGAGGTGAGGCCCTCAATC	Core staple (rect)
AGTAGAAGTGAGGCCACCGAGTAAAAGAGTCT	Core staple (rect)
ATTACATTAATAGTGAATTTATCACTCCGGCT	Core staple (rect)
CAGAAGATAGGGACATTCTGGCCACTTGCTGG	Core staple (rect)
ACCCCGGTAAAGGCTATCAGGTCAATGCAATG	Core staple (rect)
TCAGAACCCCCCTTATTAGCGTTTTCATTAAA	Core staple (rect)
TCAAAAATTTCTAAGAACGCGAGGGAAGGCTT	Core staple (rect)
GCCTGTTTTTAGTATCATATGCGTACTAGAAA	Core staple (rect) / omitted in case of TBA incorporation
GAGTCTGGAAAACTAGCATGTCAAGATTCTCC	Core staple (rect)
ATCCGGTAATCAACAATAGATAAGCAGAACGC	Core staple (rect) / omitted in case of TBA incorporation

CTTGCTGAAGTAACATTATCATTTATTATCAT	Core staple (rect)
ACTGGCATAACTGAACACCCTGAAGTTTAACG	Core staple (rect)
GGTGGCAACCATTAGCAAGGCCGGCCGTAATC	Core staple (rect)
AACCAGACAGTACCTTTAATTGCTGTTTGACC	Core staple (rect)
GTCCATCAATTAGTAATAACATCAAAGAATAC	Core staple (rect)
ATAGTTAGGAGAATAGAAAGGAACCGCCCACG	Core staple (rect)
GAAAAGGTCGAACGAGTAGATTTACCTTTTGA	Core staple (rect)
CACCATTACATATAAAAGAAACGCCCAAAAGA	Core staple (rect)
CAAAAAGAGAATATAATGCTGTAGACGGTGTC	Core staple (rect)
TTAAATCCGTCAGTTGGCAAATCAACCACCAG	Core staple (rect)
AAAACATTATGTGTAGGTAAAGATTTTTTGAG	Core staple (rect)
CCTCAGAGGGCCGGAGACAGTCAAAGCTGATA	Core staple (rect)
TGCGCCGATTTCATGAGGAAGTTTAGCGATTA	Core staple (rect)
TTCGATGGCCCACTACGTAAACCGTCTATCAGGGTTTTTCGGTTTGC	Core staple (rect)
CAGACTGTCACCAGAACCACCACCAGCGCAGT	Core staple (rect)
AATATCTGTTTGCCCGAACGTTATGCAATTCA	Core staple (rect)
GGCGGATATTTCCCCCTTTTTGGGGGTTTCAAGCCCAATAGGAACCCATGTAC	Core staple (rect)
CCAATGAATTTCCCCCTTTTTGGGGGTTTAAACGAAAGAGGCAAACGAAGGCA	Core staple (rect)
ATTATTCATTTCCCCCTTTTTGGGGGTTTTTAAATCAGCTCATTTTCGCATTA	Core staple (rect)
CCAACCTATTTCCCCCTTTTTGGGGGTTTACCATCGATAGCAGCAAAACGTCA	Core staple (rect)
AATAACATTTTCCCCCTTTTTGGGGGTTTGGAATTACGAGGCATAATACATAA	Core staple (rect)
ATTTTGACTTTCCCCCTTTTTGGGGGTTTTGGTGGTTCCGAAATCCGAAAATC	Core staple (rect)
ATGTTAGCTTTCCCCCTTTTTGGGGGTTTCCAAATCAACGTAACAACCGGATA	Core staple (rect)
GAAGGGAATTTCCCCCTTTTTGGGGGTTTCGTTAGAATCAGAGCGGGAGCTAA	Core staple (rect)
AACATACGTTTCCCCCTTTTTGGGGGTTTCAAATGAAAAATCTAACGCTGAGA	Core staple (rect)
GACGATTGTTTCCCCCTTTTTGGGGGTTTTCGGTTTATCAGCTTGGGAGCCTT	Core staple (rect)
CGCCAAAATTTCCCCCTTTTTGGGGGTTTAAAAACAGGGAAGCGCACAGAGAG	Core staple (rect)
TAATTGTATTTCCCCCTTTTTGGGGGTTTGCCTTGATATTCACAAGCAGGTCA	Core staple (rect)
ACCAGGCATTTCCCCCTTTTTGGGGGTTTCACCAGAAGGAGCGGATGCGGAAC	Core staple (rect)
TTCATTACTTTCCCCCTTTTTGGGGGTTTAAACGTAGAAAATACATACGCAGT	Core staple (rect)
AAAGAAACTTTCCCCCTTTTTGGGGGTTTAAGCGCCATTCGCCATTGCCGGAA	Core staple (rect)
AATTTTTGTTTCCCCCTTTTTGGGGGTTTTTTCAATTACCTGAGCAGAGGCGA	Core staple (rect)
GCCAGCAGTTTCCCCCTTTTTGGGGGTTTAGCCGGAAGCATAAAGTTCCACAC	Core staple (rect)

CTGTTTGATTTCCCCCTTTTTGGGGGTTTGCTCAATCGTCTGAAAATACCTAC	Core staple (rect)
GGTTGGTGTGGTTGGTTGTTGTTGTTGTTGT	TBA1
CATCATCATCATCATCAGTCCGTGGTAGGGCAGGTTGGGGTGACT	TBA2
ATATGCAACTAAAGTCTCAACAT	Replacing Staple 1
ATCCGGTAATCAACAATAGATAAGCAGAACGCGCCTGTTT	Replacing Staple 2
CAATATGATTAGCAAAATTAAGCAGGCAAGGCAAAGATACAACAACAACAACAA	Protruding Staple 1
GATGATGATGATGATGTTAGTATCATATGCGTACTAGAAA	Protruding Staple 2
GGTTGGTGTGGTTGGTTGTTGTTGTTGTTGTAATATGCAACTAAAGTCTCAACAT	TBA1 rigid
ATCCGGTAATCAACAATAGATAAGCAGAACGCGCCTGTTTCATCATCATCATCATC AGTCCGTGGTAGGGCAGGTTGGGGTGACT	TBA2 rigid
GGTTGGTGTGGTTGGTTTATCAGTACTTGTCAACACGAGCAGCCCGTATATTCTCC TACAGCACTA	TBA1-TTT-Lever_2
AGTCCGTGGTAGGGCAGGTTGGGGTGACTTTTATCAGTACTTGTCAACACGAGCA GCCCGTATATTCTCCTACAGCACTA	TBA2-TTT-Lever_2
GTGTGGTGTGTGTGGTTTATCAGTACTTGTCAACACGAGCAGCCCGTATATTCTCC TACAGCACTA	ScrambledTBA1-TTT-Lever_2
GAGCGTGTTGAGCGGAGTCGTGAGCGTGTTTTATCAGTACTTGTCAACACGAGCA GCCCGTATATTCTCCTACAGCACTA	ScrambledTBA2-TTT-Lever_2

ATTTTGTCACAAAAGAAACAGCTGACCTTCATCAAG	Core staple (box)
ATGGTAGGTCTGAGAGTTTACCTTTAGAT	Core staple (box)
GGTTGGGTGAAATTGCTGAGCAAAATTGGGCTTGAGATGG	Core staple (box)
TTCTGTGCCAACGCTCAACATTTGGGCTTCGCC	Core staple (box)
CCGACAAAAAC	Core staple (box)
GACCAGGGAACCAGTAAGCAGATAGCCGAACAAAGTGATTT	Core staple (box)
GACGCTGAGAAGGAATA	Core staple (box)
AGGCTGATGATTTAGCACGGTGTACAGACTTTGCGCAT	Core staple (box)
TTGAAAACATAGCAATTACCGTAG	Core staple (box)
TTAGCAAACGTATACCAGAAACGAGGCGCAGACGGT	Core staple (box)
TGTAGAAACCAATCTGTGCGAATTTTAGATAAAC	Core staple (box)
TTAGGCGAATTATTCATTTCGATAGCTTTTAACCTCTAAAT	Core staple (box)
AGGCTTAATTTTTTACAAAGCTGCTCATTTTTTGAATA	Core staple (box)
AACACCGGAATCATCTTCTGACCCGGCTTA	Core staple (box)
CCTGTTTATCA	Core staple (box)
CGTCGCTATTAAAACAT	Core staple (box)
AGAGAAATCAATTCATCGTAGGAATCATTACC	Core staple (box)
AGAGAATAAACAACTGAAAAGGGATGGGAAGAAAAATCTA	Core staple (box)
GAGAATATAAA	Core staple (box)

GCCGGAGGAATTTGAGGCGACCTGCTCCATTTTACTTA	Core staple (box)
AGGGAAGCGCATGAATACCCGCAT	Core staple (box)
TTATGTGAATAAAAATAAGGCGTTAAATAAGA	Core staple (box)
GAGCGTCTTGGATTATTTTTTTTAAACCGGATATTCATTAC	Core staple (box)
ACATTTAACAATTTCATTTCCTTGCTTCGCAAGACAGAAA	Core staple (box)
AATCCAAAACATATAATTAAGAAAGAACTGACCAACTTTG	Core staple (box)
AGGCATTTTCGAGCTTACCAACTTTTATTTATAT	Core staple (box)
GTGAGTGAATAAGAATTACCACTT	Core staple (box)
CCCAATAGCAAGCATGCTATTTTTTATCCC	Core staple (box)
AATATGACAAGATGGAAACAGTACAATAAAGCCCATCCTAA	Core staple (box)
GAAATAGCTATCTTACCGACAGAGAGACCATATTATGCACC	Core staple (box)
TTTAATTTTATCCTGAATCTAAGTCCTTCATCGAGTAAAC	Core staple (box)
GCCCTGAGAGAGTTGCAGCAACGTA	Core staple (box)
GTACAAATATATTTTAGTTCATGTAATAGTATAAACCAGA	Core staple (box)
CGACAAAACAAGCAAGCAAATTTTTACCTTAGG	Core staple (box)
AAGAACGCGAGGCGCCTCCCGACTTTACAG	Core staple (box)
CTGAACACCCTGAACAA	Core staple (box)
GGTCACGTTGGTGTAGATGGCAACT	Core staple (box)
TAACCCCTTAGAGAAAAAGCCTGTTTAGTATC	Core staple (box)
TGCGTTATACCGTGCTACGCGAAAGAAAC	Core staple (box)
CGATTTAATCTTTCAGAATCATTGTGAATTTTCTTATG	Core staple (box)
TTTTTGAAGCCTTAAATCATCCTAATTCAAGAACGAGCTA	Core staple (box)
TCATTTGAAATACCGACCGAATGAGAATAATTAATTAAAG	Core staple (box)
GGTTGTTTAACGTCAATTTTGAAAAGAAT	Core staple (box)
TTTAACAACGCCAAAATTTCATAATTACTAATCC	Core staple (box)
CTACGCCAGTTACAAATTTAACAGTAACC	Core staple (box)
CATATCAAAATTGAAAACAAGCCCTGACGAGAAACA	Core staple (box)
TACAGTAACAGTAGTTACAATAAGAACTGGCTCATT	Core staple (box)
GATTTGTATCATCGCCTGATGAAAT	Core staple (box)
CAGAGGCGGCTGTCTTTCCTTTTCATTCTACGA	Core staple (box)
ATAGACAGTAA	Core staple (box)
TTTTAATGCTGATGCATTTCCAATCTGTA	Core staple (box)
AAACCAGAGGGTATAGAAGGCTTATCCGGTAT	Core staple (box)

TCACAGTAGTAAAGAAGATGATGAAACATTAATTTTTATAT	Core staple (box)
AAAATAATATCCCAAGATTAGTAATCAGATAATT	Core staple (box)
ATTCAACCGATTGAGGGAGGCAGAT	Core staple (box)
AAGAATTGAGTTATAAG	Core staple (box)
CCGAAACGCAATAATAACGTAGACGGGATAGCAGCCTTGCG	Core staple (box)
GATTCAGGACGTTTCGCCTGATTGCTTTAGTCAATACAAAA	Core staple (box)
ATGTTCGGTATTAAACCAAGTTTCGCACGAACA	Core staple (box)
GAGCGCTAATATAGCCCTTTAAGA	Core staple (box)
GAGAGGCGAGCTGATTGCCCTTCACCGC	Core staple (box)
TAGCCCGATGATGGTGGAGTCTGTAGGGTTAGAACC	Core staple (box)
TGTCCGTTGTAGCAATACTTGATTGTTTTCC	Core staple (box) / omitted in case of TBA incorporation
CTGAACGCTGGTAGGCGAAAATCCTGTTGATA	Core staple (box)
CGTGTGTCAAATTTAAAAGACTCCATTCCATATAACAGTTTTTA	Core staple (box)
CACCAGTATCACCGTCTAAACAGTCCACGGAATAAG	Core staple (box)
CAATCATACCCAGCGAATACATAATCTGAAACATGAAAGTTAG	Core staple (box)
AGTGAAAATACTTATACCAAGAGGCAAAAGAATACTTTC	Core staple (box)
TTTAATTTGCGCATCGTCAGGTTTATAACGGAACGTGCCGGTCT	Core staple (box)
TCCAGCCAGGGTGGTTGCCAGCATCTTTTCTTT	Core staple (box)
AACGATATTGACCATTAAAGGTGAATTAGCAC	Core staple (box)
CAGATACAGAAAGATGAAGTTTCTTATTACGCAGT	Core staple (box)
AGCTCAATAGAGGTTTACCCATATTCCTGATTATCTGAG	Core staple (box)
AGCTTTCAGGCGGATTGACCGTAATGGG	Core staple (box)
ATTTTAACCGTGTTTGAGGGGACGACGAGTGC	Core staple (box)
CCAACCTTTTAGAACAAACTCAACATTAAATGTGAACCA	Core staple (box)
CAAATTTGCACCGGGCAACGTTTGCGTATTGGGCGTCGG	Core staple (box)
CCAGAACGCAGTGAGAGTAAAACAGCGTGGTGCTGGTCTGCACC	Core staple (box)
AAAACGAAAGCGCGAAACAAAGTACAAC	Core staple (box)
ACGTTTCGGAACCTATTATAGGTGGCATAAG	Core staple (box)
AAAGAGGAGAAGGTAACAAAGACATAATGCCCCCTGCCTAGGG	Core staple (box)
GATTTAAAACGACAACATTATTACAGGTATAA	Core staple (box)
TTTTAGCGAGTAACAACGGAAACTAACCCGTCG	Core staple (box)
TTCGACTTGTAGAACGTCAGAAATAAATATA	Core staple (box)

ATTATCATAGCGCCAAAGACAAAAGGGC	Core staple (box)
TGTGATTCCCAATTCTGCGGAAACAATACAT	Core staple (box) / omitted in case of TBA incorporation
CCAAATCAAGCGGTCCATAATGGACCATCACGCAAATTAATTTT	Core staple (box)
ATACCAGTCTCCGTGGCATCGGGAAACGAGTAGATTTAGTTAAC	Core staple (box)
GAAGACTAAAACACTTTATTGGAAACATCTTT	Core staple (box)
AGTAATCTTAACATATAAATTTCCTCTTTGATTAGTAATAATCG	Core staple (box)
AAGTTAGATGATGGCACCAGCTTGCCATTCATC	Core staple (box)
GCTTCTGCAGTATCGACATCCTCAACGTCAGATGA	Core staple (box)
GACTTCAAATATTTTAGACAGCC	Core staple (box)
ACGTGGACTCCATTTTGCCTAATGAGT	Core staple (box)
TCCCAGTCACGATTTAATCGTAAAACT	Core staple (box)
ACGTACAGCGCCTTTCAACCGTTCTAG	Core staple (box)
ACCGACTTGAGCTTTAGAAGGAGCGGA	Core staple (box)
TGAGAACCCTCATATATTTTAACTTAAATTTCCGT	Core staple (box)
AGCAAGGTGGCATCAATTTTAAGTTAAACGACCTC	Core staple (box)
TACCTTTTTTTGCCCAATA	Core staple (box)
GCCTCAGGAAGATTTCTTCCTGTAGCC	Core staple (box)
CGGCCAGTTTTGCAAATGG	Core staple (box)
TTTGACCAAAAACATTTTTTGCCGCACAGGCGATG	Core staple (box)
GCCGTAAAGCACTTTGTAATCATGGTC	Core staple (box)
AAGGGTATTTTATAGTAGT	Core staple (box)
GAGAAAGGAAGGTTTCGGTCATACCGG	Core staple (box)
GGATATTAAGAGGCTGTTTTCTG	Core staple (box)
AGCATGTCATAAGCAAATATTTAAATTGTTTTTCGCTAT	Core staple (box)
GCGGGCCGTTTTTTTTGAGCGGGC	Core staple (box)
TCATCAGTTGAGTTTAGGCACCAACCT	Core staple (box)
AGCGTTTGCCATTTTAAGGTTATCTAA	Core staple (box)
GCATTGACAGGTTTTCTGATAGC	Core staple (box)
TTTTTGCTTTTGTATAGCC	Core staple (box)
GAATGACCATAATTTTTCAGCGGAGTG	Core staple (box)
CTGATAAAAACAAGAGAATCGATGAACGTTTGGCCAGTG	Core staple (box)
ACGGTGTTTTTCAAGAGAA	Core staple (box)

GAGGCCGTTTTGTCATTGC	Core staple (box)
GAAAGCGTTTTCTTCTGAC	Core staple (box)
GGGTTTCTCCCGGGTACCGAGCTCGAATTTTAAAGGGAG	Core staple (box)
ATACCATTGCAACAGGTTTTATACATGGCTTTAAC	Core staple (box)
TTGTTAAATCAAAAATAATTCGCGTCTGTTTGCTTTCCGGCACC	Core staple (box)
CGGACGTCGAGAGGGTTTTTGGA	Core staple (box)
AACTACATCACTTGCCTTTTGTA	Core staple (box)
GAGGTGAACAGCAGCGAAAGACAGCATCTTTCCAAAATAGCGA	Core staple (box)
CTCACAACGCCTGTAGTTTTTCG	Core staple (box)
AACGGCTAAAAATACGTAATGCCACTACTTTCATTCAACTAATG	Core staple (box)
AACTCGTATTTGCGGAACAAAGAAACCATTTAGCCAGCAAAAT	Core staple (box)
CAACTTTCAACATTTCTTTACCCTGAC	Core staple (box)
TAGCGTCCAATATTTCAGCTTGCTTTC	Core staple (box)
CCCTCAGAACCGTTTCGCTGAGAGCCA	Core staple (box)
GCAGCAAACAACAGTTGAAAGGAATTGATTTAATCACCG	Core staple (box)
CTGATGGCCAACAGAGTTTTCAGTCTCTGAACAGT	Core staple (box)
GGAACTCATTTTCAGGTTTTAAT	Core staple (box)
ATCAATATGATATTTCGGAATTT	Core staple (box)
TCAATTGACCATTAGATTTTAGC	Core staple (box)
ATAGCTGTGCATAAAGTGTAAAGCCTGGTTTAAAACCGT	Core staple (box)
CTGCAACAGTGCTTTACCACCCT	Core staple (box)
ACAGCGGATCATTTTGCAATGCC	Core staple (box)
GCAGGTCAGCAGCAACTTTTAAA	Core staple (box)
CCTCGTTTACCATTTAACGAGGGTAGC	Core staple (box)
ACGACCAGCGGTGCCGTTTTCCGCCGCGCTTGCTT	Core staple (box)
GTGTGCTCGTCATAAATTTTTAGAATCAGAGACAG	Core staple (box)
AGCAGCACCGTATTTAAACAATTCGAC	Core staple (box)
CCTAATTAGTCTTTAATTTTAGGTTGAGGCAAATG	Core staple (box)
GTTCCGAAATCGTTTCCAACGCGCGGG	Core staple (box)
AGGCAGGTGTCCAGCATTTTATTAAAGGGATGCCA	Core staple (box)
AGTGCCCTTTTAGAACTCA	Core staple (box)
CCGAGTATTTTTGCCAACG	Core staple (box)
AATATCTTATTTAGAAGTATTAGACTTTTTTAATCAAGT	Core staple (box)

GAGCTAACGCCAGCTGCATTAATGAATCTTTAAATCAAAAGAA	Core staple (box)
TCCTCGTTTTTACACTGGT	Core staple (box)
AGAATAGAGCCTTTAATTGTATCGGTTTTTTTAAATATTCATT	Core staple (box)
TGGGAAGGGCGATTTAACGTTAATATT	Core staple (box)
AAAAAAATTTTGTAATACT	Core staple (box)
AACCACCACACTTTTTGCATCAG	Core staple (box)
AAGCGTCTTTTTCATGGAA	Core staple (box)
CGGAAAAGCCAGGGTCAGACGATTGGCCTTTAGAGCCCACCCCA	Core staple (box)
CATTACCCACGTTTTTTGCCTCCCTCAGCAGAACCACGCCGCCA	Core staple (box)
AAAGCAAAAGAGTTGATAATTAAGCAATAACA	Core staple (box)
AATAAAAAGGAATAGTAAGAGCAACACTTGCA	Core staple (box)
TTATATCCAGAAATATCCTGAGAAG	Core staple (box) / omitted in case of TBA incorporation
GGGTTCAGTGAGTTTAGACAGGAACGGTTTAT	Core staple (box)
ATAATGAGTGTTGGAACAAGAGTCCACTTGGC	Core staple (box)
CAGAGCCGCCACAGCCGCCA	Core staple (box)
TTACTACGTGAAAATCAAGTTTTTTGGGAGCT	Core staple (box)
CAAACTCCAAAGCCTCTCAGGGGGCCAGAGAAAAGCCCCATGTT	Core staple (box)
ATCGTCAGTATTAACACCGC	Core staple (box)
CATACCGCCACGACCTCACCGGAAACAACTTTCTCCACGCAGAA	Core staple (box)
CTGTGAACGCCAATTCGCATTAAATTTTAAAA	Core staple (box)
CACGGGGATCAACAAATGAAAGCCGGCGGCAAGTGTCTGCGCGT	Core staple (box)
CAGTGAATACGTATATTTTTGAATGGCTAAAC	Core staple (box)
GCTCCCGTAACATCACCAGTACAAACTATAGT	Core staple (box)
TAGCATGGGATTTTGCTAAA	Core staple (box)
TGTACAAAAGGAAAGGAACAACTAAAGGTTTTCTGTGTAACGAT	Core staple (box)
CCACATTGCTAACGGGAGGCAGATTCACCGAG	Core staple (box)
GACTAATCAGTATTGCTAAGTTTTA	Core staple (box)
CAGTTGAGGATCGCCAGCACGCGTGCCTCTGTGGTGAGTGTCAC	Core staple (box)
CGCCTGCAACTAAGCTTAATTGCTGAATAGAA	Core staple (box)
ATTCAAAAAAAAGATTAACCAGACTTTGA	Core staple (box)
CCTACCCTCAATCAATATCTAATAGATCGAC	Core staple (box)
GAACCAGAGCCACCCTTATT	Core staple (box)

TTGCATCAGGGTGAGATAGCTATTCGGCGCAATTCAAAAG	Core staple (box)
CCAAGCTTTCAGCAGGGTTT	Core staple (box)
CATCAAGATTGTAATCATATGTACCCCGCTGA	Core staple (box)
CCCCCGATTTAGGTCGAGGT	Core staple (box)
ACTGCCTCGTTCTTTACCAGAACCGCCATCCT	Core staple (box)
CAAATCGTTAACGCCGGGTTACCTGCAGTCCA	Core staple (box)
GTAATGGCAAATTGAAAAATCTAAAGCATGAGGCGGCCATTAAA	Core staple (box)
GTGTAGACAGTCAAATCACC	Core staple (box)
GATTAAAACGGGTCAGAGGCTTTGAGGACGCGG	Core staple (box)
CATTGCGGGGTTCCAGGCGGATAAGTGCATAG	Core staple (box)
ATACTGACGCTCAATAAAAGGGACATTCAAGC	Core staple (box)
ATAGTTAGCTATGGGGCGCGAGCTGAAATTAA	Core staple (box)
GAATCCCCAGACTGGATGCTCCTTGTCA	Core staple (box)
TTAGAAGTTTTGTAATAGTAAAATGTTTCTCA	Core staple (box)
GTGAGAGATAGATCGGCGAA	Core staple (box)
AAATGTACATTTATTTTGCTCAACA	Core staple (box) / omitted in case of TBA incorporation
ATAGGAACCCGTGAGCCTCTTATCCGCCTGG	Core staple (box)
GACGTTAGTAAATGAAAATTGCGACACTTTCGCTGAGAAA	Core staple (box)
GCCTATTATCATTTAAATCCTTTGCCCGGATA	Core staple (box)
GATCATCACCGTCCTCAGAGCCACCACCCCCA	Core staple (box)
GAGGCTTTATCATAACTGGCTTAGAAGT	Core staple (box)
CTAAAGTTTTGTCGTCTTGATATTATAAT	Core staple (box)
TACGACTCAATCGGGTAAAGGTTTCTTTTCAG	Core staple (box)
CCACTAGCGCGTATTTTCGGTCATAGCCCCAC	Core staple (box)
CTATCAGGGCGAATTAAAGA	Core staple (box)
CAGTAATCGTCTGAAATGGAACGCCAGATAAAGTTTGTTCCTTTTAA	Core staple (box)
TAACTGCTGGTACAATATTACCGCCAGCCTAC	Core staple (box)
AGAACTGGAGCATTAATGCCGGAGAGGGAAGGCCGGAGGTAAAG	Core staple (box)
CGGAGCTGGCAGTGCTGATTGCCGTTCCGGTA	Core staple (box)
GAGTGCCTTTATGGATAAAAATTTTTAGTAAT	Core staple (box)
CCACACTCAGGAGGTTTAGTGTACTGGTTTTCCGGACAAGGTCATGAG	Core staple (box)
GGTCCTTCAAAGATCTATAAACAGTTCATCAGAAGCGCCCGAAA	Core staple (box)

TTGCCTTTAGCGCCATCGAT	Core staple (box)
CAGGCAATAAATAAGCTAAATCGGTTGTCGGG	Core staple (box)
GCTAGGGCGCTGAACGTGGC	Core staple (box)
AATGAGGATTAGTTCGAGCTTCAAAGCGAAGAGGAAAAAGCGGA	Core staple (box)
AGGGCCGTTAGTGGCCTGGTCACTGTTGTCGA	Core staple (box)
GAAGATAAAACAGAGGTCACCTTGTATAGACAGGCACGGT	Core staple (box)
TGTGTACACCCTGCGGTCAGGCGATGCAACAATTCCACACGCGC	Core staple (box)
TGCTTTGACAGTCACATAGACCCACCATCAGCCGTCAATAAACG	Core staple (box)
GCGCCTGCGGCCAGAATGCG	Core staple (box)
AATACCGAACGAACCAGCGCGTACCTGAA	Core staple (box)
TATTATAGGAAAACGACGTTTTAAAGAG	Core staple (box)
CATTGCCTTGAGTTGATGATACAGGAGTACCG	Core staple (box)
CAAATAAACCCTCAGAAGTTCGGCTTTCATGCGCCGATTTTAAA	Core staple (box)
ATTTATTTGAGGTAGGAGCACTAACAACTGGT	Core staple (box)
AATTGAAAATCTCCAAAAAATACCGATACCG	Core staple (box)
CGTCAACCAGGCTCGCCATTCAGGCTGCCGAA	Core staple (box)
TCAGTACCATTAGAACGTCACCAATGAAATCAG	Core staple (box)
TCGCAGCCGGAATTCCTGTGTGAAATTGCTCA	Core staple (box)
CATACATACAGGCAAGGCAAATAATGCTCAGAGGCATTACGCTCATT	Core staple (box)
GAAAGTGGTGCCACCAGCTTACGGCTGGGCTT	Core staple (box)
GTCGCCTGTCGTTCACATTAATTGCGTTAACA	Core staple (box)
TAATCGCCGGGCGCGGTTGCGGCAAACGTGCGCCATAAAGCCCGCTT	Core staple (box)
TACGCCAGCTGGGCAACTGT	Core staple (box)
GTGTGTCACCCTTTTCTTAAACAGCTTGAAAG	Core staple (box)
TGACTATAACGTAATGCGCCGCTACAGGCCATCACGAGCGGGCA	Core staple (box)
GAGGCTATCAGGTCATTGCGTTGATAAAGAG	Core staple (box)
GGAGAAAAAATCCTGCTCATTTGCCGCCAAAAAGAGGTGGTGAA	Core staple (box)
TGAGGGATGTGCTTAAGTTGGGTAACGCAGGT	Core staple (box)
TCACCGGACGCAATCCCTCCGTTTT	Core staple (box)
TGCGCGCCTCTCACGGAGCAGTTGCGTGG	Core staple (box)
GGGATAGCTGTGCACTGTTCTTCGGGCCAGATGGCATGGT	Core staple (box)
TTATATCCAGAAATATCCTGACAACAACAACAACAACAACAACAA	Box_Thr_Protr.1

GATGATGATGATGATGATGATGATGCAACATGTGATTCCCAATTCTGCGGAAACA ATACAT	Box_Thr_Protr.2
GGTTGGTGTGGTTGGTTGTTGTTGTTGTTGTTGTTGTAGAAGTGTCCGTTGTAG CAATACTTGATTGTTTTCC	Box_Thr_TBA1-rigid
AAATGTACATTTATTTTGCTCATCATCATCATCATCATCATCAGTCCGTGGTA GGGCAGGTTGGGGTGACT	Box_Thr_TBA2-rigid

A RECONFIGURABLE DNA DEVICE FOR CONTROLLING INTER-PARTICLE DISTANCE WITH NANOMETER-SCALE RESOLUTION

Pandora's Box

Sequence	Comment
ATTTTGTCACAAAAGAAACAGCTGACCTTCATCAAG	Bottom Core Plate
ATGGTAGGTCTGAGAGTTTACCTTTAGAT	Bottom Core Plate
GGTTGGGTGAAATTGCTGAGCAAAATTGGGCTTGAGATGG	Bottom Core Plate
TTCTGTGCCAACGCTCAACATTTGGGCTTCGCC	Bottom Core Plate
CCGACAAAAAC	Bottom Core Plate
GACCAGGGAACCAGTAAGCAGATAGCCGAACAAAGTGATTT	Bottom Core Plate
GACGCTGAGAAGGAATA	Bottom Core Plate
AGGCTGATGATTTAGCACGGTGTACAGACTTTGCGCAT	Bottom Core Plate
TTGAAAACATAGCAATTACCGTAG	Bottom Core Plate
TTAGCAAACGTATACCAGAAACGAGGCGCAGACGGT	Bottom Core Plate
TGTAGAAACCAATCTGTGCGAATTTTAGATAAAC	Bottom Core Plate
TTAGGCGAATTATTCATTTCGATAGCTTTTAACCTCTAAAT	Bottom Core Plate
AGGCTTAATTTTTTACAAAGCTGCTCATTTTTTGAATA	Bottom Core Plate
AACACCGGAATCATCTTCTGACCCGGCTTA	Bottom Core Plate
CCTGTTTATCA	Bottom Core Plate
CGTCGCTATTAAAACAT	Bottom Core Plate
AGAGAAATCAATTCATCGTAGGAATCATTACC	Bottom Core Plate
AGAGAATAAACAACTGAAAAGGGATGGGAAGAAAAATCTA	Bottom Core Plate
GAGAATATAAA	Bottom Core Plate
GCCGGAGGAATTTGAGGCGACCTGCTCCATTTTACTTA	Bottom Core Plate
AGGGAAGCGCATGAATACCCGCAT	Bottom Core Plate
TTATGTGAATAAAAATAAGGCGTTAAATAAGA	Bottom Core Plate
GAGCGTCTTGGATTATTTTTTTAAACCGGATATTCATTAC	Bottom Core Plate
ACATTTAACAATTTCATTTCCTTGCTTCGCAAGACAGAAA	Bottom Core Plate
AATCCAAAACATATAATTAAGAAAGAACTGACCAACTTTG	Bottom Core Plate

AGGCATTTTCGAGCTTACCAACTTTTATTTATAT	Bottom Core Plate
GTGAGTGAATAAGAATTACCACTT	Bottom Core Plate
CCCAATAGCAAGCATGCTATTTTTTATCCC	Bottom Core Plate
AATATGACAAGATGGAAACAGTACAATAAAGCCCATCCTAA	Bottom Core Plate
GAAATAGCTATCTTACCGACAGAGAGACCATATTATGCACC	Bottom Core Plate
TTTAATTTTATCCTGAATCTAAGTCCTTCATCGAGTAAAC	Bottom Core Plate
GCCCTGAGAGAGTTGCAGCAACGTA	Bottom Core Plate
GTACAAATATATTTTAGTTCATGTAATAGTATAAACCAGA	Bottom Core Plate
CGACAAAACAAGCAAGCAAATTTTTACCTTAGG	Bottom Core Plate
AAGAACGCGAGGCGCCTCCCGACTTTACAG	Bottom Core Plate
CTGAACACCCTGAACAA	Bottom Core Plate
GGTCACGTTGGTGTAGATGGCAACT	Bottom Core Plate
TAACCCCTTAGAGAAAAAGCCTGTTTAGTATC	Bottom Core Plate
TGCGTTATACCGTGCTACGCGAAAGAAAC	Bottom Core Plate
CGATTTAATCTTTCAGAATCATTGTGAATTTTCTTATG	Bottom Core Plate
TTTTTGAAGCCTTAAATCATCCTAATTCAAGAACGAGCTA	Bottom Core Plate
TCATTTGAAATACCGACCGAATGAGAATAATTAATTAAAG	Bottom Core Plate
GGTTGTTTAACGTCAATTTTGAAAAGAAT	Bottom Core Plate
TTTAACAACGCCAAAATTTCATAATTACTAATCC	Bottom Core Plate
CTACGCCAGTTACAAATTTAACAGTAACC	Bottom Core Plate
CATATCAAAATTGAAAACAAGCCCTGACGAGAAACA	Bottom Core Plate
TACAGTAACAGTAGTTACAATAAGAACTGGCTCATT	Bottom Core Plate
GATTTGTATCATCGCCTGATGAAAT	Bottom Core Plate
CAGAGGCGGCTGTCTTTCCTTTTCATTCTACGA	Bottom Core Plate
ATAGACAGTAA	Bottom Core Plate
TTTTAATGCTGATGCATTTCCAATCTGTA	Bottom Core Plate
AAACCAGAGGGTATAGAAGGCTTATCCGGTAT	Bottom Core Plate
TCACAGTAGTAAAGAAGATGATGAAACATTAATTTTTATAT	Bottom Core Plate
AAAATAATATCCCAAGATTAGTAATCAGATAATT	Bottom Core Plate
ATTCAACCGATTGAGGGAGGCAGAT	Bottom Core Plate
AAGAATTGAGTTATAAG	Bottom Core Plate
CCGAAACGCAATAATAACGTAGACGGGATAGCAGCCTTGCG	Bottom Core Plate
GATTCAGGACGTTTCGCCTGATTGCTTTAGTCAATACAAAA	Bottom Core Plate

ATGTTCGGTATTAAACCAAGTTTCGCACGAACA	Bottom Core Plate
GAGCGCTAATATAGCCCTTTAAGA	Bottom Core Plate
GAGAGGCGAGCTGATTGCCCTTCACCGC	Bottom Core Plate
TAGCCCGATGATGGTGGAGTCTGTAGGGTTAGAACC	Bottom Core Plate
TGTCCGTTGTAGCAATACTTGATTGTTTTCC	Bottom Core Plate
CTGAACGCTGGTAGGCGAAAATCCTGTTGATA	Bottom Core Plate
CGTGTGTCAAATTTAAAAGACTCCATTCCATATAACAGTTTTTA	Bottom Core Plate
CACCAGTATCACCGTCTAAACAGTCCACGGAATAAG	Bottom Core Plate
CAATCATACCCAGCGAATACATAATCTGAAACATGAAAGTTAG	Bottom Core Plate
AGTGAAAATACTTATACCAAGAGGCAAAAGAATACTTTC	Bottom Core Plate
TTTAATTTGCGCATCGTCAGGTTTATAACGGAACGTGCCGGTCT	Bottom Core Plate
TCCAGCCAGGGTGGTTGCCAGCATCTTTTCTTT	Bottom Core Plate
AACGATATTGACCATTAAAGGTGAATTAGCAC	Bottom Core Plate
CAGATACAGAAAGATGAAGTTTCTTATTACGCAGT	Bottom Core Plate
AGCTCAATAGAGGTTTACCCATATTCCTGATTATCTGAG	Bottom Core Plate
AGCTTTCAGGCGGATTGACCGTAATGGG	Bottom Core Plate
ATTTTAACCGTGTTTGAGGGGACGACGAGTGC	Bottom Core Plate
CCAACCTTTTAGAACAAACTCAACATTAAATGTGAACCA	Bottom Core Plate
CAAATTTGCACCGGGCAACGTTTGCGTATTGGGCGTCGG	Bottom Core Plate
CCAGAACGCAGTGAGAGTAAAACAGCGTGGTGCTGGTCTGCACC	Bottom Core Plate
AAAACGAAAGCGCGAAACAAAGTACAAC	Bottom Core Plate
ACGTTTCGGAACCTATTATAGGTGGCATAAG	Bottom Core Plate
AAAGAGGAGAAGGTAACAAAGACATAATGCCCCCTGCCTAGGG	Bottom Core Plate
GATTTAAAACGACAACATTATTACAGGTATAA	Bottom Core Plate
TTTTAGCGAGTAACAACGGAAACTAACCCGTCG	Bottom Core Plate
TTCGACTTGTAGAACGTCAGAAATAAATATA	Bottom Core Plate
ATTATCATAGCGCCAAAGACAAAAGGGC	Bottom Core Plate
TGTGATTCCCAATTCTGCGGAAACAATACAT	Bottom Core Plate
CCAAATCAAGCGGTCCATAATGGACCATCACGCAAATTAATTTT	Bottom Core Plate
ATACCAGTCTCCGTGGCATCGGGAAACGAGTAGATTTAGTTAAC	Bottom Core Plate
GAAGACTAAAACACTTTATTGGAAACATCTTT	Bottom Core Plate
AGTAATCTTAACATATAAATTTCCTCTTTGATTAGTAATAATCG	Bottom Core Plate
AAGTTAGATGATGGCACCAGCTTGCCATTCATC	Bottom Core Plate

GCTTCTGCAGTATCGACATCCTCAACGTCAGATGA	Bottom Core Plate
CGGAAAAGCCAGGGTCAGACGATTGGCCTTTAGAGCCCACCCCA	Side Wall Core
CATTACCCACGTTTTTTGCCTCCCTCAGCAGAACCACGCCGCCA	Side Wall Core
AAAGCAAAAGAGTTGATAATTAAGCAATAACA	Side Wall Core
AATAAAAAGGAATAGTAAGAGCAACACTTGCA	Side Wall Core
TTATATCCAGAAATATCCTGAGAAG	Side Wall Core
GGGTTCAGTGAGTTTAGACAGGAACGGTTTAT	Side Wall Core
ATAATGAGTGTTGGAACAAGAGTCCACTTGGC	Side Wall Core
CAGAGCCGCCACAGCCGCCA	Side Wall Core
TTACTACGTGAAAATCAAGTTTTTTGGGAGCT	Side Wall Core
CAAACTCCAAAGCCTCTCAGGGGGCCAGAGAAAAGCCCCATGTT	Side Wall Core
ATCGTCAGTATTAACACCGC	Side Wall Core
CATACCGCCACGACCTCACCGGAAACAACTTTCTCCACGCAGAA	Side Wall Core
CTGTGAACGCCAATTCGCATTAAATTTTAAAA	Side Wall Core
CACGGGGATCAACAAATGAAAGCCGGCGGCAAGTGTCTGCGCGT	Side Wall Core
CAGTGAATACGTATATTTTTGAATGGCTAAAC	Side Wall Core
GCTCCCGTAACATCACCAGTACAAACTATAGT	Side Wall Core
TAGCATGGGATTTTGCTAAA	Side Wall Core
TGTACAAAAGGAAAGGAACAACTAAAGGTTTTCTGTGTAACGAT	Side Wall Core
CCACATTGCTAACGGGAGGCAGATTCACCGAG	Side Wall Core
GACTAATCAGTATTGCTAAGTTTTA	Side Wall Core
CAGTTGAGGATCGCCAGCACGCGTGCCTCTGTGGTGAGTGTCAC	Side Wall Core
CGCCTGCAACTAAGCTTAATTGCTGAATAGAA	Side Wall Core
ATTCAAAAAAAAAGATTAACCAGACTTTGA	Side Wall Core
CCTACCCTCAATCAATATCTAATAGATCGAC	Side Wall Core
GAACCAGAGCCACCCTTATT	Side Wall Core
TTGCATCAGGGTGAGATAGCTATTCGGCGCAATTCAAAAG	Side Wall Core
CCAAGCTTTCAGCAGGGTTT	Side Wall Core
CATCAAGATTGTAATCATATGTACCCCGCTGA	Side Wall Core
CCCCCGATTTAGGTCGAGGT	Side Wall Core
ACTGCCTCGTTCTTTACCAGAACCGCCATCCT	Side Wall Core
CAAATCGTTAACGCCGGGTTACCTGCAGTCCA	Side Wall Core

GTAATGGCAAATTGAAAAATCTAAAGCATGAGGCGGCCATTAAA	Side Wall Core
GTGTAGACAGTCAAATCACC	Side Wall Core
GATTAAAACGGGTCAGAGGCTTTGAGGACGCGG	Side Wall Core
CATTGCGGGGTTCCAGGCGGATAAGTGCATAG	Side Wall Core
ATACTGACGCTCAATAAAAGGGACATTCAAGC	Side Wall Core
ATAGTTAGCTATGGGGCGCGAGCTGAAATTAA	Side Wall Core
GAATCCCCAGACTGGATGCTCCTTGTCA	Side Wall Core
TTAGAAGTTTTGTAATAGTAAAATGTTTCTCA	Side Wall Core
GTGAGAGATAGATCGGCGAA	Side Wall Core
AAATGTACATTTATTTTGCTCAACA	Side Wall Core
ATAGGAACCCGTGAGCCTCTTATCCGCCTGG	Side Wall Core
GACGTTAGTAAATGAAAATTGCGACACTTTCGCTGAGAAA	Side Wall Core
GCCTATTATCATTTAAATCCTTTGCCCGGATA	Side Wall Core
GATCATCACCGTCCTCAGAGCCACCACCCCCA	Side Wall Core
GAGGCTTTATCATAACTGGCTTAGAAGT	Side Wall Core
CTAAAGTTTTGTCGTCTTGATATTATAAT	Side Wall Core
TACGACTCAATCGGGTAAAGGTTTCTTTTCAG	Side Wall Core
CCACTAGCGCGTATTTTCGGTCATAGCCCCAC	Side Wall Core
CTATCAGGGCGAATTAAAGA	Side Wall Core
CAGTAATCGTCTGAAATGGAACGCCAGATAAAGTTTGTTCCTTTTAA	Side Wall Core
TAACTGCTGGTACAATATTACCGCCAGCCTAC	Side Wall Core
AGAACTGGAGCATTAATGCCGGAGAGGGAAGGCCGGAGGTAAAG	Side Wall Core
CGGAGCTGGCAGTGCTGATTGCCGTTCCGGTA	Side Wall Core
GAGTGCCTTTATGGATAAAAATTTTTAGTAAT	Side Wall Core
CCACACTCAGGAGGTTTAGTGTACTGGTTTTCCGGACAAGGTCATGAG	Side Wall Core
GGTCCTTCAAAGATCTATAAACAGTTCATCAGAAGCGCCCGAAA	Side Wall Core
TTGCCTTTAGCGCCATCGAT	Side Wall Core
CAGGCAATAAATAAGCTAAATCGGTTGTCGGG	Side Wall Core
GCTAGGGCGCTGAACGTGGC	Side Wall Core
AATGAGGATTAGTTCGAGCTTCAAAGCGAAGAGGAAAAAGCGGA	Side Wall Core
AGGGCCGTTAGTGGCCTGGTCACTGTTGTCGA	Side Wall Core
GAAGATAAAACAGAGGTCACCTTGTATAGACAGGCACGGT	Side Wall Core
TGTGTACACCCTGCGGTCAGGCGATGCAACAATTCCACACGCGC	Side Wall Core

TGCTTTGACAGTCACATAGACCCACCATCAGCCGTCAATAAACG	Side Wall Core
GCGCCTGCGGCCAGAATGCG	Side Wall Core
AATACCGAACGAACCAGCGCGTACCTGAA	Side Wall Core
TATTATAGGAAAACGACGTTTTAAAGAG	Side Wall Core
CATTGCCTTGAGTTGATGATACAGGAGTACCG	Side Wall Core
CAAATAAACCCTCAGAAGTTCGGCTTTCATGCGCCGATTTTAAA	Side Wall Core
ATTTATTTGAGGTAGGAGCACTAACAACTGGT	Side Wall Core
AATTGAAAATCTCCAAAAAATACCGATACCG	Side Wall Core
CGTCAACCAGGCTCGCCATTCAGGCTGCCGAA	Side Wall Core
TCAGTACCATTAGAACGTCACCAATGAAATCAG	Side Wall Core
TCGCAGCCGGAATTCCTGTGTGAAATTGCTCA	Side Wall Core
CATACATACAGGCAAGGCAAATAATGCTCAGAGGCATTACGCTCATT	Side Wall Core
GAAAGTGGTGCCACCAGCTTACGGCTGGGCTT	Side Wall Core
GTCGCCTGTCGTTCACATTAATTGCGTTAACA	Side Wall Core
TAATCGCCGGGCGCGGTTGCGGCAAACGTGCGCCATAAAGCCCGCTT	Side Wall Core
TACGCCAGCTGGGCAACTGT	Side Wall Core
GTGTGTCACCCTTTTCTTAAACAGCTTGAAAG	Side Wall Core
TGACTATAACGTAATGCGCCGCTACAGGCCATCACGAGCGGGCA	Side Wall Core
GAGGCTATCAGGTCATTGCGTTGATAAAGAG	Side Wall Core
GGAGAAAAAATCCTGCTCATTTGCCGCCAAAAAGAGGTGGTGAA	Side Wall Core
TGAGGGATGTGCTTAAGTTGGGTAACGCAGGT	Side Wall Core
TCACCGGACGCAATCCCTCCGTTTT	Side Wall Core
TGCGCGCCTCTCACGGAGCAGTTGCGTGG	Side Wall Core
GGGATAGCTGTGCACTGTTCTTCGGGCCAGATGGCATGGT	Side Wall Core
GACTTCAAATA**TTTT**AGACAGCC	Side Wall Connections
ACGTGGACTCCA**TTT**TGCCTAATGAGT	Side Wall Connections
TCCCAGTCACGA**TTT**AATCGTAAAACT	Side Wall Connections
ACGTACAGCGCC**TTT**CAACCGTTCTAG	Side Wall Connections
ACCGACTTGAGC**TTT**AGAAGGAGCGGA	Side Wall Connections
TGAGAACCCTCATATA**TTTT**AACTTAAATTTCCGT	Side Wall Connections
AGCAAGGTGGCATCAA**TTTT**AAGTTAAACGACCTC	Side Wall Connections
TACCTTT**TTTT**GCCCAATA	Side Wall Connections

GCCTCAGGAAGA**TTT**CTTCCTGTAGCC	Side Wall Connections
CGGCCAG**TTTT**GCAAATGG	Side Wall Connections
TTTGACCAAAAACATT**TTTT**GCCGCACAGGCGATG	Side Wall Connections
GCCGTAAAGCAC**TTT**GTAATCATGGTC	Side Wall Connections
AAGGGTA**TTTT**ATAGTAGT	Side Wall Connections
GAGAAAGGAAGG**TTT**CGGTCATACCGG	Side Wall Connections
GGATATTAAGAGGCTG**TTTT**CTG	Side Wall Connections
AGCATGTCATAAGCAAATATTTAAATTG**TTT**TTCGCTAT	Side Wall Connections
GCGGGCCGTTTT**TTT**GAGCGGGC	Side Wall Connections
TCATCAGTTGAG**TTT**AGGCACCAACCT	Side Wall Connections
AGCGTTTGCCAT**TTT**AAGGTTATCTAA	Side Wall Connections
GCATTGACAGG**TTTT**CTGATAGC	Side Wall Connections
TTTTTGC**TTTT**GTATAGCC	Side Wall Connections
GAATGACCATAA**TTT**TTCAGCGGAGTG	Side Wall Connections
CTGATAAAAACAAGAGAATCGATGAACG**TTT**GGCCAGTG	Side Wall Connections
ACGGTGT**TTTT**CAAGAGAA	Side Wall Connections
GAGGCCG**TTTT**GTCATTGC	Side Wall Connections
GAAAGCG**TTTT**CTTCTGAC	Side Wall Connections
GGGTTTCTCCCGGGTACCGAGCTCGAAT**TTT**AAAGGGAG	Side Wall Connections
ATACCATTGCAACAGG**TTTT**ATACATGGCTTTAAC	Side Wall Connections
TTGTTAAATCAAAAATAATTCGCGTCTG**TTT**GCTTTCCGGCACC	Side Wall Connections
CGGACGTCGAGAGGGT**TTTT**GGA	Side Wall Connections
AACTACATCACTTGCC**TTTT**GTA	Side Wall Connections
GAGGTGAACAGCAGCGAAAGACAGCATC**TTT**CCAAAATAGCGA	Side Wall Connections
CTCACAACGCCTGTAG**TTTT**TCG	Side Wall Connections
AACGGCTAAAAATACGTAATGCCACTAC**TTT**CATTCAACTAATG	Side Wall Connections
AACTCGTATTTGCGGAACAAAGAAACCA**TTT**AGCCAGCAAAAT	Side Wall Connections
CAACTTTCAACA**TTT**CTTTACCCTGAC	Side Wall Connections
TAGCGTCCAATA**TTT**CAGCTTGCTTTC	Side Wall Connections
CCCTCAGAACCG**TTT**CGCTGAGAGCCA	Side Wall Connections
GCAGCAAACAACAGTTGAAAGGAATTGA**TTT**AATCACCG	Side Wall Connections
CTGATGGCCAACAGAG**TTTT**CAGTCTCTGAACAGT	Side Wall Connections
GGAACTCATTTTCAGG**TTTT**AAT	Side Wall Connections

ATCAATATGATA**TTT**CGGAATTT	Side Wall Connections
TCAATTGACCATTAGA**TTTT**AGC	Side Wall Connections
ATAGCTGTGCATAAAGTGTAAAGCCTGG**TTT**AAAACCGT	Side Wall Connections
CTGCAACAGTGC**TTT**ACCACCCT	Side Wall Connections
ACAGCGGATCA**TTTT**GCAATGCC	Side Wall Connections
GCAGGTCAGCAGCAAC**TTTT**AAA	Side Wall Connections
CCTCGTTTACCA**TTT**AACGAGGGTAGC	Side Wall Connections
ACGACCAGCGGTGCCG**TTTT**CCGCCGCGCTTGCTT	Side Wall Connections
GTGTGCTCGTCATAAA**TTTT**TAGAATCAGAGACAG	Side Wall Connections
AGCAGCACCGTA**TTT**AAACAATTCGAC	Side Wall Connections
CCTAATTAGTCTTTAA**TTTT**AGGTTGAGGCAAATG	Side Wall Connections
GTTCCGAAATCG**TTT**CCAACGCGCGGG	Side Wall Connections
AGGCAGGTGTCCAGCA**TTTT**ATTAAAGGGATGCCA	Side Wall Connections
AGTGCCC**TTTT**AGAACTCA	Side Wall Connections
CCGAGTA**TTTT**TGCCAACG	Side Wall Connections
AATATCTTATTTAGAAGTATTAGACTTT**TTT**AATCAAGT	Side Wall Connections
GAGCTAACGCCAGCTGCATTAATGAATC**TTT**AAATCAAAAGAA	Side Wall Connections
TCCTCGT**TTTT**ACACTGGT	Side Wall Connections
AGAATAGAGCCTTTAATTGTATCGGTTT**TTT**TAAATATTCATT	Side Wall Connections
TGGGAAGGGCGA**TTT**AACGTTAATATT	Side Wall Connections
AAAAAAA**TTTT**GTAATACT	Side Wall Connections
AACCACCACAC**TTTT**TGCATCAG	Side Wall Connections
AAGCGTC**TTTT**TCATGGAA	Side Wall Connections
GCAAAATTTTTTTTTTTCCCTTAT	Edge Passivation
CCACCCTTTTTTTTTTTCAGAGCC	Edge Passivation
ACGTCAATTTTTTTTTTAGGGCGA	Edge Passivation
ATGTTTATTTTTTTTTTCCAGTCC	Edge Passivation
CTGCGGATTTTTTTTTTATCGTCA	Edge Passivation
ATTTAGGTTTTTTTTTTAATACCA	Edge Passivation
TCGGTGCTTTTTTTTTTGGGCCTC	Edge Passivation
CGTTGTATTTTTTTTTTAAACGAC	Edge Passivation
GAAGAAATTTTTTTTTTGCGAAAG	Edge Passivation

ATCAGTATTTTTTTTTTGCGACAG	Edge Passivation
GACGACGTTTTTTTTTTATAAAAA	Edge Passivation
TAAATCGTTTTTTTTTTGAACCCT	Edge Passivation
CATTTGGTTTTTTTTTTGAATTAG	Edge Passivation
TCGCACTTTTTTTTTTTCCAGCCA	Edge Passivation
ATCAAAATTTTTTTTTTATCAGGT	Edge Passivation
CTTTTCATTTTTTTTTTTAATCAA	Edge Passivation
ATTCAAAAAAAAAGATTAACCAGACTTTGA-TAMRA	Fluoro Staple
Thiol-GTGGAAAGTGGCAATC	Thiolated Staple

Zelos

Sequence	Comment
CGCATGATATAAGTAAATATCCATAGCAAACCC	Core staple
ATTTTATTACCTTACATTGGCAGATTAGAA	Core staple
CACCAAAGTTAAAAACTTAAATTTCTGTAC	Core staple
ACCACTAAATCGGAACCCAAGGAGCGGGTT	Core staple
TTTTTTAATATATTCCTTATCCAGAGATTTTT	Core staple
CAAAGGACAGATACTTAGCCGGAACGAGCGGA	Core staple
CGATTCTTCGCTTCGCACTCCAGCCAGGAC	Core staple
TCAACCACCAGATTCACAAACAATTTTT	Core staple
AGCCACAAAAGGGCGACATTCCAAAAGGCATAACCC	Core staple
TTCTTCCAGACGGGCAGAGGCATTTTCGCTAG	Core staple
TGCAGGTCAGGATTAGAGAGCTCATTTGGATA	Core staple
AAGGCGAGAAAGAACGTGCTTTCCTCGTGCGG	Core staple
TTTTTCAGGGAAGCTCTTTTTTTTTTTGGGATTGGCTTAGAGCCTTT	Core staple
TGATGCCGAACAAAGTTACAAACAGAATTG	Core staple
TCGTTTACCAGACGACAAAGAAGTTGAG	Core staple
GATATTGCGGGACCTTAAATCAAGATTAACTG	Core staple
GCTGATAGCTTCTTTTTTTTTTTTTCGAAAAAAATCCCGAAAT	Core staple
TTTTTAAAGCGAACCAGACCGACATCGACACCT	Core staple
ACTAGCCAAGCTAACGTACAGCGCCATGATGT	Core staple
TTATGTCCCGGAGACGTTGTAAAACGATTT	Core staple

TTTTTCCGATGTGCTGTTTTTTTTTTAGGGGACGACGACAGTTATT	Core staple
AGTAACAGAGGCCGCTTTTGCGGGATCGCCAT	Core staple
AATAGAAAACAAAATTAATTATCGGGAGCCAG	Core staple
TCAATATGTGAGTGAATAAAAGACGCAAAA	Core staple
TTTTTGATTCCCAATTCTGCGCCACGGGACCAT	Core staple
TTTCCAAGAGTAATCTTGACTTGAAAGACTCC	Core staple
TCATCGGGTAAAATACGTAACAACGGCTGATT	Core staple
GCAATTCATCAATATATTTGGATT	Core staple
TCAATCAATATCTGGTTAGGAGCATTTT	Core staple
TATACTTTTGATAAGAGGTCGCAGAAACCTGC	Core staple
GTGTTGAGAATCGAACGCGCCTGTTTATTAAG	Core staple
AGCCCAACCTAAAACGAAAGAGCCGCAATG	Core staple
ATTAATCAGATAGCTAACGAGCGTCTTTAAAT	Core staple
TTTTGCCAAGCATTTTTTTTTTAAATTATTCGCCATTCAGGC	Core staple
TTTTTAACATTGTGCCCTGTCATCATTTTTTT	Core staple
TTTTTGAGCAAATTACTTTGAGAAACATTTTT	Core staple
CGTTACCGATATATTCGGTCGCAGGGAGAATTAGCATTTTT	Core staple
GGCAGCGAAACAAAGTACAAGCGCAGACAATA	Core staple
AGTATTCCACACACTCAATCCGCCGGGCTATG	Core staple
CATAATAGGGTTTTCACCGCCTGGCCCTATTG	Core staple
GGCGAAACAATAAATTGCGTAGATTTTCGAAA	Core staple
AAAAGCACGTATGAAGGGAAGAAAGCGATAAA	Core staple
ATCACGTCACCAGTACAAACTACAACGCCTT	Core staple
ACGTTAACCGTTGTAGCACAGAACAAACGA	Core staple
AGAGCTGACCTGAAAGCGTACACCAGTCCGCA	Core staple
GTGCATTTACCGTTCCAGTATCTGTATGTAAT	Core staple
GGGGTGCGCTCACTGCCCGCAGCGGAATAACC	Core staple
TTTTTGCGAGAGGCTTTTGCAGATAAAAATTCA	Core staple
TTCCAAGAACGGGTATTAAACTCCCGACGAAC	Core staple
TAAACGCCTGATAAATTGTGCGACCTGCTCATTCCATTTTT	Core staple
AACTTCATAGCGTGAAATTGTTATCCTCAC	Core staple
AACAACTAAAGTACGGTGTCCGGAAACATGTA	Core staple
ACCGCCGCCAGCGGCGGCCTTTAGTGATCAAA	Core staple

TGTTATACCGACCGTGTGATTTAGGTTGGCCC	Core staple
AGAATTTAGAGCTTGACGGGGAACGTGGCGTT	Core staple
GCGGATAATCAGGAGGAGCTCATT	Core staple
GCATTCGAGAACAAGCAAGTATTCTATGGC	Core staple
GCTAGAATAGAAGTTAGTAAATGAATTTAGCG	Core staple
CCGGTTGATAATCAGAATTGACCG	Core staple
TTTTTAGACAGTCAAATCACCGGGT	Core staple
TTTTTAGACTTGAACTTGCGCTACAAATTTTT	Core staple
CAAAGTACGCCAGAATCCTGTGCGCCGCTTCT	Core staple
GCAGGCCCACGTTAGGTGGAGAGGGTATCA	Core staple
GGTGTAATGAGTGAGCTAACGCTCACAAAGCA	Core staple
TTTTTGTCTCGTCGCTGGCAGAAAAATCATTAGCAAGAGAATCAAGTTTTTTT	Core staple
AGTTTCCATGTTGAACGGTGTACAGACCGCTG	Core staple
TTTTTTTGCGGAACAAAGAAACCACCAGAAGGTTTC	Core staple
TTTTTCTTTGCCACCAGTAACCCGAACTTTTT	Core staple
AACATGCAGCAATAAATCAAAAGAATAAAG	Core staple
TTTTTAAAAGTCTGTTAAATCTTGAGTTTTTT	Core staple
TTTTTATCGTGGTGAATTTTTTTTTTAAGTTGGGTAACGCCATATT	Core staple
GGCTTTTAACGGGGTCAGTGCCTGTAGCAACGGTAA	Core staple
AAAGAGCGGATCACGATGCTGATTGCCGCTAT	Core staple
TATAGTAGCGACGCCGGAAACGTCACCACCAG	Core staple
GTACACACGACCCCTTGCTGGTAATATCATAC	Core staple
AGGATATCCTGTTGTTTCATCATATTCCATGTACCGCCGGGATG	Core staple
TGAGGGATTTTGCTTTCAACAGTTTCAGAAGG	Core staple
GAGGATAACGGAATACCCAAGAGGATCCAGCTCGAA	Core staple
TTTAGGTCAATCATAAGCCCCCTTATTGCGA	Core staple
GGCTACTATCGGAGTAATAAAAGGGACACAGA	Core staple
GCGCCTTTAATTGTATCGACAGGAGGTAAT	Core staple
ACGACTAACAACTAGAGCCGTCAATAGACGCC	Core staple
ACAGAACGAACCACCAGCATGAAAAAGAAG	Core staple
GTTTACGCAGTTTTTTTTTTTTTATAAGATAACCTCACTGGA	Core staple
ATATCCCGGAATAGGTGTATCACCGTACGTGC	Core staple
AAATACCGGAATCATAATTAAGCCAGTATAAA	Core staple

CAGGTCTAGATTAATAAAGCATCACCTCAA	Core staple
AACGCAAAGCGGATTGCATGAAGGGTAGAA	Core staple
TCATAACTTTAATCATTGTGTGCGATTTCGTTTTAATTTTT	Core staple
GGGGCCAGTGAATCGAGCCAGAATTTTT	Core staple
GATTATCGGCGATTCAGAGGTGGAGCCGAACG	Core staple
GTGCCGGTTAAGAGCAGCGTGGGCCA	Core staple
CAGGTAATAACATCACTTGCGAACTCAAGTCT	Core staple
CTTTATAGGGAACCGAACTGACCAACTAAGA	Core staple
GGTTAGGTAAAGATTCAAAAATCAATATACAT	Core staple
CAACATACCAAGAAATTATTTGCACGTACAGA	Core staple
GATATTTGCACCAGGCGTTTTAGCGAACCCAA	Core staple
GCGTGCCTGCAGTATGGCTTTCGCAACATACGAGCCGGAATAAA	Core staple
TTCGTAATCATGCGGGCGGTTGGGGCA	Core staple
GAGCATAAGAGACCGACAAAAGGTAAAGAATC	Core staple
TTCACAACATTAGGCTCATTATACCAGTGAGA	Core staple
TTCAGCCACCACCACCCTCAGAGTTTTT	Core staple
TTTTTTGCAACGCGGTTTTTTTTTTTTCACGGAAAAAGAGACATTT	Core staple
CAAACAGAGCACTGGTCAGCAGCAACCGTTACCTGC	Core staple
GTGCAATCCAATAGCGATAGCTTAGATTCCTT	Core staple
TGGTGCCGCACAAGTTGGGCGGTTGTGTGAAG	Core staple
CATTAGCAGCGAATCGGAACGAGGGTAGTGCC	Core staple
GGCGTGAGAAGAAACTATATGTAAATGATT	Core staple
AGCCCGTCCGTGAGCCTCCTCACAGTTAAG	Core staple
GTCAATTCTACTAATAGTAGCGGGCCAGTT	Core staple
TTTTTTCGTATGAGGCTCAGTTAAATCTTTTT	Core staple
CATAGAAAATCTCCAAAAAACGGAGTGAAATC	Core staple
ATAACACCGAGTAAAAGAGTGGAAAAACGAAC	Core staple
CCGACGTGGACTCCAACGTCAGCCCGAGAATC	Core staple
TCCATTGACCATTAGATACACGGCCAGTCGAA	Core staple
CGTCAACGCCATTGAGAGCCAGCAGCAAAGAA	Core staple
TTCACTTTTTTAATGGAAACTCAAAATCTTAA	Core staple
CGTAGAGGCGGTTTGCGTGAGAGAGTAACA	Core staple
TTACTTAACGTCAAAAATGATACAAAATAAATCAACAGTTGAAAGGATTTTT	Core staple

GCAACCAGTCACATTTGTGAGAGATAGATTAA	Core staple
AGACGTAATTTAACGACAATAAACAACCTA	Core staple
AATTAGTATAAAGCCAACGCGGCTTAATTTTT	Core staple
CAGTCCATATCATTACAAAATCGCGCAGTTCA	Core staple
CCGAACTGTAATAGGGGTGTAGAACGTCAACA	Core staple
TAGTATAAATCATACAGGCAAGGCTGCGCACG	Core staple
GCTCATGCTGTAGCTCAACTTTACCAACCA	Core staple
CGATTTTGCCAGAGTAAAATGTTTAGACAATA	Core staple
CTATAATTACGAGGCATAGGCCCCCTGTTAC	Core staple
AAATGAGCAAAAGAAGATGATGCTTTGAGCGC	Core staple
TACGAGAACGCGCAGCTACAATTTTATAAA	Core staple
AAAGTTAAAGGCTTTGAGGACTAAAGACGGAA	Core staple
CCGAAGCCCTTTTTAAAGGTTTAAGGGG	Core staple
TAATGGCGCTAGCGTACTATGGTTGCTTTT	Core staple
GGGAGGTTATATGTCAATAGTGAATTTAAGTA	Core staple
TGACCGTATAAACAGTTACTGAGTTTTATGTACC	Core staple
ACTAATGCAGATACATAACGCAAC	Core staple
AAGATTTGGGAATTAGAGATGAAACCAGAA	Core staple
TTAAGATTGCCCGAGTGTTGTTCCAGTTGTCC	Core staple
ATTATTACCAACTAGAAGGCTTATCCGGCCGT	Core staple
GGCACTTGAATATCAGTTAGCGTTTTTT	Core staple
GGAGAAGGTGAATTATCACCTAACGGAATTGA	Core staple
GAGTTGAGAGATACCGTTCTAGCTGATATGCC	Core staple
TTTTTGGATTATGCCAGCCATTGCAACACTGT	Core staple
AACATGCCACGCCAAAAATA	Core staple
GGGTTTAGACGGGAGAATTAGTTGCTATAAAC	Core staple
TTTTTATAAAGCCTCAGAGCAGGCAAAGCTTCA	Core staple
GAGATTCCAGACAGGAACAACTAAAGGAATAA	Core staple
GATATAAGACTCCTTATTACGTTCTTCGGGGTCACTGTTGCCCT	Core staple
TTAAGATAGCCCTAAAACATTAATACATGCCT	Core staple
ACCTCGTCGCTATTAATTAAGAATCCTTCGTG	Core staple
TTTTTGATAACAAGTAATATACCACAATTTTT	Core staple
CTCAGTAGAAACCAATCAATTAATTCTGTTGA	Core staple

TCGTAAAACTAGCATGGCTATTTTAACA	Core staple
GTTCATCTCTAAAAAGATAGCAGCACGAAA	Core staple
TGCCGTTTTTCTTTTCACCACAACAGCTCAAT	Core staple
ATTAAATAAAGAACGGATTCGCCTGATTGA	Core staple
GCCTCGTCAGATTAACAGTACCTTTTACACAT	Core staple
CGATTACCCAAATCAACGTTTCGGTCAATT	Core staple
CGCACACCAGCAAGACCTCAGAACCGATAC	Core staple
CCGTAACAATGCCCCCTAATGGGATGGTGTAGATGGGCGCTTTT	Core staple
CTCCACCAACACACTAAGGAACCTTTTT	Core staple
TTTTAACCAATGAACCTTGCTAGGGAGA	Core staple
CGCCCAACTGTTCTGGTGCCGGAAACCATAAA	Core staple
AACCTCAAGTTTTTTGGGGTAGCGGTCAAGTT	Core staple
ATCCAAGCCCGAAAGACTTCTAAAAAAATTAA	Core staple
ATCAATAACCTGTTTAGCTAGGGTTTTCAAGA	Core staple
ATCACAGGAAGAATTACGCCAGCTGGCGTGAA	Core staple
TGAATAGTATCATATGCGTCCAACATAGGA	Core staple
AAGACGTAGGAATCATTACCGCAAGCAAGTCT	Core staple
CCATCTAATGCAGCCATATTTAACAACGTATA	Core staple
TCCTGCTCATGGATTTTGACGCTCAATCGGCT	Core staple
TTTTTCTGGAGCAAACAAGAGGTCATTGCTAAT	Core staple
TCATAGGCTTGCCCTGACGACGTAATCAGTCA	Core staple
TTTTTATTGAGGAAGGTTAGAAGTATTTTTTT	Core staple
TTAGAGGCCGATTAAAGGGATTTGACGAAGCC	Core staple
ATTAGGAAGGTAAATATTGAATACCACACCAAAATATTTTT	Core staple
TTGTAGAGAGAATAACATAACCTGAATCAAAA	Core staple
TACCGACAATATTTTTGAATGTCTGAAAATTT	Core staple
AAGCGTCTATCAGGGCGATGATCGGCAACTGT	Core staple
GTGTGTACCAAAAACATTATCTTTCCGGAAAA	Core staple
AAGTTTTGATGATACAGGAGTGTCGTCTAAGGCCGGTTTTT	Core staple
GATGATTCCACAGACAGCCCTCATAGTTTGTACTGGCTGAGAGTTTTTT	Core staple
TCATTTGCGGGAGAAGCCTTATCGGCCTGCTT	Core staple
TTTCGCAGGCGATGATGGTGGTTCCGAAGCCC	Core staple
AAACAGCTGCATTAATGAATTTGCCCCAAATT	Core staple

TTTTTGAATTGTAAACAAGAAAGTTAATTTTT	Core staple
CATATGGTCATCAGACAGCCAGCG	Core staple
TTTTTATGAAATACAGGAATATAGCAATTTTT	Core staple
GAAGAGAATGACCATAAATCCCTCCGGCATCACCAGTAGCACCATTATTTTT	Core staple
TTTTTCCAGGTTTTTCTTTTTTTTTTTCCGTTCTTTACCCTGATTCC	Core staple
GCTTTTTCTTAAACAGCTTGCCACCCTCTGGC	Core staple
TTTTTCTGCGGAATCGTCATATGGATAGCATTC	Core staple
CAGCTGCTGGTCATCCTCATAACGGAAACA	Core staple
ATACAATAAAACGCTTCTGAATAAAGAACCTACGGG	Core staple
AAGGAGAGCCACCGGAACCGCCTCCCTCAGAG	Core staple
TCATGATATTCACTACAAAGGCTATCAGAATC	Core staple
TTCAGTAGTAAATTGGGCTTCAGGACGTTTAA	Core staple
GGAGCCGACAATGACAACAATCACCCTCAACA	Core staple
TACCTCATCTTCTGACCTAACTGATGCACGTA	Core staple
TTGCCCATCTTTGCGTTTTCATCGGCATTAAC	Core staple
TTTTTCCACGCGTTTGTTTTTTTTTTTTGCCAAAGGATAAAAAATCGTAACAATCCTCA	Core staple
TAGACCTTGATAGCCGCCGCCAGCATTGGTTT	Core staple
ATCGTAAGAACTTTACAGGTAGAAAGATCGGAAATTGTCCAATATTTTT	Core staple
AGCATTGAGGATTTATCTAAAATATCTTCAGT	Core staple
TTTTTGCCCAAACTACGAGAGTAATAATTTTT	Core staple
ACTAATAGGTCTCTTTTTAACCTCCGGCAAAT	Core staple
ACTTATATTTTAAATGCAAAATTAATTCTC	Core staple
CAAATACAGGGCGGGCGCTGGCAAGTGTCGAG	Core staple
CCTGTTGACAACTAAAGGCAGGTCAGAAGC	Core staple
AAGATGGGAAGACGTTAATAAAACGAACGTCA	Core staple
GAGGCCCTCAAATGCTTTAACGTGCCGGCTTG	Core staple
TTTTTAGATTTCGATTTTTTTTTTTTTCAAGGGGGGCGCGAGCAAAG	Core staple
TCATAAAATAATATCCCATCATGTTCAGCACG	Core staple
CTCCCACCGCTTGGGAAGGGCGATCGGTGTAG	Core staple
GCTTAATCCCTTAGCGGTCCACGCTGGTCGGC	Core staple
TGGCAAACAGCCATATTATTTATCCCAAAGAA	Core staple
ACTAGAAAACATCGCAAGACAAAGAACGTATA	Core staple
TTTTTGTTATTCCAAAATCACAATTTTTTTTT	Core staple

TTTTTGTAATTTGAAGGGTTTGAGCGCTTTTT	Core staple
TTAAAGCCAGAATGGAACGATTGGACCC	Core staple
TTTTTCAATTCCCTACAAATAGACAACTTTTT	Core staple
ATACTCATCTTTGACCCCCAAGCGTTTGTGAA	Core staple
CCTTGTGAGGCGGTCAGTATTGCAACAGCCCTGAAC	Core staple
TTTTCGCTGCGCCACCCGCCGCGCTTAAAGAA	Core staple
TTGCACTGTAGCTCATAATCAAATTTTT	Core staple
TTTTCCAGTATTTGTTTT	Core staple
AAAGTCAGAGGTTTTT	Edge staple (passivated)
TTTTCCTTATTTTCTTTT	Edge staple (passivated)
TTTTGATTGATCCTTTTT	Edge staple (passivated)
TTTTTTCAGATAGAATTTTT	Edge staple (passivated)
TTTTTCCTTAAATTATTTTT	Edge staple (passivated)
TTTTTCATAGAGGCGTTTTT	Edge staple (passivated)
TTTTTATCCGTCGAATTTTT	Edge staple (passivated)
TTTTTCATGATTTTTTTTTT	Edge staple (passivated)
TTTTTGGCTTGCTGATTTTT	Edge staple (passivated)
TTTTGGGTTTGGAATTTT	Edge staple (passivated)
TTTTAATTAAGGCGTTTT	Edge staple (passivated)
TTTTATAGACAACATTTT	Edge staple (passivated)
TTTTTTAGAACTGAGTTTTT	Edge staple (passivated)
TTTTTAGGAAGATTTTTT	Edge staple (passivated)
TTTTTGAATAATTGCTTTTT	Edge staple (passivated)
TTTTAGTAGTCAACTTTT	Edge staple (passivated)
TTTTTCCGGCGAAAGTTTTT	Edge staple (passivated)
TTTTTATCAGTGATTTTTTT	Edge staple (passivated)
TTTTTAGTTGTCATCTTTTT	Edge staple (passivated)
TTTTGCCTACCAGATTTT	Edge staple (passivated)
TTTTTAACGAAGCGTTTTTT	Edge staple (passivated)
TTTTCAATAGCGCCTTTT	Edge staple (passivated)
TTTTTAAGTGGCATATTTTT	Edge staple (passivated)
TTTTTTAGCTATCTTA	Edge staple (passivated)

TTTTTGCCAATTCTGTTTTT	Edge staple (passivated)
TTTTTACGGGGTGAGTTTTT	Edge staple (passivated)
TTTTTCCGCCTAACATTTTT	Edge staple (passivated)
TTTTTCAAGATGGAATTTTT	Edge staple (passivated)
TTTTTAGTTTTCTAATTTTT	Edge staple (passivated)
GCATATGCTAGCAAACGTAGAAAATATCACAATCAATAGAAAATT	Fuel and Anti-Fuel staples
AATTTTCTATTGATTGTGATATTTTCTACGTTTGCTAGCATATGC	Fuel and Anti-Fuel staples
CGACTTGAATTCGCGTCTGGCTGGGAACAAACGGCG	Fuel and Anti-Fuel staples
CGCCGTTTGTTCCCAGCCAGACGCGAATTCAAGTCG	Fuel and Anti-Fuel staples
TGTGCACGTTAGTACCGCCACCCTCACCCAATAGGAACCCATGTA	Fuel and Anti-Fuel staples
TACATGGGTTCCTATTGGGTGAGGGTGGCGGTACTAACGTGCACA	Fuel and Anti-Fuel staples
GATCCAGCGCAGTGTCACTCGGGGGTTTCTGCCAGCACCTTGACT	Fuel and Anti-Fuel staples
AGTCAAGGTGCTGGCAGAAACCCCCGAGTGACACTGCGCTGGATC	Fuel and Anti-Fuel staples
AAGCCCCAAAAACAGTTTTTGTTAAATCGTTCAGAC	Fuel and Anti-Fuel staples
GTCTGAACGATTTAACAAAAACTGTTTTTGGGGCTT	Fuel and Anti-Fuel staples
TGCCTATTTCGGAACCTATGGGTTTTGCTCAGTACCAACGTACTG	Fuel and Anti-Fuel staples
CAGTACGTTGGTACTGAGCAAAACCCATAGGTTCCGAAATAGGCA	Fuel and Anti-Fuel staples
AAGAATGCCAACGGCGGTCATTGCAGGCAACGCTTG	Fuel and Anti-Fuel staples
CAAGCGTTGCCTGCAATGACCGCCGTTGGCATTCTT	Fuel and Anti-Fuel staples
TGAGGTTCGCGGCTGGTAATGGGCATCAGATGCCGG	Fuel and Anti-Fuel staples
CCGGCATCTGATGCCCATTACCAGCCGCGAACCTCA	Fuel and Anti-Fuel staples
GCATATGCTAGCAAACGTAGAAAATACATTTGTCACAATCAATAGAAAATT	Fuel and Anti-Fuel staples
AATTTTCTATTGATTGTGACAAATGTATTTTCTACGTTTGCTAGCATATGC	Fuel and Anti-Fuel staples
CGACTTGAATTCGCGTCTGGCCTTCCGTGGGAACAAACGGCG	Fuel and Anti-Fuel staples
CGCCGTTTGTTCCCACGGAAGGCCAGACGCGAATTCAAGTCG	Fuel and Anti-Fuel staples
TGTGCACGTTAGTACCGCCACCCTCAGAAAAGCCCAATAGGAACCCATGTA	Fuel and Anti-Fuel staples
TACATGGGTTCCTATTGGGCTTTTCTGAGGGTGGCGGTACTAACGTGCACA	Fuel and Anti-Fuel staples
GATCCAGCGCAGTGTCACTGCGTACCGGGGGTTTCTGCCAGCACCTTGACT	Fuel and Anti-Fuel staples
AGTCAAGGTGCTGGCAGAAACCCCCGGTACGCAGTGACACTGCGCTGGATC	Fuel and Anti-Fuel staples
AAGCCCCAAAAACAGGAAAAATTTTTGTTAAATCGTTCAGAC	Fuel and Anti-Fuel staples
GTCTGAACGATTTAACAAAAATTTTTCCTGTTTTTGGGGCTT	Fuel and Anti-Fuel staples
TGCCTATTTCGGAACCTATTATGCGGGGTTTTGCTCAGTACCAACGTACTG	Fuel and Anti-Fuel staples

CAGTACGTTGGTACTGAGCAAAACCCCGCATAATAGGTTCCGAAATAGGCA	Fuel and Anti-Fuel staples
AAGAATGCCAACGGCAGCCGGGGTCATTGCAGGCAACGCTTG	Fuel and Anti-Fuel staples
CAAGCGTTGCCTGCAATGACCCCGGCTGCCGTTGGCATTCTT	Fuel and Anti-Fuel staples
TGAGGTTCGCGGCTGGTAATGGGTAACGGCATCAGATGCCGG	Fuel and Anti-Fuel staples
CCGGCATCTGATGCCGTTACCCATTACCAGCCGCGAACCTCA	Fuel and Anti-Fuel staples
GCATATGCTAGCAAACGTAGAAAATACATACAATTTTGTCACAATCAATAGAAAATT	Fuel and Anti-Fuel staples
AATTTTCTATTGATTGTGACAAAATTGTATGTATTTTCTACGTTTGCTAGCATATGC	Fuel and Anti-Fuel staples
CGACTTGAATTCGCGTCTGGCCTTCCTTCTCCGTGGGAACAAACGGCG	Fuel and Anti-Fuel staples
CGCCGTTTGTTCCCACGGAGAAGGAAGGCCAGACGCGAATTCAAGTCG	Fuel and Anti-Fuel staples
TGTGCACGTTAGTACCGCCACCCTCAGAACCGAGCAAGCCCAATAGGAACCCATGTA	Fuel and Anti-Fuel staples
TACATGGGTTCCTATTGGGCTTGCTCGGTTCTGAGGGTGGCGGTACTAACGTGCACA	Fuel and Anti-Fuel staples
GATCCAGCGCAGTGTCACTGCGCGCTCATACCGGGGGTTTCTGCCAGCACCTTGACT	Fuel and Anti-Fuel staples
AGTCAAGGTGCTGGCAGAAACCCCCGGTATGAGCGCGCAGTGACACTGCGCTGGATC	Fuel and Anti-Fuel staples
AAGCCCCAAAAACAGGAAGATATTAAATTTTTGTTAAATCGTTCAGAC	Fuel and Anti-Fuel staples
GTCTGAACGATTTAACAAAAATTTAATATCTTCCTGTTTTTGGGGCTT	Fuel and Anti-Fuel staples
TGCCTATTTCGGAACCTATTATTCTTTAGCGGGGTTTTGCTCAGTACCAACGTACTG	Fuel and Anti-Fuel staples
CAGTACGTTGGTACTGAGCAAAACCCCGCTAAAGAATAATAGGTTCCGAAATAGGCA	Fuel and Anti-Fuel staples
AAGAATGCCAACGGCAGCACCCAGCGGGGTCATTGCAGGCAACGCTTG	Fuel and Anti-Fuel staples
CAAGCGTTGCCTGCAATGACCCCGCTGGGTGCTGCCGTTGGCATTCTT	Fuel and Anti-Fuel staples
TGAGGTTCGCGGCTGGTAATGGGTAAAGTTAACGGCATCAGATGCCGG	Fuel and Anti-Fuel staples
CCGGCATCTGATGCCGTTAACTTTACCCATTACCAGCCGCGAACCTCA	Fuel and Anti-Fuel staples
GCATATGCTAGCAAACGTAGAAAATACATACATAAAGGAAGTTTATTTTGTCACAATCAATAGAAAATT	Fuel and Anti-Fuel staples
AATTTTCTATTGATTGTGACAAAATAAACTTCCTTTATGTATGTATTTTCTACGTTTGCTAGCATATGC	Fuel and Anti-Fuel staples
CGACTTGAATTCGCGTCTGGCCTTCCTGTAGCCTCGGATTCTCCGTGGGAACAAACGGCG	Fuel and Anti-Fuel staples
CGCCGTTTGTTCCCACGGAGAATCCGAGGCTACAGGAAGGCCAGACGCGAATTCAAGTCG	Fuel and Anti-Fuel staples
TGTGCACGTTAGTACCGCCACCCTCAGAACCGCCACCCAGGGATAGCAAGCCCAATAGGAACCCATGTA	Fuel and Anti-Fuel staples
TACATGGGTTCCTATTGGGCTTGCTATCCCTGGGTGGCGGTTCTGAGGGTGGCGGTACTAACGTGCACA	Fuel and Anti-Fuel staples
GATCCAGCGCAGTGTCACTGCGCGCCTGTGCTCACGGTCATACCGGGGGTTTCTGCCAGCACCTTGACT	Fuel and Anti-Fuel staples
AGTCAAGGTGCTGGCAGAAACCCCCGGTATGACCGTGAGCACAGGCGCGCAGTGACACTGCGCTGGATC	Fuel and Anti-Fuel staples
AAGCCCCAAAAACAGGAAGATTGTATAATTCGCATTAAATTTTTGTTAAATCGTTCAGAC	Fuel and Anti-Fuel staples
GTCTGAACGATTTAACAAAAATTTAATGCGAATTATACAATCTTCCTGTTTTTGGGGCTT	Fuel and Anti-Fuel staples
TGCCTATTTCGGAACCTATTATTCTGAAACATTAGGATTAGCGGGGTTTTGCTCAGTACCAACGTACTG	Fuel and Anti-Fuel staples
CAGTACGTTGGTACTGAGCAAAACCCCGCTAATCCTAATGTTTCAGAATAATAGGTTCCGAAATAGGCA	Fuel and Anti-Fuel staples

AAGAATGCCAACGGCAGCACCGTCGGTCAGCATCAGCGGGGTCATTGCAGGCAACGCTTG	Fuel and Anti-Fuel staples
CAAGCGTTGCCTGCAATGACCCCGCTGATGCTGACCGACGGTGCTGCCGTTGGCATTCTT	Fuel and Anti-Fuel staples
TGAGGTTCGCGGCTGGTAATGGGTAAAGGTTTCCAAATCGTTAACGGCATCAGATGCCGG	Fuel and Anti-Fuel staples
GCATATGCTAGCAAACGTAGAAAATACATACATAAAGGTGGCAGACACCACGGAATAAGTTTATTTTGTCACAATCAATAGAAAATT	Fuel and Anti-Fuel staples
CGACTTGAATTCGCGTCTGGCCTTCCTGTAGCCAGCTTTCATCAACAACCCGTCGGATTCTCCGTGGGAACAAACGGCG	Fuel and Anti-Fuel staples
TGTGCACGTTAGTACCGCCACCCTCAGAACCGCCACCCTCAGCCACCCTCATTTTCAGGGATAGCAAGCCCAATAGGAACCCATGTA	Fuel and Anti-Fuel staples
GATCCAGCGCAGTGTCACTGCGCGCCTGTGCACTCTGTGGTGGCCGTTTTCACGGTCATACCGGGGGTTTCTGCCAGCACCTTGACT	Fuel and Anti-Fuel staples
AAGCCCCAAAAACAGGAAGATTGTATAAGCAAATATTTTTGTTAAAATTCGCATTAAATTTTTGTTAAATCGTTCAGAC	Fuel and Anti-Fuel staples
TGCCTATTTCGGAACCTATTATTCTGAAACATGAAAGTATTAAGAAGGATTAGGATTAGCGGGGTTTTGCTCAGTACCAACGTACTG	Fuel and Anti-Fuel staples
AAGAATGCCAACGGCAGCACCGTCGGTGGTGCCATCCCAAGGTGTCCAGCATCAGCGGGGTCATTGCAGGCAACGCTTG	Fuel and Anti-Fuel staples
TGAGGTTCGCGGCTGGTAATGGGTAAAGGTTTCTTTGCTCGTGTGTGTTCAGCAAATCGTTAACGGCATCAGATGCCGG	Fuel and Anti-Fuel staples
CTGAACGCTGGTAGGCGAAAATCCTGTTGATATTTACCACTAAATCGGAACCCAAGGAGCGGGTT	Hybridization of DNA boxes on Zelos
AGCTCAATAGAGGTTTACCCATATTCCTGATTATCTGAGTTTACGTTAACCGTTGTAGCACAGAACAAACGA	Hybridization of DNA boxes on Zelos
TTACTACGTGAAAATCAAGTTTTTTGGGAGCTTTTAGAATTTAGAGCTTGACGGGGAACGTGGCGTT	Hybridization of DNA boxes on Zelos
ATTTATTTGAGGTAGGAGCACTAACAACTGGTTTTCAGGTAATAACATCACTTGCGAACTCAAGTCT	Hybridization of DNA boxes on Zelos
CTGAACGCTGGTAGGCGAAAATCCTGTTGATATTTCGCACACCAGCAAGACCTCAGAACCGATAC	Hybridization of DNA boxes on Zelos
AGCTCAATAGAGGTTTACCCATATTCCTGATTATCTGAGTTTCTTTATAGGGAACCGAACTGACCAACTAAGA	Hybridization of DNA boxes on Zelos
CTGATAAAAACAAGAGAATCGATGAACGTTTGGCCAGTGTTTTTCAGCCACCACCACCCTCAGAGTTTTT	Hybridization of DNA boxes on Zelos
ATTTATTTGAGGTAGGAGCACTAACAACTGGTTTTTTGCACTGTAGCTCATAATCAAATTTTT	Hybridization of DNA boxes on Zelos
[FAM]GAATTGTAAACAAGAAAGTTAA	Fluorophore staple (FRET)
CTCCACCAACACACTAAGGAACC[TAMRA]	Fluorophore staple (FRET)
TTCAGCCACCACCACCCTCAGAG	Changed edge staple set for FRET
CCGGCGAAAG	Changed edge staple set for FRET
TAGAACTGAG	Changed edge staple set for FRET
GTAATATACCACAAGATAACAA	Changed edge staple set for FRET
AGATTTCGATTCAAGGGGGGCGCGAGCAAAG	Changed edge staple set for FRET
TACGAGAGTAATAAGCCCAAAC	Changed edge staple set for FRET
ATCGTGGTGAAAAGTTGGGTAACGCCATATT	Changed edge staple set for FRET
TCAGATAGAA	Changed edge staple set for FRET
TTGCACTGTAGCTCATAATCAAA	Changed edge staple set for FRET

Primer for scaffold sequencing

Sequence	Comment
CGTAAAGCACTAAATCGGAACCCT	P1
TCACTGCCCGCTTTCCA	P2
GTTTTCCCAGTCACGACGTTGTAA	P3
GAAAAGCCCCAAAAACAGGAAGAT	P4
ATCATACAGGCAAGGCAAAGAATT	P5
AAAAAGATTAAGAGGAAGCCCGAA	P6
CGATAAAAACCAAAATAGCGAGAG	P7
TTGACCCCCAGCGATTATACCA	P8
TGACAACAACCATCGCCCAC	P9
ATAAGTGCCGTCGAGAGGGTTG	P10
CATAATCAAAATCACCGGAACCAG	P11
GAAACCGAGGAAACGCAATAATAA	P12
GACTTGCGGGAGGTTTTGAA	P13
CAAGACAAAGAACGCGAGAAAACT	P14
CCTGAGCAAAAGAAGATGATGAAA	P15
ACCTCAAATATCAAACCCTCAATC	P16
GTCCATCACGCAAATTAACCG	P17
ATAGGGGCCTTGAATCGGCT	P18
GCGGTCCGTTTTTTCGTC	P19
GCGGCTGGTAATGGGTAAA	P20

Scaffold p7249

TTCCCTTCCTTTCTCGCCACGTTCGCCGGCTTTCCCCGTCAAGCTCTAAATCGGGGGCTCCCTTTAGGGTTCCGATTTAGTGCTT
TACGGCACCTCGACCCCAAAAAACTTGATTTGGGTGATGGTTCACGTAGTGGGCCATCGCCCTGATAGACGGTTTTTCGCCCT
TTGACGTTGGAGTCCACGTTCTTTAATAGTGGACTCTTGTTCCAAACTGGAACAACACTCAACCCTATCTCGGGCTATTCTTTT
GATTTATAAGGGATTTTGCCGATTTCGGAACCACCATCAAACAGGATTTTCGCCTGCTGGGGCAAACCAGCGTGGACCGCTTG
CTGCAACTCTCTCAGGGCCAGGCGGTGAAGGGCAATCAGCTGTTGCCCGTCTCACTGGTGAAAAGAAAAACCACCCTGGCGC
CCAATACGCAAACCGCCTCTCCCCGCGCGTTGGCCGATTCATTAATGCAGCTGGCACGACAGGTTTCCCGACTGGAAAGCGG
GCAGTGAGCGCAACGCAATTAATGTGAGTTAGCTCACTCATTAGGCACCCCAGGCTTTACACTTTATGCTTCCGGCTCGTATG
TTGTGTGGAATTGTGAGCGGATAACAATTTCACACAGGAAACAGCTATGACCATGATTACGAATTCGAGCTCGGTACCCGGG
GATCCTCTAGAGTCGACCTGCAGGCATGCAAGCTTGGCACTGGCCGTCGTTTTACAACGTCGTGACTGGGAAAACCCTGGCGT
TACCCAACTTAATCGCCTTGCAGCACATCCCCCTTTCGCCAGCTGGCGTAATAGCGAAGAGGCCCGCACCGATCGCCCTTCCC
AACAGTTGCGCAGCCTGAATGGCGAATGGCGCTTTGCCTGGTTTCCGGCACCAGAAGCGGTGCCGGAAAGCTGGCTGGAGTG
CGATCTTCCTGAGGCCGATACTGTCGTCGTCCCCTCAAACTGGCAGATGCACGGTTACGATGCGCCCATCTACACCAACGTGA
CCTATCCCATTACGGTCAATCCGCCGTTTGTTCCCACGGAGAATCCGACGGGTTGTTACTCGCTCACATTTAATGTTGATGAAA
GCTGGCTACAGGAAGGCCAGACGCGAATTATTTTTGATGGCGTTCCTATTGGTTAAAAAATGAGCTGATTTAACAAAAATTTA
ATGCGAATTTTAACAAAATATTAACGTTTACAATTTAAATATTTGCTTATACAATCTTCCTGTTTTTGGGGCTTTTCTGATTATC
AACCGGGGTACATATGATTGACATGCTAGTTTTACGATTACCGTTCATCGATTCTCTTGTTTGCTCCAGACTCTCAGGCAATGA
CCTGATAGCCTTTGTAGATCTCTCAAAAATAGCTACCCTCTCCGGCATTAATTTATCAGCTAGAACGGTTGAATATCATATTGA
TGGTGATTTGACTGTCTCCGGCCTTTCTCACCCTTTTGAATCTTTACCTACACATTACTCAGGCATTGCATTTAAAATATATGA
GGGTTCTAAAAATTTTTATCCTTGCGTTGAAATAAAGGCTTCTCCCGCAAAAGTATTACAGGGTCATAATGTTTTTGGTACAAC
CGATTTAGCTTTATGCTCTGAGGCTTTATTGCTTAATTTTGCTAATTCTTTGCCTTGCCTGTATGATTTATTGGATGTTAATGCT
ACTACTATTAGTAGAATTGATGCCACCTTTTCAGCTCGCGCCCCAAATGAAAATATAGCTAAACAGGTTATTGACCATTTGCG
AAATGTATCTAATGGTCAAACTAAATCTACTCGTTCGCAGAATTGGGAATCAACTGTTATATGGAATGAAACTTCCAGACACC
GTACTTTAGTTGCATATTTAAAACATGTTGAGCTACAGCATTATATTCAGCAATTAAGCTCTAAGCCATCCGCAAAAATGACC
TCTTATCAAAAGGAGCAATTAAAGGTACTCTCTAATCCTGACCTGTTGGAGTTTGCTTCCGGTCTGGTTCGCTTTGAAGCTCGA
ATTAAAACGCGATATTTGAAGTCTTTCGGGCTTCCTCTTAATCTTTTTGATGCAATCCGCTTTGCTTCTGACTATAATAGTCAG
GGTAAAGACCTGATTTTTGATTTATGGTCATTCTCGTTTTCTGAACTGTTTAAAGCATTTGAGGGGGATTCAATGAATATTTAT
GACGATTCCGCAGTATTGGACGCTATCCAGTCTAAACATTTTACTATTACCCCCTCTGGCAAAACTTCTTTTGCAAAAGCCTCT
CGCTATTTTGGTTTTTATCGTCGTCTGGTAAACGAGGGTTATGATAGTGTTGCTCTTACTATGCCTCGTAATTCCTTTTGGCGTT
ATGTATCTGCATTAGTTGAATGTGGTATTCCTAAATCTCAACTGATGAATCTTTCTACCTGTAATAATGTTGTTCCGTTAGTTC
GTTTTATTAACGTAGATTTTTCTTCCCAACGTCCTGACTGGTATAATGAGCCAGTTCTTAAAATCGCATAAGGTAATTCACAAT
GATTAAAGTTGAAATTAAACCATCTCAAGCCCAATTTACTACTCGTTCTGGTGTTTCTCGTCAGGGCAAGCCTTATTCACTGAA
TGAGCAGCTTTGTTACGTTGATTTGGGTAATGAATATCCGGTTCTTGTCAAGATTACTCTTGATGAAGGTCAGCCAGCCTATGC
GCCTGGTCTGTACACCGTTCATCTGTCCTCTTTCAAAGTTGGTCAGTTCGGTTCCCTTATGATTGACCGTCTGCGCCTCGTTCCG
GCTAAGTAACATGGAGCAGGTCGCGGATTTCGACACAATTTATCAGGCGATGATACAAATCTCCGTTGTACTTTGTTTCGCGC
TTGGTATAATCGCTGGGGGTCAAAGATGAGTGTTTTAGTGTATTCTTTTGCCTCTTTCGTTTTAGGTTGGTGCCTTCGTAGTGG
CATTACGTATTTTACCCGTTTAATGGAAACTTCCTCATGAAAAAGTCTTTAGTCCTCAAAGCCTCTGTAGCCGTTGCTACCCTC
GTTCCGATGCTGTCTTTCGCTGCTGAGGGTGACGATCCCGCAAAAGCGGCCTTTAACTCCCTGCAAGCCTCAGCGACCGAATA
TATCGGTTATGCGTGGGCGATGGTTGTTGTCATTGTCGGCGCAACTATCGGTATCAAGCTGTTTAAGAAATTCACCTCGAAAG
CAAGCTGATAAACCGATACAATTAAAGGCTCCTTTTGGAGCCTTTTTTTTGGAGATTTTCAACGTGAAAAAATTATTATTCGCA
ATTCCTTTAGTTGTTCCTTTCTATTCTCACTCCGCTGAAACTGTTGAAAGTTGTTTAGCAAAATCCCATACAGAAAATTCATTT
ACTAACGTCTGGAAAGACGACAAAACTTTAGATCGTTACGCTAACTATGAGGGCTGTCTGTGGAATGCTACAGGCGTTGTAGT
TTGTACTGGTGACGAAACTCAGTGTTACGGTACATGGGTTCCTATTGGGCTTGCTATCCCTGAAAATGAGGGTGGTGGCTCTG
AGGGTGGCGGTTCTGAGGGTGGCGGTTCTGAGGGTGGCGGTACTAAACCTCCTGAGTACGGTGATACACCTATTCCGGGCTAT
ACTTATATCAACCCTCTCGACGGCACTTATCCGCCTGGTACTGAGCAAAACCCCGCTAATCCTAATCCTTCTCTTGAGGAGTCT
CAGCCTCTTAATACTTTCATGTTTCAGAATAATAGGTTCCGAAATAGGCAGGGGGCATTAACTGTTTATACGGGCACTGTTAC
TCAAGGCACTGACCCCGTTAAAACTTATTACCAGTACACTCCTGTATCATCAAAAGCCATGTATGACGCTTACTGGAACGGTA
AATTCAGAGACTGCGCTTTCCATTCTGGCTTTAATGAGGATTTATTTGTTTGTGAATATCAAGGCCAATCGTCTGACCTGCCTC
AACCTCCTGTCAATGCTGGCGGCGGCTCTGGTGGTGGTTCTGGTGGCGGCTCTGAGGGTGGTGGCTCTGAGGGTGGCGGTTCT
GAGGGTGGCGGCTCTGAGGGAGGCGGTTCCGGTGGTGGCTCTGGTTCCGGTGATTTTGATTATGAAAAGATGGCAAACGCTA
ATAAGGGGGCTATGACCGAAAATGCCGATGAAAACGCGCTACAGTCTGACGCTAAAGGCAAACTTGATTCTGTCGCTACTGA
TTACGGTGCTGCTATCGATGGTTTCATTGGTGACGTTTCCGGCCTTGCTAATGGTAATGGTGCTACTGGTGATTTTGCTGGCTC
TAATTCCCAAATGGCTCAAGTCGGTGACGGTGATAATTCACCTTTAATGAATAATTTCCGTCAATATTTACCTTCCCTCCCTCA
ATCGGTTGAATGTCGCCCTTTTGTCTTTGGCGCTGGTAAACCATATGAATTTTCTATTGATTGTGACAAAATAAACTTATTCCG
TGGTGTCTTTGCGTTTCTTTTATATGTTGCCACCTTTATGTATGTATTTTCTACGTTTGCTAACATACTGCGTAATAAGGAGTCT
TAATCATGCCAGTTCTTTTGGGTATTCCGTTATTATTGCGTTTCCTCGGTTTCCTTCTGGTAACTTTGTTCGGCTATCTGCTTACT
TTTCTTAAAAAGGGCTTCGGTAAGATAGCTATTGCTATTTCATTGTTTCTTGCTCTTATTATTGGGCTTAACTCAATTCTTGTGG
GTTATCTCTCTGATATTAGCGCTCAATTACCCTCTGACTTTGTTCAGGGTGTTCAGTTAATTCTCCCGTCTAATGCGCTTCCCTG
TTTTTATGTTATTCTCTCTGTAAAGGCTGCTATTTTCATTTTTGACGTTAAACAAAAAATCGTTTCTTATTTGGATTGGGATAAA
TAATATGGCTGTTTATTTTGTAACTGGCAAATTAGGCTCTGGAAAGACGCTCGTTAGCGTTGGTAAGATTCAGGATAAAATTG
TAGCTGGGTGCAAAATAGCAACTAATCTTGATTTAAGGCTTCAAAACCTCCCGCAAGTCGGGAGGTTCGCTAAAACGCCTCGC
GTTCTTAGAATACCGGATAAGCCTTCTATATCTGATTTGCTTGCTATTGGGCGCGGTAATGATTCCTACGATGAAAATAAAAA
CGGCTTGCTTGTTCTCGATGAGTGCGGTACTTGGTTTAATACCCGTTCTTGGAATGATAAGGAAAGACAGCCGATTATTGATT
GGTTTCTACATGCTCGTAAATTAGGATGGGATATTATTTTTCTTGTTCAGGACTTATCTATTGTTGATAAACAGGCGCGTTCTG
CATTAGCTGAACATGTTGTTTATTGTCGTCGTCTGGACAGAATTACTTTACCTTTTGTCGGTACTTTATATTCTCTTATTACTGG
CTCGAAAATGCCTCTGCCTAAATTACATGTTGGCGTTGTTAAATATGGCGATTCTCAATTAAGCCCTACTGTTGAGCGTTGGCT
TTATACTGGTAAGAATTTGTATAACGCATATGATACTAAACAGGCTTTTTCTAGTAATTATGATTCCGGTGTTTATTCTTATTT
AACGCCTTATTTATCACACGGTCGGTATTTCAAACCATTAAATTTAGGTCAGAAGATGAAATTAACTAAAATATATTTGAAAA

AGTTTTCTCGCGTTCTTTGTCTTGCGATTGGATTTGCATCAGCATTTACATATAGTTATATAACCCAACCTAAGCCGGAGGTTA
AAAAGGTAGTCTCTCAGACCTATGATTTTGATAAATTCACTATTGACTCTTCTCAGCGTCTTAATCTAAGCTATCGCTATGTTT
TCAAGGATTCTAAGGGAAAATTAATTAATAGCGACGATTTACAGAAGCAAGGTTATTCACTCACATATATTGATTTATGTACT
GTTTCCATTAAAAAAGGTAATTCAAATGAAATTGTTAAATGTAATTAATTTTGTTTTCTTGATGTTTGTTTCATCATCTTCTTTT
GCTCAGGTAATTGAAATGAATAATTCGCCTCTGCGCGATTTTGTAACTTGGTATTCAAAGCAATCAGGCGAATCCGTTATTGT
TTCTCCCGATGTAAAAGGTACTGTTACTGTATATTCATCTGACGTTAAACCTGAAAATCTACGCAATTTCTTTATTTCTGTTTTA
CGTGCAAATAATTTTGATATGGTAGGTTCTAACCCTTCCATTATTCAGAAGTATAATCCAAACAATCAGGATTATATTGATGA
ATTGCCATCATCTGATAATCAGGAATATGATGATAATTCCGCTCCTTCTGGTGGTTTCTTTGTTCCGCAAAATGATAATGTTAC
TCAAACTTTTAAAATTAATAACGTTCGGGCAAAGGATTTAATACGAGTTGTCGAATTGTTTGTAAAGTCTAATACTTCTAAAT
CCTCAAATGTATTATCTATTGACGGCTCTAATCTATTAGTTGTTAGTGCTCCTAAAGATATTTTAGATAACCTTCCTCAATTCCT
TTCAACTGTTGATTTGCCAACTGACCAGATATTGATTGAGGGTTTGATATTTGAGGTTCAGCAAGGTGATGCTTTAGATTTTTC
ATTTGCTGCTGGCTCTCAGCGTGGCACTGTTGCAGGCGGTGTTAATACTGACCGCCTCACCTCTGTTTTATCTTCTGCTGGTGG
TTCGTTCGGTATTTTTAATGGCGATGTTTTAGGGCTATCAGTTCGCGCATTAAAGACTAATAGCCATTCAAAAATATTGTCTGT
GCCACGTATTCTTACGCTTTCAGGTCAGAAGGGTTCTATCTCTGTTGGCCAGAATGTCCCTTTTATTACTGGTCGTGTGACTGG
TGAATCTGCCAATGTAAATAATCCATTTCAGACGATTGAGCGTCAAAATGTAGGTATTTCCATGAGCGTTTTTCCTGTTGCAAT
GGCTGGCGGTAATATTGTTCTGGATATTACCAGCAAGGCCGATAGTTTGAGTTCTTCTACTCAGGCAAGTGATGTTATTACTA
ATCAAAGAAGTATTGCTACAACGGTTAATTTGCGTGATGGACAGACTCTTTTACTCGGTGGCCTCACTGATTATAAAAACACT
TCTCAGGATTCTGGCGTACCGTTCCTGTCTAAAATCCCTTTAATCGGCCTCCTGTTTAGCTCCCGCTCTGATTCTAACGAGGAA
AGCACGTTATACGTGCTCGTCAAAGCAACCATAGTACGCGCCCTGTAGCGGCGCATTAAGCGCGGCGGGTGTGGTGGTTACG
CGCAGCGTGACCGCTACACTTGCCAGCGCCCTAGCGCCCGCTCCTTTCGCTTTC

Scaffold p8064

GGCAATGACCTGATAGCCTTTGTAGATCTCTCAAAAATAGCTACCCTCTCCGGCATTAATTTATCAGCTAGAACGGTTGAATA
TCATATTGATGGTGATTTGACTGTCTCCGGCCTTTCTCACCCTTTTGAATCTTTACCTACACATTACTCAGGCATTGCATTTAAA
ATATATGAGGGTTCTAAAAATTTTTATCCTTGCGTTGAAATAAAGGCTTCTCCCGCAAAAGTATTACAGGGTCATAATGTTTTT
GGTACAACCGATTTAGCTTTATGCTCTGAGGCTTTATTGCTTAATTTTGCTAATTCTTTGCCTTGCCTGTATGATTTATTGGATG
TTAATGCTACTACTATTAGTAGAATTGATGCCACCTTTTCAGCTCGCGCCCCAAATGAAAATATAGCTAAACAGGTTATTGAC
CATTTGCGAAATGTATCTAATGGTCAAACTAAATCTACTCGTTCGCAGAATTGGGAATCAACTGTTATATGGAATGAAACTTC
CAGACACCGTACTTTAGTTGCATATTTAAAACATGTTGAGCTACAGCATTATATTCAGCAATTAAGCTCTAAGCCATCCGCAA
AAATGACCTCTTATCAAAAGGAGCAATTAAAGGTACTCTCTAATCCTGACCTGTTGGAGTTTGCTTCCGGTCTGGTTCGCTTTG
AAGCTCGAATTAAAACGCGATATTTGAAGTCTTTCGGGCTTCCTCTTAATCTTTTTGATGCAATCCGCTTTGCTTCTGACTATA
ATAGTCAGGGTAAAGACCTGATTTTTGATTTATGGTCATTCTCGTTTTCTGAACTGTTTAAAGCATTTGAGGGGGATTCAATGA
ATATTTATGACGATTCCGCAGTATTGGACGCTATCCAGTCTAAACATTTTACTATTACCCCCTCTGGCAAAACTTCTTTTGCAA
AAGCCTCTCGCTATTTTGGTTTTTATCGTCGTCTGGTAAACGAGGGTTATGATAGTGTTGCTCTTACTATGCCTCGTAATTCCTT
TTGGCGTTATGTATCTGCATTAGTTGAATGTGGTATTCCTAAATCTCAACTGATGAATCTTTCTACCTGTAATAATGTTGTTCC
GTTAGTTCGTTTTATTAACGTAGATTTTTCTTCCCAACGTCCTGACTGGTATAATGAGCCAGTTCTTAAAATCGCATAAGGTAA
TTCACAATGATTAAAGTTGAAATTAAACCATCTCAAGCCCAATTTACTACTCGTTCTGGTGTTTCTCGTCAGGGCAAGCCTTAT
TCACTGAATGAGCAGCTTTGTTACGTTGATTTGGGTAATGAATATCCGGTTCTTGTCAAGATTACTCTTGATGAAGGTCAGCCA
GCCTATGCGCCTGGTCTGTACACCGTTCATCTGTCCTCTTTCAAAGTTGGTCAGTTCGGTTCCCTTATGATTGACCGTCTGCGC
CTCGTTCCGGCTAAGTAACATGGAGCAGGTCGCGGATTTCGACACAATTTATCAGGCGATGATACAAATCTCCGTTGTACTTT
GTTTCGCGCTTGGTATAATCGCTGGGGGTCAAAGATGAGTGTTTTAGTGTATTCTTTTGCCTCTTTCGTTTTAGGTTGGTGCCTT
CGTAGTGGCATTACGTATTTTACCCGTTTAATGGAAACTTCCTCATGAAAAAGTCTTTAGTCCTCAAAGCCTCTGTAGCCGTTG
CTACCCTCGTTCCGATGCTGTCTTTCGCTGCTGAGGGTGACGATCCCGCAAAAGCGGCCTTTAACTCCCTGCAAGCCTCAGCG
ACCGAATATATCGGTTATGCGTGGGCGATGGTTGTTGTCATTGTCGGCGCAACTATCGGTATCAAGCTGTTTAAGAAATTCAC
CTCGAAAGCAAGCTGATAAACCGATACAATTAAAGGCTCCTTTTGGAGCCTTTTTTTTGGAGATTTTCAACGTGAAAAAATTA
TTATTCGCAATTCCTTTAGTTGTTCCTTTCTATTCTCACTCCGCTGAAACTGTTGAAAGTTGTTTAGCAAAATCCCATACAGAA
AATTCATTTACTAACGTCTGGAAAGACGACAAAACTTTAGATCGTTACGCTAACTATGAGGGCTGTCTGTGGAATGCTACAGG
CGTTGTAGTTTGTACTGGTGACGAAACTCAGTGTTACGGTACATGGGTTCCTATTGGGCTTGCTATCCCTGAAAATGAGGGTG
GTGGCTCTGAGGGTGGCGGTTCTGAGGGTGGCGGTTCTGAGGGTGGCGGTACTAAACCTCCTGAGTACGGTGATACACCTATT
CCGGGCTATACTTATATCAACCCTCTCGACGGCACTTATCCGCCTGGTACTGAGCAAAACCCCGCTAATCCTAATCCTTCTCTT
GAGGAGTCTCAGCCTCTTAATACTTTCATGTTTCAGAATAATAGGTTCCGAAATAGGCAGGGGGCATTAACTGTTTATACGGG
CACTGTTACTCAAGGCACTGACCCCGTTAAAACTTATTACCAGTACACTCCTGTATCATCAAAAGCCATGTATGACGCTTACT
GGAACGGTAAATTCAGAGACTGCGCTTTCCATTCTGGCTTTAATGAGGATTTATTTGTTTGTGAATATCAAGGCCAATCGTCTG
ACCTGCCTCAACCTCCTGTCAATGCTGGCGGCGGCTCTGGTGGTGGTTCTGGTGGCGGCTCTGAGGGTGGTGGCTCTGAGGGT
GGCGGTTCTGAGGGTGGCGGCTCTGAGGGAGGCGGTTCCGGTGGTGGCTCTGGTTCCGGTGATTTTGATTATGAAAAGATGGC
AAACGCTAATAAGGGGGCTATGACCGAAAATGCCGATGAAAACGCGCTACAGTCTGACGCTAAAGGCAAACTTGATTCTGTC
GCTACTGATTACGGTGCTGCTATCGATGGTTTCATTGGTGACGTTTCCGGCCTTGCTAATGGTAATGGTGCTACTGGTGATTTT
GCTGGCTCTAATTCCCAAATGGCTCAAGTCGGTGACGGTGATAATTCACCTTTAATGAATAATTTCCGTCAATATTTACCTTCC
CTCCCTCAATCGGTTGAATGTCGCCCTTTTGTCTTTGGCGCTGGTAAACCATATGAATTTTCTATTGATTGTGACAAAATAAAC
TTATTCCGTGGTGTCTTTGCGTTTCTTTTATATGTTGCCACCTTTATGTATGTATTTTCTACGTTTGCTAACATACTGCGTAATA
AGGAGTCTTAATCATGCCAGTTCTTTTGGGTATTCCGTTATTATTGCGTTTCCTCGGTTTCCTTCTGGTAACTTTGTTCGGCTAT
CTGCTTACTTTTCTTAAAAAGGGCTTCGGTAAGATAGCTATTGCTATTTCATTGTTTCTTGCTCTTATTATTGGGCTTAACTCAA
TTCTTGTGGGTTATCTCTCTGATATTAGCGCTCAATTACCCTCTGACTTTGTTCAGGGTGTTCAGTTAATTCTCCCGTCTAATGC
GCTTCCCTGTTTTTATGTTATTCTCTCTGTAAAGGCTGCTATTTTCATTTTTGACGTTAAACAAAAAATCGTTTCTTATTTGGAT
TGGGATAAATAATATGGCTGTTTATTTTGTAACTGGCAAATTAGGCTCTGGAAAGACGCTCGTTAGCGTTGGTAAGATTCAGG
ATAAAATTGTAGCTGGGTGCAAAATAGCAACTAATCTTGATTTAAGGCTTCAAAACCTCCCGCAAGTCGGGAGGTTCGCTAA

AACGCCTCGCGTTCTTAGAATACCGGATAAGCCTTCTATATCTGATTTGCTTGCTATTGGGCGCGGTAATGATTCCTACGATGA
AAATAAAAACGGCTTGCTTGTTCTCGATGAGTGCGGTACTTGGTTTAATACCCGTTCTTGGAATGATAAGGAAAGACAGCCGA
TTATTGATTGGTTTCTACATGCTCGTAAATTAGGATGGGATATTATTTTTCTTGTTCAGGACTTATCTATTGTTGATAAACAGG
CGCGTTCTGCATTAGCTGAACATGTTGTTTATTGTCGTCGTCTGGACAGAATTACTTTACCTTTTGTCGGTACTTTATATTCTCT
TATTACTGGCTCGAAAATGCCTCTGCCTAAATTACATGTTGGCGTTGTTAAATATGGCGATTCTCAATTAAGCCCTACTGTTGA
GCGTTGGCTTTATACTGGTAAGAATTTGTATAACGCATATGATACTAAACAGGCTTTTTCTAGTAATTATGATTCCGGTGTTTA
TTCTTATTTAACGCCTTATTTATCACACGGTCGGTATTTCAAACCATTAAATTTAGGTCAGAAGATGAAATTAACTAAAATATA
TTTGAAAAAGTTTTCTCGCGTTCTTTGTCTTGCGATTGGATTTGCATCAGCATTTACATATAGTTATATAACCCAACCTAAGCC
GGAGGTTAAAAAGGTAGTCTCTCAGACCTATGATTTTGATAAATTCACTATTGACTCTTCTCAGCGTCTTAATCTAAGCTATCG
CTATGTTTTCAAGGATTCTAAGGGAAAATTAATTAATAGCGACGATTTACAGAAGCAAGGTTATTCACTCACATATATTGATT
TATGTACTGTTTCCATTAAAAAAGGTAATTCAAATGAAATTGTTAAATGTAATTAATTTTGTTTTCTTGATGTTTGTTTCATCAT
CTTCTTTTGCTCAGGTAATTGAAATGAATAATTCGCCTCTGCGCGATTTTGTAACTTGGTATTCAAAGCAATCAGGCGAATCCG
TTATTGTTTCTCCCGATGTAAAAGGTACTGTTACTGTATATTCATCTGACGTTAAACCTGAAAATCTACGCAATTTCTTTATTTC
TGTTTTACGTGCAAATAATTTTGATATGGTAGGTTCTAACCCTTCCATTATTCAGAAGTATAATCCAAACAATCAGGATTATAT
TGATGAATTGCCATCATCTGATAATCAGGAATATGATGATAATTCCGCTCCTTCTGGTGGTTTCTTTGTTCCGCAAAATGATAA
TGTTACTCAAACTTTTAAAATTAATAACGTTCGGGCAAAGGATTTAATACGAGTTGTCGAATTGTTTGTAAAGTCTAATACTTC
TAAATCCTCAAATGTATTATCTATTGACGGCTCTAATCTATTAGTTGTTAGTGCTCCTAAAGATATTTTAGATAACCTTCCTCA
ATTCCTTTCAACTGTTGATTTGCCAACTGACCAGATATTGATTGAGGGTTTGATATTTGAGGTTCAGCAAGGTGATGCTTTAGA
TTTTTCATTTGCTGCTGGCTCTCAGCGTGGCACTGTTGCAGGCGGTGTTAATACTGACCGCCTCACCTCTGTTTTATCTTCTGCT
GGTGGTTCGTTCGGTATTTTTAATGGCGATGTTTTAGGGCTATCAGTTCGCGCATTAAAGACTAATAGCCATTCAAAAATATTG
TCTGTGCCACGTATTCTTACGCTTTCAGGTCAGAAGGGTTCTATCTCTGTTGGCCAGAATGTCCCTTTTATTACTGGTCGTGTG
ACTGGTGAATCTGCCAATGTAAATAATCCATTTCAGACGATTGAGCGTCAAAATGTAGGTATTTCCATGAGCGTTTTTCCTGTT
GCAATGGCTGGCGGTAATATTGTTCTGGATATTACCAGCAAGGCCGATAGTTTGAGTTCTTCTACTCAGGCAAGTGATGTTAT
TACTAATCAAAGAAGTATTGCTACAACGGTTAATTTGCGTGATGGACAGACTCTTTTACTCGGTGGCCTCACTGATTATAAAA
ACACTTCTCAGGATTCTGGCGTACCGTTCCTGTCTAAAATCCCTTTAATCGGCCTCCTGTTTAGCTCCCGCTCTGATTCTAACG
AGGAAAGCACGTTATACGTGCTCGTCAAAGCAACCATAGTACGCGCCCTGTAGCGGCGCATTAAGCGCGGCGGGTGTGGTGG
TTACGCGCAGCGTGACCGCTACACTTGCCAGCGCCCTAGCGCCCGCTCCTTTCGCTTTCTTCCCTTCCTTTCTCGCCACGTTCGC
CGGCTTTCCCCGTCAAGCTCTAAATCGGGGGCTCCCTTTAGGGTTCCGATTTAGTGCTTTACGGCACCTCGACCCCAAAAAAC
TTGATTTGGGTGATGGTTCACGTAGTGGGCCATCGCCCTGATAGACGGTTTTTCGCCCTTTGACGTTGGAGTCCACGTTCTTTA
ATAGTGGACTCTTGTTCCAAACTGGAACAACACTCAACCCTATCTCGGGCTATTCTTTTGATTTATAAGGGATTTTGCCGATTT
CGGAACCACCATCAAACAGGATTTTCGCCTGCTGGGGCAAACCAGCGTGGACCGCTTGCTGCAACTCTCTCAGGGCCAGGCG
GTGAAGGGCAATCAGCTGTTGCCCGTCTCACTGGTGAAAAGAAAAACCACCCTGGCGCCCAATACGCAAACCGCCTCTCCCC
GCGCGTTGGCCGATTCATTAATGCAGCTGGCACGACAGGTTTCCCGACTGGAAAGCGGGCAGTGAGCGCAACGCAATTAATG
TGAGTTAGCTCACTCATTAGGCACCCCAGGCTTTACACTTTATGCTTCCGGCTCGTATGTTGTGTGGAATTGTGAGCGGATAAC
AATTTCACACAGGAAACAGCTATGACCATGATTACGAATTCGAGCTCGGTACCCGGGGATCCTCAACTGTGAGGAGGCTCAC
GGACGCGAAGAACAGGCACGCGTGCTGGCAGAAACCCCCCGGTATGACCGTGAAAACGGCCCGCCGCATTCTGGCCGCAGCA
CCACAGAGTGCACAGGCGCGCAGTGACACTGCGCTGGATCGTCTGATGCAGGGGGCACCGGCACCGCTGGCTGCAGGTAACC
CGGCATCTGATGCCGTTAACGATTTGCTGAACACACCAGTGTAAGGGATGTTTATGACGAGCAAAGAAACCTTTACCCATTAC
CAGCCGCAGGGCAACAGTGACCCGGCTCATACCGCAACCGCGCCCGGCGGATTGAGTGCGAAAGCGCCTGCAATGACCCCGC
TGATGCTGGACACCTCCAGCCGTAAGCTGGTTGCGTGGGATGGCACCACCGACGGTGCTGCCGTTGGCATTCTTGCGGTTGCT
GCTGACCAGACCAGCACCACGCTGACGTTCTACAAGTCCGGCACGTTCCGTTATGAGGATGTGCTCTGGCCGGAGGCTGCCA
GCGACGAGACGAAAAAACGGACCGCGTTTGCCGGAACGGCAATCAGCATCGTTTAACTTTACCCTTCATCACTAAAGGCCGC
CTGTGCGGCTTTTTTTTACGGGATTTTTTTTATGTCGATGTACACAACCGCCCAACTGCTGGCGGCAAATGAGCAGAAATTTAAG
TTTGATCCGCTGTTTCTGCGTCTCTTTTTCCGTGAGAGCTATCCCTTCACCACGGAGAAAGTCTATCTCTCACAAATTCCGGGA
CTGGTAAACATGGCGCTGTACGTTTCGCCGATTGTTTCCGGTGAGGTTATCCGTTCCCGTGGCGGCTCCACCTCTGAAAGCTTG
GCACTGGCCGTCGTTTTACAACGTCGTGACTGGGAAAACCCTGGCGTTACCCAACTTAATCGCCTTGCAGCACATCCCCCTTT
CGCCAGCTGGCGTAATAGCGAAGAGGCCCGCACCGATCGCCCTTCCCAACAGTTGCGCAGCCTGAATGGCGAATGGCGCTTT
GCCTGGTTTCCGGCACCAGAAGCGGTGCCGGAAAGCTGGCTGGAGTGCGATCTTCCTGAGGCCGATACTGTCGTCGTCCCCTC
AAACTGGCAGATGCACGGTTACGATGCGCCCATCTACACCAACGTGACCTATCCCATTACGGTCAATCCGCCGTTTGTTCCCA
CGGAGAATCCGACGGGTTGTTACTCGCTCACATTTAATGTTGATGAAAGCTGGCTACAGGAAGGCCAGACGCGAATTATTTTT
GATGGCGTTCCTATTGGTTAAAAAATGAGCTGATTTAACAAAAATTTAATGCGAATTTTAACAAAATATTAACGTTTACAATT
TAAATATTTGCTTATACAATCTTCCTGTTTTTGGGGCTTTTCTGATTATCAACCGGGGTACATATGATTGACATGCTAGTTTTAC
GATTACCGTTCATCGATTCTCTTGTTTGCTCCAGACTCTCA

6.4 List of Abbreviations and Physical Parameters

Abbreviation	Description
%	Percentage
1D	One-dimensional
2D	Two-dimensional
3D	Three-dimensional
Å	Angstroms
°C	Degree Celsius
ΔG	Change in free energy
$\Delta G^{\ddagger}$	Energy difference between ES and $ES^{\ddagger}$
ΔG_{ES}	Energy difference between E + S and ES
$\Delta G^{\ddagger}_{TS}$	Energy difference between E + S and $ES^{\ddagger}$
$\Delta\Delta G^{\ddagger}$	Difference of $\Delta G^{\ddagger}$ between two enzyme species
$\Delta\Delta G_{ES}$	Difference of ΔG_{ES} between two enzyme species
$\Delta\Delta G^{\ddagger}_{TS}$	Difference of $\Delta G^{\ddagger}_{TS}$ between two enzyme species
ε	Absorption coefficient
A	Adenosine
Au	Gold
ABTS	2,2’-azino-bis(3-ethylbenzothiazoline-6-solfonic acid)
AFM	Atomic force microscopy
AGE	Agarose gel electrophoresis
B	Boric acid
b(s)	Base(s)
bp(s)	Base pair(s)
c	Concentration

C	Cytosine
Da	Dalton
DNA	Deoxyribonucleic acid
ds	Double stranded
E_0	Initial enzyme concentration
EDTA	Ethylenediaminetetraacetat
ES	Enzyme-substrate complex
$ES^{\ddagger}$	Enzyme-substrate transition state
EtBr	Ethidium bromide
FAM	6-Carboxyfluorescin
FDTD	Finite difference time-domain
G	Guanine
G6pDH	Glucose-6-phosphate dehydrogenase
GOx	Glucose Oxidase
h	Hour
H_2O	Water
HCl	Hydrogen chloride
HJ	Holliday junction
HRP	Horseradish peroxidase
k_x	Rate coefficient
k_{cat}	Turnover number, catalytic rate
K_M	Michaelis constant
Mb	Apo-myoglobin
MDH	Malic dehydrogenase
M-FRET	Metal-enhanced Förster resonance energy transfer
$MgCl_2$	Magnesium chloride

min	Minute
NaCl	Sodium chloride
NAD^+	Nicotinamide adenine dinucleotide
NC	Nanocube
NP	Nanoparticle
NS	Nanosphere
P	Product
PEG	Polyethylene glycol
rcf	Relative centrifugal force
rmsf	Root mean square flexibility
RNA	Ribonucleic acid
RT	Room temperature
S	Substrate concentration
SDS-PAGE	Sodium dodecyl sulfate polyacrylamide gel electrophoresis
SERS	Surface-enhanced Raman scattering
ss	Single stranded
STM	Scanning tunneling microscope
Sulfo-SMCC	Sulfosuccinimidyl 4-(N-maleimidomethyl)cyclohexane-1-carboxylate
T	Thymine
TAMRA	Carboxytetramethylrhodamine
TBA1	Thrombin binding aptamer 1
TBA2	Thrombin binding aptamer 2
TEM	Transmission electron microscopy
T_m	Melting temperature
v_0	Initial reaction rate
v_{max}	Maximum reaction rate

6.5 List of Figures

6.6 List of Supplementary Figures

6.7 List of Tables

6.8 List of Supplementary Tables

6.9 List of Equations

7 Appendix

7.1 Thermal folding of a three-domains DNA origami structure

Parts of this chapter are published in the following article: Kosinski, R. *et al.* Sites of high local frustration in DNA origami. *Nature Communications* **10**, 1061 (2019)[178]

7.1.1 Introduction

The self-assembly of a DNA origami structure necessitates the folding of a long single-stranded sequence (named *scaffold*) by hundreds of pre-designed short oligonucleotides (named *staple strands*). Thereby, the scaffold is arranged into a 2D or 3D structure, ideally shaping into a pre-designed conformation. Interestingly, the self-assembly of a DNA origami appears quite similar to the folding of proteins. While in protein folding the side chains of the amino acids basically inherit the information that is responsible for the proteins folding trajectory,[211,248] in DNA origami folding, the staple strands carry that information and dictate the final shape by connecting discontinuous regions of the scaffold sequence. Maybe surprisingly, the folding of DNA origamis manifests an extremely high yield of correctly folded structures and rather low error rates.[249]

Several studies regarding the subject of DNA origami folding have contributed intriguing insights into this process[162,163,165,167–169,171,175,250–252] and revealed three main aspects of the problem: (i) well defined folding trajectories do exist, leading to local or absolute energy minima to which the structure quickly evolves; (ii) the occupancy of each folding trajectory may be manipulated by addition of mechanical triggers, which usually target continuous regions of the scaffold (i.e. oftentimes the edges); (iii) the mechanical triggers induce a reconfiguration of the Holliday junctions (HJs) within the structure.

While many works have reported the presence of different folding paths and even the post-assembly reconfiguration of DNA origamis, the aim of this work is to highlight not only the importance of topological strain, but also the significance of sequence-encoded information

and seeded growth in order to eventually combine all these aspects into a multi-facet picture of the folding process.

7.1.2 Results

Holliday junctions, the "intersection" of four single stranded DNA strands at a common point (called crossover), can exist in two states (iso I and iso II). While the base content of these two isomers is identical, the nucleobases that stack with each other at the crossover point are different in the two forms. It has been demonstrated that since the HJ is the fundamental building unit of every DNA origami, the triggered change of some HJs at a region of the structure collectively propagates to the entire DNA origami shape, which eventually assumes one of two different iso-forms (iso I or iso II).[170,171,174,177] Whereas in the iso I form, the staple strands connect the scaffold in an antiparallel fashion via staple crossovers, in the iso II state, antiparallel stretches of staple strands are connected via scaffold crossovers (Figure 30). But what factors guide the assembly process, favoring one iso-form over the other?

To answer this question, a novel DNA origami system was developed. The system consists of a monolayer DNA origami that is made up of three topologically identical domains (named A, B and C), linked to one another by two to three free scaffold bases (Figure 31). Hence, from a strict mechanical perspective, these domains are identical. They however diverge in their chemical make-up, since their component sequences are different. Since, during the folding process, all domains experience the same physical conditions, differences in their isomerization rates can solely be attributed to the differences in their sequences. Each domain consists of a core of 56 staple strands, flanked by unpaired scaffold regions. These scaffold regions (left and right) are exposed to three kinds of edge staples (e(0), e(1), e(2)), which induce scaffold crossovers at favorable or unfavorable positions. Edges of type 0 (e(0)) bind in a U-shape to two antiparallel helices of the scaffold. On the other hand, edges type 1 (e(1)) and type 2 (e(2)) each contain an additional 5T-spacer and bind to three different scaffold helices (Figure 30), resulting in a S-shape and O-shape, respectively. It is therefore expected that different amounts of mechanical strain are exerted by each type of edge staples.

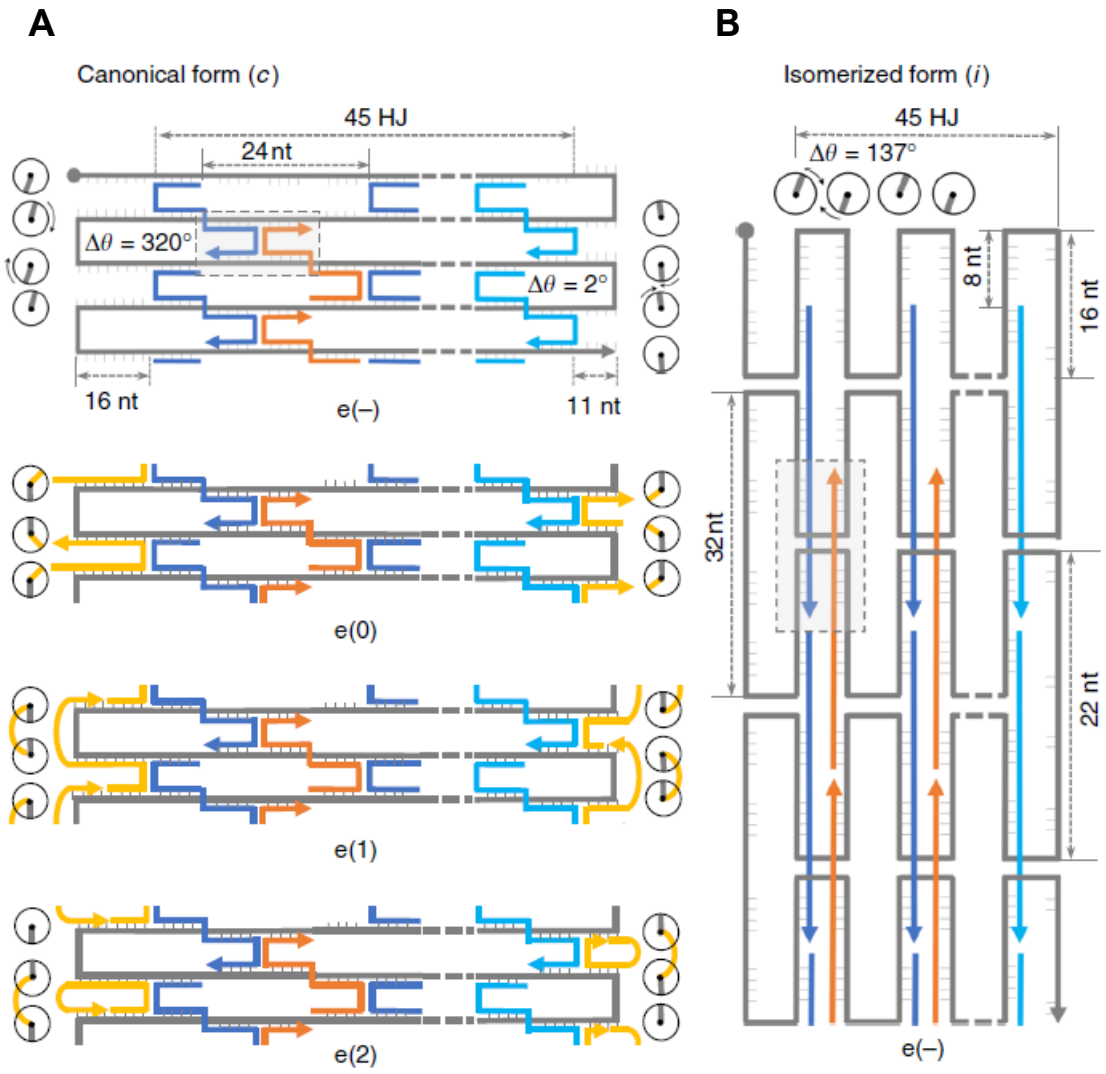

Figure 30: Design of the DNA origami in both isomerization states. (A) In the canonical form the staples form crossovers between the scaffold strand. When no edge staples are applied, the scaffold experiences a certain freedom laterally and vertically, with several nucleotides being unpaired. Three different edge staples were used to target the exposed regions on the left and right side. **(B)** In the isomerized form the scaffold forms crossovers between the staples. Note that the right staples (cyan) are expected to not perfectly bind in the isomerization state and induce mechanical stress, since their length is 32 nt, while the scaffold loops are only 22 nt long. Circular symbols at the scaffold edges indicate the relative orientations of the bases. The angular displacement gives information about how much the orientation has to rotate in order to make a crossover at the designed position. Reprinted and adapted with permission from reference [178].

7.1.2.1 Topology

AFM imaging of the DNA constructs showed that each of the three domains may assume one of two different conformations, either a canonical (c) or an isomerized (i) form, in agreement with previous reports.[170,175,177] Therefore, a total of $2^3 = 8$ different conformations are possible, although in case the domains cannot be distinguished, the number of possible conformations reduces to four (Figure 31) (ccc, icc, iic and iii). Both iso-forms have approximately the same surface area, however, the isomerized form has about twice the length and only half the width of the canonical one. For simplicity, in the course of this work, we will interchangeably refer to the canonical or isomerized form of a DNA origami domain as to the iso I or iso II forms, respectively, intending the collection of iso I or iso II conformations of the constituent HJs (even if this might not be true for each HJ).

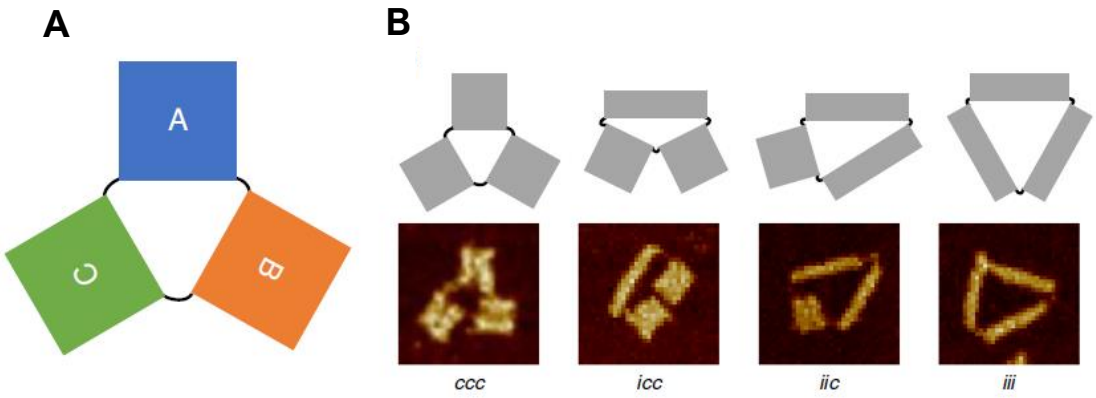

Figure 31: Possible conformations of the three-domain origami. The origami is composed of three, conformationally identical, quasi-independent domains (**A**, **B** and **C**) that are connected via short single stranded scaffold region. (**B**) Since domains can take on two isomerization states, but are non-distinguishable, in total four global conformations can be reached (shown schematically (top) and as observed with AFM (bottom)). Reprinted and adapted with permission from reference [178].

Isomerization yields were investigated in presence or absence of edge staples of each type, added at the left or right side of free scaffold segments, respectively. AFM analysis of the final assemblies showed that in absence of edge staples about 15 % of all domains appeared in iso II form (Figure 32). Addition of right edge staples increased isomerization rates only by an insignificant amount (ca. 17-19 %). On the other hand, in presence of left edge staples, a serious increase in the fraction of isomerized domains was recognized (about 62% for e(0)), confirming the hypothesis that scaffold turns at unfavorable positions become points of high local frustration to which the structure responds by searching an alternative folding route.

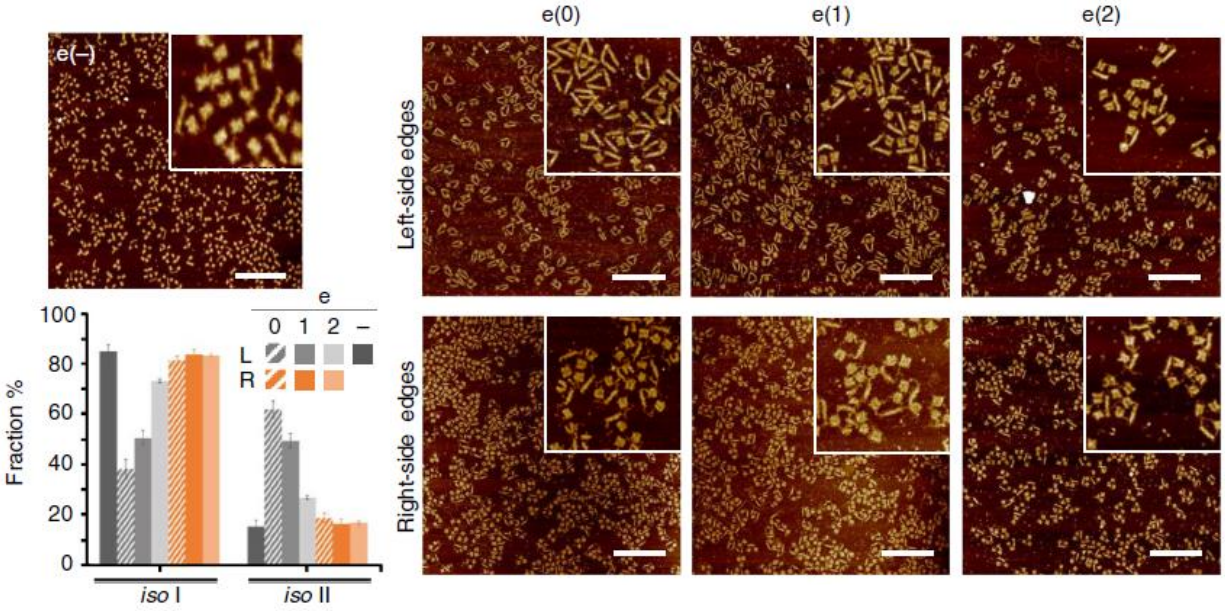

Figure 32: Distribution of global isomers. DNA origamis were assembled either in absence (e-) or in presence of edge staples on the right (orange) or the left (grey) side. Structures were analyzed and counted by AFM. The graph (bottom left) shows the total distribution of iso I to iso II faces. Scale bars are 600 nm. Insets are 1 µm x 1 µm. Error bars were obtained from three independent images of the same sample. Reprinted and adapted with permission from reference [178].

This result can be understood as follows: upon binding of staple strands to the edges and assuming formation of B-DNA duplexes, the scaffold at the left side of the structure should turn about 320° in order for the scaffold ends to align each other, while only 2° are necessary to achieve the same result at the right side of the structure (Figure 30A). Contrarily, in the iso II form, a rotation of only 137° is necessary. Additionally, for iso II, these regions are usually single stranded, offering far more orientational freedom to the scaffold and thus facilitating the formation of crossovers (Figure 30B). Noteworthy, isomerization rates varied considerably among the different edge types (e(0) = 62 %, e(1) = 47 %, e(2) = 29 %). A possible explanation might be that, while e(0) has two domains of 16 bp binding regions, e(1) and e(2) have three 8-16-8 binding regions. Hence, the 8 bp regions might not be strong enough to fully bind to their complementary part of the scaffold, therefore exerting less mechanical strain and eventually resulting in a lower isomerization extent. This might be true especially for e(2), where the staples have to inverse their direction. Noteworthy, when shorter e(0) staple strands were used in the assembly, dramatically reduced isomerization rates were observed (from 62 % to 19 %), suggesting that shorter oligos apply less torque on the structure and allow enough rotational freedom for the scaffold to arrange itself in the correct orientation (Figure 33A).

While edge staples could be used to shift the ratio between iso I and iso II forms by *destabilizing* the iso I state, the next step was to investigate whether this shift could also be

triggered by the *stabilization* of the iso II form. For this purpose, an additional set of staples (cyan strands in Figure 30) was left out in order to reduce mechanical strain in iso II structures. As expected, an increased formation of iso II was observed (Figure 33B).

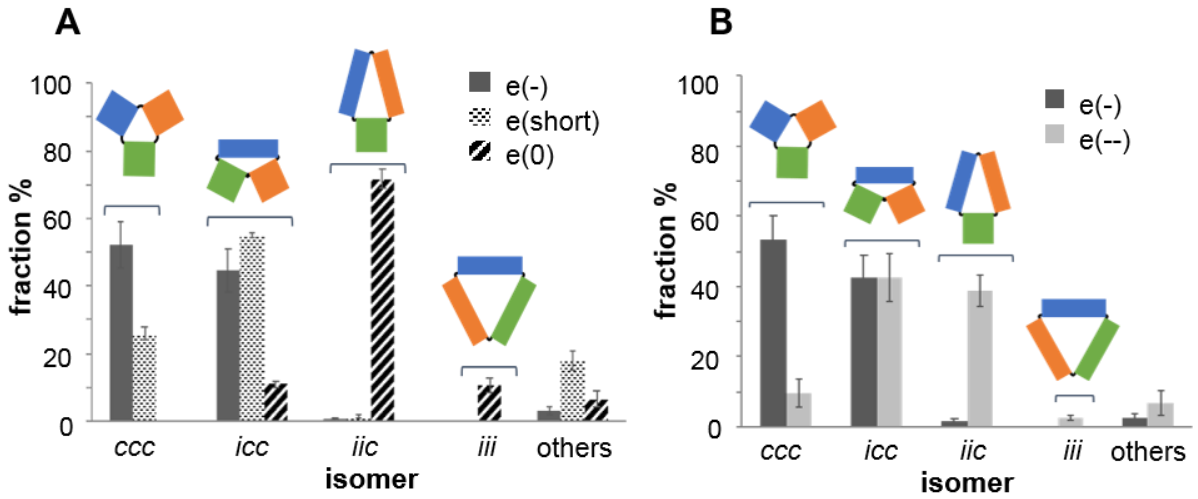

Figure 33: Statistical analysis of global origami configurations in presence of absence of different stimuli. (**A**) In presence of short edge staples (punctuated bars) isomerization rates are higher than in their absence (grey bars), but significantly lower than for full length edge staples (striped bars). (**B**) Absence of the last row of right-side staples (cyan staple strands in Figure 30) (light grey bars) leads to a significant increase in isomerized domains. Assembly conditions: 5 nM scaffold at -1 °C/min in 1X TEMg with 50X staple strands. Reprinted and adapted with permission from references [178].

Taken together, these results clearly indicate that mechanical strain early in the assembly process manifests itself in the appearance of an isomerized state of the structure, in the attempt to reduce structural frustration at those critical early-assembled sites. Nevertheless, the occurrence of iso II states even in absence of any edge staples, i.e. without any mechanical triggers, suggests that also other factors play a role in determining the fate of the assembly, which have not yet been determined.

7.1.2.2 Sequence

Since all domains of the DNA origami structure share the same topology, yet they demonstrate different isomerization behavior, only sequence-dependent effects may justify this discrepancy. To display these differences, each domain was individually assembled and the appearance of iso I and iso II forms were recorded by AFM (Figure 34A, B). While domain A showed significant rates of isomerization in absence of e(0) (41 %), domains B and C were

almost exclusively in the canonical form. Contrarily, if e(0) were added to the assembly mix, the equilibrium shifted towards the isomerized form, with domain A and B displaying 94 % and 85 % of isomerization, respectively. Domain C on the other hand was hardly affected by this, with more than 80 % of structures still in the canonical form. These results indicate that DNA origami domains can take different folding pathways, even if their topology, their assembly conditions and the type of mechanical stress they experience are exactly the same, further strengthening the idea that the base content is of crucial importance for the folding process as well.

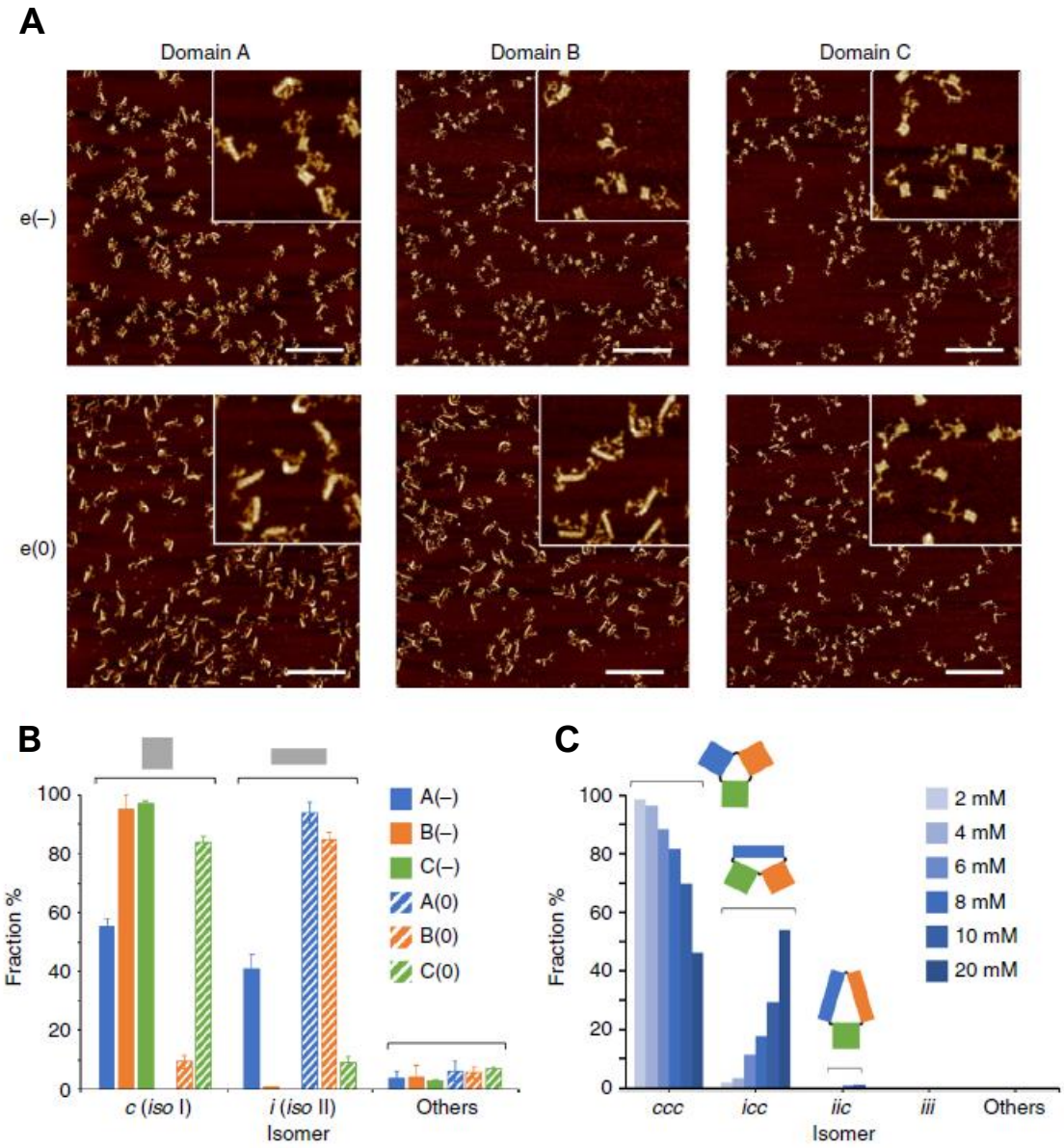

Figure 34: Observation of single-domain isomerization. (A) Representative AFM images of single-domain origamis in absence (e-) or presence of edge staples of type 0 (e0). Scale bars are 600 nm. Insets are 1 µm x 1 µm. (**B**) Statistical analysis of the obtained AFM images. Error bars were obtained from three independent images of the same sample. (**C**) Mg-screening of the origami assembly. Increasing Mg^{2+} concentrations seem to favor iso II. Reprinted and adapted with permission from reference [178].

It has been previously stated that magnesium ions have an effect on the transformation rate of HJs, while stacking forces at the junction points of HJs were shown to be responsible for the equilibrium ratio.[173] To test whether the magnesium concentration affects the isomerization process, a magnesium screening was performed (Figure 34C). Surprisingly, a strong relationship was observed, where increasing magnesium concentrations are related to increasing iso II appearance. Interestingly, only the ratios of ccc and icc changed, while occurrence of iic and iii were still insignificant, suggesting that again a sequence-dependency is in play.

To further investigate the sequence dependency of isomerization, another set of experiments was carried out. Here, the global e(-) structure was assembled in presence of distinct pairs of e(0) staples, targeting the left free helices of the scaffold (Figure 35, indicated from 1 to 9). The results indicate that a single pair of edge staples was enough to trigger an increase in the isomerization rate, with a maximum of 90 % for position 3/4 and a minimum of 47 % for position 8/9. The fact that the same mechanical forces acting on distinct edges of the structure cause such significantly different responses reinforces the view that topological stress alone is not sufficient to explain the final folding trajectory of a DNA origami, but that the sequence content plays a decisive role as well. Also, the addition of one staple pair alone resulted in isomerization rates that are almost as high as for assemblies where all edge staples are added, proposing a cooperative mechanism for the reconfiguration of HJs.[177]

Analysis of the T_m values of the staple pairs (calculated by Mfold)[227] showed a good match between the melting temperatures and the degree of isomerization, therefore suggesting that staples with a high T_m (e.g. 3/4) bind early in the folding process, probably directing the assembly path towards iso II. Furthermore, the base stacking contributions at the HJs[46,253] were taken into consideration to investigate whether one of the two iso-forms is energetically favored. The analysis did not reveal any trend that would match the observed isomerization rates of each domain, suggesting either a minor role of the base stacking contributions or inaccuracies in their estimated values.

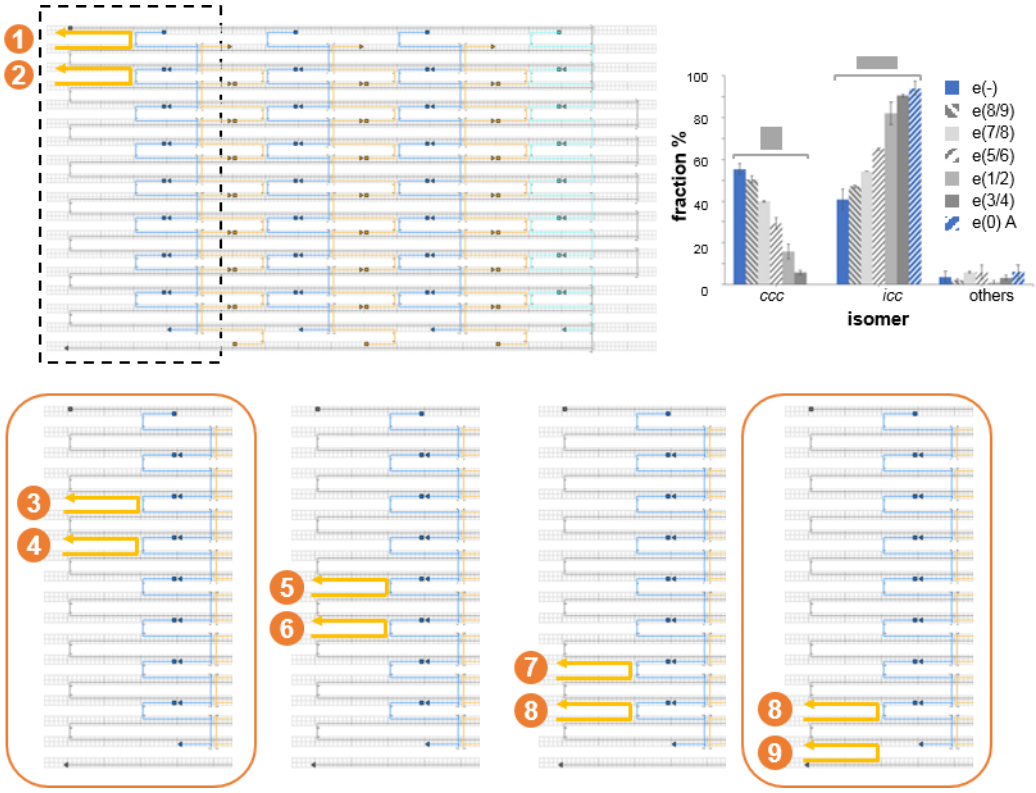

Figure 35: Individual edge staple pairs trigger vastly differing isomerization rates. DNA origami structures were assembled with different pairs of edge staple strands (1-9) of domain A. AFM analysis revealed vastly different isomerization rates, depending on the staple position (top right). Reprinted and adapted from reference [178]

7.1.2.3 Energy landscape

In order to get a better grasp on the energetic costs associated to each isomerization state, cooling and melting curves were recorded for every structure in presence or absence of edge staples. The assembly and disassembly of domain A was followed by the incorporation of two orthogonal FRET pairs, that specifically yield a fluorescence signal for iso I or iso II, respectively (Figure 36). Thermal profiles for the canonical iso I state could only be recorded for e(-) and e(2), since no significant amount of canonical shapes appeared for e(0) and e(1). On the other hand, thermal profiles could be obtained for iso II in all cases, in full agreement with the results obtained by AFM analysis (Figure 36B).

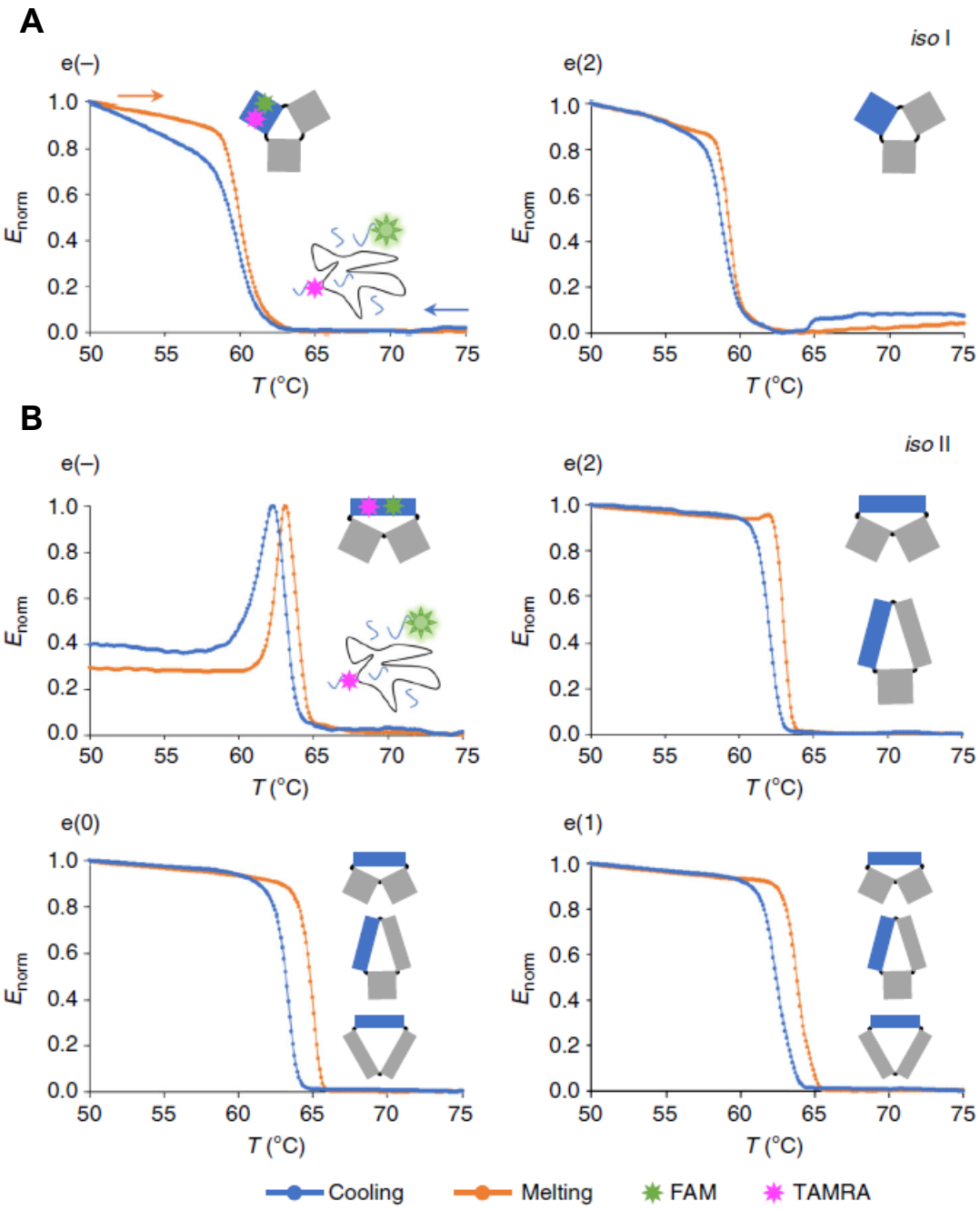

Figure 36: Cooling and melting curves of domain A. Two FRET pairs were used to record formation of exclusively iso I (**A**) or iso II (**B**). Upon assembly/disassembly FRET signal should increase/decrease respectively. Cooling/Melting rate was ± 0.1 °C/min. Data were averaged from four replicates of two independent experiments. Since no canonical faces were present in e(0) and e(1) samples, no thermal profiles could be obtained here. FRET pair was FAM (green) and TAMRA (magenta). Reprinted and adapted with permission from reference [178].

While the cooling and melting curves of iso I are overlapping (T_m is about 60 °C for both e(-) and e(2)), proposing a reversibility of the transition in the vicinity of the FRET labels, the

thermal profile of iso II formation shows a hysteresis of about 1-2 °C, with T_m of cooling and melting profiles being ca. 63 and 64 °C (e(-) and e(2), slightly higher for e(0) and e(1), Figure 36B). Clearly, folding of iso II is not fully reversible and it is generally associated to higher energetic costs. A peculiarity is displayed by the thermal behaviour of e(-) in the iso II form. Here, a biphasic curve was recorded, with a steep increase in the FRET signal at about 64-65 °C (associated to 1.0 FRET signal) and a strong FRET decrease down to 0.4 at ca. 62-63 °C, that approximatively corresponds to the T_m of iso I formation. Interestingly, this biphasic behaviour corresponds very well with the distribution of iso I and iso II observed at the AFM, with about 60 % iso I and 40% iso II. It can therefore be assumed that early in the folding process, when the energy of the system is still high enough (high temperatures), formation of iso II starts earlier, since it is energetically more stable. Once the temperature drops further though, more staples disfavoring the iso II state bind to the scaffold, thus triggering a reconfiguration of the total structure to iso I in about 60% of the cases.

Mathematical treatment of the thermal profiles by van't Hoff analysis was prevented by the lack of reversibility of iso II assembly and disassembly. Therefore, the Friedman-Ozawa isoconversional method was used[254–257] to estimate the activation energies of the assembly and disassembly of the structures. Investigation of the e(2) thermal profiles enabled to draw a full picture of the energetic landscape and to derive an explanation for the aforementioned observations: within this unified view (Figure 37), the assembly of iso I is kinetically favored over iso II due to its lower energy barrier that must be overcome to start the assembly process ($E_{act}^{U\text{-}I} < E_{act}^{U\text{-}II}$, Figure 37). Conversely, also the unfolding process is facilitated for iso I, since its local energy minimum is higher than that that of iso II ($E_{act}^{I\text{-}U} << E_{act}^{II\text{-}U}$). On the other hand, reaching iso II is less probable due to its higher activation energy. Once assembled though, the structure reaches an energy minimum from which it cannot easily escape. Both iso states are connected via an intermediate open state of the HJs, which is not only apparent from the thermal profile of e(-), but also from the magnesium screening experiments, where it appeared evident that more canonical domains are formed when the reconfiguration is facilitated by decreased Mg concentrations.

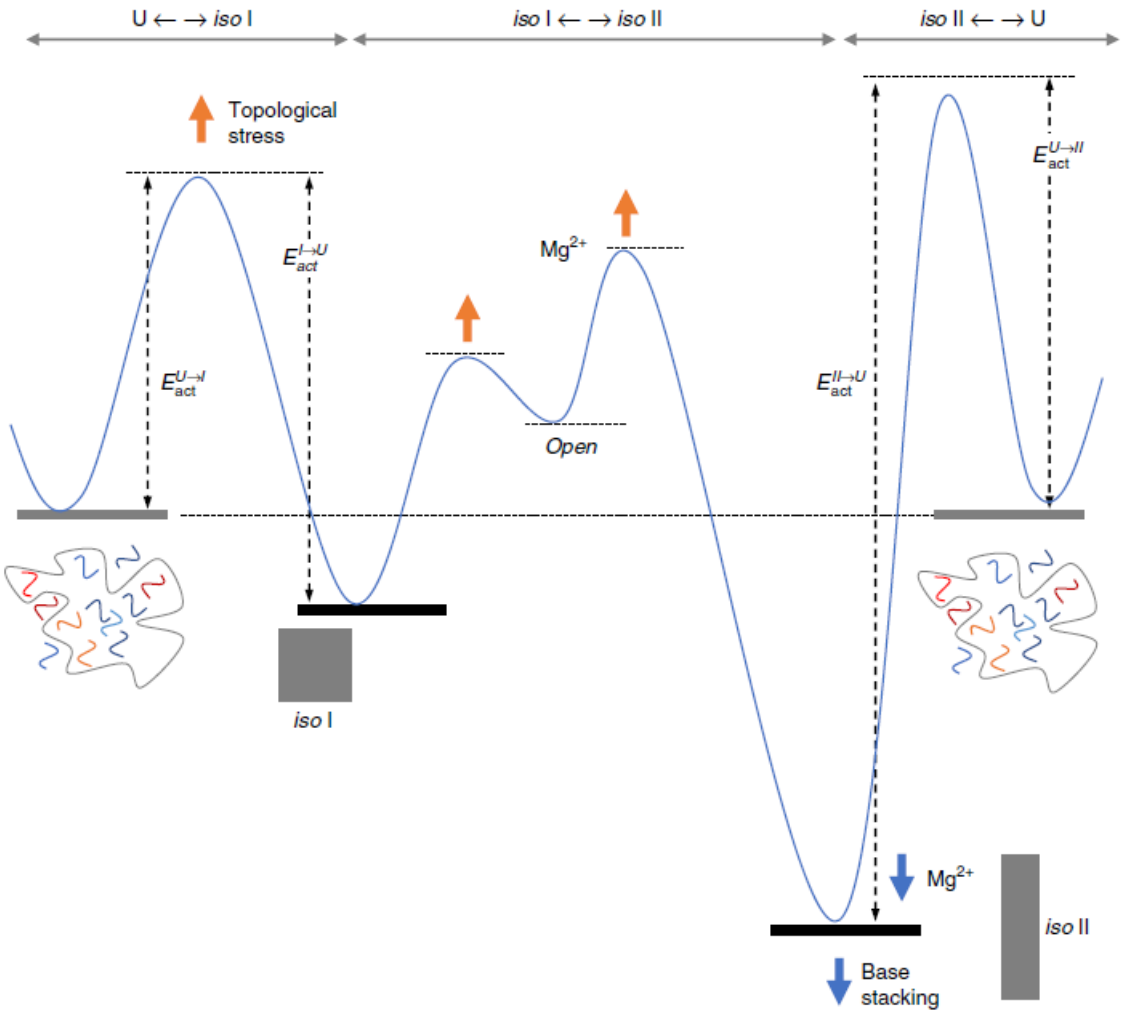

Figure 37: Schematic energy diagram for the folding and unfolding process of the DNA origami. Both configurations reach local energy minima that are connected via a post-assembly reconfiguration (open form, energy level is set arbitrarily). Iso I has a lower activation energy, favoring its formation as well as the reversibility of the folding/unfolding process. Iso II has a higher energy barrier. Once overcome the structure is more stable than iso II though and the process is not easily reversed. Note that Mg^{2+} does increase the energy barrier for the post-assembly reconfiguration, stabilizing both iso forms once they are fully assembled. Reprinted and adapted with permission from reference [178].

7.1.3 Conclusion

Previous works on the folding and post-assembly reconfiguration of DNA origamis have identified important mechanisms that steer the assembly fate of a given structure. While scaffold turns have been shown to guide the initial folding process[163,165] and serve as attacking spots for mechanically propagated structural reconfiguration,[171,175,177] the staples with a high T_m were proven to act as nucleation sites from which the folding process progresses.[251]

In this work, topological as well as sequence-dependent factors were merged into a unified view, from which quantitative data could be harnessed in order to build a model that explains not only the occurrence of two distinct folding pathways but also the distribution among them. Within this model, and in agreement with preceding findings, the nucleation sites from which the folding process begins is of crucial importance. While iso II may be energetically favored by an increased number of base stacking interactions, its formation is greatly disturbed by the high entropic costs associated with its formation, favoring the appearance of iso I. The situation is reversed however, if the nucleation site is moved to a location of high structural frustration. In this case, the increased energetic barrier for iso I swings the equilibrium towards the iso II state, where high torsional stress can be evaded. It is therefore expected that careful design and manipulation of these sites can serve as a tool for the rational construction of DNA structures that can take on different shapes.

7.2 A reconfigurable DNA device for controlling inter-particle distance with nanometer-scale resolution

Parts of this chapter are published in the following article: *Erkelenz, M., *Kosinski, R. *et al.* (*equal contribution) Site-specific facet protection of gold nanoparticles inside a 3D DNA origami box: a tool for molecular plasmonics. *Chemical Communications* **57**, 3151-3153 (2021).[231] An additional first co-authorship publication is currently in preparation.

7.2.1 Introduction

The site-specific functionalization of gold nanoparticles (AuNP) is a pre-requisite for the creation of ordered AuNP assemblies, such as e.g. dimers.[258–260] Particle dimers are of particular interest since the plasmonic coupling of two closely located AuNPs leads to a tremendously enhanced electric field at the inter-particle space (hot spot). This phenomenon is applied in advanced biosensing technologies, such as surface-enhanced Raman scattering or surface-enhanced fluorescence (SERS or SEF).[192,261–263] Due to the chemical and topological symmetry of spherical AuNP and, to a lower extent, nanocubes (AuNC), it is challenging to address exclusively a specific location of the particle for functionalization. While offering a lower enhancement factor, AuNCs bear the advantage of a hugely increased hot spot volume[264,265] that can be used to bind and detect a huge number of ligand molecules. In both cases however, the addressability issue remains and a method is needed to break the symmetry of these objects. In this work, a DNA origami box is used to encage AuNCs of different sizes and to shield five out of their six facets, leaving only one side available for further functionalization. Two distinct DNA-AuNC hybrid structures are then fixed in a face-to-face orientation on top of a dynamic DNA origami platform and their inter-molecular distance is controlled with nanometer-scale accuracy through the triggered reconfiguration of the device among five distinct states. This lays the basis for a plasmonic device with hot spots of customizable dimensions.

7.2.2 Results

7.2.2.1 Binding of AuNCs into the DNA host

To host the AuNCs and ensure protection of 5 out of 6 of their facets, a lidless, 3D DNA box was designed that can incorporate bare AuNPs. To achieve this, up to 28 thiolated oligonucleotides were attached to single stranded DNA handles that protrude into the cavity of the box (Figure 38). Using this strategy, bare AuNPs can be bound inside the box, preventing the need for AuNP surface functionalization with complementary oligonucleotides and thus making the DNA-free facet available and accessible for other ligands. The DNA box consists of a bottom plate and four walls, which can be individually folded and lift up in order to control the steric accessibility to the box cavity in a stepwise manner. Within this work, if not stated otherwise, box structures were folded with all four walls lifted up to ensure sufficient structural integrity and rigidity. The box features a ca. 25 nm x 25 nm x 26 nm inner cavity, as derived by statistical analysis of TEM images (n = 100). These values correspond very well with the theoretical expectations (21.3 nm x 21.3 nm x 25.4 nm) according to calculations of inter-helical distances in previously reported studies.[266]

In a first experiment, 18 nm AuNCs were used for the loading of DNA boxes. Since uncoated AuNPs are not stable in buffers of high ionic strength,[267] stabilization with 0.2 % [w/v] Tween20 was required. Thiolated boxes were incubated with 10 equivalents of AuNPs over night at room temperature. Figure 38 shows representative TEM images of stained samples. Since successful incorporation was achieved, a set of follow-up experiments were set up to test the efficiency of incorporation, depending on the amount of thiolated staples within the DNA box cavity and on the size and shape of AuNPs (Table 5). Two trends emerge from the collected data: (i) increasing the number of thiolated staples inside the cavity results in a higher incorporation efficiency in all cases (up to 69 % for 28 staples and 10 nm spheres).

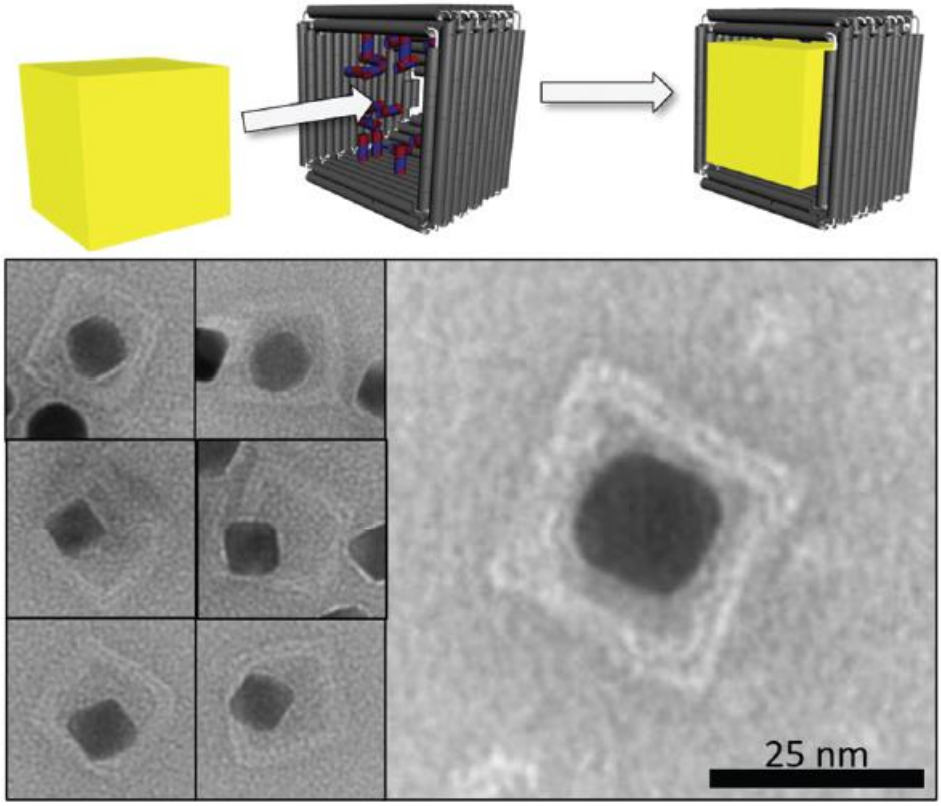

Figure 38: Binding of AuNCs into its DNA host. Up to 28 thiol-modified staple strands are incorporated inside the DNA box to bind AuNCs (top). Representative TEM images of DNA boxes with successfully incorporated 18 nm AuNCs (bottom). Reprinted and adapted with permission from reference [231].

Importantly, the system shows a high specificity. Control samples without thiolated oligos show in most cases no incorporation at all, with a maximum of only 12 % binding for the very small 8 nm spheres. (ii) Loading efficiency drops for increasing sizes of AuNPs. While 8 nm spheres show an atypical binding behaviour, the trend is consistent for AuNPs with sizes greater than 10 nm. Almost 70 % incorporation was achieved for 10 nm AuNPs, while the lowest binding yield was observed for 18 nm AuNCs. However, still 16% of DNA boxes appeared loaded. Interestingly, when compared to the commonly applied method based on DNA-coated AuNPs,[268] this method worked equally well or even better, depending on the sizes of the AuNPs chosen for encapsulation (data not shown). This may be attributed to the increased sizes of the AuNPs upon DNA coating or to the significant electrostatic repulsion between DNA boxes and coated AuNPs.

Table 5: Systematic evaluation of incorporation efficiencies. Differently sized and shaped AuNPs were used for the loading of the DNA host (top: Scheme) with varying amounts of thiol-modified staples inside its cavity. Top: Scheme. Middle: Representative TEM images. Bottom: Statistical analysis. n = 130 origami boxes at least. Tween20 was used for stabilization of AuNPs. Reprinted and adapted with permission from reference [231].

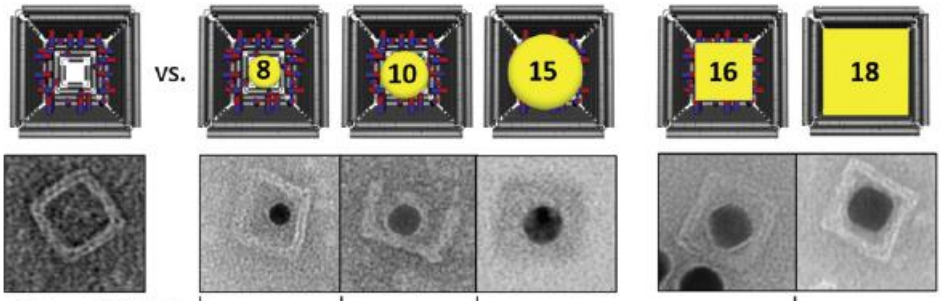

No. of thiols					
0	12%	0%	0%	0%	0%
16	17%	59%	12%	13%	3%
28	57%	69%	50%	28%	16%
Tween20 w/v	0.1%	0.15%	0.2%	0.2%	0.2%

To achieve a plasmonic hot spot, two AuNPs must be brought into close and programmable nanometer-sized proximity. Since successful incorporation of AuNPs into DNA boxes was achieved, these particles must now be precisely positioned one in front of the other. For this purpose, a DNA platform, termed "Zelos", was designed. Zelos is a square lattice bilayer of 20 parallel helices. Importantly, Zelos consists of two halves that are connected via eight helices. These helices can be adjusted in length so that both halves can be moved closer or farther apart from one another in a programmable fashion. The Zelos platform is designed to be actuated interchangeably among five distinct states, spanning a distance between the two halves that ranges from a minimum of 0 nm (i.e. the duplexes connecting the two halves are 0 bp-long) to a maximum of 15 nm (corresponding to 43 bp-long duplexes). Such a controllable distance among the two halves of the platform will translate into a predictable distance among the two facing facets of the NPs. Inter-particle gap will ultimately depend on the relative positions at which the two box/ANPs will be fixed on top of the reconfigurable platform.

Figure 39 illustrates the strategy used to control the gap distance between the two halves of the Zelos platform. For a matter of clarity, the scheme reports the design approach used for one staple, although the same procedure is adopted identically for a total of eight staples. Essentially, the scaffold is routed back and forth along the bilayered platform leaving eight

single stranded portions (each 63 bases-long) at the central seam. These scaffold loops at the seam are those regions that will be targeted by sequential addition of fuel/antifuel strands, thus dictating the distance between the two halves of the platform.

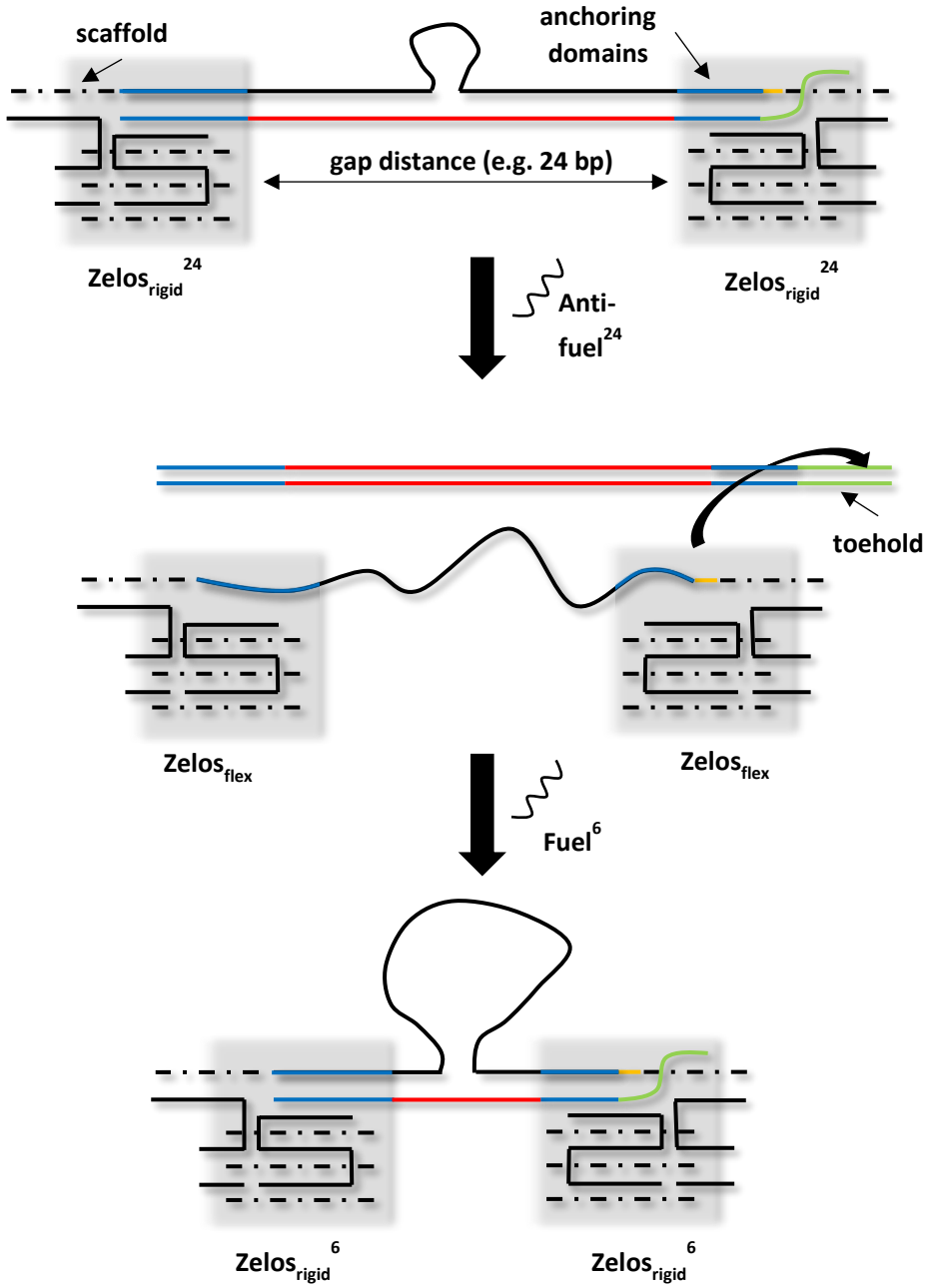

Figure 39: Schematic representation of the toehold mediated strand displacement reaction for Zelos gap distances. When fuel strands of defined lengths are hybridized to Zelos, a distinct gap distance can be adjusted, and the structure is rigid (top). Once anti-fuel is added, it can bind to the toehold of the fuel strand and displace it from the origami. The structure is now in a flexible state (middle). By addition of a new fuel-strand, the gap distance can be regulated again (bottom). A single free base in the scaffold (yellow) aids in releasing possible tension arising from the hybridization of fuel-strands.

To adjust the gap distance, so-called “fuel staples” are designed to bind at both halves of the structure, thus forming eight duplexes of defined length. Each of these fuel staples can be partitioned into several domains. A first, anchoring domain hybridizes to the scaffold within the structure and tightly secures the staple at each of the two halves of Zelos (blue segments). A second domain binds to a portion of the scaffold that spans the gap region in between the two halves (red segment). Since fuel staples do not fully hybridize to the entire unpaired scaffold segment, a scaffold loop is formed. The larger the size of this loop (that is, the portion of the scaffold which is excluded from the duplex bridges), the shorter will be the gap distance between the two halves of Zelos. Finally, a third domain is represented by a toehold region at the termini of each fuel staple (green segment). This single-stranded DNA domain consists of 8 nucleobases and serves as the starting point of a toehold-mediated strand displacement reaction. Upon addition of so-called anti-fuel strands that are fully complementary to the fuel staples, these latter are displaced from the origami, thereby resulting in the two halves being connected only by eight unstructured single-stranded scaffold segments. In this flexible configuration, the distance between the two halves is basically undefined; nevertheless, this intermediate gives room for binding of another set of fuel staples that can adjust the length of the duplexes and thus the gap distance to another desired value. Basically, the platform was designed to assume five distinct gap distances. The predictable actuation of the device from one rigid state of defined gap distance to another rigid state of different gap distance always requires the transition through an intermediate state of undefined gap distance. Finally, one terminal nucleobase of the scaffold was left unbound (yellow region) in order to relieve the orientational strain that can arise upon fuel binding.

To test the programmable reconfiguration of the device into pre-defined gap distances, Zelos was assembled with five different sets of fuel staples, which should yield a theoretical distance of 0, 2, 4, 8 and 15 nm, respectively. Figure 40 shows analysis of representative TEM images of the generated structures. The platform appears well-folded and gap distances, estimated by statistical analysis of TEM images (Figure 40), correspond exceptionally well with the expected theoretical values (assuming 0.33-0.34 nm / bp[48]), indicating that a highly precise arrangement of AuNPs is indeed possible.

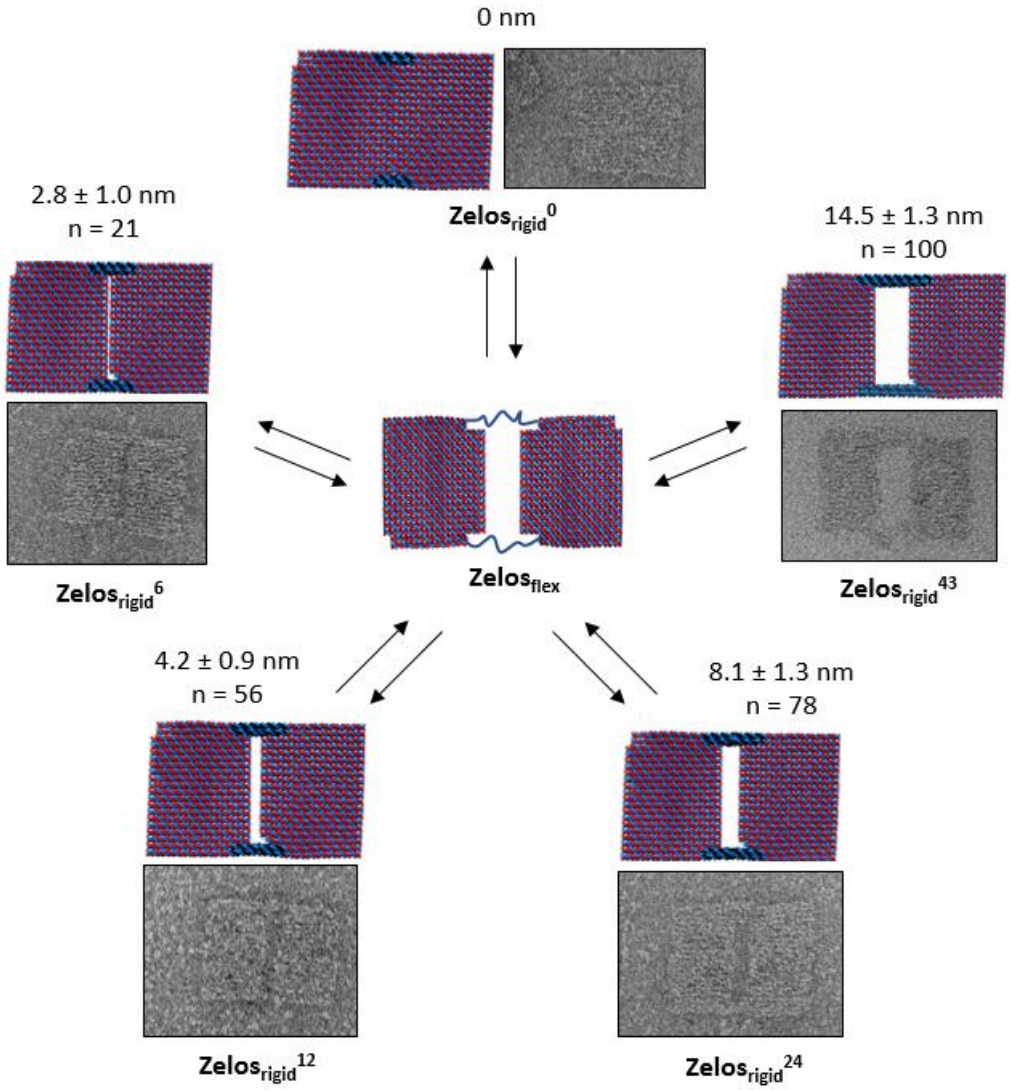

Figure 40: Schematic representation of the dynamic regulation of Zelos. By addition and removal of fuel-staples, the gap distance in Zelos can be adjusted. The structure must pass a flexible (flex) intermediate state that has no defined gap distance. TEM images show representative images of assemblies with defined gaps. Statistical analysis was used to calculate the recorded distances. No gap was observed for 0 nm samples. Atomic models were generated with the CanDo software. TEM images and statistical evaluation was done by Dr. Michael Erkelenz from the group of Prof. Schlücker (University Duisburg-Essen).

7.2.2.2 Hierarchical assembly of the plasmonic DNA device

In the next step, AuNPs need to be fixed in a face-to-face orientation on top of the Zelos platform and at well-defined positions. Only in this way, the precision achieved in the structural reconfiguration of the platform can be reliably translated into a predictable hot spot gap between the DNA-free nanoparticles. For this purpose, four staple strands are designed to protrude from each half of Zelos. These staples, while being anchored within the DNA platform, have a second domain that can incorporate into four distinct positions within the DNA boxes (Figure 41B). In this way, the relative orientation of each DNA box on top of the Zelos platform can be fully predicted. Two distinct DNA boxes, each one carrying a single AuNP, can be thus positioned with the DNA-free metal surfaces facing each other at a predictable distance. The entire architecture thus consists of three DNA origami structures and has an approximate molecular weight of about 15 MDa. The hierarchical assembly of such a large structure is clearly hampered by steric hindrance and strong electrostatic repulsions among the negatively charged DNA origami structures. For this reason, hybridization of Zelos and DNA boxes was performed over seven days at 30 °C in 1X TEMg11 buffer, using a 1:4 (Zelos:Box) ratio. Figure 41A summarizes the results of the AGE analysis and the corresponding TEM images of the individual bands. It is apparent, that the hybridization event led to the occurrence of two new bands (1 and 2) that migrate significantly slower than the monomer band (4) and the dimer band (3) and are therefore expected to be species of higher molecular weight. Interestingly, the Zelos monomer band disappears after hybridization, suggesting an almost complete binding of Zelos to at least one DNA box. Subsequently, bands were cut out and visualized by TEM. As expected, bands 3 and 4 refer to the DNA box dimer and monomer species, respectively. Band 2 represents Zelos bound to one DNA box. Finally, about 16 % of all the structures show a complete hybridization of two DNA boxes to the Zelos platform.

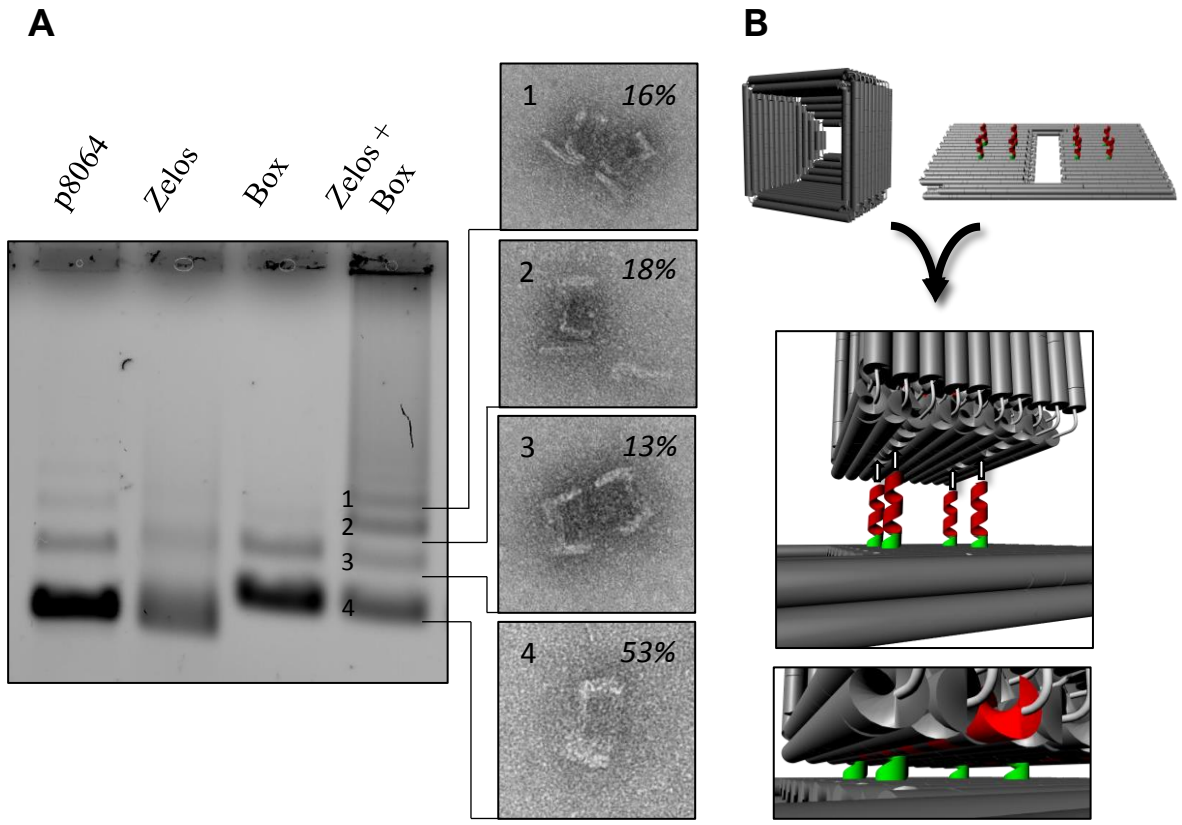

Figure 41: Hybridization of Zelos and Box. (A) AGE (left) of individual DNA origamis as well as the hybridization sample of Zelos and Box. Hybridization was performed for seven days at 30 °C, 11 mM $MgCl_2$ in a 4:1 (Box:Zelos) stoichiometry. Two new bands appear (1 and 2). TEM analysis (right) revealed the identity of each band. Percentages give information about the yield of each species, calculated from the EtBr intensity. Gel and TEM images were acquired by Dr. Michael Erkelenz. The agarose gel was run at 80 V for 2 hours in an ice bath. (**B**) Schematic representation of the hybridization event. Protruding staples (red) reach from Zelos into the box, thereby anchoring it on the surface. 3T spacers (green) are used to give some flexibility and reduce electrostatic repulsion. Pictures created by Dr. Michael Erkelenz from the group of Prof. Schlücker (University Duisburg-Essen).

7.2.3 Conclusion

The rapid development of structural DNA nanotechnology led to its merging with multiple scientific disciplines. One of the most fruitful combinations unifies the spatial precision of DNA origami and the optical properties of plasmonically active particles, as noble metal nanoparticles. DNA-based nanoplasmonics has launched a wealth of research publications as well as novel nanomaterials with advanced optical properties. Several of these

have been shown to be extremely useful in the field of ultrasensitive vibrational spectroscopy, as e.g. SERS.

The goal of this work was to develop a hierarchical DNA origami superstructure that can accommodate bare AuNPs at a predictable distance and that is able to dynamically alter this gap to achieve intense electric field enhancement. In the first part of the work, the successful stabilization of bare AuNPs of several sizes and shapes, as well as their incorporation into rationally tailored DNA hosts have been demonstrated using AuNCs with a maximum size of 18 nm. Furthermore, a DNA platform was constructed that enables the placement of DNA boxes with control over their relative orientation and inter-molecular distance. The actuation of the platform through five distinct states, each one characterized by a defined distance between the two halves of the structure, has been proven and suggests that, once AuNC are incorporated within the DNA boxes, also the gap distance between them can be accurately adjusted.

In the future, three main experimental routes should be pursued: (i) the full assembly of the origami superstructure, i.e. the 18 nm AuNC loaded DNA boxes hybridized to both halves of the DNA platform, must be shown, (ii) the dynamic switching of the loaded platform between varying gap distances has to be proven; (iii) once established, bare AuNC facets should be loaded with Raman reporters for single molecule measurements and calculations of the SERS enhancement factor. Upon completion of these steps it is expected that this novel hybrid-structure may serve as a valuable tool within the field of vibrational spectroscopy and may be beneficial for the structural investigation of numerous analytes.

7.3 Publications

Peer-reviewed publications	Kosinski, R., Mukhortava, A., Pfeifer, W. *et al*. Sites of high local frustration in DNA origami. *Nature Communications* **10**, 1061 (2019) Erkelenz, M.*, Kosinski, R.*, Sritharan, O. *et al.* Site-specific facet protection of gold nanoparticles inside a 3D DNA origami box: a tool for molecular plasmonics. *Chemical Communications* **57**, 3151-3153 (2021) - * Equal contribution Kosinski, R., Perez, J. M., Schöneweiß, E. *et al.* The role of DNA nanostructures in the catalytic properties of an allosterically regulated protease. *Science Advances* **8**, (2022)
Publications in progress	Kosinski, R., Giesler, H., Erkelenz, M., et al. A reconfigurable DNA device for controlling inter-particle distance with nanometer-scale resolution.
Book Chapter	"The Effect of DNA Boundaries on Enzymatic Reactions, Kosinski R., Saccà, B.) in "DNA Origami: Structures, Technology, and Applications", **in Press**, (2022) John Wiley and Sons Inc.
Posters	Erkelenz, M., Kosinski, R., Sritharan, O., Saccá, B., Schlücker. S., Detection of Protein-Protein Interactions with DNA Origami assisted Dynamic Gold Nanocube Dimerization. *CRC 1093 Symposium*, Supramolecular Principles in Biological Systems, **2019**, Essen, Germany Kosinski, R., Mukhortava, A., Pfeifer, W., Candelli, A., Rauch, P., Saccà B., Sites of High Local Frustration in DNA Origami. *NanTech* **2019**, Aalto, Finland Kosinski, R., Mukhortava, A., Pfeifer, W., Candelli, A., Rauch, P., Saccà B., Sites of High Local Frustration in DNA Origami. *3rd CRC International Symposium*, **2019**, Essen, Germany Erkelenz, M., Kosinski, R., Schöneweiß, E.-C., Saccà, B., Ottmann, C., Schlücker, S., Nanopositioning of Supramolecular Ligands on DNA Origami for Multivalent Protein Recognition. *16th World Medical Nanotechnology Congress*, **2018**, Tokyo, Japan

7.4 Acknowledgements

First of all, I would like to take the opportunity to thank Prof. Andrea Musacchio and Prof. Kurt Vesterager Gothelf to spend much of their valuable time to evaluate this thesis.

Furthermore, I would like to thank the group of Prof. Sánchez-García and the group of Prof. Sebastian Schlücker for their support, time, material and data that they contributed to this thesis. Having the opportunity to engage in such fruitful cooperations throughout my PhD time is something that I am especially thankful for.

Obviously also a big thanks to all the members of the AG Saccà and AG Kaiser for their scientific input, conversations, laughs, parties and in general the time together, which made the last years so much more enjoyable. Special ones to mention here are of course Pierre "Panzer-Pierre" Stegemann, Andreas "AJ" Jaekel, Lena "Lenomon" Stenke, Sabrina "Brinka" Gambietz, Sabrina "Brynamite, Brine, Brunai, Brincess" Ninck and Leonard "Lönard" Sewald. Spending basically every lunch time for the past four years and countless drinking sessions with you is something that I truly appreciate. It is my pleasure to work with you. Additionally, I want to thank some people of the "alte Garde", which pursue their careers outside these groups by now: Wolfgang "Pfeifi" Pfeifer, Elisa "Lutz" Schöneweiß, Geronimo „Gero" Heilmann, Florian „Bo" Schulz, Michelle "Meech" Hechler and Sarah "Sarotte Ida" Urban. You welcomed me with an open heart when I started here and especially Pfeifi and Lutz helped me countless times when I had no clue what to do. I would like to say that I will always remember the numerous evenings and events together, but for this to happen clearly, we would have needed to drink less alcohol.

Special thanks also to Jenny "Jenjen" Bormann, Svenja "SvenH" Blaskowski for keeping everything running smoothly in the lab and to Svenja "SvenK" Kernchen for explaining to me for the last four years, over and over again, the bureaucracy of this university and how to survive it.

I would also like to express my admiration for "the incredible Wing". Your music brightened my days and put a smile on my face. Furthermore thanks to Lichess.org for being a free-of-charge chess-website where I have apparently spent 27 days, 1 hour and 8 minutes of my life and thank you Barbara for letting me play even when I played a match in my work time ("It's ok Ricky, it exercises your brain. But no mobile games!"). An honorable mention here is of

course the coffee-machine. The daily supply of a mixture of coffee, decade-old-deposits and probably a blend of various microorganisms made my days.

A special “thank you” to Viktoria “Viki, or Vicky?” and Michael “Disco Mikey” Erkelenz. This friendship was as unexpected then as it is special to me now and I am forever grateful that I have met you.

A person which I owe so much is my supervisor, Prof. Barbara Saccà. You have impressed me the first day I listened to your lecture and you continued to do so for the last four years. You showed me how to be a scientist, motivated me when I was struggling and sometimes just showed up at our office to chat with us for half an hour. Asking you to do my PhD thesis in your group has easily been one of the best decisions of my life.

Certainly, my greatest supporter is my family. Having my back for almost 30 years now, always helping me out and motivating me to do the things I am interested in is something rare and I am truly thankful for that. Specifically, I have to mention my sister who “endured me 30 years, taught me things, motivated me, made me more intelligent, why are you even asking?” (her words). We may never have known what the other one is doing (no, I am not doing something with bacteria!!!), but despite this mutual ignorance about each other’s profession, I knew I could always count on you!

Finally, I want to say thank you to the most beautiful girl there is, Melanie “Melo” Weiß, who makes my life happier every day. Thank you for spending so much time with me.

7.5 Curriculum Vitae

Aus datenschutzrechtlichen Gründen nicht in der Onlineversion enthalten.

7.6 Declaration

Hiermit erkläre ich, gem. § 7 Abs. (2) d) + f) der Promotionsordnung der Fakultät für Biologie zur Erlangung des Dr. rer. nat., dass ich die vorliegende Dissertation selbständig verfasst und mich keiner anderen als der angegebenen Hilfsmittel bedient, bei der Abfassung der Dissertation nur die angegeben Hilfsmittel benutzt und alle wörtlich oder inhaltlich übernommenen Stellen als solche gekennzeichnet habe.

Essen, den 24.03.2022 _____

Unterschrift des/r Doktoranden/in

Hiermit erkläre ich, gem. § 7 Abs. (2) e) + g) der Promotionsordnung der Fakultät für Biologie zur Erlangung des Dr. rer. nat., dass ich keine anderen Promotionen bzw. Promotionsversuche in der Vergangenheit durchgeführt habe und dass diese Arbeit von keiner anderen Fakultät/Fachbereich abgelehnt worden ist.

Essen, den 24.03.2022 _____

Unterschrift des/r Doktoranden/in

Hiermit erkläre ich, gem. § 6 Abs. (2) g) der Promotionsordnung der Fakultät für Biologie zur Erlangung der Dr. rer. nat., dass ich das Arbeitsgebiet, dem das Thema „DNA origami tools for biophysical and biochemical applications“ zuzuordnen ist, in Forschung und Lehre vertrete und den Antrag von (Richard Kosinski) befürworte und die Betreuung auch im Falle eines Weggangs, wenn nicht wichtige Gründe dem entgegenstehen, weiterführen werde.

Essen, den 24.03.2022 _____

Unterschrift eines Mitglieds der Universität Duisburg-Essen